Experimental and Numerical Investigation of Masonry Infilled Reinforced Concrete Frames with Rubber Joints

Prateek Kumar Dhir

Department of Civil and Environmental Engineering

University of Strathclyde, Glasgow

13th May 2022

Contents

Declaration of Originality

This thesis is the result of the author's original research. It has been composed by the author and has not been previously submitted for examination which has led to the award of a degree.

Dedicated to my grandmother the late Suryamani Dhir

Acknowledgments

I am greatly thankful to my supervisor Dr. Enrico Tubaldi who continuously provided me with all the necessary support to complete my research. My second supervisor Dr. Shangtong Yang and Dr. John Douglas provided valuable suggestions during my annual reviews that helped me to improve my work further. It was a nice experience to collaborate with Ms. Alessandra Orfeo within our research group as well as with Hamid Ahmadi, Dr. Julia Gough, Dr. Bartolomeo Panto, and Prof. Ivo Calio outside the university where we shared our research skills with each other.

In my present research, I had to perform extensive experimental tests in our department Lab and for which our lab technicians James Francis, Gavin Gibson, and Derek McNee provided me with all the necessary help needed. It wouldn't have been possible to successfully carry out the tests without their support. Again, I am grateful to my hero, Mara Knapp, who always stood beside me when I struggle either with my university access or placing a purchase order for my experiments. Thanks to Morag McIntosh for providing all the academic assistance and Maggi for the emails when my online orders get delivered. I am grateful to Darren Grant and Matthew McLean, who provided uninterrupted IT support throughout my research.

Thank you, Diana and family, for offering me food uncountable times and my elder brother Dr. Krishna and my brother Sandeep who never let me feel that I am thousands of miles away from my home. Had an exciting time with my football team "Strathlabamba". Thank you, Ryan, Euan, Andrea, Valerio, Alessandra, Francesca, Thanos, Christos, and Christoph for sharing lunch hours with me. Euan never shares food, but he shares food with me!

Lastly, my parents, my girlfriend Reena, and brother Sandeep always stood beside me on my good and bad days. Thank you, Glasgow, you are awesome!

Abstract

Masonry infill walls are among the most vulnerable components of reinforced concrete (RC) frame structures. Numerous models have been developed in the last decades to describe the seismic response of masonry-infilled RC frames, by focusing on the description of the interaction between the infill and the frame and/or the global seismic response of the composite frame-infill system. More recently, some techniques for enhancing the performance of the infills have been proposed, with the aim to improve the capacity of the infills and/or the performance of infilled frames.

Recent experimental and numerical studies have investigated innovative solutions for protecting these walls by reducing their interaction with the RC frame. Among the most promising ones, there are those that aim to decouple or reduce the infill-frame interaction by means of flexible or sliding joints at the interface between horizontal subpanels or between the panels and the frame.

Rubber joints have emerged as a very efficient technical solution with the possibility to tailor the properties through the selection of suitable compounds and geometries. The present thesis aims to improve current knowledge of the mechanical behaviour of rubber joints and of the seismic performance of infilled frames equipped with them. For this purpose, both numerical and experimental studies have been carried out. With regards to the numerical work, a novel computational modelling strategy has been developed using ABAQUS to investigate the in-plane behaviour of RC frames with infill walls and rubber joints. The proposed approach employs three-dimensional solid finite elements to simulate the concrete components, 3D beam elements for the reinforcing bars, and a meso-scale approach for the infill wall with rubber joint. The results of the application of the numerical strategy shed light on the effectiveness of the rubber in minimizing the in-plane seismic damage to the bricks, by localizing the deformation mostly in the rubber joints and reducing the overall stiffness of the infilled system. They also provide some insight into the effect of the rubber joints' layout and stiffness on the behaviour and capacity of the system and its components. In particular, it is shown that, using vertical rubber joints with low stiffness in addition to the horizontal ones further improves the behaviour in terms of reduction of compressive stresses and cracking in the masonry at large displacements. Even the plastic deformations in the frame can be reduced by using vertical joints with low stiffness.

Detailed numerical analyses involving micro and meso-scale descriptions of masonry can accurately simulate the behaviour of the system at hand, but they can be computationally expensive and unsuitable for the analysis of large-scale structures. On the other hand, the use of simplified macro-models, characterised by a reduced number of degrees of freedom and parameters that are required to define them, would enable the analysis of larger scale structural systems. In this thesis, a novel two-dimensional macro-element model has been proposed for describing the in-plane behaviour of RC infilled frames with flexible or sliding joints, which is an extension of a discrete 2-D macro-element previously developed for the case of traditional infill panels. The proposed modelling approach, implemented in OpenSees, is calibrated and validated against quasi-static tests from the previous literature, carried out on masonry-infilled RC frames with sliding and rubber joints. The study results show the capabilities of the proposed modelling approach to evaluate the benefits of using flexible joints in terms of minimising the negative effects of the interaction between infill and RC frame. The addition of the sliding/flexible joints enhances the energy dissipation capabilities with more stable and larger hysteresis loops under cyclic loading. However, it has been observed that for a given level of drift demand, the internal forces in the columns of the RC frame with infill and rubber joints have similar maximum values, if not inferior to those of the bare frame, with the exception of the axial and shear force in the windward column. The maximum absolute values of the internal forces in the case of infill with rubber joints are lower than the corresponding values obtained in the system with traditional infill.

Although past tests have characterised the behaviour of multi-layer flexible joints, no in-depth investigation has been carried out to date on the hysteretic and dissipative behaviour of mortar-rubber joints. In order to fill this gap, a series of experimental tests were conducted at the University of Strathclyde to characterise the mechanical behaviour of the various components of the rubber-masonry triplets as well as the behaviour of the composite system, with particular focus on the cyclic shear response and the bond strength. The hysteretic responses of the triplets obtained from the experiments are simulated using a finite element micro-modelling strategy using Abaqus. The mortar-rubber joints exhibit an equivalent damping ratio value of the order of 20% or more which is much higher than that of the rubber compound (of the order of 6%). This is due to the frictional mechanism activated at the interface between the rubber joints and the mortar, enhanced by the presence of pins in the surface of the rubber joints. The bond between the rubber layers and the mortar layers was found to be the weakest component of the composite system. While the failure

of this bond reduces the stiffening effect of the infills and increases even further the damping capabilities of the joints due to the activation of the frictional mechanism, it may be not desirable because it may result in residual deformations and a weakening of the infill panel in the out-of-plane direction. The study results are useful for informing the development of future models for the design and analysis of rubber joints, and for the selection of the most suitable rubber compound and layer geometrical properties.

Key Words: Masonry Infill, Sliding-Joint, Rubber-Joints, Finite Element Analysis, Masonry Triplets, Monotonic Shear, Cyclic Shear, Hysteretic Behaviour.

List of Figures

List of Tables

Symbols

A_p	cross-section area tributary volume of the subpanel
b_p	width of the subpanel
$b_w t_w$	nominal cross-section area
c	cohesion
c_j	cohesion at the joint
C_{i0}	material parameters
d_{cm}	ultimate displacement in compression
d_{tm}	ultimate tensile displacement
d_n	normal deformations of the 2D links
d_s	tangential deformations of the 2D links
d_d	diagonal spring elongation
d_{2d}	yielding displacement
d_{3d}	peak-force displacement
d_{4d}	residual-force displacement
D_k, D_r	damage indexes
E	young's modulus
E_{mon}	ultimate cumulative energy
E_{cum}	cumulative energy at the current step of the analysis
f_{cm}	compression strengths of masonry
f_{tm}	tensile strengths of masonry
f_{rm}	residual compressive strength of the masonry
f_{cj}	compressive strength of the joint
F_{rm}	residual compressive force
F_d	diagonal spring force
F_{1d}	cracking force of the masonry panel
F_{2d}	yielding force

F_{3d}	peak force
F_{4d}	residual force
F_n	internal panel forces in normal direction
F_s	internal panel forces in shear direction
F_c	maximum compressive force
F_t	maximum tensile force
F_R	the residual compressive strength
F_{cm}	maximum compressive force of the masonry panel
F_{tm}	maximum tensile force of the masonry panel
γ_{cr}	diagonal shear drift of the masonry panel
G_f^I	mode-I fracture energy
G_f^{II}	mode-II fracture energy
G_{eff}	secant shear modulus of the rubber
G_r	shear modulus of the rubber joint
h_p	panel width of the macro-element
I_1	first invariant of strain tensor
IP_c	in-plane capacity
IP_d	in-plane demand
OP	out-of-plane capacity
OP_d	out-of-plane demand
k_n	normal stiffness
$k_{n,s,t}^{mr}$	stiffness of the mortar-rubber joint in the normal and shear directions
$k_{s,t}$	in-plane stiffness along two orthogonal shear directions
k_{nj}	initial normal stiffness per unit area of the joint
k_s^m	in-plane (s) shear stiffness of the mortar joint
k_s^r	in-plane (s) shear stiffness of the rubber joint
k_n^m	normal stiffness of the mortar joint
k_n^r	normal stiffness of the rubber joint

k_t^m	out-of-plane (t) shear stiffness of the mortar joint
k_t^r	out-of-plane (t) shear stiffness of the rubber joint
k_{tj}	tensile strength of the joint
K_s	shear stiffness of the 2D link
K_n	tangent stiffnesses of the link in the normal directions
K_{nm}	normal stiffness of the contact link
K_{sj}	stiffness of the joint
K_{d_0}	initial stiffness of the masonry panel
K_{n0}	initial elastic stiffness
K_{nj}	normal stiffness of the joint
l	length between the two supports
l_p	length of the tributary volume of the subpanel associated with the link
R_f	failure load
S	shape factor
t_r	thickness of the rubber joint
t_m	thickness of mortar joint
V_i	vertexes of the macro-element
w_p	thickness of the subpanel
W	strain energy
τ_0	peak force
γ_0	peak shear drift
τ_r	residual force
γ_r	residual shear drift
τ	peak shear strength
γ_y	yield shear drift
τ_y	yielding sterss
$\lambda_B - 1$	nominal creep strain
α	angle between the diagonal and the first edge of the panel
μ	coefficient of friction

σ_c	compressive strength,
τ_{cr}	cracking stress
ξ_{eq}	damping ratio
σ_B	effective stress.
ϕ	friction angle
$\dot{\varepsilon}$	effective creep strain rate
τ	nominal shear stress
Δ_i	length of rigid offsets
$\tau_{s,t}^{\max}$	maximum shear stresses along two orthogonal shear directions
n_i	nodes of the of the macro-element
σ	nominal tensile stress
σ_n	normal strength
σ_t	tensile strength
ν	poison's ratio
σ_p	shear strength
$\tau_{s,t}$	shear stresses along two orthogonal shear directions
ζ_{eq}	equivalent damping ratio
μ_j	friction coefficient of the joint
γ	nominal shear strain
λ	ratio of unloading stiffness and the initial stiffness
ε_{cu}	ultimate strains in compression
ε_{tu}	ultimate strains in tension
u_i, v_i	translations of nodes of the macro-element
ϕ_i	rotations of nodes of the macro-element
ε	nominal tensile strain

Abbreviations

2D	Two dimensional
3D	Three dimensional
AAC	Autoclaved aerated concrete
B31	3D 2-node linear beam element in space.
BBM	Bottom beam-masonry
BF	Bare frame
BF_CY	Bare frame tested for cyclic loading
BF_MO	Bare frame tested for monotonic loading
C3D20R	3D 20-node quadratic element with reduced integration.
C3D8R	8-node linear element with reduced integration and hourglass control.
CDP	Concrete damage plasticity
CLC	Cellular lightweight concrete
CM	Column-masonry
CoV	Coefficient of Variation
DMEM	Discrete macro-element method
DRES	Damage reduction enclosure system
FC. MJ	Plain masonry fully infilled frame
FE	Finite element
FEAP	Finite element analysis program
HDNR	High-damping natural rubber
IDA	Incremental dynamic analysis
IFSJ	Infilled frame with sliding joints
IFSJ_CY	Infilled frame with sliding joints tested for cyclic loading
IFSJ_MO	Infilled frame with sliding joints tested for monotonic loading

INSYSME	INnovative SYStems for earthquake-resistant Masonry Enclosures
J3.LB	Lateral boards and three joints
OpenSees	Open System for earthquake engineering simulation
PPH	Panel-panel interface in horizontal direction
PPV	Panel-panel interface in vertical direction
RAM	Random access memory
RC	Reinforced concrete
RJ_H	Rubber joint with horizontal joint
RJ_HV	Rubber joint with horizontal and vertical joint
RJ_HVH	Rubber joint with high stiffness vertical rubber
RJ_HVL	Rubber joint with low stiffness vertical rubber
SIWIS	Seismic infill wall isolator sub frame
SJ	Sliding joints
$SP_{\_1,2,3,4}$	Sub-panels numbered from bottom to top
TARRC	Tun abdul razak research centre
TBM	Top beam-masonry
TIF	Frame with traditional infills
TIF_CY	Traditional infilled frame tested for cyclic loading
TIF_MO	Traditional infilled frame tested for monotonic loading
URM	Unreinforced masonry

1 Introduction

1.1 Problem statement

Enclosures along the perimeter of building constructions are needed to form a separation between the internal space and the external environment. Infill walls represent the most traditional enclosure system for reinforced concrete (RC) building frame structures in many countries worldwide, exhibiting a reasonable performance and durability against fire, noise, moisture and temperature hazard (Santos 2006 2014; Vicente et al. 2010, 2012; Silva et al. 2016, 2019; Martins et al. 2017).

Infill walls have the unique static function to bear their own weight. However, they are also subjected to other type of loadings, such as wind loading and earthquake-induced loadings. Seismic events throughout the world (Duzce (Turkey 1999), L'Aquila (Italy 2009), Lorca (Spain 2011), Christchurch (New Zealand 2011), Emilia Romagna (Italy 2012). 2015 Nepal earthquake (Nepal 2015), Sulawesi earthquake and tsunami (Indonesia 2018), Haiti earthquake (Haiti 2021) have shown the high vulnerability associated with the masonry infills in RC building frames. This is because the masonry infills are treated as non-structural components and often ignored in the design calculations.

A significant number of numerical and experimental studies and post-earthquake reconnaissance reports have analysed and discussed the importance of infills in the seismic performance of RC framed buildings (Di Trapani et al. 2015). An irregular distribution in plan and/or elevation of infills can also trigger torsional responses in the building and undesired collapse mechanisms (Karami and Ahmadi 2021). Moreover, infill walls interact significantly with the RC frame members surrounding them, inducing local failures. The failure experiences in the walls can be characterised by sudden reduction of resistance, accompanied by severe damage, partial collapse or disintegration.

Infill wall damage can cause injuries or even casualties, even under moderate earthquakes that not able to induce structural collapse. The direct and indirect losses associated to infill wall damage can be significant, with some studies (Villaverde 1997; Filiatrault and Sullivan 2014; Cardone and Perrone 2017; Del Vecchio et al. 2018; De Risi et al. 2019) showing the cost of repair for masonry infills can be significantly higher than the structural components. This problem of infill walls has been known for decades. For example, 34 years ago (Rojahn et al.

1988) RC framed buildings with unreinforced masonry infill were assigned the worst "Basic Structural Hazard" score and studies (Boussabah and Brunea 1992; Bruneau 1994; Bothara et al. 2010) also have shown the low performance of URM infills even under moderate earthquakes. However, damage of masonry infills continues to be recorded even in the more recent constructions (Hermanns et al. 2012). This highlights the need of improved infill construction techniques and design approaches for these components.

An EU-funded project, INnovative SYStems for earthquake-resistant Masonry Enclosures in reinforced concrete buildings (INSYSME 2016), was run in 2016-2021 with the principal objective of identifying and developing optimised new masonry enclosure solutions for enhanced earthquake resistance, respecting local materials and construction practice, and providing clear design rules, so that the proposed systems could be used effectively. Among the various technical solutions proposed within the project for this purpose, one of the most promising one involved the use of rubber joints within the panel and between the panel and the frame (Figure 1.1).

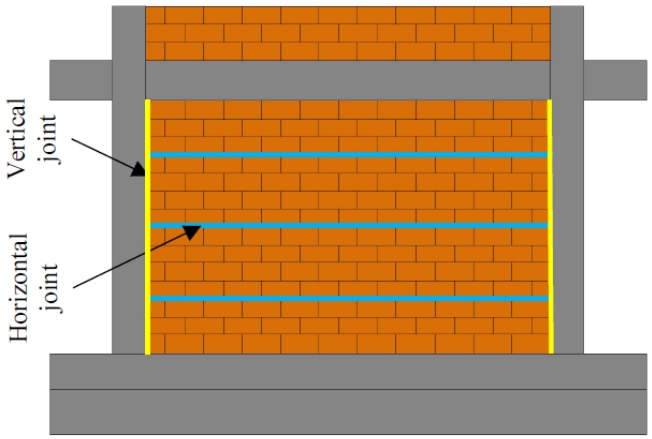

Figure 1.1. Masonry infilled walls with horizontal and vertical joints.

The effectiveness of the rubber joints was tested by in-plane and out-of-plane quasi-static tests carried out at the University of Padova (Verlato 2017) on an infilled RC frame with and without rubber joints. The tests demonstrated the "proof of concept" of the technology and showed that the introduction of the rubber joints considerably reduces the masonry infill damage and provides a satisfactory out-of-plane performance in terms of stiffness and strength. Moreover, they showed that the rubber joints may contribute to increase the energy dissipation capabilities of the system, although this potential contribution was not investigated in depth. However, these tests demonstrated only the "proof of concept" of the rubber joint technology, and they were not accompanied by the development of modelling strategies that could be

employed for designing the joints and/or evaluating the complex performance of infilled RC frames with added rubber joints. Thus, further numerical and experimental analyses are needed to advance the technology and develop it further, so that rubber joints can be effectively employed in RC frame construction practice to protect infill walls and enhance the performance of infilled systems.

1.2 Aims and objectives

This thesis aims to further advance the knowledge of the behaviour of rubber joints and of masonry-infilled RC frames equipped with them. In particular, the main objectives of the study are

- To conduct an extensive literature study on the available techniques on infill protection and highlight their merits and limitations.
- To develop a numerical modelling strategy for the assessment of RC frames with masonry infill and rubber joints under in-plane loading.
- To develop simplified models suitable for investigating large scale structural systems with infills and flexible/sliding joints.
- To characterise the cyclic performance of masonry walls with rubber joints, both experimentally and numerically.

1.3 Thesis outline

The thesis is structured as follows. This Chapter provides a general overview of the motivations and objectives of the research. Chapter 2 contains an extensive review of the current state-of-the-art of modelling strategies available for infill safety.

Chapter 3 presents a meso-scale modelling strategy using Abaqus to investigate the performance of infilled RC frames with the introduction of rubber joints against in-plane loading. Validation studies are carried out against two past experimental campaigns considering the cases of RC infilled frame with traditional infill as well as infill with rubber joints. The study results show that the proposed modelling strategy is capable to accurately describe the main features of the response of RC frames with masonry infills and rubber joints: the minimisation of the in-plane damage of the infill thanks to the localisation of deformations in the rubber joints, and the significant reduction of the overall stiffness of the infilled system.

Chapter 4 proposes a two-dimensional discrete macro-element model for describing the in-plane behaviour of RC infilled frames with flexible or sliding joints. The proposed modelling approach, implemented in OpenSees, is an extension of a discrete macro-element previously developed for the case of traditional infill panels. The study results show the capabilities of the proposed modelling approach, allowing to describe the behaviour of RC frames with masonry infills and rubber joint at a fraction of the computational cost required by the meso-scale approach.

Chapter 5 presents the outcomes of an extensive experimental campaign and of numerical analyses aimed at characterising the cyclic shear behaviour of masonry triplets with mortar-rubber joints under both monotonic and cyclic loading. The hysteretic responses of the triplets obtained from the experiments are simulated using a micro-modelling strategy developed in Abaqus. The study results are useful for informing modelling strategies for the design and analysis of rubber joints, and for the selection of the most suitable mechanical and geometrical properties of these seismic protection devices.

Chapter 6 summarises the major findings of this doctoral dissertation, discusses the outcome of the research project and outlines future research work.

1.4 List of publications

The following is the full list of peer reviewed journal papers, conference papers and reports that resulted and/or are related with this content of this thesis.

1 Dhir, P.K., Tubaldi, E., Ahmadi, H. and Gough, J., 2021. Numerical modelling of reinforced concrete frames with masonry infills and rubber joints. *Engineering Structures*, 246, p.112833. Chapter 3 is based on this article.

2 Dhir, P.K., Tubaldi, E., Panto, B. and Calio, I., 2022. A macro-model for describing the in-plane seismic response of masonry-infilled frames with sliding/flexible joints. *Earthquake Engineering & Structural Dynamics.* Chapter 4 is based on this article.

3 Dhir, P., Tubaldi, E., Orfeo, A. and Ahmadi, H., 2022. Cyclic shear behaviour of masonry triplets with rubber joints. *Construction and Building Materials.* Chapter 5 is based on this article.

4 Dhir, P. K., Tubaldi, E., Ahmadi. H., and Gough, J. Modelling of masonry infill walls with rubber joints. In SECED 2019 Conference: Earthquake Risk and Engineering towards a

Resilient World. 9-10 September 2019, Greenwich, London. Chapter 3 is based on this article.

5 Dhir, P. K., Tubaldi, E. Introduction of rubber joints within traditional masonry infill walls: A numerical modelling approach, 1st Doctoral School Multidisciplinary Symposium (DSMS19), the University of Strathclyde, Glasgow, UK, 19 June 2019, ISBN: 978-1-909522-53-4. Chapter 3 is based on this article.

6 Tubaldi, E., Dhir, P. K., & Orfeo, A. (2021). Optimal design of rubber joints for seismic protection of masonry-infilled frame structures. *A report from a project funded by a 2019 EEFIT Research Grant winner.* Available at: https://www.istructe.org/resources/report/optimal-design-of-rubber-joints-for-seismic-protec/. Chapter 3,4, and 5 are based on this report.

2 Literature Review

2.1 Introduction

Masonry infill walls used as enclosure in RC or steel frame structures are in some way an evolution of traditional masonry whose main function is to delimit the architectural space and to thermally and acoustically insulate buildings rather than to carry any load (Santos 2006 2014; Vicente et al. 2010, 2012; Dias et al. 2014; Tran et al. 2014; Silva et al. 2016, 2019; Martins et al. 2017). RC and steel framed structures use masonry infills, which are very usual around the world. Although, investigating the response of infilled frame has become an interest of researchers and engineers since last 40 years (Moghaddam and Dowling 1987), the interest has increased significantly in recent years (Kaushik et al. 2006; Asteris et al. 2013) only.

The state of the art of masonry infill construction and modelling presented in this chapter by drawing the outcomes from the existing literature. In Section 2.2, an overview of infill construction techniques throughout the world is provided. Section 2.3 describes the seismic performance and failure modes of infill walls under different types of loading. Section 2.4 describes the various numerical methods developed for RC infilled frames, whereas the analytical solutions available for capacity assessment are detailed in Section 2.5. The techniques developed for improving the seismic performance of infill walls are presented in Section 2.6, followed by a summary of the chapter.

2.2 Overview of masonry infill construction techniques

Masonry infills can be classified based on the construction topology, and the properties of the masonry bricks and blocks. These are reviewed and analysed in the following subsections.

2.2.1 Construction typology

Masonry infills can be classified based on the construction topology, the material properties of the masonry components (bricks and mortar), and their geometry.

- *Single leaf masonry* (Figure 2.1a). The simplest type of wall, where the wall thickness is the thickness of the masonry unit.
- *Double leaf masonry* (Figure 2.1b). Two parallel leaves joined together either by mortar or tie arrangements.
- *Cavity wall* (Figure 2.1c). Two parallel single-leaf walls separated by a hollow space. This space can be unfilled, filled, or partially filled with non-loadbearing thermal insulating material. The two walls could be tied together with wall ties.
- *Veneer walls* (Figure 2.1d). They consist of one leaf confined in the reinforced concrete frame and of an external leaf (veneer). The internal leaf interacts with the structure, whereas the external one protects the building from penetration of moisture.

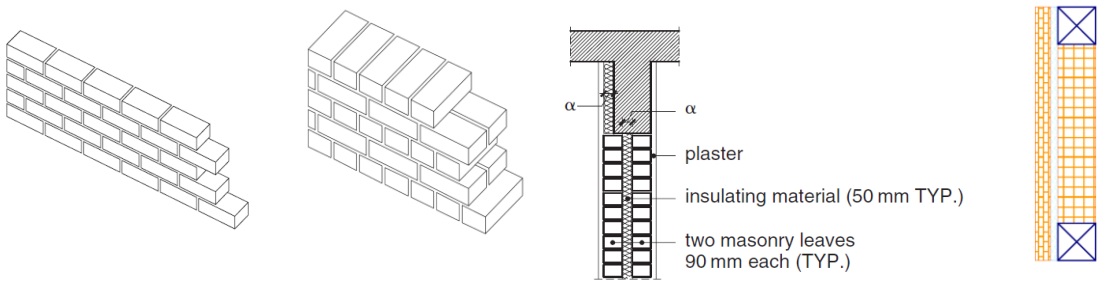

(a) (b) (c) (d)

Figure 2.1. Construction typology of popular masonry walls. Figure taken from Santos (2006) and INSYSME project (INSYSME 2015).

2.2.2 Brick/block typology

The masonry bricks/blocks can be made of burnt (fired) clay (Figure 2.2a,b), unburnt (i.e., unfired) clay (Figure 2.2c), Fly-ash clay (Figure 2.2d), Fly ash-lime-gypsum (Figure 2.2e), Autoclaved Aerated Concrete (Figure 2.2f), Cellular light-weight concrete (Figure 2.2g) and aggregate concrete (Figure 2.2h, Figure 2.2i). Stone can also be used in some situations.

a) Solid fired clay bricks

b) Fired hollow clay bricks

a) Unburnt solid clay (Adobe) Bricks

d) Fly ash clay bricks

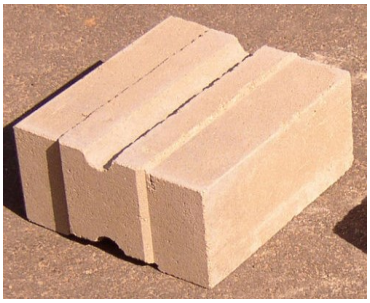

e) Fly ash-lime-gypsum brick

f) Autoclaved Aerated Concrete (AAC) blocks

g) Cellular light concrete (CLC) blocks

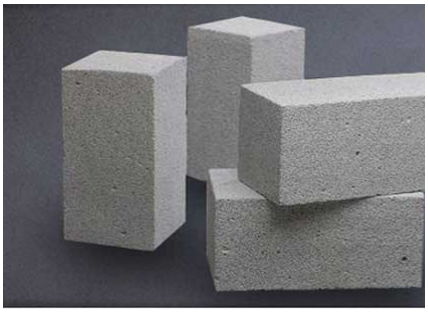

h) Solid Concrete bricks

i) Hollow concrete blocks

Figure 2.2. Types of bricks used for masonry infill wall construction.

Solid fired clay bricks were widely used in the past in many countries such as Italy, but they were then replaced with hollow fired clay bricks. Nowadays, solid masonry units are the most used in the construction of external veneers (INSYSME 2016).

The adobe infill walls exhibit low strength and stiffness causing larger deformation capacity and lower in-plane resistance in lateral directions. This provides good thermal-hygrometric performances during hot weather. It is getting attentions due to its contributions towards sustainable building construction (Preti et al. 2012).

Fly ash brick masonry exhibits weaker, more flexible, and more deformable behaviour under compression in comparison with burnt clay brick masonry (Basha and Kaushik 2016). Moreover, the use of fly ash bricks is limited in the countries like India due to its lower density, higher water absorption and porosity as compared to that of burnt clay bricks.

Autoclaved Aerated Concrete (AAC) is prepared from a mixture of cement, lime, sand and that expands with the addition of aluminium powder (Penna et al. 2008). The reaction between the concrete and the aluminium forms microscopic hydrogen bubbles expanding the concrete to about five times its original volume. This product is a non-toxic and air-tight material having fine cellular structure and a high strength/weight ratio. No hazardous solid waste or air pollutant is released during its manufacturing process. The use of lightweight AAC significantly reduces imposed dead load on the system causing reduced seismic inertia forces. It also shows additional properties like non-combustible and fire-resisting nature that makes it popular in the construction industry.

Cellular lightweight concrete (CLC) having low strength and low density is used as partition walls, thermal insulation material on roofing systems and also as infill in RC and steel frames buildings. Functional properties like low density, thermal insulation and good acoustic insulation makes it a viable alternative against conventional clay brick masonry (Rasheed and Prakash 2018).

The dimensions of brick or block units can vary from case to case. Moreover, units can be classified based on the extent of voids (void ratio).

- *Massive blocks* (Figure 2.3a). This typology is mostly used for structural masonry to form load-bearing walls or eternal veneers rather than infill walls.
- *Hollow blocks with vertical perforations* (Figure 2.3b). Typical values of the void ratio range from 25% to 65%.
- *Hollow blocks with horizontal perforations* (Figure 2.3c).

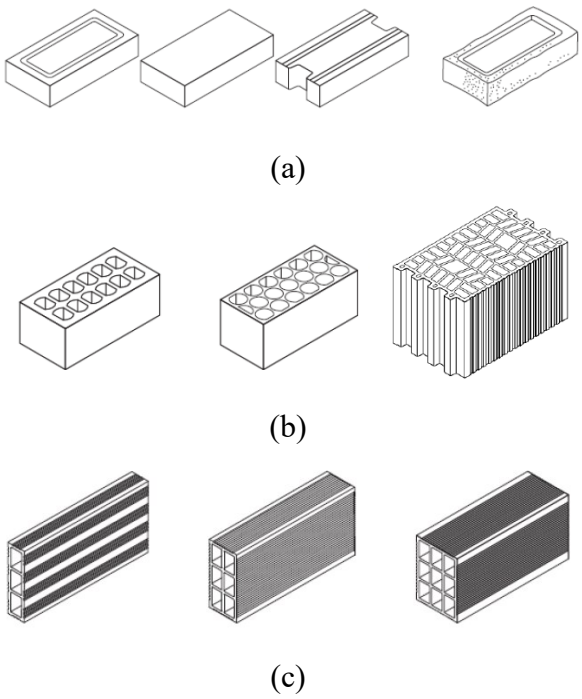

Figure 2.3. Types of blocks used in masonry infill constructions as per their shapes.

The mortar used to lay bricks and blocks is usually composed of a water, sand, and binder (lime or cement) in variable proportions (e.g., 1:1.5:5). It is usually classified according to its compressive strength (usually M2.5 to M10 according to Eurocode 6). The horizontal mortar joints have a thickness between 5 mm and 15 mm. The vertical joints between bricks and blocks can also be conventional mortar joint with a thickness of 5 mm to 15 mm or can be dry joints (INSYSME 2016).

2.2.3 Typical masonry infills in seismic countries

In this subsection, the most diffused typologies of infill walls in seismic countries in Europe and worldwide are reviewed:

Europe: A report from INSYSME project (INSYSME 2016) provides a very exhaustive review of the construction typologies of masonry infill walls in Europe. In most parts of Europe, single leaf and cavity walls are used except for Portugal where veneer walls are more common. Again, the characterisation of enclosure wall systems in Europe is based on the masonry properties like material properties, existence, and orientation of holes, the shape of the holes, the existence of interlocking, etc.

According to the INSYSME project (INSYSME 2016), In Italy, single-leaf walls are mostly used for RC framed buildings. Other alternatives are double leaf and cavity walls.

Greece uses single-leaf walls and cavity walls. In Romania, single-leaf walls are the most common ones. Single leaf and cavity walls are the common types in Turkey. Hollow clay tile and gas–concrete masonry infill walls are widely used in the Kokaeli epicentral region (Sezen et al. 2003) where single and double-leaf walls are very frequent. Similarly, single leaf and cavity walls are mostly used in Germany.

In Italy, other than fired clay, aggregate concrete (dense and lightweight), and autoclaved aerated concrete are also quite popular in Italy, Romania, Turkey, and Germany. Aggregate concrete is the only type used in Portugal and Greece. Although the use of stone masonry is quite uncommon in Europe, Greece reports some use of stone walls as decorative materials. Lastly, another material rarely employed for the masonry units is calcium silicate, with Germany being the only one to mention its use.

Considering the direction of the holes in the masonry block, Italy mostly uses masonry units with vertical holes for either single leaf or cavity walls. In Greece, masonry units with horizontal holes and vertical holes are the two mainly used types of bricks for the construction of cavity walls and partition walls. Single leaf and partition walls with vertical holes are the common types in Romania. In Portugal, masonry units with horizontal holes are the most common types and used for cavity walls and partitions whereas masonry units with vertical holes and solid bricks are rare. Units with horizontal holes are mostly used in Turkey for the construction of single leaf, cavity walls, or partitions walls. The use of masonry unit with vertical holes are rare. Lastly, the situation is a bit opposite in Germany. The most used masonry unit types are with vertical holes or are solid units. Units with horizontal holes are rare to find.

Interlocking bricks aren't that common in Europe. Only in Italy, Germany, and Portugal vertical interlocking units are used for the construction of internal leaf and partition walls. In Romania, horizontal interlocking units are used for partition walls and veneers, but recourse to this type of interlocking is rare.

With reference to the characterisation of the mortars used in enclosures systems in Europe, in Italy the most used mortar is of class M2.5, and more rarely M5. Mortar joints have a thickness in the range between 5- 15 mm. In the case of the vertical joints, the two most used options, are ordinary joints, with a thickness of 5 to 15 mm, or dry joints. The Greek case is similar to the Italian, with some differences in the class of mortar. In Greece, M4 and M10 classes are the most employed, with the use of lime instead/or in addition to

cement. In Romania, M1; M2.5; M5, and M10 mortars are used. Germany mostly uses M5 class mortars for general joints, and M10 class in the case of thin layer joints.

India and Nepal: cladding and partition walls are usually constructed using concrete blocks, clay brick, or stone masonry, with solid clay bricks and cement mortar being the most diffused materials (Dizhur et al. 2016; Rai et al. 2016). Solid bricks with a double-leaf arrangement (alternative disposition) are used for exterior walls (Varum et al. 2017). These types of infills are very stiff and provide a significant increase in global stiffness (Brando et al. 2015).

Pakistan: burnt clay bricks are the most used infill elements (Khan and Raza 2015). The thickness of brick infills is 230mm for external walls and 115 mm for the internal or partition walls. Concrete solid and hollow blocks are also being increasingly used as infill materials, and their thickness varies from 150 to 200 mm. Brick prisms consisting of solid brick units, commonly employed for masonry infill wall construction in Pakistan, were tested by Ali et al. (2017). Brick prisms, made of solid units of size 225 × 110 × 260 mm^3 each, laid with mortar joints 10 to 12 mm thick, were tested under compression. The average compressive strength obtained was 5 MPa.

Iran: Solid bricks (25cm thick) were used for the infill walls in Bam Telephone Center, whose performance during Bam Earthquake was analysed by Hossein and Toshimi 2004). Hollow bricks were also used for the partitions. Damage to masonry infill walls made with hollow clay brick has been reported following the Ezgeleh earthquake (DRES 2017). Thin unreinforced hollow or solid brick walls are the most diffused typology in Iran (Sherafati and Sohrabi 2016).

Jordan: RC structures are widely used in Jordan, with the exterior infill walls composed usually of three layers; stone facing, plain concrete, and hollow concrete blocks. The total thickness ranges from 300 to 350 mm. The walls are bounded by slender RC columns. For the partition walls inside the building, hollow concrete blocks of thickness ≈100mm are used (Alwashali and Maeda 2013).

China: Masonry walls are built with shale hollow bricks, concrete hollow bricks, aerated concrete blocks, or fly ash bricks (Feng et al. 2014). Solid bricks are also employed (Cai and Su 2019). In Zhai et al. (2016), concrete hollow block units with dimensions 190 × 190 × 390 mm^3 were utilised to build masonry infill walls to be tested in the lab. These

units are typical in infill construction in China. Recently, aerated, and hollow concrete blocks are the most common types of masonry used in China (Huang et al. 2016).

2.3 Seismic performance of infill walls

The performance of infills subjected to in-plane and out-of-plane loads is discussed in this section.

2.3.1 In-plane behaviour

Several experimental and numerical investigations (Mehrabi et al. 1996; Mehrabi and Shing 1997; Al-Chaar et al. 2002; Shing and Mehrabi 2002; Stylianidis 2012; Anić et al. 2021) have been performed which have shed light on the effect of different geometrical and mechanical parameters of the infill and the frame on the response and collapse modes. Studies (Paulay and Priestley 1992; Crisafulli 1997; El-Dakhakhni et al. 2003) have identified four main failure modes of the infill panel shown in Figure 2.4:

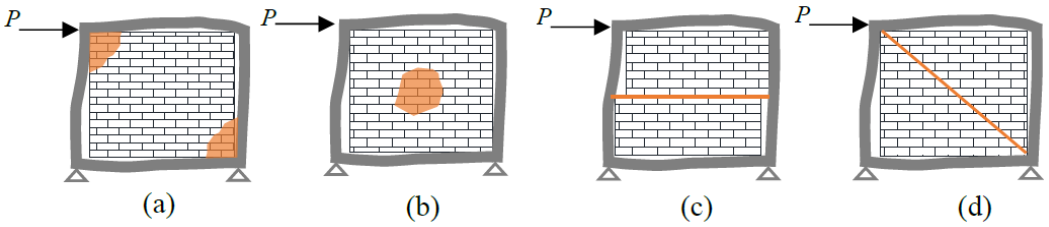

Figure 2.4. Compression failure at (a) corners (b) centre of the infill (c) shear failure at the centre of the infill along a mortar joint, (d) diagonal tensile failure (El-Dakhakhni et al. 2003).

Additionally, the infilled frame may fail due to the formation of plastic hinges in the beams and columns or in the beam-column joints due to increased bending and shear forces caused by the interaction with the masonry infills (Liauw and Kwan 1984a, 1984b; Mehrabi and Shing 1997; Milanesi et al. 2018). This mode is characteristic of weak frames equipped with strong infills. The formation of a gap between the frame and infill may not be called a failure but this influences the performance of the system.

The occurrence of various modes of failure is dependent on the frame geometry, infill thickness, and the material properties of both infill and the frame. As observed by (El-Dakhakhni et al. 2003), compression failure occurred in the corner regions and the sliding shear at the bed joints are the most significant ones. The diagonal cracking is not regarded

as a failure mode since after cracking, the resistance of the infill and of the infilled frame continues to increase.

2.3.2 Out-of-plane behaviour

The bending in the out-of-plane direction of masonry infill panels is induced by the inertia forces acting on the panels as well as the differential motion of floors. Several studies have investigated the behaviour of infills against the out-of-plane load. Figure 2.5a show one of the failure modes where the entire panel tilt out of the frame due to gaps or weak connections of the panel to the surrounding frame. Other failure modes can be individuated depending on the type of boundary conditions. Mode of failures for infill supported at two sides (horizontal direction, vertical direction) and all four sides are shown in Figure 2.5 (b-d).

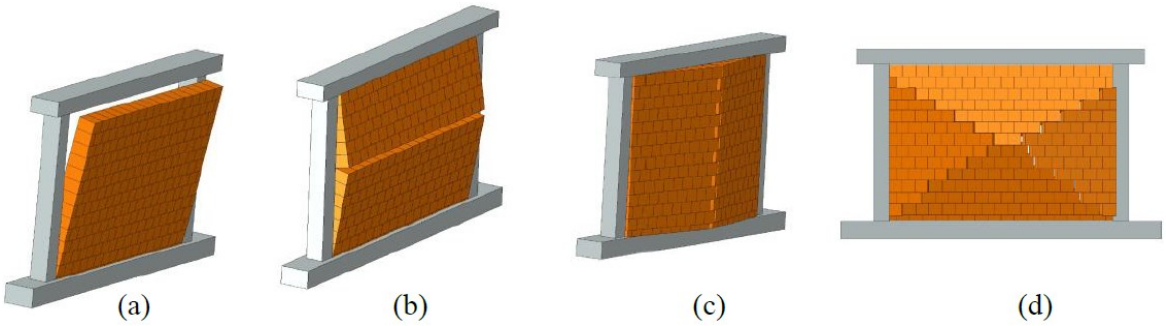

Figure 2.5. Failure modes of infill against out-of-plane load (Kubalski et al. 2017)

During a seismic event, the failure of infill in the out-of-plane direction can be caused by the following three factors:

- previously acting or already existing in-plane load.
- inertia forces developed by earthquakes.
- relative displacements between top and bottom levels of wall.

This subsection focuses on the studies assuming no infill damage has occurred previously. It is also noteworthy that the out-of-plane capacity of the infill can be largely reduced by the previous in-plane damage that weakens the connection between infill joints and frame (Manfredi and Masi 2014) or by the shrinkage of the mortar.

As observed by Dawe and Seah (1989), the out-of-plane behaviour can be categorised into four stages based on the application of load as well as the selected drift limit. In the initial phase, until the generation of the first crack, a linear elastic behaviour is

observed. The second phase characterises the formation and propagation of initial cracks. The third phase demonstrated the arching effect initiation, and the final phase continues with the crushing of the masonry, and it ends when the collapse load is attained.

The out-of-plane action of infill is greatly influenced by the infill-frame interaction. When the infill is fully connected with the frame, an arching mechanism can be observed. This arching effect is dependent on factors like wall compressive strength, thickness of wall, dimensions of the panel and most importantly the boundary condition of infill-frame interaction surface (Figure 2.6). This arching action significantly increases the out-of-plane resistance of the masonry infill (Braga et al. 2011).

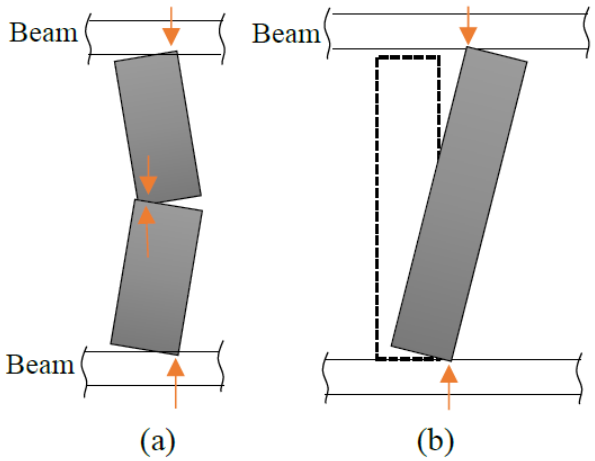

Figure 2.6. Mechanism showing (a) arching action (b) rigid-body effect of infill wall.

Asteris et al. (2017) performed an extensive study on the existing capacity models available for out-of-plane actions and the typical crack patterns developed during the experimental campaigns against out-of-plane load. This study confirms the performance of the masonry infilled frame in both horizontal and vertical directions based on the stiffness of the infill-frame stiffness. Again, the failure in the masonry infill may be caused when it reaches its peak compressive strength, or the surrounding frame is incapable of providing the desired confinement.

2.3.3 Behaviour of infill under sequential loading

Paulay and Priestley (1992) first observed the significant influence of in-plane stresses on the out-of-plane resistance of the infill. The in-plane behaviour is responsible for the reduction in the out-of-plane resistance due to the decrease in stiffness at the infill-frame

interaction surfaces. Again, the gaps formed between the frame and masonry panel are quite common and may be caused either by in-plane stress or due to the shrinkage also responsible for influencing the resistance to out-of-plane loading.

L'Aquila earthquake in 2009 demonstrated that most of the out-of-plane overturning collapses occurred in the lower storeys (Braga et al. 2011). This can be explained by the fact that the overturning effects caused by the out-of-plane action are exacerbated by the in-plane deformation, which develops an infill-top beam detachment (Hanounet al. 2017). A typical X-pattern crack can be formed weakening the infill and making the structure more vulnerable. Other researchers (Al-Chaar et al. 2002; Morandi et al. 2013; Donà et al. 2017; Asteris et al. 2017; DiTrapani et al. 2018) have also observed that prior in-plane damage may be responsible for influencing the collapse of infills against out-of-plane loading.

The combined in-plane and out-of-plane behavior of infill at various levels of out-of-plane pressure were studied by Kuang and Yuen (2010) and the significant influence of the secondary moment generated by the diagonal compressive force on the out-of-plane deformation was observed. Recently, several studies were carried out (Yuen and Kuang 2013, 2014, 2015; Yuen et al. 2016) on modeling of masonry infilled RC frames against bi-directional loading and highlighted the importance of interaction effects against the in-plane and out- of-plane load.

A simplified macro-model developed by Furtado et al. (2014, 2015) considered the out-of-plane response as well as in-plane and out-of-plane interaction of infill. OpenSees, was used to study the combined influence of in-plane and out-of-plane loads on infill. Incremental Dynamic Analysis (IDA) was performed responses evaluated considering separately the in-plane and out-of-plane loading and the one where in-plane and out-of-plane loading are considered together were significant.

Longo et al. (2016) performed a numerical study considering the macro-model developed by Mosalam and Günay (2015) and implemented in OpenSees (McKenna et al. 2010). This model calibrated the previous experimental tests (Calvi and Bolognini 2001; Da Porto et al. 2013) under bi-directional ground acceleration confirming Eurocode 8 (EN 1998-1 2004). The analysis outcomes demonstrate that, until the first cracks occur in the panels due to in-plane loading, negligible out-of-plane displacement was observed. However, the formation of the first crack increases the out-of-plane displacement

significantly. The numerical results were found to be consistent with the damage that occurred to the buildings in recent seismic events.

2.3.4 Behaviour of infills with openings

Infills with openings (e.g., doors, windows) are often disregarded in numerical models of infilled frames, by assuming that their contribution to the lateral stiffness and strength is negligible compared to that of infills with no openings. However, this is not always the case. Nevertheless, it is important to study the interaction between infills with openings and the surrounding frame and how the openings affect the strength of the infills under in-plane and out-of-plane loading.

Fiorato et al. (1970) and Mallick and Garg (1971) found an 85-90% reduction of lateral stiffness and a 75% reduction of lateral strength due to the presence of openings. Studies (Liauw 1972; Dawe and Seah 1989), have shown that infilled frames with more than 50% infill panel opening area may possess almost the same stiffness as of bare frame. Again, the presence of door openings, especially the central doors lower the initial stiffness of the system. Kakaletsis and Karayannis (2009) stated that the presence of door openings is more vulnerable than the window openings. Mansouri et al. (2011) studied on various shapes, sizes, and locations of openings (windows and doors) and found that the openings are responsible for a significant reduction in the strength, ductility, and stiffness of the infilled frame system.

In the experimental test carried out by Zhai et al. (2016), the central window opening was found to be responsible for the reduction of lateral strength and stiffness and resulted in the improved global performance of the infill as compared to the case of solid infill wall. Similarly, a full-scale RC infilled frame with a door opening was tested by Tu et al. (2016) under cyclic loading and it was observed that, with the addition of loading, the frame and panel start to separate.

Drougkas et al. (2021) developed a method based on analytical modelling for the prediction of the damage initiation mode and capacity of stand-alone masonry piers against in-plane loading. The model for walls with openings can be applied to simple buildings however can likewise be reached out to additional intricate designs with straightforward alterations.

2.4 Numerical modelling of masonry infill

The need to understand and simulate the infill response has motivated the development of numerical and analytical models for the last four decades (Moghaddam and Dowling 1987). Experimental tests are expensive and time-consuming, whereas the numerical models are economical and efficient once validated while investigating the influence of parameters in a problem. Various approaches, with different degree of complexity, are available for modelling masonry infills. These are briefly presented here, and then described more in detail in the next sections.

Micro-modelling: This approach involves accurately modelling the masonry units, the mortar, the mortar-unit interface as well as masonry-frame interface. Figure 2.7 (a) shows that the masonry unit and the mortar joints are considered as continuum elements whereas the interface between the unit and mortar are considered as discontinues. The high nonlinearity associated with the masonry including the mortar and bricks make it challenging to model the infill wall behaviour. Although the micro-modelling approach is computationally expensive, it is the most accurate in predicting the infill wall behaviour.

Meso-scale modelling (Simplified Micro-modelling): Due the large computational cost involved with the micro-modelling; global analysis of infilled frames becomes impractical. The micro-modelling approach can be simplified by merging the mortar joint and the interface in to a zero-thickness element (Figure 2.7b). Thus, the dimensions of the units are extended by half of the thickness of mortar joint at all of its sides and interface element was assigned between the mortar and contact surface. This approach is potentially less accurate than the micro-modelling one, but it is more efficient in terms of computational cost.

Smeared homogeneous modelling approach: This method considers the masonry unit, mortar and the brick-mortar interfaces as a homogeneous part (Figure 2.7c), which is assigned one single material. Masonry is considered as a homogeneous unit with anisotropic properties. This approach can be very useful for investigating large walls or multi-span multi-storey frames without an impractical computational cost.

Macro-modelling approach: This considers the global behaviour of infilled framed system and ignores the local failures occurring in the masonry panel shown by diagonal structs (Figure 2.7d). Due to its simplicity and easy applicability, macro-modelling is of great interest for engineers and designers.

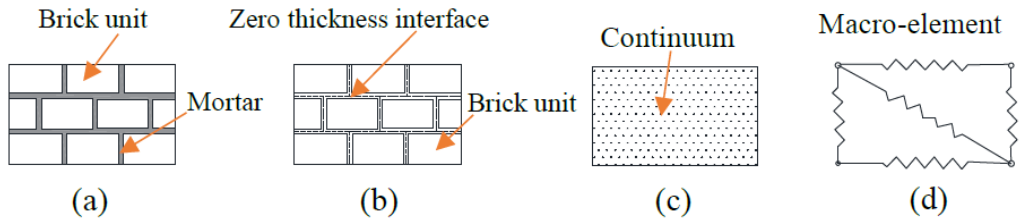

Figure 2.7. (a) Micro-modelling (b) meso-scale modelling (c) smeared homogeneous modelling (d) macro-modelling approaches for masonry infill (Lourenço 1997).

Different approaches are also available for describing the behaviour of the frame surrounding the infill and the interaction between the infill and the frame elements. For example, the frame can be modelled using beam element or more complex three-dimensional elements. These approaches are not analysed further in the next subsections, which focus on the masonry infill modelling.

2.4.1 Micro-modelling

Micro-modelling of infills entails the full representation of units, mortar, and the units-mortar and infill-frame interfaces, with the geometrical and mechanical properties of each constituent individually taken into account. Although this modelling approach provides a realistic prediction of local and global failure modes of masonry infill walls, its use is restricted by its high computational cost, which makes it impossible to apply it to investigate large-scale structures.

The first attempt to study the behaviour of infill using the finite element method (FEM) was made by Mallick and Severn (1967) where special attention was given to model the frame-infill interaction. Page (1978) and Rots (1991) used continuum elements to model the masonry units and interface elements for mortar joints.

An elastic interface model was developed by Lourenço and Rots (1997) combining the plasticity for compression, tension, and shear. This model was further expanded by Oliveira and Lourenço (2004) by incorporating nonlinear unloading/reloading behaviour to describe the response under cyclic loading. On the other side, instead of using interface elements for defining the infill-frame interaction, Asteris (2003) developed a step-by-step strategy that used the concept of contact length and a separation criterion.

The combination of smeared and discrete crack approaches to visualise the various failure modes infilled frame system was proposed by Stavridis (2009) and Stavridis and

Shing (2010). Both the frame and the masonry units were modelled using a smeared-crack element. Interface elements were assigned to the mortar element and also to the middle of the bricks to capture the formation of crack within it. Koutromanos et al. (2011) expanded the modelling strategy by introducing a smeared-crack model that also allows the consideration of cyclic behaviour with cohesive crack elements. A detailed 3-D modelling approach was proposed by D'Altri et al. (2018) to investigate the in-plane and out-of-plane response of the masonry panel. This This novel approach can be fully characterised by the properties obtained on small-scale experimental tests on brick and mortar and on small masonry assemblages.

2.4.2 Meso-modelling

The meso-scale approach (Lourenço and Rots 1997; Lourenço 1997; Dolatshahi and Aref 2011; Macorini and Izzuddin 2011, 2013, 2014; Nasiri and Liu 2017) uses a zero-thickness interface to simulate the behaviour of the mortar joints. This approach provides an accurate description of the development of cracks in the bricks and at the mortar interfaces. Compared to macro-modelling approaches it allows for a better evaluation of the effects of the on the in-plane behaviour of the infill and frame. Sarhosis et al. (2014) developed a computational model using the Discrete Element Method (DEM) and the software UDEC to investigate the behaviour of masonry infilled steel frames with openings and their interactions subjected to in-plane monotonic loading. It was found that the inclusion of multiple openings significantly reduces the strength and stiffness of the system. In particular, placing an opening close to the point of application of the lateral load will result in further reduction of masonry infill's stiffness.

Expanded units, representing the brick units plus half mortar joint thickness per side (Figure 2.8a), are modelled as a series of continuum elements and the interaction between the expanded units along the bed and head joints is modelled through surface-to-surface contact behaviour (Dhir et al. 2021). The initial response of the cohesive interfaces is linear elastic, followed by a cracking behaviour that describes the most critical failure modes of masonry joints, namely, tensile cracking and shear sliding. The inelastic behaviour of the masonry units is also considered in a simplified way by employing the concrete damage plasticity (CDP) model. Each brick unit is modelled with 16 8-noded elements (C3D8R) as shown in Figure 2.8b.

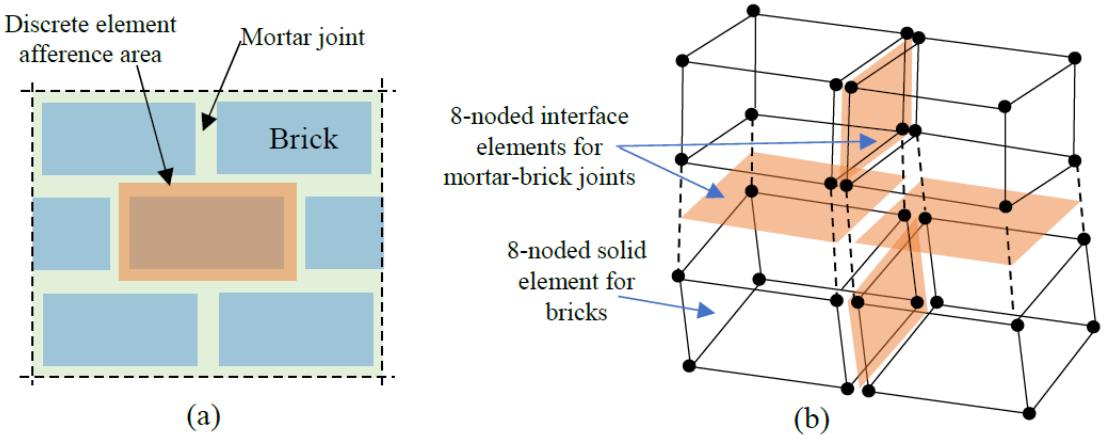

Figure 2.8. (a) Masonry portion describing meso-scale model for masonry components (b) element model for brick units (Dhir et al. 2021).

It is noteworthy that the interfaces cannot fail under compressive loads, but failure in compression of masonry can be taken indirectly into account through the CDP model employed for the bricks. Further details about the interface model can be found in Abdulla et al. (2017).

Lemos and Sarhosis (2022) proposed a detailed meso-scale modelling approach based on the discrete element method, considering the nonlinear behaviour of the joints and the units. The failure of units is addressed by the bonded-block concept, in which a random network of potential cracks is made, allowing progressive collapse mechanisms. Uniaxial compression tests are dissected exhaustively. The re-enactment of a remarkable investigation of a block board under shear shows the great exhibition of the proposed approach. The examination results exhibit the model's capacities and guidelines for its application.

2.4.3 Smeared homogeneous models

In this method, the masonry is considered as anisotropic or orthotropic homogeneous equivalent material in which the mechanical characteristic of units and mortar are smeared over the infill domain. Dhanasekar and Page (1986) performed a parametric study that has shown that it resulted that the load-displacement response, ultimate strength, and failure modes are greatly influenced by the tensile and shear strengths of masonry infill.

A smeared FE model was proposed by Lotfi, and Shing (1991) based on the plasticity theory of brittle materials, isotropic properties of uncracked infill, and orthotropic

property of cracked infill. But this approach fails to provide a realistic representation of the brittle-shear response of the masonry infill. Lourenço (1997) used a continuum model combining the anisotropic and plastic behaviour by considering the Hill-type yield criteria in compression and Rankine-type criterion in tension.

Again, a smeared crack model was used by Mosalam et al. (1997) for a homogeneous and continuum material obtained from a homogenisation process to simulate the experimental test performed on the infilled frame system. Asteris (2003) used anisotropic materials for analysing the performance of infilled frames with openings where infill-frame interaction was considered in compression zones only. More recently, Mohyeddin et al. (2013) proposed a homogeneous 3D discrete FE model for analysing the performance study of masonry walls. Similar studies (Pela et al. 2013; Milani and Bertolesi 2017) have also been proposed to analyse the infill performance using homogenisation theory.

2.4.4 Macro-modelling

Different approaches have been proposed in the last decades that fall into the category of macro-modelling approaches. Among these, the "equivalent strut" is found to be the most popular approach. However, other approaches have also been proposed by several researchers to study the infill wall behaviour. Sachanski (1960) proposed an FE approach for analysing the infilled frame. This approach was further updated by Barua and Mallick (1977) with that allows the consideration of infill-frame gap and also the effect of slip. A FE approach was proposed by Dawe and Charalambous (1983) that employed beam and membrane elements for describing the frame and infill respectively. Rigid links were considered to model the interface between the frame and the infill.

2.4.4.1 Strut approach

The reduced computational simplicity and efficiency in the analyses make the diagonal struct approach attractive for engineers and researchers. Polyakov (1960) studied the behaviour of infill by replacing it with one or few beam elements. Several models have been proposed over the last years aiming at improving the modelling schemes and estimate the important mechanical properties of infill like stiffness, strength, failure mechanism, and hysteresis response.

Holmes (1961) first introduced the concept of equivalent diagonal strut. As shown in Figure 2.9, the infill wall acts as diagonal compression struct of same thickness and

young's modulus equal to 1/3rd of the diagonal length. Smith and Carter (1970) statistically estimated the lateral stiffness of the infilled system. Later, Liauw and Kwan (1984a) confirmed that, under lateral load, the stresses developed at the tensile corners are quite low and bracing action is effective only in diagonal region.

Paulay and Priestley (1992) also used diagonal bracings connected by pins to the frame elements to represent the infill wall. Then, Saneinejad and Hobbs (1995) performed an experimental study followed by a nonlinear finite element analysis and observed that the infill system can be represented with pin-jointed diagonal struts (equivalent) with significant accuracy if the mechanical properties are known correctly.

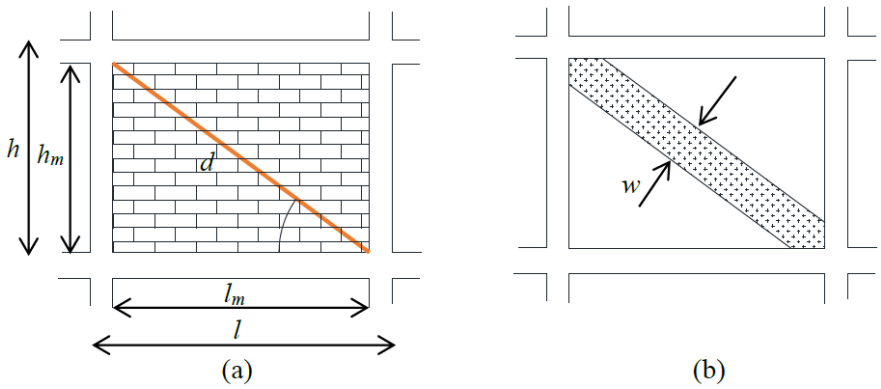

Figure 2.9. Infill with (a) diagonal strut in compression (b) equivalent strut (Liberatore and Mollaioli 2015).

Many simplified models for masonry infilled frames rely on the concept of equivalent single (or multiple) struts (Smith and Carter 1970; El-Dakhakhni et al. 2003; Di Trapani et al. 2018). Al-chaar (2002) proposed a strut model where pins are eccentrically connected to the columns at a distance from the face of the beam. Although the equivalent diagonal strut models are efficient in predicting the global stiffness of the infilled frame, still, analysing the model with just one diagonal strut element can't provide enough justice to the results while considering shear force and bending moment diagrams along the length of the column due to the influence of infill. Asteris (2008) reported the ineffectiveness of this approach in capturing the complex response of infilled frames. Figure 2.10a shows five parallel compressive struts employed in each direction (Syrmakezis and Vratsanou 1986) that is capable of predicting the influence of contact length between the infill and frame on moment distribution capacity.

A series of cyclic tests were conducted by Zarnic and Tomazevic (1988) a model was proposed where equivalent compression structs were used that are not associated with the node connecting the upper beam and the column (Figure 2.10b). Schmidt (1989) proposed a model with increased number of struts with offsets at both the ends (see Figure 2.10c). Chrysostomou (1991) and Chrysostomou et al. (2002) used a strut model with one diagonal and two off diagonal compressive struts arrange parallelly in each direction (Figure 2.10d). The off-diagonal struts are placed at the critical locations (position of the formation of a plastic hinge) along the frame members.

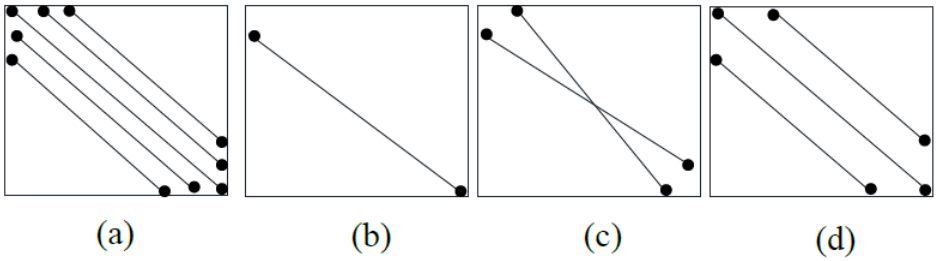

Figure 2.10. Macro-models with various structs and orientations (Sattar 2013).

The strut models presented above have suffered could not predict the horizontal shear sliding in a direct way rather, indirectly estimated the relation between shear and diagonal force. So, there was a need to improve the equivalent strut modelling to further level. Crisafulli and Carr (2007) developed an improved model (Figure 2.11) with four nodded panels connected to the frame at beam-column joints. This model considers the panel element from Crisafulli (1997) that consists of a shear spring and two parallel struts and in each direction. Still, it suffered from the limitation that, the shear force and the bending moments in the surrounding frames couldn't be correctly predicted.

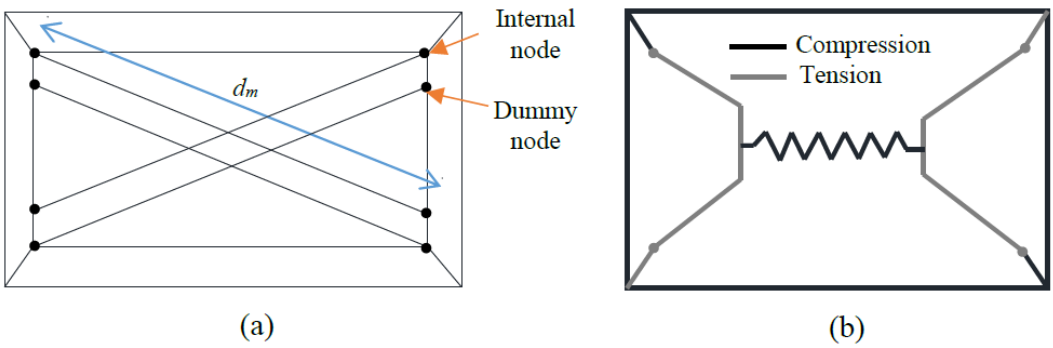

Figure 2.11. (a) Compression/tension structs (b) shear spring (Crisafulli and Carr 2007).

Rodrigues et al. (2010) modelled each masonry panel represented by four rigid struts and a central shear element. This approach was further improved by Furtado et al. (2015) that investigates the in-plane and out-of-plane interactions of the infilled frame. The limitations associated with the model were the load-displacement relationship of the masonry wall must have been known in advance of modelling and it couldn't capture the failure of infill with openings.

Cavaleri et al. 2017 assessed the seismic performance of the RC school building by involving concentric equivalent struts for modelling infills. The qualities of the new methodology, first time applied to a real case. The improved assessment of the extra shear demand delivered by infills only for the base columns is adequate to caution that a simplified model ignoring infills or considering the use of concentric struts for the infills may extensively overestimate the structural capacity.

2.4.4.2 Macro-elements

More recently, macro-models with improved capabilities with respect to the equivalent strut models have been introduced. Figure 2.12a presents a single strut model at each diagonal and multilinear plastic link elements and rigid link elements near to beam-column connections (Cavaleri and Di Trapani 2014). In the same year, the more complex model was proposed by Caliò and Pantò (2014) that considers infill-frame interface elements, and the in-plane nonlinear masonry response was captured by the equivalent discrete quadrilateral elements of four edges connected by four hinges and two diagonal nonlinear springs. This model showed significant accuracy and was later improved by Panto et al. (2017) to study the out-of-plane performance.

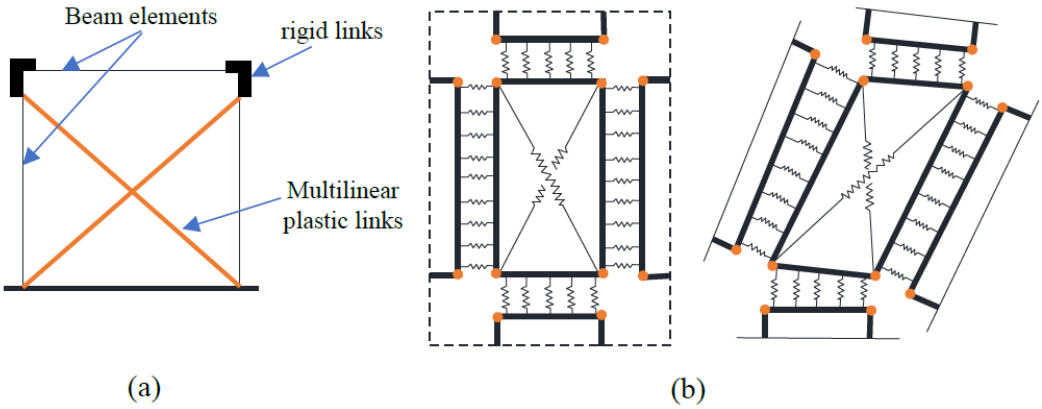

Figure 2.12. Macro-models proposed by (a) Cavaleri and Di Trapani (2014) and (b) Caliò and Pantò (2014).

Mosalam and Günay (2015) introduced a model in OpenSees capable of removing the macro-element representing an infill panel when it exceeds the interaction curve. It suffered from a limitation of not accounting for the arching action of the masonry wall. This limitation was eliminated by Donà et al. (2017) by considering two similar equivalent struts but with half of the resistance. Asteris et al. (2017) developed a 2-D equivalent strut model of nonlinear fiber-section elements where concrete-type constitutive law was assigned to the diagonal elements. Although this model could account for the arching mechanism, the potential local shear failure of columns due to the local increase of shear forces couldn't be predicted. This approach was further developed by Di Trapani et al. (2018) by defining a four-strut macro-element that can account for both in and out-of-plane resistance.

Anic et al. (2021) investigated the contribution of openings inside the infill walls that are confined by an RC frame and subjected to seismic events in both in-plane and out-of-plane directions. It was seen that the micro-models were sensitive and insensitive toward several parameters, in regard to the model's way of performance and computational stability. The in-plane behaviour of infilled frames was found to be greatly influenced by the interface material model.

2.5 Infill wall capacity models

This section summarizes the discussions from different authors for evaluating the capacity of infill walls under in-plane loading, out-of-plane loading, and combined loading.

2.5.1 In-plane capacity

Holmes (1963) proposed a semi-empirical method based on the experimental test results to study the infilled frame behavior against vertical and horizontal loading. Wood (1978) predicted the failure load of the infilled frame using plastic analysis whereas Liauw and Kwan (1983, 1984b, 1985) considered the effect of infill-frame interaction and proposed analytical expressions to calculate the peak shear force. Four types of failure mechanisms were proposed that allowed to analyze the multi-storey infilled frames using simplified techniques. Mehrabi and Shing (1994) considered five failure mechanisms and proposed equations that can calculate the resistance force of the system. Despite of the usefulness of these approaches, the approaches are limited in use as they considered limited h/l ratios, geometries, infilling brick types, etc. Therefore, there are not used much in practice.

2.5.2 Out-of-plane capacity

Although earthquakes are dynamic forces, during analysis, it's a common practice to use equivalent static forces while analyzing the buildings. Therefore, while estimating the out-of-plane capacity of masonry infill, the maximum uniform lateral pressure responsible for the failure of the infill panel is usually taken into consideration.

The initially proposed methods for analyzing the infill walls against out-of-plane loads were based on elastic model approaches (Lawrence 1979). As the elastic model overestimate the stiffness of the system, several studies (Hendry 1973; Hendry and Kheir 1976; Drysdale and Essawy 1988) were conducted that consider two-way action by using yield line analysis. The major limitation associated with this approach was, flexural or tensile strength is considered as the governing parameter, but this is significant only until the cracking of the masonry.

Studies (Anderson 1984; Dawe and Seah 1989) in their experimental campaign found that, after the initiation of crack, the wall tries to deform and leading the generation of in-plane membrane forces occur in the wall as shown in (Figure 2.13a). The infill panel exhibiting predominant resisting mechanism is due to the arching action (Flanagan and Bennett 1999) and the expression on arching action was developed by McDowell et al. (1956, 1957). This is referred as a one-way arching considering masonry compressive strength instead of tensile strength.

It was observed that, when there is a good connection between the infill wall and the frame along all the sides, two-way action should be considered. Dawe and Seah (1989) carried out an extensive experimental test program steel infilled frames with hollow concrete blocks and the influence of support conditions and the presence of openings was studied. Empirical relationships were developed that consider the two-way arc mechanism when the bending panel occurs.

Angel et al. (1994) and Shapiro et al. (1994) added few more improvements to the existing models by introducing simplified expressions for predicting the out-of-plane strength based not just on the compressive strength of masonry and the slenderness ratio, but also on the amount of in-plane damage, and the stiffness of the bounding frame. Al-chaar (2002) added few extra features like consideration of openings to the model developed by Angel et al. (1994) and Shapiro et al. (1994).

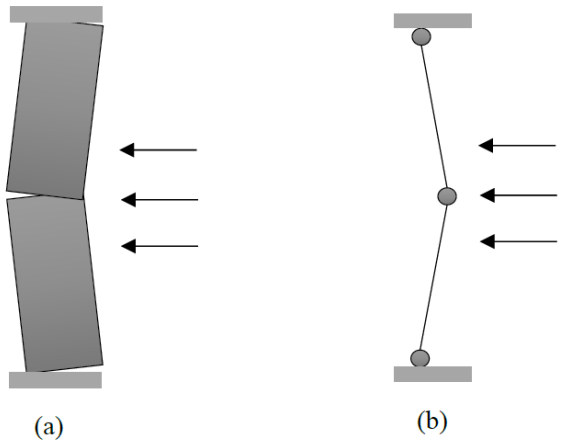

Figure 2.13. Development of (a) arching action (b) three-pin arch against out-of-plane loading (Asteris et al. 2017).

Flanagan and Bennett (1999) associated the experimental outcome from studies (Anderson 1976; Dawe and Seah 1989; Fricke et al. 1992; Angel et al. 1994; Flanagan and Bennett 1999) with the analytical equations proposed by Dawe and Seah (1989) and Angel et al. (1994). It was concluded that the empirical expressions suggested by Dawe and Seah (1989) should be the basis of the evaluation of the out-of-plain strength of infill walls.

Morandi et al. (2013) followed Eurocode 8 (EN 1998-1 2004) to predict the out-of-plane demand pressure acting on infill walls under seismic excitations and proposed an expression to determine lateral pressure resistance. Marinkovic (2018) in his study

mentioned that expression developed for predicting the lateral pressure resistance mayn't be appropriate as the wall could have been previously damaged by the in-plane loading.

Anic et al 2020 investigated the out-of-plane performance of masonry infilled frames and assessed the influence of bi-directional loads, openings, slenderness, boundary conditions, etc. It was found that arching action fosters extra compressive strengths that resist the traversal ones. Models have shown dispersed results among themselves and the outcomes from the experiments. with trial information. Likewise, the governing factors, impacts of the frame, its boundary conditions, and other parameters were found.

Anic et al 2021 performed an experimental investigation to examine the cyclic, out-of-plane performance of RC infilled frames, using non-contact optical techniques. It was found that neither the infill walls nor the openings altogether influenced the overall behaviour of the specimens. In any case, the infill walls experienced considerable damage within 1.25-2.50% inter-story drift, which represents an endanger to life and jobs. Moreover, it was found that masonry walls containing openings, sustained further damage, particularly those with eccentrically positioned openings compared with the fully infilled frames.

2.5.3 Simultaneous in- and out-of-plane loading

Al-chaar (2002) suggested that the influence of out-of-plane loading cannot be ignored while analyzing the in-plane strength a masonry infilled system and vice versa. He proposed a formulation that considers the simultaneous effect of in-plane and out-of-plane loading with a condition that, the in-plane capacity should not be reduced when the out-of-plane demand is less than or equal to 20% of the out-of-plane capacity.

$$\frac{IP_d}{IP_c} = 1 + \frac{1}{4}\frac{OP_d}{OP_c} - \frac{5}{4}\left(\frac{OP_d}{OP_c}\right)^2 \qquad \text{Eq. 2.1}$$

where IP_d is the in-plane capacity considering out-of-plane loading, IP_d is the in-plane capacity of infilled frames using pushover analyses, OP_d is the out-of-plane demand placed on the infilled frame and OP_c is the out-of-plane capacity.

Anic et al 2021b proposed a 3D micro-model for the assessment of the vulnerability of masonry-infilled RC frames. The contributions of openings inside the infill walls subjected to both in-plane and out-of-plane loads were investigated. It was found that, even inside the similar material model, some parameters had more effects when attributed to

concrete rather than to masonry. The in-plane behaviour was largely influenced by the interface materials whereas the out-of-plane behaviour was governed by the tensile strength of both the interface and masonry material model.

Pradhan et al 2021a investigated the out-of-plane behaviour of infill walls based on various influencing parameters. Further experimental campaigns have been recognized and suggested. An empirical equation was proposed by Pradhan et al 2021b for the assessment of the infilled frame's OOP capacity, with or without IP damage. The OOP strength was greatly affected by compressive strength, slenderness ratio, aspect ratio, and IP damage. The proposed equations give reliable predictions of the OOP limit, by firmly showing the suitability of the adopted macro-element model in estimating the OOP performance of URM infills.

2.6 Solutions for improving the performance of infill walls

As described in the previous sections, several experiments have been performed and numerical models have been developed to understand the seismic behavior of infill walls and their effect on the performance of infilled RC frames. At the same time, various solutions for improving the behavior and capacity of infill walls are proposed. These are categorized, depending on the degree of frame-infill interactions (Figure 2.14).

The first approach aims to make the infill stronger while ensuring a rigid connection to the frame (Figure 2.14a). The second approach aims to increase the flexibility of the infill wall and/or of the connection between the infill wall and the frame through alternative techniques (Figure 2.14b). The third approach aims to detach the infill the frame so that the frame can deflect independently from the infill, without transmitting any force to it (Figure 2.14c).

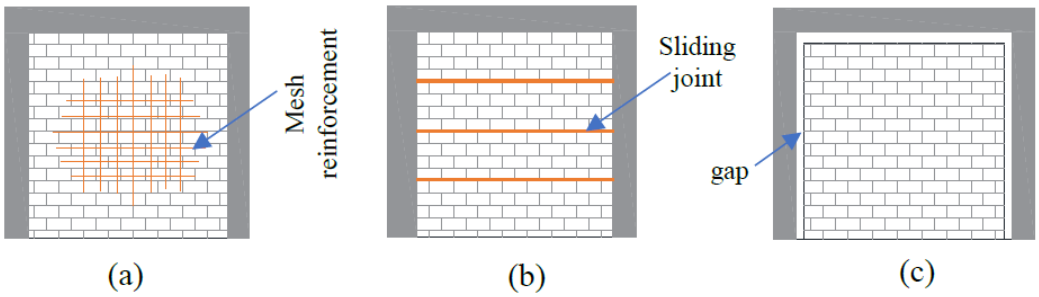

Figure 2.14. Alternative approaches with (a) mesh reinforcements, (b) sliding joints, and (c) gaps for improving the behaviour of infilled frames under earthquake loading.

Despite the availability of alternative construction techniques, in most of newly built RC frames the masonry infills are rigidly attached to the frame. Various solutions available till date on infill safety are discussed in the following subsections.

2.6.1 Strengthening of infill walls rigidly attached to the frame

Several techniques are available for increasing the strength of infill walls rigidly attached to frames. For example, Braga et al. (2011) proposed to add extra reinforced concrete elements in the middle of the walls, connected to the columns, with the aim of reducing the slenderness of the wall and stabilizing the infill panels. Nevertheless, the costs for the implementation of this technique are high. Moretti et al (2014) proposed the idea of connecting the wall with the surrounding frame with dowels. Alternatively, an additional layer of mortar can be added to the outer surfaces of the infill wall which can also be a quite time-consuming and expensive technique (Prawel and Reinhorn 1985; Mander and Nair 1994; El-Dakhakhni 2002; Korkmaz et al. 2010; Kyriakides 2011; Ozkaynak et al. 2014; Valluzzi et al. 2014; da Porto et al. 2015; Akhoundi et al. 2018;) can also be used.

Reinforcing is popularly used as a solution for strengthening the masonry walls. A study by Brokken and Bertero (1981) has shown a significant increase in the resistance force as well as an improvement in the infill stiffness as well as the energy dissipation capacity. Dawe and Seah (1989) observed that the joint reinforcement in the infill panel has a minor contribution towards the ultimate load capacity. Whereas Hendry and Liauw (1994) have shown the benefits of horizontal joint reinforcements in decreasing the formation of infill crack. Crisafulli (1997) proposed an interesting reinforcement detailing where diagonal reinforcements were introduced at the beam-column joints as well as the upper corners of

the infill. This arrangement improved the resistance by about 110% as compared to the traditional reinforcing approach.

The benefits of introducing reinforcements in bed mortar joints and the external plaster were studied by Calvi and Bolognini (2001) where the out-of-plane damage was investigated as a function of previous in-plane damage considering with and without reinforcement conditions. In particular, the reinforcing mesh caused the increase in the collapse resistance in both in-plane and out-of-plane directions.

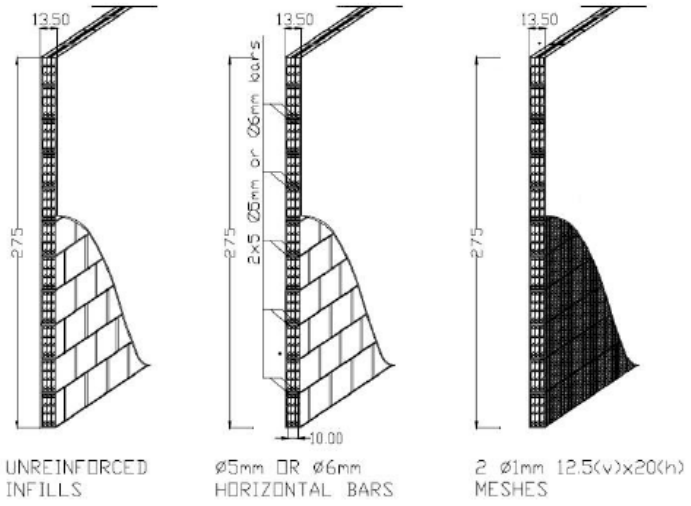

Figure 2.15. Specimens tested by Calvi and Bolognini (2001)

Similar studies (Da Porto et al. 2013; Vintzileou 2014; Silva et al. 2016; Vintzileou et al. 2016) also have demonstrated the reduction of the global damage of infill due to the presence of embedded reinforcement due to the increase of in-plane drift. Although a large number of techniques are available for retrofitting URM, some of them are complex and their applicability needs the consideration of the presence of infill while preparing the design, which is very complicated due to the complex behavior of infill walls. Again, a proper design of the critical section was needed as the stiffened infill wall influence the fundamental frequency of vibration of the system leading to increased structural demand.

2.6.2 Decoupling systems

This aim to allow the frame to deform independently from the infill. In this way, the infills don't influence the infilled system performance. Having a gap (Figure 2.16) between the infill and the frames are the simplest way of separating them. However, this is vulnerable against out-of-plane load and there is a need for strengthening of non-structural components.

The benefit of such a system is its implementation hardly alters the design of structural members. Significant developments have been experienced only in the last few years where the insertion of highly deformable materials or introduction of sliding joints can lead to the expected in-plane frame-infill detachment without significant lowering in the out-of-plane resistance.

Figure 2.16. Introduction of gaps in the infilled frame system (Aliaari and Memari 2005).

As mentioned earlier, the decoupling approach originated from the concept of preventing the wall during in-plane deflections of the frame and therefore to make it an actual non-structural element. Initial attempts were made by considering the infilled frame. This may be either due to the formation of shrinkage cracks/poor connection or purposely presented to enhance the infill wall performance.

Riddington (1984) investigated the influence of top and side gap width on the performance of infilled systems. The presence of the top gap was responsible for a slight decrease in the initial stiffness, whereas a considerable reduction was observed when the side gaps are introduced. In the case of frames with both top and side gaps, the development of moments in the columns and beams are close to the ones of a bare frame for the same drift level. Viscoelastic or similar material can be introduced to overcome the problem caused by the presence of unintentional gaps.

Liauw and Kwan (1984b,1985) compared to the case with no gap, and the studies discussed so far considered a gap smaller than 2mm that usually appear due to workmanship or shrinkage. Valiasis and Stylianidis (1989) tested RC frames with infills not connected to

the surrounding members, showing that at small lateral drifts the infill does not increase the strength of the structure. However, at higher drifts, the strength was increased up to 50% compared to the bare frame case. Dawe and Seah (1989) showed that a 20 mm gap at the top between the infill and frame results in a 50% reduction in the stiffness as compared to the bare frame and a reduction of the ultimate strength of 60%. Flanagan (1994) showed that a gap of 1inch (=2.54 cm) between the columns and the infill does not cause any further lowering of ultimate load, which was however attained for a higher drift level.

Aliaari and Memari (2005, 2006) investigated the "Seismic infill wall isolator subframe" (SIWIS). This isolator system was designed in such a way that, after reaching the load limit it fails and behaves like the bare frame. This allows the infill wall to contribute towards the in-plane stiffness of the system at lower drift levels and protect the infill by isolating it from the frame. Although the fuse mechanism could manage to isolate the infill wall from the frame preventing the infill damage, the fuses are designed to yield in case of a seismic event, and thus replacing them is costly and time-consuming. Aliaari and Memari (2006) form experimental tests found that the SIWIS added a very brittle nature to the global behavior which was undesirable, and the system was not convincing for practical applications. Charleson (2012) pointed out the problem of a short column which can appear in the case of masonry infills extending for a portion of the column height which is in rigid contact with the columns.

In the action of out-of-plane forces, the vulnerability of the wall increases by separating the infill for in-plane movement. To prevent the out-of-plane failure, Charleson (2012) suggested two solutions where the first approach considers the infill wall was built as a cantilever wall at its base. The limitations associated with these solutions were, the first one needed L-shaped steel to be used which increased the cost and made the plastering process difficult. The shortcoming associated with the second method was this can't be used for hollow bricks and the gap between the beam and infill causes acoustics and fire protection like issues.

Kuang and Wang (2014) suggested an air gap between the columns and the masonry (Figure 2.17) where steel connectors were placed in the bed joints connecting to columns to prevent the failure against the out-of-plane failure. Although the test results demonstrated the effectiveness of the airgap in isolating the infill from the surrounding frame, the connections are costly, time-consuming and thermal isolations of the air gaps also need extra efforts. Again, the steel connectors present at the bed joints may cause damage to the infill

as it tries to restrain the system in the in-plane direction. Similar issues were studied by Jiang et al. (2015), who investigated the behavior of infilled RC frame with a presence of 20mm horizontal (at top beam-masonry interaction) and vertical gap (at column masonry interaction) between the infill and frame. polystyrene plates were introduced between the gaps and the steel ties introduced in the column and bed joints caused significant protection in the in-plane direction leading to the formation of early damage in the infill.

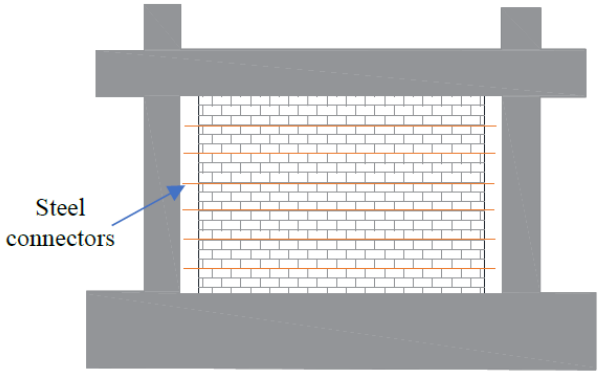

Figure 2.17. Isolated masonry infill with steel connectors (Kuang and Wang 2014).

Tasligedik (2014) and Tasligedik and Pampanin (2017) proposed solutions for improving the infilled frame performance by dividing the infill vertically into three parts which enabled the individual rocking of the panel instead of single shear dominated infill wall. The introduction of gaps between the subpanels causes a delay in the formation of a strut. Again, the infill panes confined into a steel subframe further attached to the structural frame provide a considerable restraining resistance against the out-of-plane action. Still, this technique is found to be expensive and complicated to implement. Tsantilis and Triantafillou (2018) investigated the response of infilled frame system both experimentally where the infill panels were isolated by the introduction of thin layered cellular materials. Furtado et al. (2016) suggested the decoupling of infills as a good solution for reducing wall damage and improving the performance of infilled frames.

To conclude this section, the decoupling solutions summarized here are very promising, although they have been used rarely in practice. Further developments are needed in order to ensure adequate performance under both in-plane and out-of-plane loading.

2.6.3 Hybrid systems

A combination of multiple approaches for the seismic protection of infill called as hybrid system was recently introduced in USA developed for concrete masonry surrounded by steel frames (Biggs 2007; Abrams and Biggs 2012). Type I, Type II and Type III hybrid walls were developed as shown in Figure 2.18. Type-I consists of gaps between the top beam and masonry as well as the masonry and the columns. Type-II has gap at the masonry-column interface only whereas the Type-III has gap only at top beam- masonry interface. These systems if the masonry is damaged the gravity load can be transferred to the frame through the adjacent columns and vice versa.

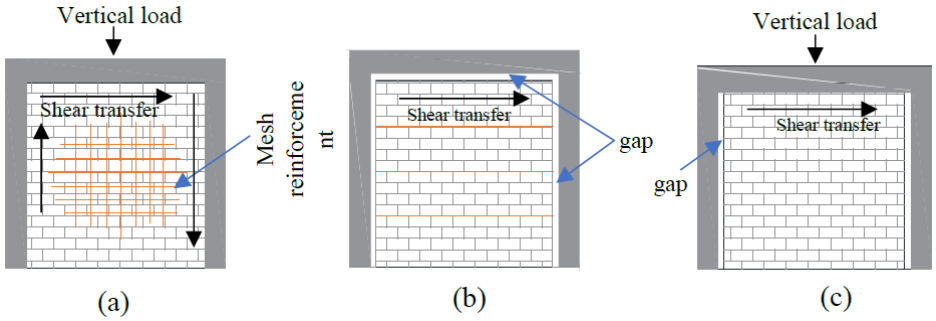

Figure 2.18. Hybrid Masonry Frames: (a) Type I (b) Type II, and (c) Type III (Abrams and Biggs 2012).

The proposed hybrid systems were developed for the steel frames with concrete masonry and it's difficult to make it compatible with RC frames with hollow clay masonry infills. Also, the systems couldn't provide expected out-of-plane resistance in case of simultaneous in-plane and out-of-plane loading.

2.6.4 Infill walls with sliding/flexible joint

In recent years, alternative design solutions have been proposed for engineered flexible infill walls with enhanced behaviour, exhibiting reduced interaction with the building structural components. The idea behind most of the proposed techniques is to increase the flexibility of the infill panel and to reduce the interaction with the surrounding frame through the introduction of sliding/flexible layers and flexible/soft layers (Mojsilović 2012; Anglada 2014; Vögeli et al. 2015; Mojsilović et al. 2015; Calabria et al. 2016; INSYSME 2016; Verlato et al. 2016; Ahmadi et al. 2017; Petrović et al. 2017; Verlato 2017;

Mojsilović et al. 2019). These can be horizontal layers inserted between the bricks or horizontal and vertical layers placed between the infill and the frame.

The improved deformability of the infill by the introduction of a horizontal sliding plane was achieved by Mohammadi and Akrami (2010) and Mohammadi et al. (2011). This plane consists of two prestressed steel plates which allow maximum wall forces to be controlled by friction. Experimental observations show that crushing at the lower boundary of the wall can occur if the amount of friction is not properly adjusted. Again, allowing high drifts may lead to the introduction of shear failure in the RC columns.

A notable study was carried out (Preti et al. 2012; Preti et al. 2015; Preti et al. 2016; Bolis et al. 2017) who have proposed solutions to infill protection by introducing horizontal sliding joints that allows the infill sub-panel to slide over each other in the in-plane direction and the out-of-plane resistance is taken care by the lateral shear connectors as shown in Figure 2.19. This system confirmed high drift capacity (i.e., up to 2.5%) with negligible infill damage by a significant reduction of stiffness and maximum strength. The limitation associated with this mechanism is that, at higher drift limits, masonry sub-panels cause high-stress concentrations in the columns and the openings.

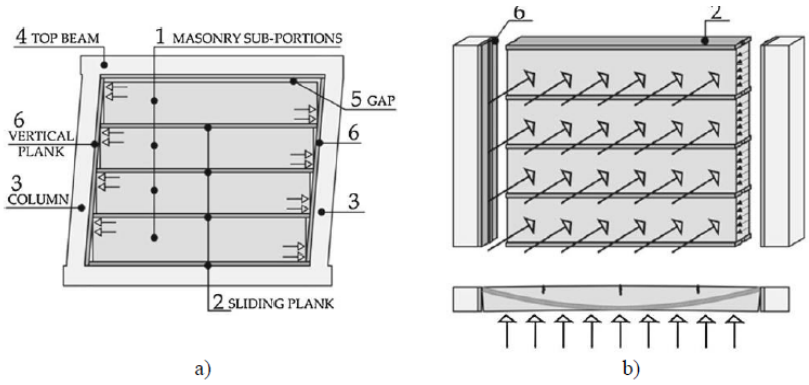

Figure 2.19. (a) Details of the proposed solution and (b) out-of-plane resisting mechanism (Preti et al. 2015).

Preti and Bolis (2017) proposed an approach where vertical sliding surfaces were introduced in the infill wall that allows the individual parts of the wall to slide and rotate independently. The out-of-plane resistance is offered vertically by the shear connectors. Dividing the infill vertically instead into subpanels eliminated the generation of stress concentration at the frame-infill interactions which couldn't be avoided in the horizontally divided infill. Although this technique significantly increases the flexibility and ductility,

the construction technique is complicated and involves complex stages like installation of shear keys.

Morandi et al. (2016) proposed a similar system with additional shear keys and C-shaped units to enhance the out-of-plane resistance. this system divides the infill wall into horizontal parts that slide on each other. The proposed system demonstrated a significant reduction in infill damage as compared to traditional infill. The effectiveness of this system against out-of-plane action was limited for the walls with openings.

The sliding mechanisms developed by researchers (Preti et al. 2012; Preti et al. 2015; Preti et al. 2016) have established the basis of more sophisticated systems. Among the different materials that can be employed for the soft layers, rubber is one of the most promising, because of the wide range of stiffness and dissipation capacity achievable by the choice of suitable compound and geometry. The Tun Abdul Razak Research Centre (TARRC) has developed an innovative rubber joint (Figure 2.20) made from a high-damping natural rubber (HDNR) compound. The joint has a non-flat profile whose shape has been defined in order to achieve different stiffness in the in-plane and out-of-plane direction and improve the out-of-plane capacity of the infills by invoking an arching mechanism (Ahmadi et al. 2017). The joint does not require skilled labour to be deployed and is available in two versions, DRES-V1 and DRES-V2 (Verlato 2017), which differ only for the presence of pins in the second one. These pins are introduced to enhance the bond between the rubber and the mortar and avoid sliding. In fact, even if sliding can be considered as an excellent mechanism for both reducing infill damage and dissipating energy through friction (Morandi et al. 2016), it is not desirable since it does often result in residual displacements.

Figure 2.20. Horizontal rubber joints developed by TARRC (Ahmadi et al. 2017).

(a) (b)

Figure 2.21. (a) TARRC's rubber joint used at SAIE Bologna (SAIE 2015) (b) masonry infilled frame with horizontal and vertical rubber joints tested within INSYSME project (INSYSME 2016).

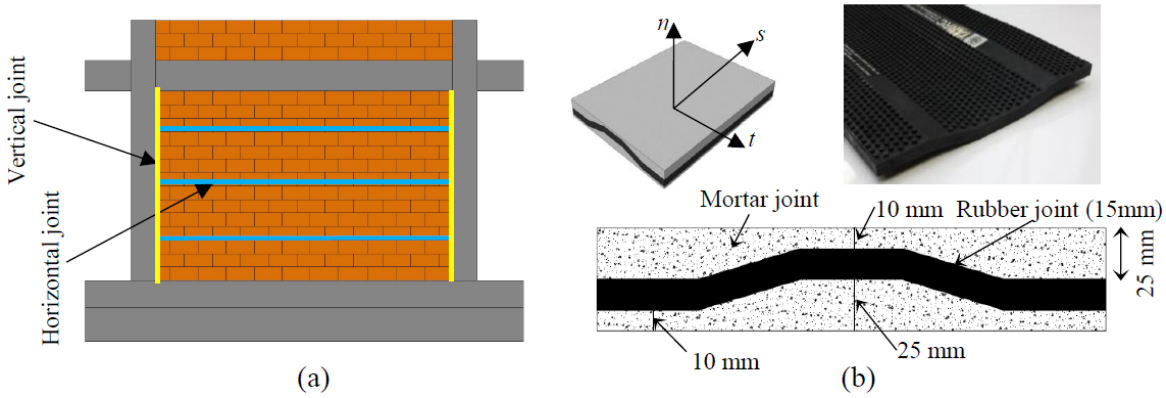

Figure 2.22. (a) Masonry infilled frame with rubber joints (b) HDNR joint developed by TARRC.

The effectiveness of the rubber joints was proved during tests carried within the European research project INnovative SYStems for earthquake-resistant Masonry Enclosures in reinforced concrete buildings (INSYSME 2016) on seismic protection of infill walls. In particular, in-plane and out-of-plane quasi-static tests were carried out at University of Padova (Verlato 2017) on an infilled reinforced concrete frame with and

without rubber joints. The tests demonstrated the "proof of concept" of the technology and showed that the introduction of the rubber joints considerably minimises the masonry infill damage and provides excellent out-of-plane performance in terms of stiffness and strength. Moreover, they showed that the rubber joints may contribute to increase the energy dissipation capabilities of the system, although this potential contribution was not investigated in depth.

The gap in the knowledge of the dynamic behaviour of infilled frames with rubber joints can be better investigated by more experiments as the rubber joints introduce flexibility and dissipate the seismic energy by deforming in shear. A characterization of the cyclic shear behaviour of the HDNR compound and of the rubber-mortar joints is needed.

Recently, a preliminary study by Dhir et al. (2021) has developed a modelling strategy in Abaqus for evaluating the in-plane quasi-static behaviour of RC frames with masonry infills and rubber joints, using a meso-scale approach. The test results are simulated in this study by using a detailed micro-modelling strategy, with the constitutive properties of the constituent materials of the triplets informed by material tests on mortar, brick, and rubber samples. The results of the experimental and numerical investigations of this study are useful for informing future numerical research on the analysis of the seismic performance of masonry infilled frames with rubber joints and on the evaluation of optimal mechanical and geometrical properties of the rubber joint properties.

Very recently, Dhir et a. 2022a proposed a macro-model for describing the in-plane seismic response of masonry-infilled frames with sliding/flexible joints. This study aims to fill this gap by proposing a two-dimensional macro-element model for describing the in-plane behaviour of RC infilled frames with flexible or sliding joints. The proposed modelling approach, implemented in OpenSees, is an extension of a discrete macro-element previously developed for the case of traditional infill panels. It is calibrated and validated in this study against quasi-static tests from the literature, carried out on masonry-infilled RC frames with sliding and rubber joints. The study results show the capabilities of the proposed modelling approach to evaluate the benefits of using flexible joints in terms of minimising the negative effects of the interaction between infill and RC frame and limiting the increase of global stiffness of the system with respect to the bare frame condition.

Dhir et al. 2022b performed an extensive experimental campaign and of numerical analyses aimed at characterising the cyclic shear behaviour of masonry triplets with mortar-rubber joints under both monotonic and cyclic loading. These joints consist of rubber strips

placed between two mortar layers with the aim of enhancing the flexibility of masonry components while providing some auxiliary energy dissipation. The hysteretic responses of the triplets obtained from the experiments are simulated using a micro-modelling strategy developed in Abaqus. The mortar-rubber joints exhibit very good dissipative properties, with an equivalent damping ratio value of the order of 20% or more which is much higher than that of the rubber compound (of the order of 6%). The bond between the rubber layers and the mortar layers was found to be the weakest component of the composite system. The bond between the rubber joints and the mortar layers exhibited higher strengths under cyclic loading compared to monotonic loading.

The solutions presented here definitively present several advantages over other solutions involving the strengthening of the infills or the full decoupling of the infills from the frame. Furthermore, the use of rubber or of sliding joints is expected to provide higher damping levels compared to the traditional infills. However, at high drift levels, premature shear failure of the columns occurs due to the punching of the horizontal masonry subpanels. Additionally, some issues are related to the out-of-plane capacity and the possibility of the arching mechanism to form even when flexible joints are added between the infill and the frame.

2.7 Summary

The state-of-the-art review on the available solutions to infill safety shows that the strengthening of unreinforced masonry walls requires the strengthening of the frame members adjacent to the infills, due to the increased forces transmitted to them. Thus, they may not be cost-effective. So, alternative design solutions have been proposed for engineered infill walls with enhanced behavior, exhibiting minimal interaction with the building structural components. The idea behind most of the proposed techniques is to increase the flexibility of the infill panel and to isolate it from the surrounding frame through the introduction of soft layers. Some finite element studies have been carried out to evaluate the behavior of RC frames with masonry infill walls and soft or sliding joints, but the case of rubber joints has not been fully investigated yet. Thus, a modelling strategy is needed to further study the complex interaction of infilled frames with rubber joints and shed light on the potential benefits stemming from the use of rubber joints and on the optimal layout and stiffness properties. No numerical study has analyzed yet the problem of the contribution of the joints to energy dissipation capabilities of the system, which can be significant. The

European research project INSYSME tests demonstrated the “proof of concept” of the technology and showed that the introduction of the rubber joints considerably minimizes the masonry infill damage and provides excellent out-of-plane performance in terms of stiffness and strength. Moreover, they showed that the rubber joints may contribute to increase the energy dissipation capabilities of the system, although this potential contribution was not investigated in depth.

3 Numerical modelling of reinforced concrete frames with masonry infills and rubber joints

3.1 Introduction

Seismic events throughout the world have demonstrated the high vulnerability of masonry infills in reinforced concrete (RC) frame structures. While structural members such as columns and beams are designed to be earthquake-resistant, masonry infills are often disregarded in design calculations, since they are treated as non-structural components. For this reason, they often undergo severe damage even under minor earthquakes, which may lead to injury and death of occupants as well as hampering the rescue operations.

Recent experimental and numerical studies have focused on the development of technological solutions for protecting infill walls. One way to do this is to increase their resistance, and a significant number of techniques is available for this purpose (Elgawady et al. 2004) for a state of the art review of strengthening techniques of unreinforced masonry walls and Koutas et al. (2015) for recently proposed solutions). However, these techniques also require the strengthening of the frame members adjacent to the infills, due to the increased forces transmitted to them. Thus, they may not be cost-effective. In the recent years, alternative design solutions have been proposed for engineered infill walls with enhanced behaviour, exhibiting minimal interaction with the building structural components. The idea behind most of the proposed techniques is to increase the flexibility of the infill panel and to isolate it from the surrounding frame through the introduction of soft layers (Mojsilović et al. 2015; Vögeli et al. 2015; Calabria et al. 2016; Ahmadi et al. 2017; Petrović et al. 2017). These can be horizontal layers inserted between the bricks or horizontal and vertical layers placed between the infill and the frame. Among the different materials that can be employed for the soft layers, rubber is one of the most promising, because of the wide range of stiffness and dissipation capacity achievable by the choice of suitable compound and geometry. The Tun Abdul Razak Research Centre (TARRC) has recently developed an innovative rubber layer (Figure 2.20), with different stiffnesses along

the three orthogonal directions. This is an essential requisite in order to achieve an optimal behaviour in the in-plane and out-of-plane directions. The effectiveness of the rubber joints was proved during tests carried out within the European research project INSYSME (INSYSME 2016) on seismic protection of infill walls (Figure 3.1).

In the last decades, significant research effort has been directed towards the implementation of finite element (FE) models for simulating the complex interaction between infill walls and RC frames (Mehrabi and Shing 1997; El-Dakhakhni et al. 2006; Caliò et al. 2012; Caliò and Pantò 2014; Xavier et al. 2015; Zhai et al. 2016; Kubalski et al. 2016; Okail et al. 2016; Nasiri and Liu 2017; Pantò et al. 2017; Breveglieri et al. 2018; Peng et al. 2018). Different modelling approaches have been investigated, including macro-modelling (Pietruszczak and Niu 1992; El-Dakhakhni et al. 2006; Caliò et al. 2012; Uva et al. 2012; Caliò and Pantò 2014; Pantò et al. 2017; Nicoletti et al. 2020; Ruggieri et al. 2020; Ruggieri et al. 2021), micro-modelling (Pantò et al. 2017), discrete-element modelling (Sarhosis et al. 2014) and meso-scale modelling (Lourenço and Rots 1997; Lourenço 1997; Dolatshahi and Aref 2011; Macorini and Izzuddin 2011, 2013, 2014; Nasiri and Liu 2017). Some finite element studies have been carried out to evaluate the behaviour of RC frames with masonry infill walls and soft or sliding joints (Preti et al. 2012; Mojsilović et al. 2015; Vögeli et al. 2015; Petrović et al. 2017; Di Trapani et al. 2020), but the case of rubber joints has not been fully investigated yet. Thus, a modelling strategy is needed to further study the complex interaction of infilled frames with rubber joints and shed light on the potential benefits stemming from the use of rubber joints and on the optimal layout and stiffness properties.

The proposed modelling strategy, developed using Abaqus (Dassault Systèmes 2016), is based on the use of three-dimensional solid elements for describing the RC frame, and a meso-scale approach for describing the masonry infill, where zero-thickness interfaces simulate the behaviour of the mortar joints and the rubber layers. The proposed strategy, never used before for studying the problem at hand, provides an accurate description of the development of cracks in the bricks and at the mortar interfaces and compared to macro-modelling approaches it allows for a better evaluation of the effects of the introduction of the rubber joints on the in-plane behaviour of the infill and frame.

After introducing the modelling approach, a validation study is carried out by considering the experimental quasi-static tests carried out by Mehrabi et al. (1996) on a RC frame with traditional masonry infills made of solid bricks under in-plane loading. The rubber layers are added to the model, and a parametric analysis is performed to evaluate the

influence of their layout (horizontal layers only, or horizontal and vertical layers) and stiffness on the in-plane behaviour. In the second part of the study, the modelling approach is validated against the experimental results described in INSYSME project (INSYSME 2016) on a RC frame with traditional hollow bricks and horizontal rubber joints subjected to in-plane load and further numerical analyses are performed by changing the layout and stiffness of the rubber layers.

It is noteworthy that although the present study focuses on the behaviour under in-plane quasi-static loading only, the developed three-dimensional models can also be used to simulate the out-of-plane behaviour of infills and the contribution of the rubber joints to the damping capacity of the system. Several studies have investigated numerically the out-of-plane behaviour of traditional infills using different modelling approaches (see e.g., Mohyeddin et al. 2013; Pantò et al. 2017, 2019; Pantò et al. 2018), but few (Ahmadi et al. 2017) have analysed the case of infills with sliding/flexible, using oversimplified models. No numerical study has yet analysed the problem of the contribution of the rubber joints to the energy dissipation capabilities of the system, which can be significant (Verlato 2017). Thus, a detailed numerical investigation of these problems is also warranted, although this is out of the scope of this study.

Figure 3.1. Masonry infilled frame with horizontal and vertical rubber joints tested within INSYSME project (INSYSME 2016).

3.2 Modelling strategy

The proposed modelling strategy employs material models and elements already available in the commercial FE software Abaqus (Dassault Systèmes 2016) as shown in Figure 3.2. The RC members of the frame are described with a continuum approach and

discretised using 3D 20-noded solid elements (C3D20R), whereas 3D linear beam elements (B31) are used for the reinforcing bars. The concrete behaviour is initially linear elastic, and then it follows the Concrete Damage Plasticity (CDP) model once cracking of the concrete in tension or crushing in compression occur. A damage model with linear loss of strength after cracking and a plasticity model are considered respectively for tension and compression. The constitutive behaviour of the steel reinforcing bars is assumed to be elasto-plastic with kinematic hardening (with constant post-yield stiffness) and the Von-Mises criterion defines the yielding condition. The longitudinal and transverse reinforcement are rigidly embedded within the concrete through the "embedded element technique" (Dassault Systèmes 2016). Bond-slip effects are disregarded, assuming perfect adherence at the rebar-concrete interface. It is noteworthy that this approach may lead to a slight overestimation of the stiffness of the RC frame, but this can be acceptable since the overall behaviour in terms of strength and stiffness of the system is significantly influenced by the infills.

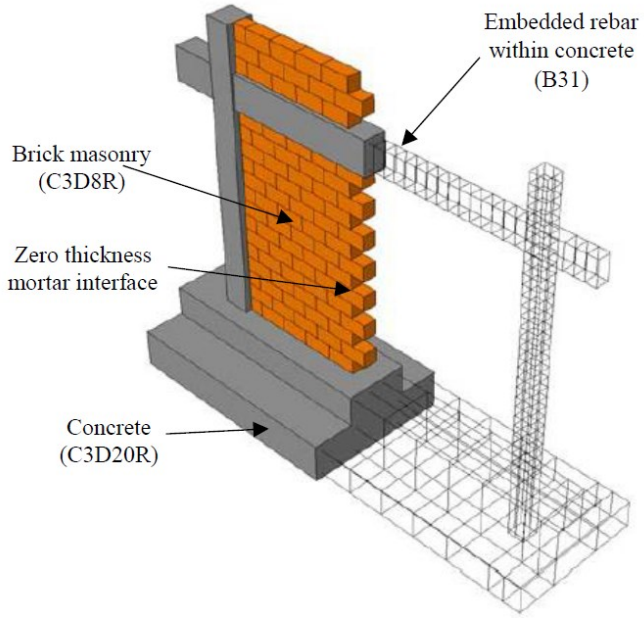

Figure 3.2. Schematic diagram of meso-modelling strategy.

The masonry infill walls are described employing a meso-scale approach (Lourenço and Rots 1997; Lourenço 1997). Expanded units, representing the brick units plus half mortar joint thickness per side (Figure 2.8a), are modelled as a series of continuum elements and the interaction between the expanded units along the bed and head joints is modelled through surface-to-surface contact behaviour. The initial response of the cohesive interfaces

is linear elastic, followed by a cracking behaviour that describes the most critical failure modes of masonry joints, namely, tensile cracking and shear sliding. This approach models the actual arrangement of masonry in the infill walls and the development of cracks in the mortar joints. The inelastic behaviour of the masonry units is also considered in a simplified way by employing the CDP model. Each brick unit is modelled with 16 8-noded elements (C3D8R) as shown in Figure 2.8 (b).

The mortar joints and rubber-mortar interfaces can be assigned different behaviour along the three orthogonal directions, which is useful to account for the particular shape of the rubber layers, resulting in orthotropic behaviour. The surface-to-surface contact is described by a linear elastic traction separation relationship for the condition prior to damage. Assuming uncoupled behaviour, this is controlled by the stiffness along the direction normal to the joint, k_n, and along two orthogonal shear directions in the plane of the joint, k_s and k_t. The values of the joint stiffnesses depend on the elastic properties of the components and on the geometry of the joints (Lourenço 1997).

A damage model is used to describe the crack formation and separation, with cracks that can form under tensile stresses, shear stresses, or a combination of the two. The damage criterion under uniaxial tensile stress is defined by the tensile strength σ_t. The critical shear stress at onset of damage is defined by a Mohr-Coulomb criterion (Lourenço 1997):

$$\tau_{s,t}^{\max} = c + \mu\sigma_n \qquad \text{Eq. 3.1}$$

where c is the cohesion between the masonry joints interfaces, μ is the coefficient of friction between the masonry joints interfaces, and σ_n is the normal contact pressure.

A quadratic stress criterion is used to define the damage initiation under combined stresses.

$$\left(\frac{\langle\sigma_n\rangle}{\sigma_t}\right)^2 + \left(\frac{\tau_s}{\tau_s^{\max}}\right)^2 + \left(\frac{\tau_t}{\tau_t^{\max}}\right)^2 = 1 \qquad \text{Eq. 3.2}$$

where $\langle\sigma_n\rangle = \sigma_n$ if σ_n is tensile (positive), and $\langle\sigma_n\rangle = 0$ if it is compressive (negative) (Abaqus manual; 2017; Abdulla et al. 2017), τ_s, τ_t = shear stresses along the first and second shear direction, respectively.

The post-elastic behaviour is controlled by the Mode I and Mode II fracture energies, namely G_f^I and G_f^{II} (Lourenço 1997). It is noteworthy that the interfaces cannot fail under compressive loads, but failure in compression of masonry can be taken indirectly into account through the CDP model employed for the bricks. Further details about the interface model can be found in Abdulla et al. (2017).

Figure 3.3 illustrates schematically a rubber-mortar joint. The properties of the interfaces describing these joints are derived hereinafter.

For the normal direction, the rubber joint stiffness (force per unit area per unit displacement) k_n^r can be evaluated as (Gent and Lindley 1959):

$$k_n^r = \frac{4G_r}{t_r}\left(1+S^2\right) \qquad \text{Eq. 3.3}$$

where G_r is the shear modulus of the rubber, t_r is the thickness of the layer, and S is the shape factor. Its expression for rectangular layers is:

$$S = \frac{BL}{2t_r(B+L)} \qquad \text{Eq. 3.4}$$

where B is the width of the rubber layer, which coincides with the thickness of the wall.

In the case of plane stain, this expression reduces to:

$$S = \frac{B}{2t_r} \qquad \text{Eq. 3.5}$$

For the shear direction along the plane of the wall (*s*), the rubber stiffness can be evaluated as:

$$k_s^r = \frac{G_r}{t_r} \qquad \text{Eq. 3.6}$$

In the out-of-plane shear direction (*t*), Eq. 3.6 provides only an approximation of the rubber stiffness k_t^r in the case of specially shaped rubber joints such as those of Figure 3.3. In fact, the shape of these joint results in a higher value of the transverse stiffness, allowing the formation of an arching mechanism under out-of-plane conditions (Ahmadi et al. 2017). In the case of simple rectangular rubber joints $k_t^r = k_s^r$.

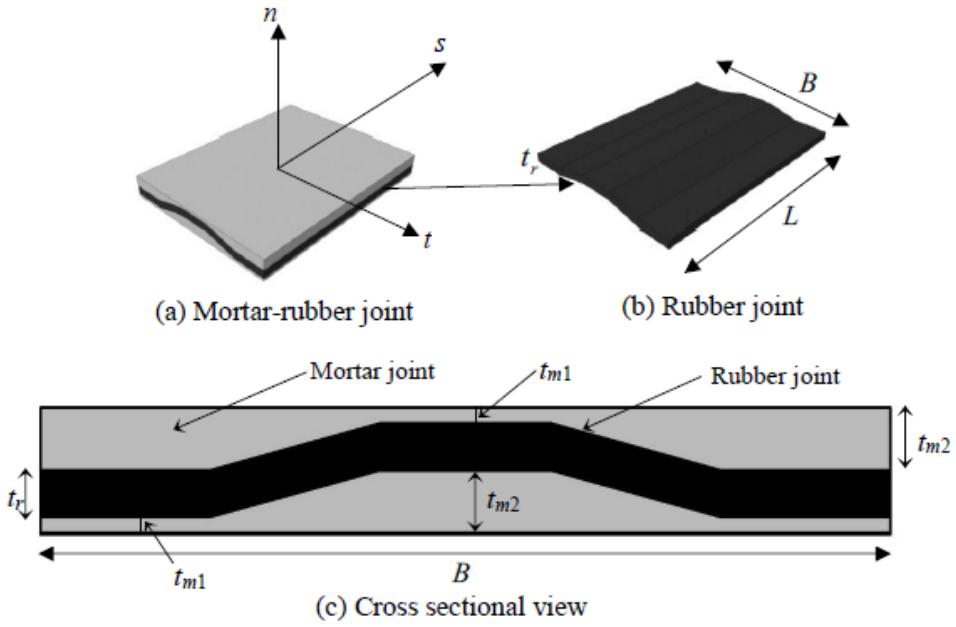

Figure 3.3. Schematic diagrams for a rubber-mortar joint (all dimensions are in mm units).

As per Figure 3.3, the rubber joint is sandwiched between two layers of mortar joints i.e., the mortar-rubber-mortar joints work, from a mechanical point of view, as a series system. Thus, if k_n^m , k_s^m , and k_t^m denote the stiffness of each mortar joint in the normal and shear directions respectively, then the composite stiffness of the mortar-rubber-mortar joint in the normal and shear directions can be approximated as follows:

$$\frac{1}{k_i^{mr}} = \frac{1}{k_i^m} + \frac{1}{k_i^r} + \frac{1}{k_i^m} \qquad i = n, s, t \qquad \text{Eq. 3.7}$$

Eq. 3.7 can be simplified and rewritten as;

$$k_i^{mr} = \frac{1}{\frac{1}{k_i^r} + \frac{2}{k_i^m}} \qquad i = n, s, t \qquad \text{Eq. 3.8}$$

The values of k_n^{mr} are controlled by the compliance of the rubber, which is much higher than of the mortar in order to accommodate large displacements of the in-plane motion of the frame and the wall. It is also noteworthy that these stiffness values should be adjusted to account for the fact that the joint has zero thickness and each brick unit in contact with the joint has to be expanded by the half joint thickness (Lourenço 1997).

With regards to the maximum allowable stresses in the mortar-rubber-mortar joints, under the series system approximation they can be assumed to coincide with the lowest

among the values of the strengths of the constitutive components and the values of the bond resistance. A failure either in unit brick or mortar or rubber can lead to the failure of the joint. However, rubber is highly deformable in shear which allows the total deformation of the system to localise in the rubber only leading to almost no damage to the masonry unit or mortar joints. In fact, failure could also occur in the bonds between the mortar and the rubber or in the bonds between the mortar and the bricks. It is noteworthy that the joint of Figure 3.3 is equipped with studs that increase the bond between the rubber and the mortar, thus providing an increased bond resistance in shear with respect to the case of smooth rubber joints (Verlato 2017).

Although the proposed model is valid for all types of structural configurations of RC infilled frames, it suffers from some limitations, among which the most important ones are the simplification of the stress field of the mortar and mortar/rubber joints, the use of an isotropic behaviour for the bricks, and the high computational cost. While the first two limitations could be eliminated by using a micro-modelling strategy with an orthotropic constitutive model for the bricks, at the cost of an increased computational burden, the latter limitation could be overcome by resorting to macro-models for describing the infills (e.g. Panto and Rossi 2019). This would allow to investigate the seismic performance of a full building with infills and rubber joints. Nevertheless, the proposed strategy can still be useful for simulating and interpreting experimental results, and for calibrating/validating simplified modelling approaches when experimental tests are not possible.

3.3 Validation study

The differences in the frame sizes, brick types used, the mortar joint type/position, and the frame-infill interaction may influence the modelling strategies significantly. So, in order to develop an efficient model with the objective of attending to diverse conditions two case studies are considered for simulating the behaviour of RC frames with traditional and innovative masonry infill walls. The first one is RC frame with traditional infill walls made with solid blocks, experimentally tested by Mehrabi et al. (1996). This case study has been selected because it is widely employed by other authors (Flanagan and Bennett 2001; Stavridis and Shing 2010; Mohyeddin et al. 2013; Caliò and Pantò 2014; Filiatrault and Sullivan 2014), including also Mehrabi et al. (1997) to validate their modelling strategy for RC frames with masonry infills. Moreover, together with the results of the tests of the infilled frame, various data from material and component tests were made available. These

latter data have been used to calibrate the model parameters, whereas the experimental test results on the structural systems (i.e., bare frame and infilled frames) have been used for model validation. After validating the proposed approach, the infilled frame is studied numerically by performing pushover analyses for different layouts and stiffnesses of the rubber joints. The second case study is a RC frame that has been experimentally studied in three configurations: with no infills, with traditional infills made of hollow masonry blocks, and with these infills and rubber joints. The results of the tests, available in INSYSME project (INSYSME 2016), are very detailed and useful for validating the proposed modelling strategy for RC frames with masonry infills and rubber joints.

3.3.1 Case study I

In the first case, reference is made to the experimental tests of Mehrabi et al. (1996), and to the ensuing numerical study (Mehrabi and Shing, 1997). Specimen 1 (bare frame) and specimen 3 (frame infilled with solid concrete masonry blocks) of the experimental campaign are considered. The height/length (h/L) ratio of the frames is 2/3. The infill panels are made with solid concrete masonry blocks arranged in a running bond pattern (Figure 3.4). The bed joints are fully filled with mortar, whereas the head joints are only partially filled with mortar. The bed and head joints are 9.5 mm thick. Some details regarding the frame, including the concrete member sizes, rebar diameter and detailing scheme and masonry block dimensions, are given in Figure 3.4. Further details are available in Mehrabi et al. (1996). Experimental tests were carried out by Mehrabi et al. (1996) on the bare frame as well as on the infilled frame. The tests consisted of the application of vertical loads (146.8 kN) at the top of each column, simulating the effect of permanent loads acting on the frame, followed by in-plane horizontal loads (monotonically increasing) applied at the beam extreme, as shown in Figure 3.4.

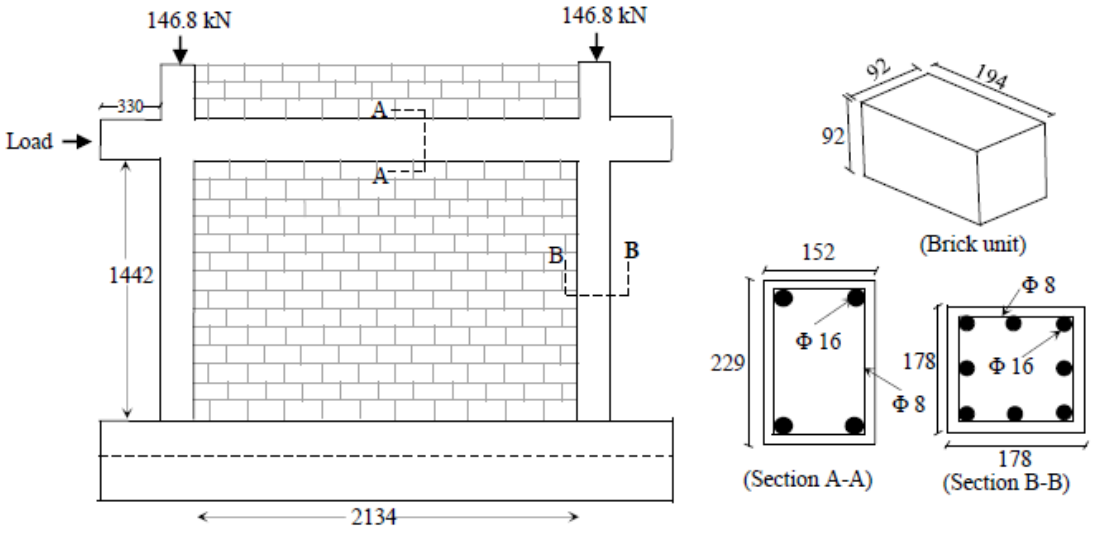

Figure 3.4. Geometric details of the selected infilled frame available in Mehrabi et al. (1996) with RC section details and brick dimensions (dimensions in mm).

The FE models of the bare frame and infilled frame have been developed by following the approach outlined in Section 2. The main mechanical properties of the concrete material employed for the frame components, brick units, and steel reinforcement are reported in Table 3.1. The properties of the zero-thickness interface elements describing the mortar joints are reported in Table 3.2. Most of the values reported in Table 3.1 and Table 3.2 are based on the results of the experimental tests carried out by Mehrabi et al. (1996), e.g. on the concrete and mortar samples, and masonry units and prisms. For some parameters where it couldn't be directly measured, they were assumed based on literature and/or calibrated to provide the best fit to results (Lourenço 1997) and are marked separately. The head joints have been given different properties to account for the fact that they were only partially filled with mortar. The wall to frame mortar interfaces have been assigned the same properties as the head joints.

Table 3.1. Mechanical properties of the frame components and brick units.

Mechanical properties	Concrete	Brick units	Steel reinforcement
Young's modulus, E (MPa)	21930	9520	210000
Poisson's ratio, ν (-)	0.18	0.15	0.30
Compressive strength, σ_c (MPa)	30.90	15.59	-
Strain at peak compressive stress	0.002	0.002	-
Ultimate strain (zero residual stress)	0.0035	0.0035	-
Yield strength (MPa)	-	-	400
Peak tensile strength, σ_t (MPa)	3.29	1.57	-
Fracture energy in tension, G_f^I (MPa·mm)	0.09	0.07	-
Post-elastic to elastic stiffness ratio	-	-	0.002

Table 3.2. Properties of the contact interfaces describing the mortar joints.

Mortar Interaction Properties	Bed joints	Head joints	Source
k_n^m per unit area (N/mm^3)	500	500	Lourenço 1997*
k_s^m , k_t^m per unit area (N/mm^3)	250	250	Lourenço 1997*
σ_t (MPa)	0.14	0.034	Mehrabi et al. 1997
Cohesion, c (MPa)	0.20	0.07	Mehrabi et al. 1997*
Coefficient of friction, μ (-)	0.90	0.70	Mehrabi et al. 1997
Normal fracture energy per unit area, G_f^I (MPa·mm)	0.015	0.005	Mehrabi et al. 1997*
Shear fracture energy per unit area, G_f^{II} (MPa·mm)	0.09	0.07	Mehrabi et al. 1997*

*Not directly measured but assumed based on literature and/or calibrated to provide best fit to results

3.3.1.1 Bare frame

After applying the vertical static loads at the top of the columns, an in-plane horizontal displacement was applied incrementally to the end of the beam (see Figure 3.5). The beam-end was free to deflect in the vertical and out-of-plane horizontal directions. Figure 3.5a shows the plastic strain distribution of the bare frame (specimen 1 in Mehrabi et al. 1996) for a horizontal displacement of 28.4 mm (corresponding to an inter-storey drift of 2.0%) and Figure 3.5b compares the experimental and numerical force-deformation curves. The overall agreement is reasonable, although the proposed model overestimates the initial stiffness of the system. This is thought to be because the compliance due to the slip behaviour between the steel reinforcement and concrete is neglected. In the same figure, the numerical curve according to the model developed by Mehrabi et al. (1996) is plotted for comparison.

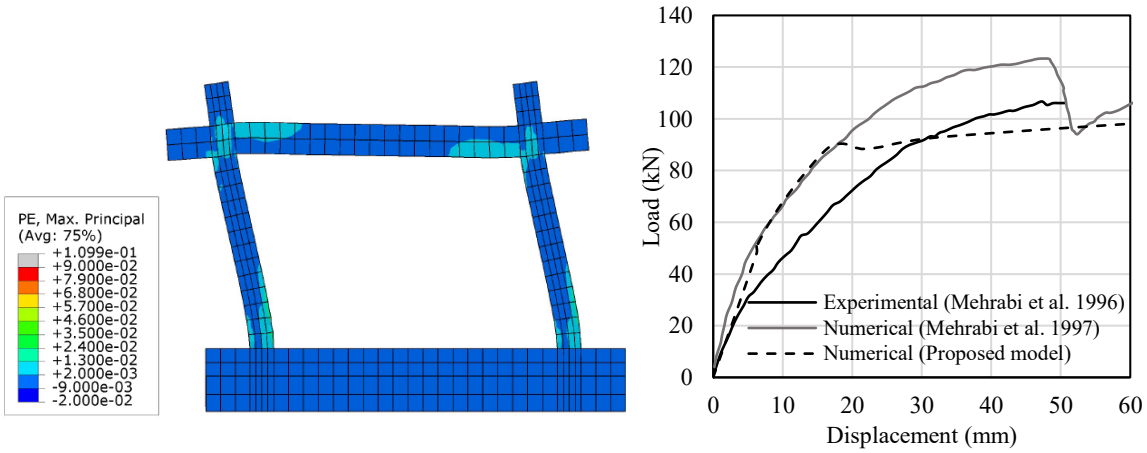

(a) (b)

Figure 3.5. (a) Plastic strain distribution at a deformation of 28.4 mm (2.0% drift) (b) load-displacement curves for the bare frame.

3.3.1.2 Frame with traditional infill

Figure 3.6a shows the model's predictions of the deformed shape and cracking pattern of the masonry infilled RC frame for a horizontal displacement of 14.2 mm, corresponding to a drift of about 1.0%. It can be observed that the horizontal load induces the formation of several diagonal cracks in the infill wall. The cracks affect both the bed, and the head mortar joints. Figure 3.6b illustrates and compares the experimental and numerical force-displacement curves obtained for the infilled frame. Again, the proposed

model describes the initial as well as the post-peak behaviour of the wall with good accuracy.

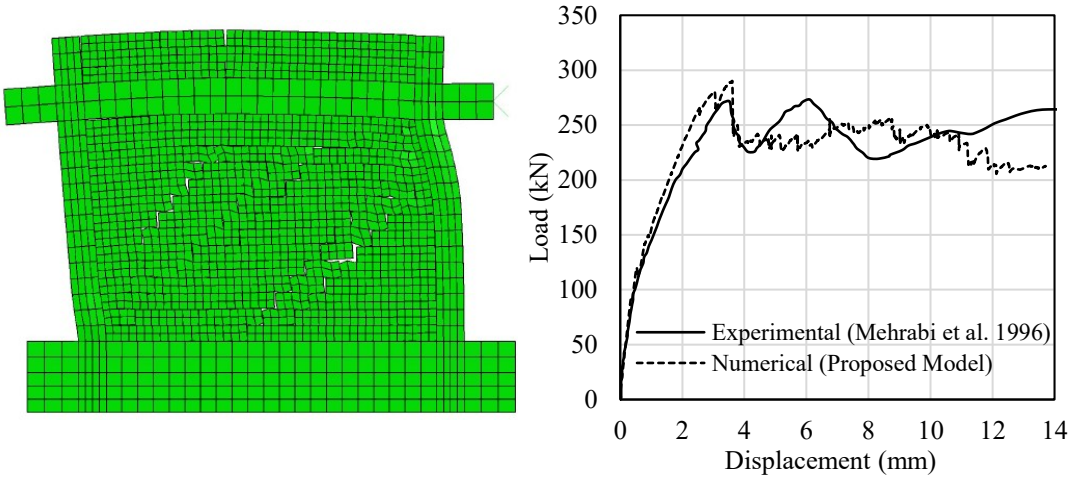

(a) (b)

Figure 3.6. (a) Simulated cracking pattern of the masonry infill wall at 14.2 mm (1.0% drift) (b) comparison between numerical and experimental load-displacement curves.

Figure 3.7a shows a contour plot of the minimum principal compressive stresses in the masonry and concrete components for a horizontal displacement of 14.2 mm (1.0% drift). The distribution of these stresses is significantly affected by the cracks forming along the main diagonal of the wall, with the highest absolute values observed in the corner regions. The plot of the plastic deformations (Figure 3.7b), indicates that the frame and many bricks are significantly damaged.

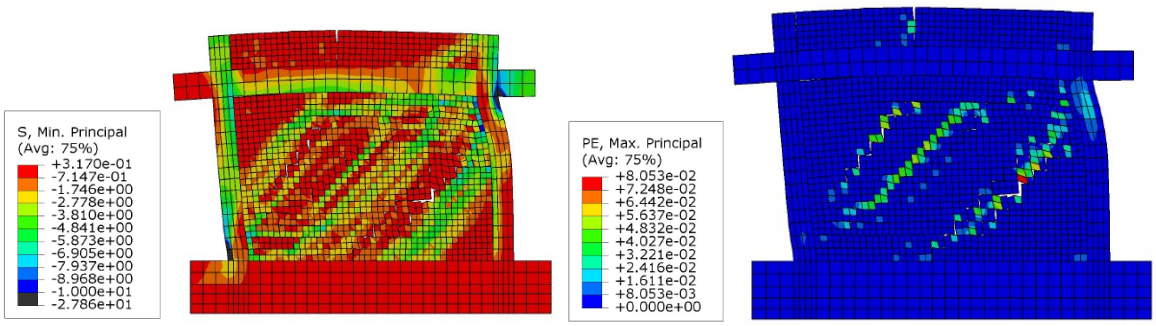

(a) (b)

Figure 3.7. (a) Minimum compressive principal stress distribution (in MPa unit) (b) Plastic strain distribution showing cracking of bricks for a horizontal displacement of 14.2 mm (1.0% drift).

3.3.1.3 Frame with infill and rubber joints

In this section, the effectiveness of rubber joints for the seismic protection of masonry infills is investigated by considering different cases, corresponding to the use of horizontal mortar-rubber joints only, and no vertical rubber joints present between the columns and the wall (RJ_H) or horizontal and vertical joints (RJ_HV). The horizontal layers of rubber joints are introduced between three or four courses of bricks and the vertical layers are introduced between the masonry infill and the frame, as shown in Figure 3.8. The rubber joints are assumed to be flat.

The horizontal rubber joints are characterised by a relatively high compression stiffness in the vertical direction, and low shear stiffness of masonry sub-panels in the in-plane direction, in order to reduce the displacement demand on the infill. The shear modulus of the rubber is equal to G_r= 0.5 MPa and the thickness of the horizontal joints is assumed equal to 7.5 mm. This value has been chosen such that each joint can undergo up to a shear deformation of approximately 125% (i.e., 9.5 mm), under a peak inter-storey drift of 2.0% (i.e., 28.4 mm relative displacement between top and bottom beams), assuming that the blocks of masonry between the joints behave rigidly under the horizontal forces. Table 3.3 reports the properties of the cohesive interfaces representing the mortar-rubber joints. The stiffness values evaluated are based on Eqs. 3.3-3.8, assuming mortar layers with thickness t_m = 10 mm.

The vertical rubber joints are characterised by a low compression stiffness to accommodate the relative displacements between the infill blocks and the frame and thus minimise the stresses between the frame columns and the masonry infill itself. Again, the idea of introducing vertical rubber joints was also to protect the frame from the infill during in-plane sliding. Unlike horizontal rubber joints, the vertical rubber joints are introduced between the masonry infill and the frame without any adhesion with the frame or infill. This led to the consideration of zero shear stiffness of the vertical joint. This reduced stiffness in compression can be achieved by using joints of the same rubber as the horizontal joints, with a higher thickness of 30 mm, or by using a softer rubber compound. These joints, placed between the wall and the frame, are not bonded with vertical mortar joints. Thus, the interfaces used to represent these joints are characterised by zero cohesion and zero tensile resistance, and a friction coefficient of 0.31. The values of fracture energies are taken from Verlato (2017) which are also consistent with the range of values reported in Lourenco (1997).

In order to investigate the effect of the stiffness of the vertical rubber layers on the system behaviour, two further sub-cases are considered, where the rubber stiffness is increased by 10 times (RJ_HVH) and decreased by 10 times (RJ_HVL) with respect to the RJ_HV case.

Table 3.3. Interaction properties of the mortar-rubber joints.

Interaction properties	Horizontal joint	Vertical joint			
		RJ_H	RJ_HV	RJ_HVH	RJ_HVL
k_n^{mr} per unit area (N/mm^3)	10.0	300	0.87	8.70	0.087
k_s^{mr} , k_t^{mr} per unit area (N/mm^3)	0.067	-	-	-	-
σ_t (MPa)	0.15	-	0	0	0
c (MPa)	0.05	0	0	0	0
μ (-)	0.36	0.4	0.31	0.31	0.31
G_f^I (MPa·mm)	0.005	-	-	-	-
G_f^{II} (MPa·mm)	0.05	-	-	-	-

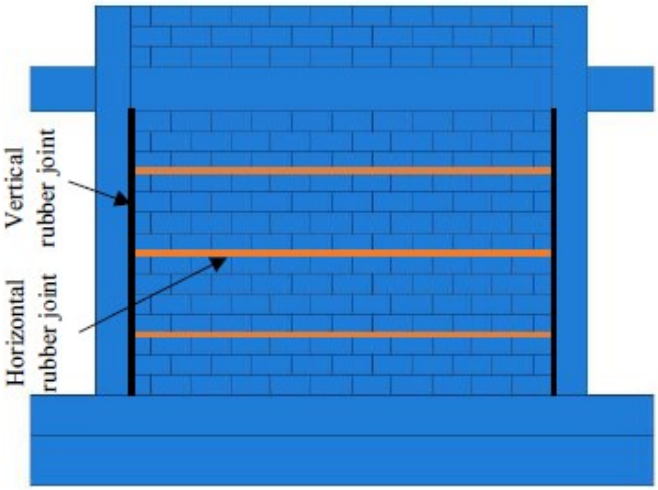

Figure 3.8. Masonry infilled frame with horizontal and vertical rubber joints (RJ_HV).

Figure 3.9a shows the deformed shape of the infilled frame for RJ_H where, no mortar joints have been considered between the columns and the wall; the corresponding interfaces have only frictional behaviour, with very high stiffness (300 N/mm^3) to avoid penetration along the normal direction. Figure 3.9b shows the load-deflection curve of the

system with horizontal rubber joints, compared to the curves obtained in the bare frame and the frame with traditional infills. Figure 3.9 shows the predicted response of the proposed numerical model considering the experimentally evaluated mechanical properties of rubber joints tested from the INSYSME project (INSYSME 2016). The addition of the rubber joints is found to increase the compliance of the infill wall, and it can be observed that most of the deformation/sliding is located at these joints, whereas the masonry blocks between the rubber joints behave rigidly. From the plots, it is possible to appreciate the remarkable flexibility of the system with rubber joints, which is similar to a bare frame. It is noteworthy that the reduction of stiffness can also help to reduce the demand of absolute accelerations in the infilled frame under seismic excitation, due to increase in natural period. This in turn helps to protect acceleration-sensitive components.

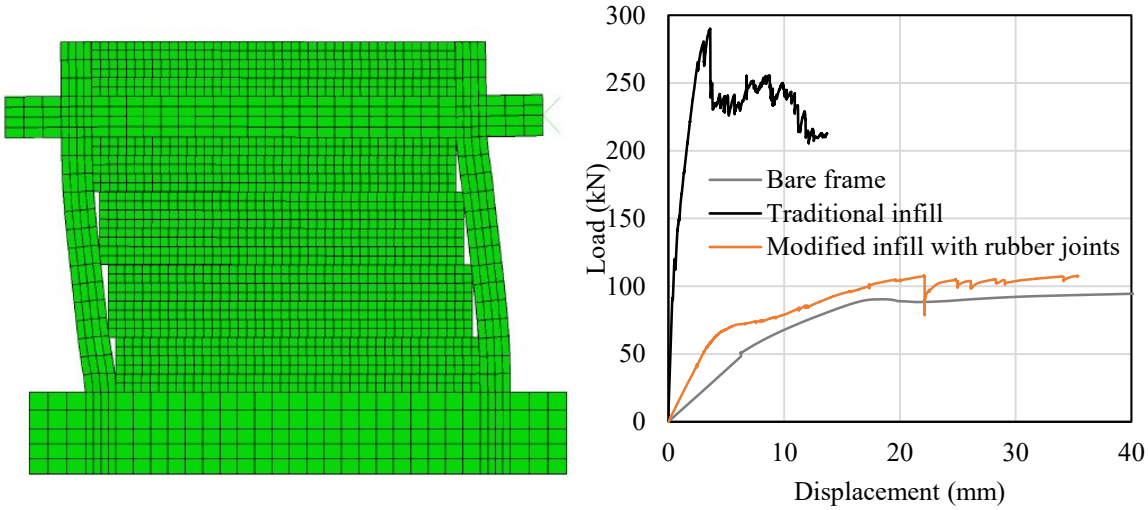

Figure 3.9. (a) Deformed shape of infilled RC frame with horizontal rubber joints (RJ_H) (b) numerical responses of the bare frame, infilled frame with traditional infills and infilled frame with horizontal rubber joints (RJ_H).

Figure 3.10 and Figure 3.11 show the principal stress distribution in the concrete and masonry components for a horizontal deflection of 14.2 mm (1.0% drift) and 28.4 mm (2.0% drift) respectively. These stresses are significantly lower compared to the case of the frame with traditional infill (see Figure 3.7a), with the exception of two small regions at the interface of the bottom subpanel and the right column, and the top subpanel with the left column. The plot of the plastic deformations (Figure 3.12 and Figure 3.13), also confirms

the effectiveness of the rubber joints in minimizing the damage to the masonry components, with bricks experiencing almost no damage even under a 2.0% drift.

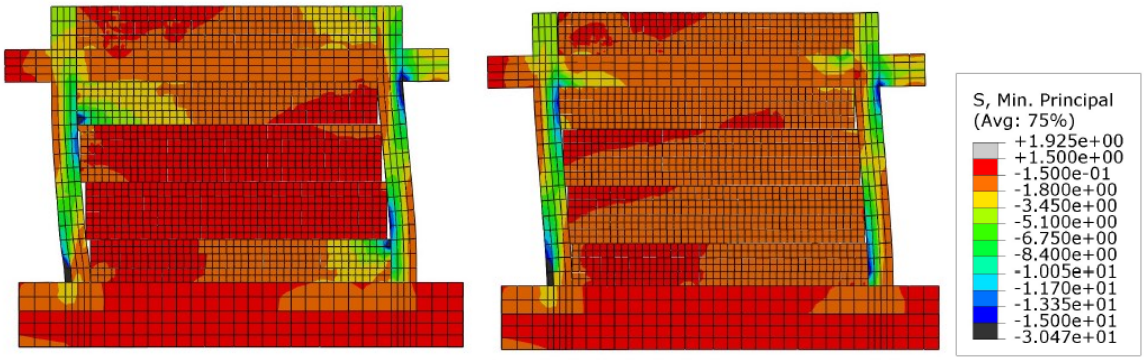

(a) RJ_H (b) RJ_HV

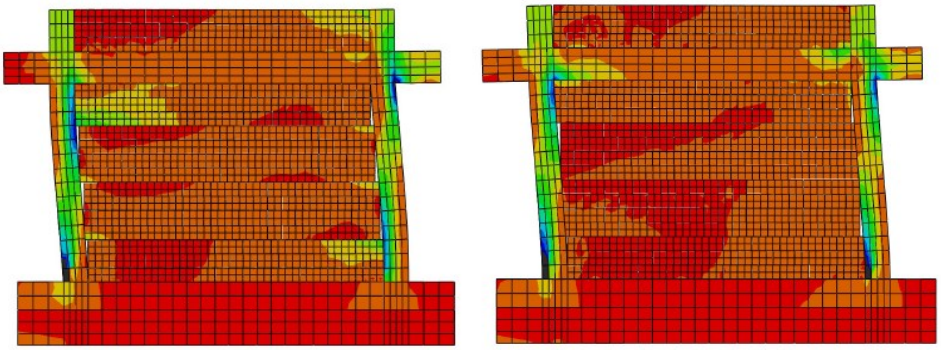

(c) RJ_HVH (d) RJ_HVL

Figure 3.10. Minimum compressive principal stress (in MPa unit) distribution under a horizontal displacement of 14.2 mm (1.0% drift).

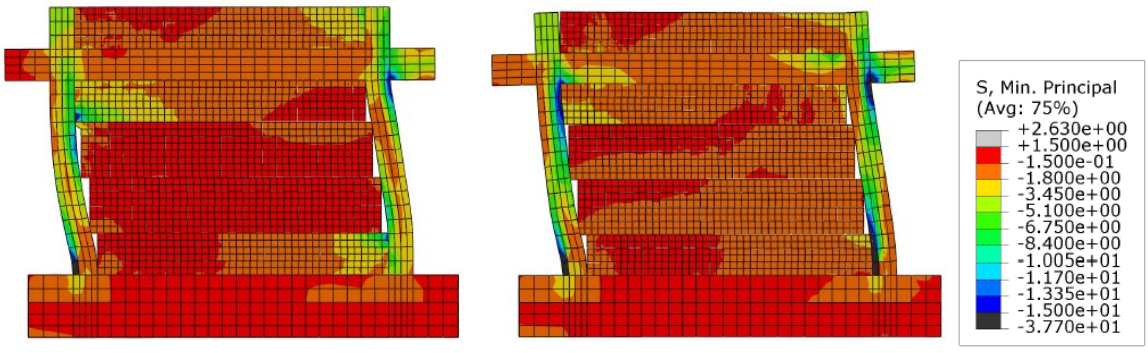

(a) RJ_H (b) RJ_HV

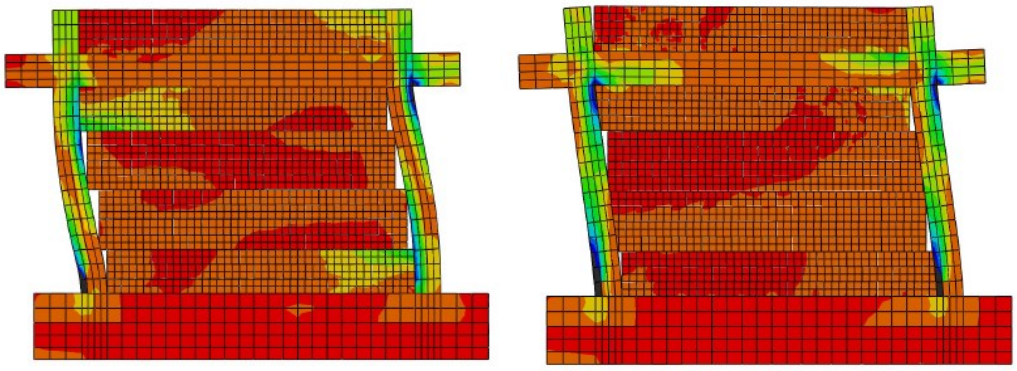

(c) RJ_HVH (d) RJ_HVL

Figure 3.11. Minimum principal compressive stress (in MPa unit) distribution under a horizontal displacement of 28.4 mm (2.0% drift).

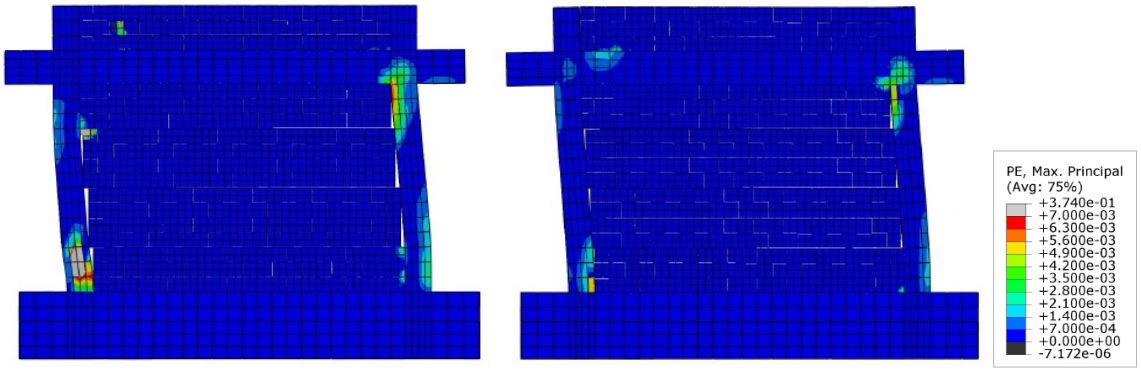

(a) RJ_H (b) RJ_HV

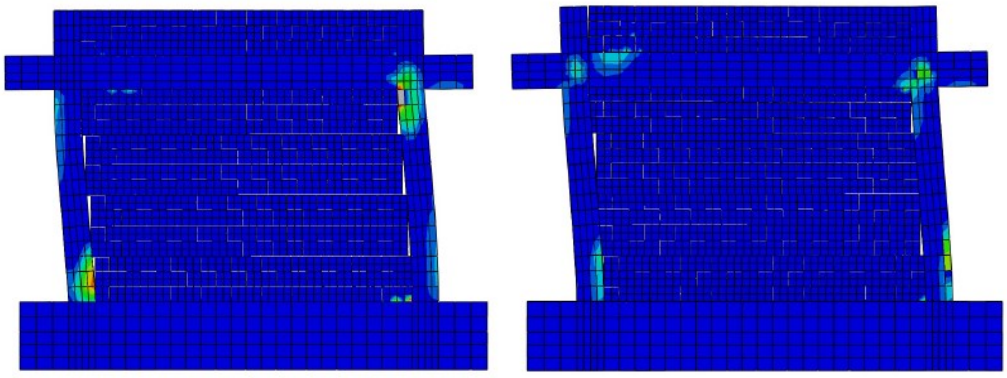

(c) RJ_HVH (d) RJ_HVL

Figure 3.12. Plastic strain distribution under a horizontal displacement of 14.2 mm (1.0% drift).

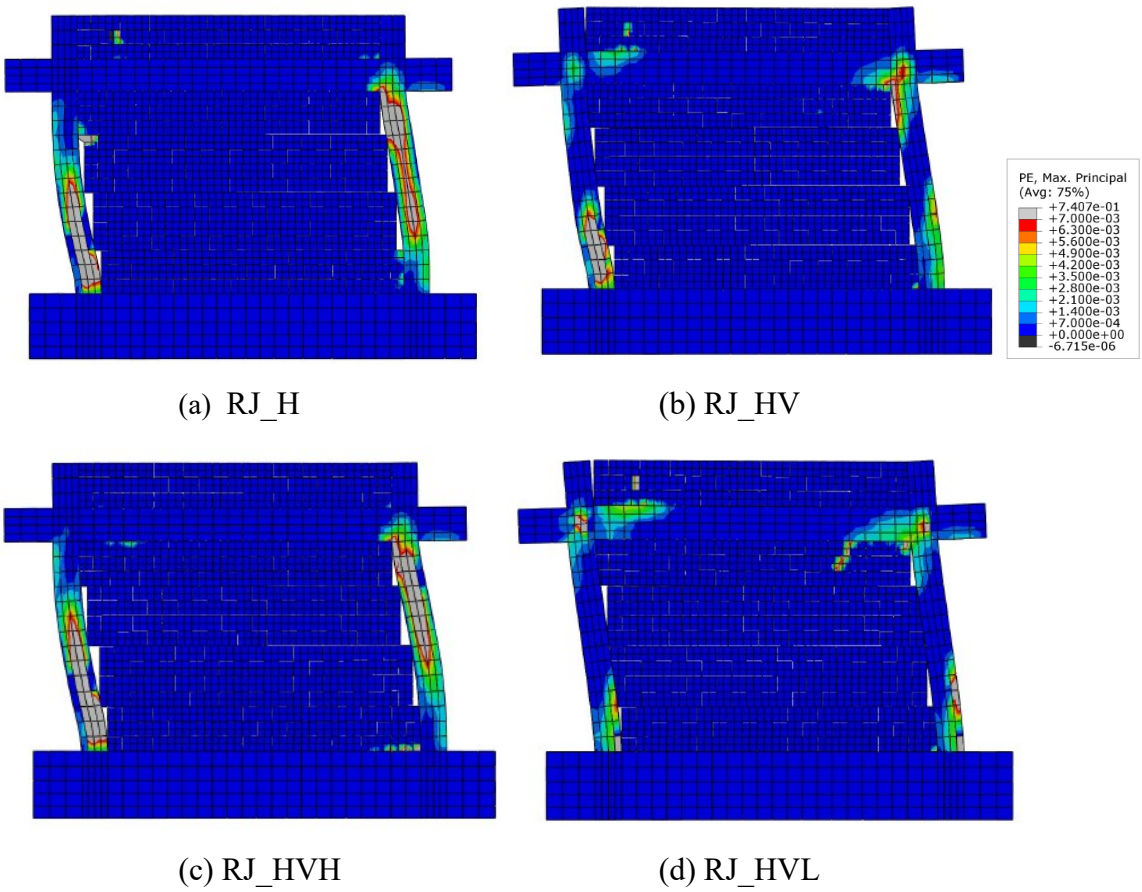

(a) RJ_H (b) RJ_HV

(c) RJ_HVH (d) RJ_HVL

Figure 3.13. Plastic strain distribution under a horizontal displacement of 28.4 mm (2.0% drift).

In order to highlight the effect of the vertical rubber joints on the system behaviour, Figure 4.15 shows the plot of the horizontal force-deflection curve for the different cases considered. It can be observed that adding the vertical rubber joints does not change significantly the global behaviour of the system compared to the case with only horizontal rubber joints. The initial stiffness is lower for the case of horizontal and vertical rubber joints compared to the case of only horizontal joints, and it reduces by reducing the vertical joint stiffness. The maximum forces achieved by the various systems are quite similar. The peak force obtained for the system RJ_HV is slightly higher than the one obtained for the system RJ_H, and it is attained for a higher displacement. With the systems RJ_HVH and RJ_HVL slightly lower peak forces are attained compared to the system denoted to as RJ_HV. However, in Figure 3.10 and Figure 3.11, it can be seen that adding the vertical rubber joints reduces the compressive stresses in the bricks adjacent to the frame. This reduction is more significant for the case of flexible vertical joints (RJ_HVL) compared to the case of ordinary or stiff vertical joints (RJ_HV, RJ_HVL). Moreover, comparing the various contour plots

of the plastic deformations in Figure 3.12 and Figure 3.13, it can be noted that the solution with vertical joints with low stiffness reduces significantly the damage of the frame, compared to the other solutions.

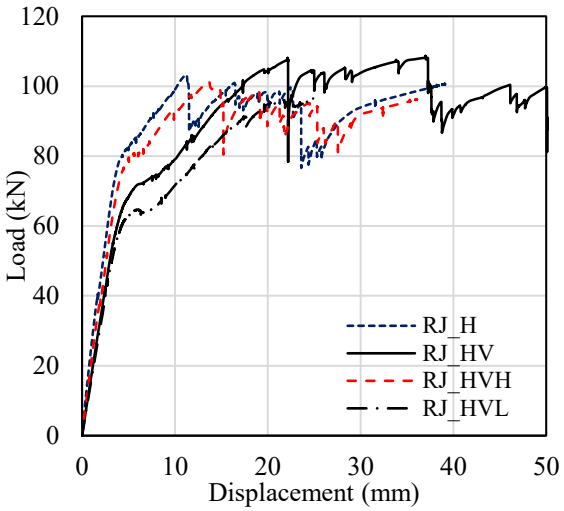

Figure 3.14. Comparison of rubber joints with various layouts and stiffnesses.

3.3.2 Case study II

The second case study considers a set of prototypes experimentally tested by University of Padova within INSYSME project (INSYSME 2016) and described in Verlato (Verlato 2017). Experimental results for bare frame, infilled frame with mortar joints (4th frame specimen, FC. MJ enclosure) and infilled frame with rubber joints (DRES-V2) are considered for the validation of the numerical modelling strategy. Figure 3.15 illustrates the infilled frame prototype, whose aspect ratio is of 2/3. The infill panels are made with hollow clay masonry blocks (D-type as in Verlato 2017) arranged in a running bond pattern (Figure 3.15). D-type blocks are characterised by a lower percentage of holes, equal to 50%, and "tongue and groove" lateral surfaces that do not require the application of vertical mortar joints (Verlato 2017). The transfer of shear stress under in-plane shear loading relies on friction. For modelling and computational simplicity, the hollow block behaviour is assumed to be isotropic, with properties based on the results of the compression test carried out along the direction parallel to the holes. The bed joints are fully filled with mortar, and they are 10 mm thick, whereas there are no mortar head joints and the transfer of stresses from a brick to the adjacent ones relies on the brick interlocking. Some details regarding the frame, including the concrete member sizes, rebar diameter and detailing scheme and masonry block dimensions, are given in Figure 3.15. Further details are available in Verlato

(2017). The experimental quasi-static tests conducted on the bare frame and the frame infilled with traditional mortar joints and TARRC's innovative mortar-rubber joints, shown in Figure 2.20, consisted of the application of vertical loads (200 kN) at the top of each column, simulating the effect of permanent loads acting on the frame, followed by in-plane horizontal loads (monotonically increasing) applied at the beam extreme, as shown in Figure 3.15.

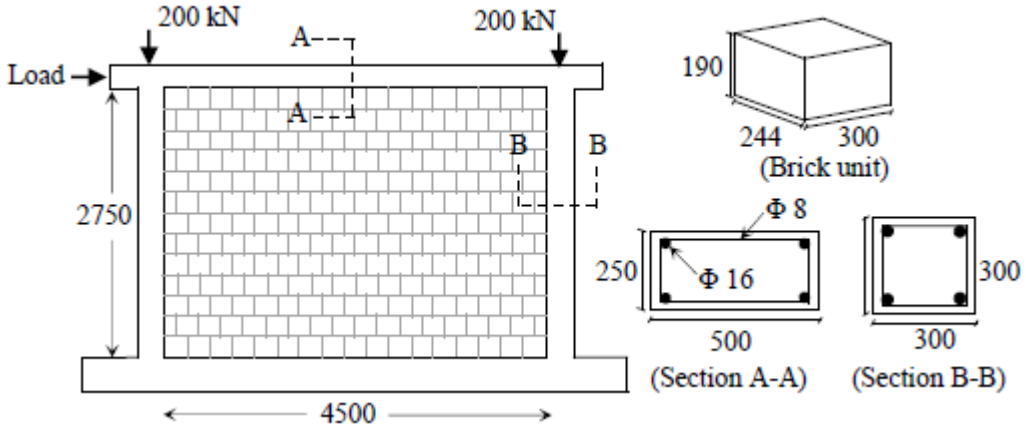

Figure 3.15. Geometric details of the selected infilled frame (INSYSME 2016) with RC section details and block dimensions (dimensions in mm).

Table 3.4 reports the main mechanical properties of the concrete material employed for the frame components, the brick units, and the steel reinforcement. Table 3.5 reports the properties of the zero-thickness interfaces describing the mortar joints. The values reported in Table 3.4 and Table 3.5 are based on the results of the experimental tests carried out by INSYSME project (INSYSME 2016) and numerical models developed by Verlato et al. (2016) to simulate these tests. The head joints have been given different properties to account for the fact that they were not filled with mortar. The wall to frame mortar interfaces have been assigned the same properties as the head joints.

Table 3.4. Mechanical properties of concrete for frame components and brick units.

Mechanical properties	Concrete	Brick units	Steel reinforcement
E (MPa)	22000	3693	180000
ν (-)	0.15	0.40	0.30
σ_c (MPa)	40	4.25	-
Strain at peak compressive stress	0.002	0.002	-
Ultimate strain (zero residual stress)	0.0035	0.0035	-
Yield strength (MPa)	-	-	535
σ_t (MPa)	3.90	0.22	-
G_f^I (MPa·mm)	0.075	0.04	-
Post-elastic to elastic stiffness ratio	-	-	0.002

Table 3.5. Properties of the contact interfaces describing the mortar joints.

Mortar Interaction Properties	Bed joints	Head joints
k_n^m per unit area (N/mm^3)	200	200
k_s^m , k_t^m per unit area (N/mm^3)	100	-
σ_t (MPa)	0.346	-
c (MPa)	0.485	-
μ (-)	1.13	0.80
G_f^I (MPa.mm)	0.005	-
G_f^{II} (MPa.mm)	0.05	-

3.3.2.1 Bare frame

After applying the vertical static loads at the top of the columns, an in-plane horizontal displacement was applied incrementally to the end of the beam (see Figure 3.16a). Figure 3.16 (a) shows the plastic strain distribution of the numerical model of the bare frame for a horizontal displacement of 55mm (2.0% drift) and Figure 3.16 (b) compares the experimental and numerical force-deformation curves. The overall agreement is good although the proposed model slightly overestimates the initial stiffness of the system.

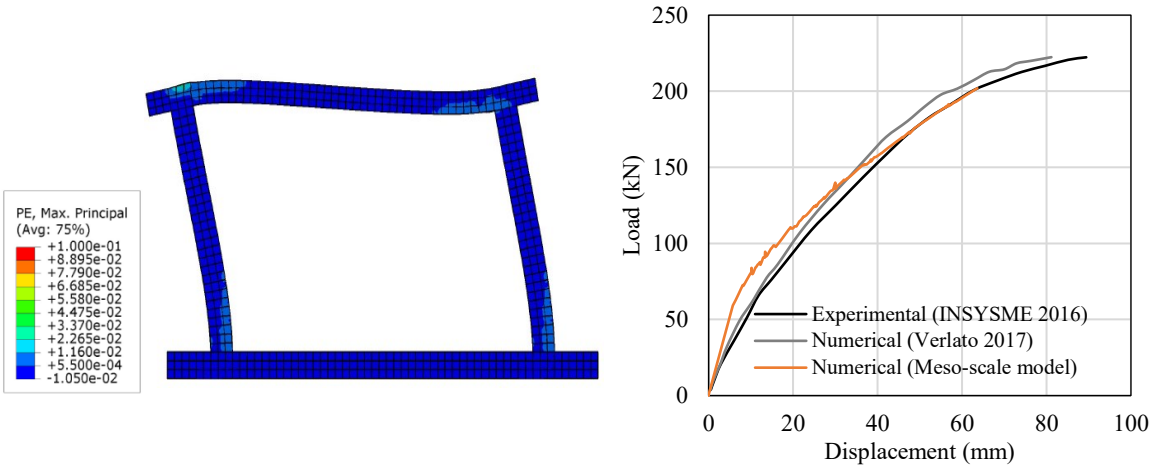

(a) (b)

Figure 3.16. (a) Plastic strain distribution at 55 mm (2.0% drift) (b) load-displacement curves for bare frame.

3.3.2.2 Frame with traditional infill

The analysis was run with a computer architecture of 16gb RAM, intel i5-8500 processor (3GHz clock speed) and 64-bit operating system. With the 3D model with traditional infill (12812 nodes), 24.07 hours of analysis are required to reach a displacement of 27.5 mm (equivalent to 1.0% of inter-storey drift). Figure 3.16 (a) shows the crack pattern of FC. MJ specimen (INSYSME 2016) at 1.2% drift. Figure 3.16 (b) shows the deformed shape and cracking pattern of the masonry infilled wall for a horizontal displacement of 27.5 mm. It can be observed that the horizontal load induces the formation of several diagonal cracks in the wall. Figure 3.16 (c) illustrates and compares the experimental and numerical force-displacement curves obtained for the infilled frame. Again, the proposed model describes the initial as well as the post-peak behaviour of the wall with good accuracy.

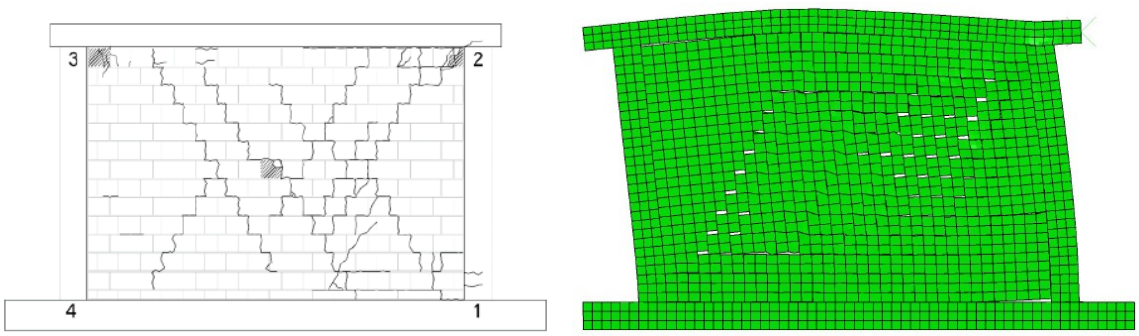

(a) (b)

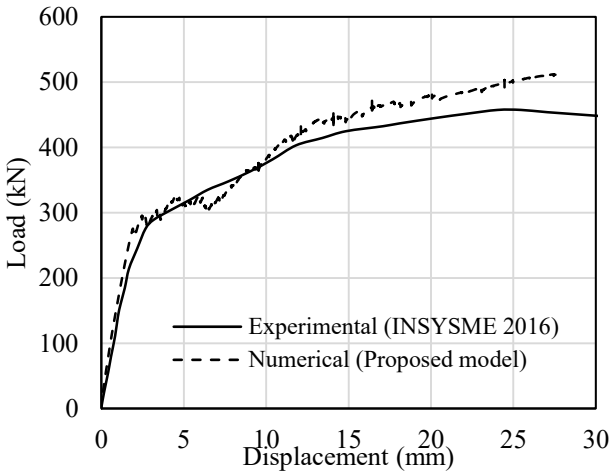

(c)

Figure 3.17. (a) Crack pattern of FC. MJ specimen (INSYSME 2016) at 1.2% drift (b) simulated cracking pattern of the masonry infill wall (c) comparison between numerical and experimental load-displacement curves.

Figure 3.18 (a) shows a contour plot of the minimum principal compressive stresses in the masonry and concrete components for a horizontal displacement of 27.5 mm (1.0% drift). The highest values of the compressive stresses are observed at the top right corner and at the bottom left corner, where they attain the compressive resistance of the bricks (Table 3.4). The principal stresses at the other two corners are tensile ones, as expected. Figure 3.18 (b) shows the plastic strain distribution indicating the cracking of the bricks for the same horizontal displacement. The cracks are localised in correspondence of diagonal bands. Also, the plastic deformations, shown in Figure 3.18(b), are localised along diagonal bands with an inclination angle of about 60 degrees with respect to the horizontal plane.

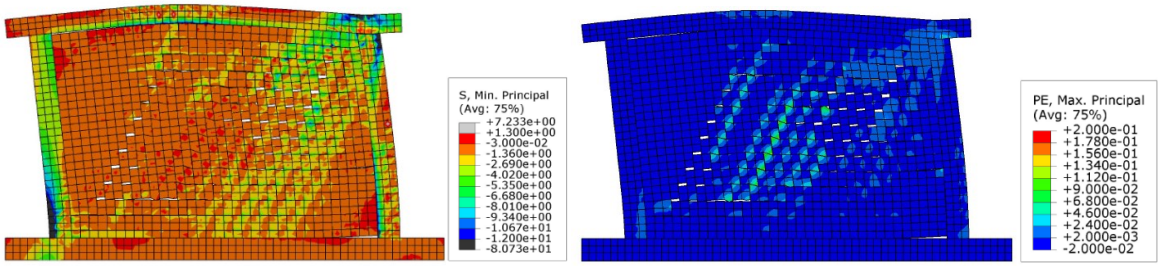

(a) (b)

Figure 3.18. (a) Minimum principal compressive stress (in MPa unit) distribution showing cracking of bricks with (b) plastic strain distribution showing cracking of bricks with mortar joints for a horizontal displacement of 27.5 mm (1.0% drift).

3.3.2.3 Infill frames with rubber joints

The horizontal layers of rubber joints are placed between four courses of the bricks and the vertical layers are introduced between the masonry infill and the frame, as shown in Figure 3.19. They have a thickness of 15 mm and are made with a rubber compound with shear modulus of 0.5MPa. The mortar layers have a maximum thickness t_{m2}= 20 mm and a minimum thickness t_{m1}= 5 mm. The vertical joints are made with a different compound, which comprises recycled styrene-butadiene rubber and ethylene propylene monomer rubber granules anchored to a support of nonwoven fabric (Verlato 2017).

Table 3.6 reports the values of the mechanical parameters describing the horizontal mortar-rubber joints and the vertical rubber joints. These properties of the cohesive interfaces representing the mortar-rubber joints, have been evaluated based on Eqs. 3.3-3.8, assuming an average mortar thickness of 10 mm. It is noteworthy that the value assumed for the mortar layer thickness does not affect significantly the composite joint properties, which are controlled by the rubber layer compliance. The interfaces used to represent these vertical joints are characterised by zero cohesion and zero tensile resistance, and a friction coefficient of 0.31 evaluated experimentally during tests carried out within INSYSME project (INSYSME 2016).

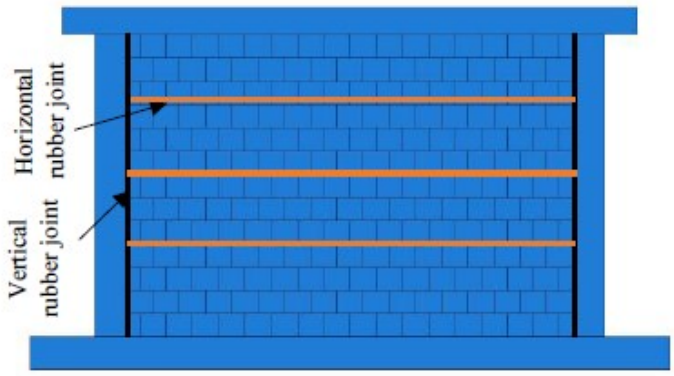

Figure 3.19. Masonry infilled frame with horizontal and vertical rubber joints (INSYSME 2016).

Table 3.6. Interaction properties of the mortar-rubber joints.

Interaction properties	Horizontal joint	Vertical joint				Source
		RJ_H	RJ_HV	RJ_HVH	RJ_HVL	
k_n^{mr} per unit area (N/mm^3)	11.7	200	1.0	10.0	0.1	Eq. 3.3
k_s^{mr} , k_t^{mr} per unit area (N/mm^3)	0.033	-	0	0	0	Eq. 3.7
σ_t (MPa)	0.15	-	0	0	0	Verlato (2017) *
c(MPa)	0.05	0	0	0	0	Verlato (2017) *
μ (-)	0.36	0.4	0.31	0.31	0.31	Verlato (2017)
G_f^I (MPa·mm)	0.005	-	-	-	-	Verlato (2017) *
G_f^{II} (MPa·mm)	0.04	-	-	-	-	Verlato (2017) *

*Not directly measured but assumed based on literature and/or calibrated to provide best fit to results

Figure 3.20 (a) shows the deformed shape of the infilled frame with both horizontal and vertical rubber joints. Overall, the addition of the rubber joints is found to enhance the compliance of the infill wall, and it can be observed that most of the deformation/sliding is located at these joints. Some cracks are observed at the top left corner of the lower portion of the wall, just below the first rubber layer. Other cracks are found on the right side of the top three subpanels. It is noteworthy that all these cracks were also observed experimentally (Verlato 2017). Figure 3.20 (b) compares the load-deflection curve of the bare frame, the frame with traditional infills, and the frame with infill walls and rubber joints. It can be seen that the infilled frame with rubber joints keeps gaining the load up to a displacement of 55mm and then after the strength drops until complete failure in attended. In contrast to the case analysed previously, the frame with the innovative infills is significantly stiffer than the bare frame. Nevertheless, using the rubber joints yields significant reduction of stiffness compared to the case with traditional infills. The model used for the simulation is found to

be quite accurate, with a global force-deflection curve very close to the experimental one (Figure 3.21).

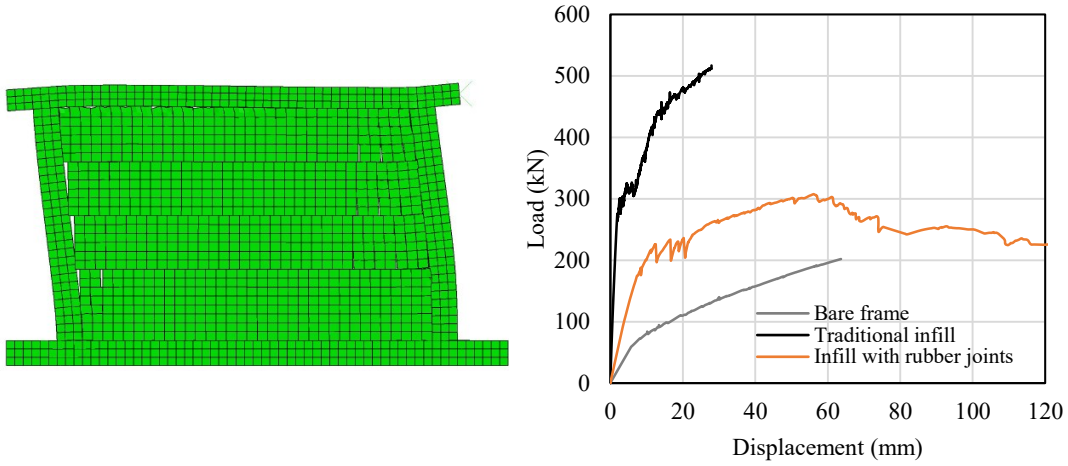

(a) (b)

Figure 3.20. (a) Deformed shape for the case RJ_HV at 55 mm (2.0% drift) (b) comparison between numerical responses of the bare frame, infilled frame with traditional infills and with rubber joints (RJ_HV).

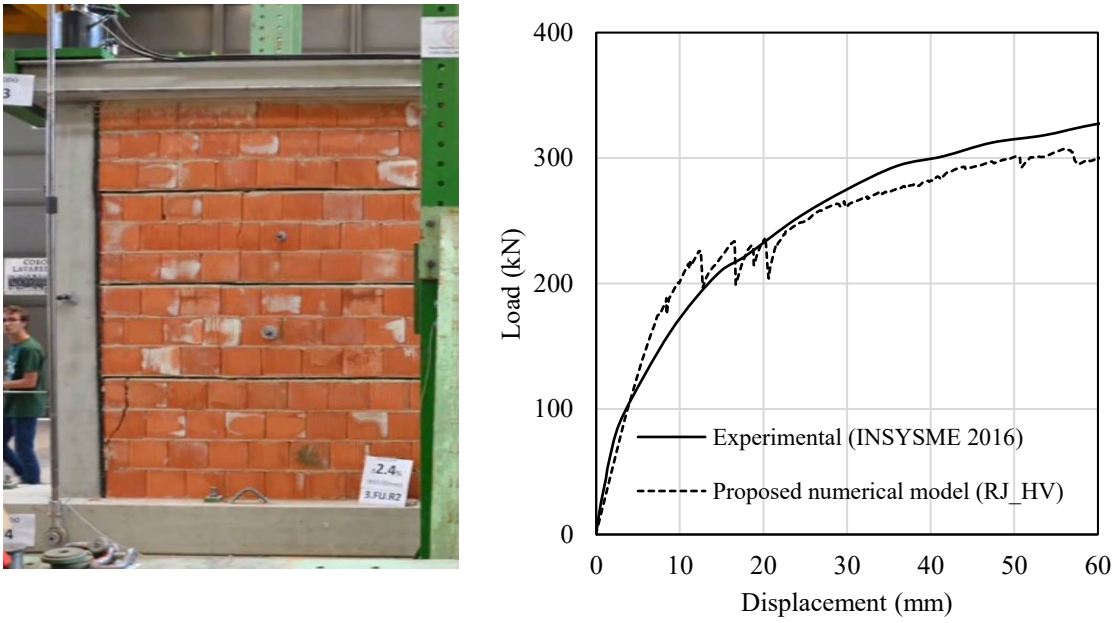

(a) (b)

Figure 3.21. (a) Failed infill with DRES-V2 at 2.4% drift (INSYSME 2016) and (b) load-deflection curve of the system with horizontal and vertical rubber joints

As for the previous case study, a comparison is carried out of the performances obtained considering horizontal rubber joint only and vertical rubber joints with higher and lower stiffness values compared to the reference model. Figure 3.22 and Figure 3.23 show the minimum compressive principal stress distribution for all selected cases, respectively under 1% and 2% imposed drift. It is clearly visible that the frame with vertical rubber joint of lower stiffness is performing better than the other cases (and the traditional infill, see Figure 3.18a) in terms of minimization of the compression stresses in the bricks.

Figure 3.24 and Figure 3.25 show the distribution of plastic strains at 1% and 2% drift limits respectively. The solution with least damage is that corresponding to the lower vertical rubber stiffness (RJ_HVL), which performs significantly better than the frame with traditional infill (Figure 3.18b) and exhibits less cracking in the masonry at high drift levels (Figure 3.25) with larger gaps opening at the interface between the masonry subpanels and the frame compared to the other solutions investigated. The plastic deformations in the frame are also slightly reduced. It can be seen from Figure 3.26 (b) that the present numerical model could successfully predict the failure as seen from the experimental test performed by INSYSME 2016 (See Figure 3.21a). During the experimental test, the formation of a vertical crack in the brick unit in the bottom-most sub-panel and the stress concentrations in the corners of the infill is quite identical to the predicted failure from the present numerical model. The force-displacement curves, presented in Figure 3.26, indicate that the use of rubber joints with low stiffness (case RJ_HVL) also corresponds to a further decrease of global stiffness and strength compared to the reference case (RH_HV).

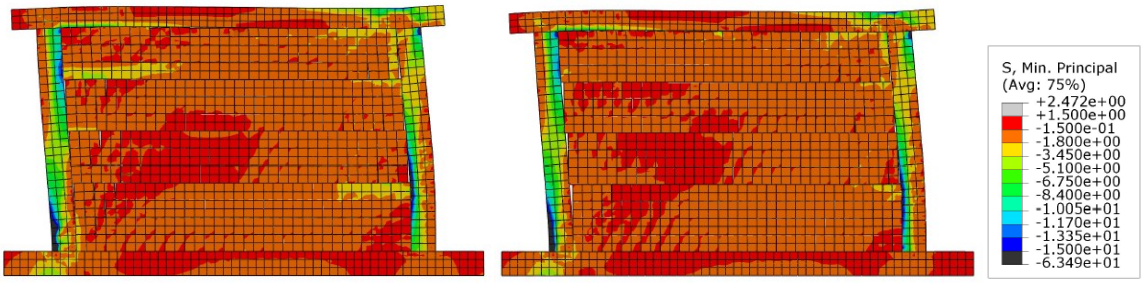

(a) RJ_H (b) RJ_HV

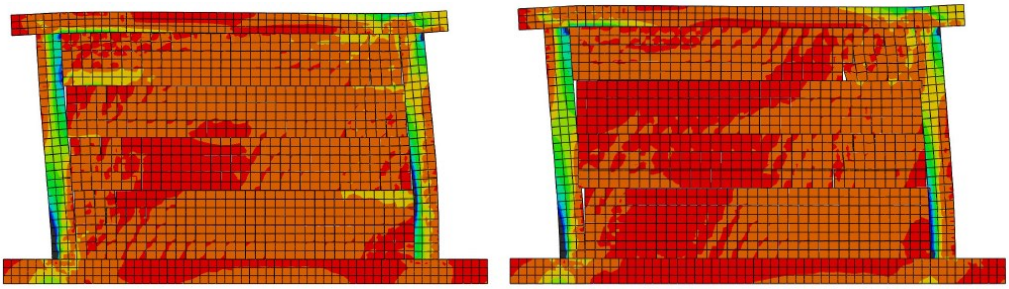

(c) RJ_HVH (d) RJ_HVL

Figure 3.22. Minimum principal compressive stress (in MPa unit) distribution for infilled frame with rubber joints for a horizontal displacement of 27.5 mm (1.0% drift).

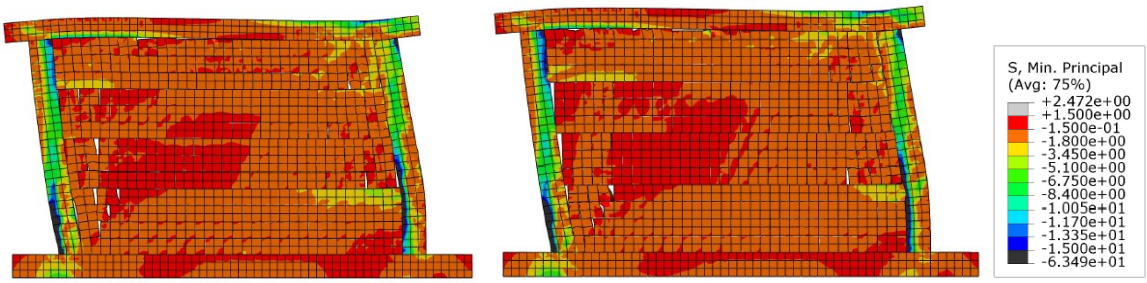

(a) RJ_H (b) RJ_HV

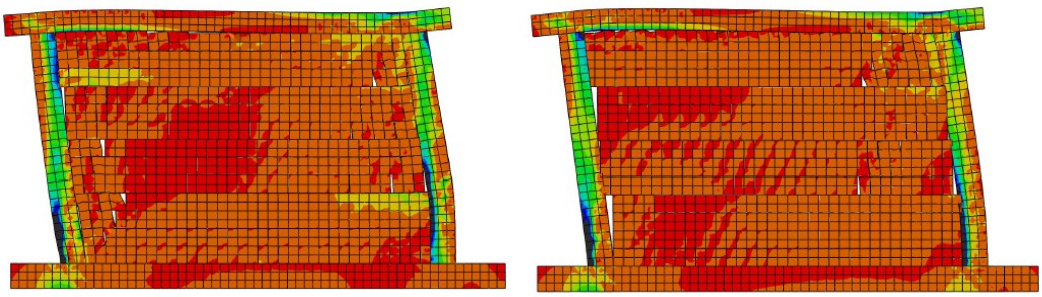

(c) RJ_HVH (d) RJ_HVL

Figure 3.23. Minimum principal compressive stress (in MPa unit) distribution for infilled frame with rubber joints for a horizontal displacement of 55 mm (2.0% drift).

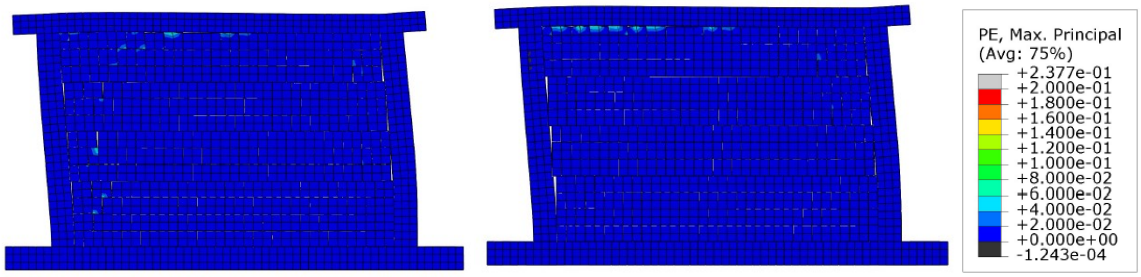

(a) RJ_H (b) RJ_HV

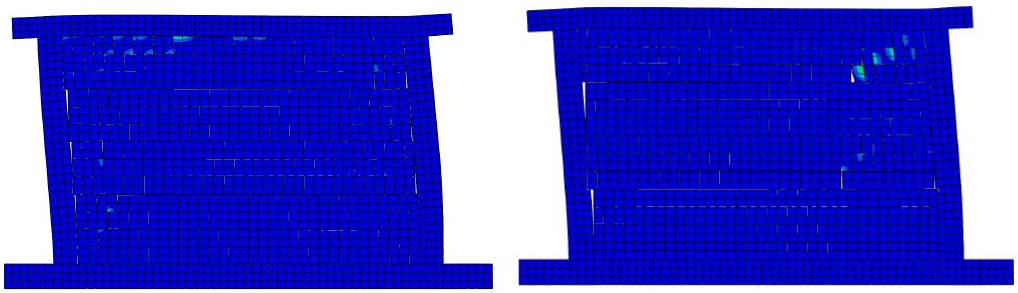

(c) RJ_HVH (d) RJ_HVL

Figure 3.24. Plastic strain contour plots for the case infill wall with rubber joints under a horizontal displacement of 27.5 mm (1.0% drift).

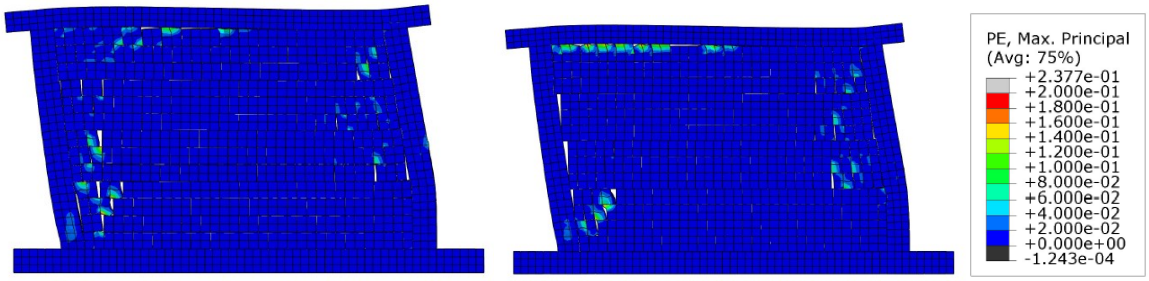

(a) RJ_H (b) RJ_HV

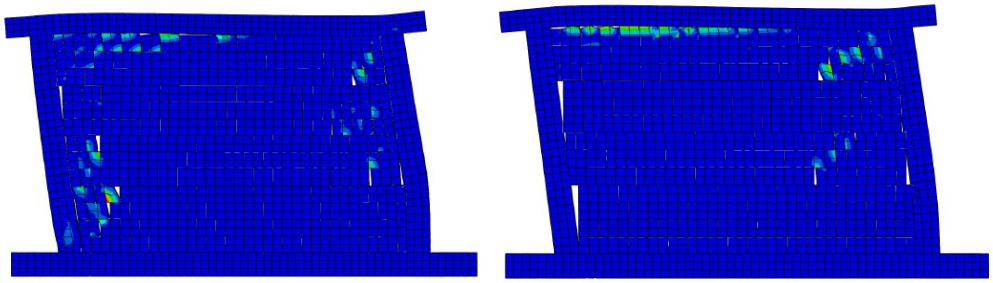

(c) RJ_HVH (d) RJ_HVL

Figure 3.25. Plastic strain contour plots for the case infill wall with rubber joints under a horizontal displacement of 55 mm (2.0% drift).

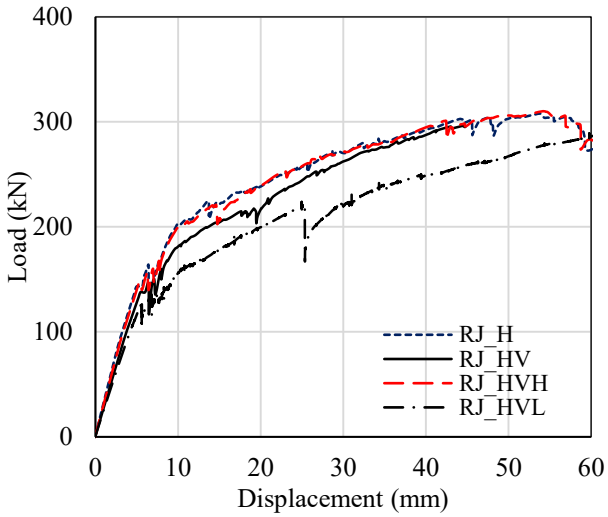

Figure 3.26. Comparison of rubber joints with various layouts and stiffness.

3.4 Summary

In this study, a novel meso-scale approach is developed for simulating the response of RC frames equipped with masonry infill walls and rubber joints under horizontal loads such as those induced by earthquakes. The behaviour of the RC frame is described using solid elements and embedded rebars, whereas the mortar-rubber joints are described by means of zero-thickness interfaces, whose behaviour is calibrated to simulate the in-series arrangement of the components. This approach, employed for the first time to investigate the system at hand, illuminates the response at local level of the components of the system, such as the bricks or the joints. The proposed strategy is validated against experimental results conducted on two case studies; a RC frame with traditional infills and a RC frame with both traditional and TARRC's innovative infills with rubber joints. A good agreement is observed between experimental and numerical results, in terms of global force-displacement response and location of cracks in the bricks.

The study results show that adding the rubber joints significantly increases the compliance of the system, helping to avoid or reduce the damage to the frame and the infills. Moreover, using vertical rubber joints with low stiffness in addition to the horizontal ones further improves the behaviour in terms of reduction of compressive stresses and cracking in the masonry at large displacements, while providing a horizontal force-deflection response similar to the case with only horizontal joints. Even the plastic deformations in the frame can be reduced by using vertical joints with low stiffness.

The proposed modelling strategy can be employed to investigate the optimal combination of strength, deformability and dissipation capacity of the rubber joints for enhancing the seismic performance for a wide variety of infilled frames. It is also useful for calibrating simplified modelling strategies, such as those based on diagonal equivalent struts. Further analyses will be carried out, using the same modelling approach developed here and simplified ones, to evaluate the combined in-plane and out-of-plane behaviour of the system. Moreover, a more complex constitutive model of the joints, describing also the energy dissipation capabilities of the rubber, will be developed and calibrated based on experimental results to investigate the benefits of introducing the rubber joints in terms of enhancement of the global damping capacity of the system.

4 A macro-model for describing the in-plane seismic response of masonry-infilled frames with sliding/flexible joints

4.1 Introduction

Masonry infills are among the most vulnerable components of reinforced concrete (RC) building frames. They are often disregarded in the design stage, and because of this, they often undergo severe cracking and damage even under moderate earthquakes. Their collapse can cause injuries, life losses, and delays in rescue operations and post-earthquake recovery. Many studies (e.g., Del Vecchio et al. 2018; De Risi et al. 2019) have highlighted the considerable economic losses associated with infill walls' damage and have shown that the repair cost of these can be significantly higher than that of structural components.

The improvement of the seismic performance of infill walls and RC infilled frames has been a subject of considerable research in the last decades, with many technical solutions proposed and experimentally evaluated. Some solutions aim at increasing the resistance of the infill (Elgawady et al. 2004; Koutas et al. 2015). However, these techniques are often not cost effective and require the strengthening of the frame members, due to the transmission of increased forces to them from the infills. Alternative solutions have been proposed that aim to increase the flexibility of the infill panel and/or to reduce its interaction with the surrounding frame, through the introduction of sliding joints (Preti et al. 2012; Preti et al. 2015; Morandi et al. 2016; Bolis et al. 2017; Preti and Bolis 2017; Preti et al. 2019; Di Trapani et al. 2020) or flexible/soft layers (Mojsilović et al. 2015; Vögeli et al. 2015; Calabria et al. 2016; Preti et al. 2016; Ahmadi et al. 2017; Petrović et al. 2017) within the panel or between the panel and the surrounding frame. The use of joints, where most of the deformations are localised, allows reducing the stresses, and thus the damage, in the infill panel as well as minimising the interaction between the panel and the surrounding frame. Another benefit brought by the joints is that they permit to control the increase of global stiffness of the infilled frame, which can significantly alter the seismic demand with respect to the bare frame condition. The joints can also contribute to the energy dissipation, reducing

the seismic demand on structural and non-structural components.

The numerical simulation of the seismic performance of infilled frames is a computationally challenging task due to the nonlinearity of the materials involved, the complex interaction between the infills and the main frame structure, and the various possible failure modes that could occur. Different modelling approaches have been proposed, including macro-modelling and micro/meso-scale modelling (Lourenço 1997; Asteris et al. 2011; Caliò and Pantò 2014; Pantò et al. 2017), where some of these approaches have also been applied to model infilled frames with flexible/sliding joints (Mojsilović et al. 2015; Vögeli et al. 2015; Calabria et al. 2016; Preti et al. 2016; Ahmadi et al. 2017; Bolis et al. 2017; Petrović et al. 2017; Preti et al. 2019; Di Trapani et al. 2020).

Detailed numerical analyses involving micro and meso-scale descriptions of masonry can be computationally costly and unsuitable for large scale structures. In this case, macro-models are found to be very appealing due to the reduced number of degrees of freedom and parameters that are required to define them. Many of the simplified models for masonry infilled frames rely on the concept of equivalent strut (Smith and Carter 1970; El-Dakhakhni et al. 2003; Di Trapani et al. 2018). A two-dimensional (2D) discrete macro-element model (DMEM) for infill frames was proposed by Caliò and Pantò (Caliò and Pantò 2014) to avoid the main limitations of the equivalent strut approach. This macro-model, originally proposed for unreinforced masonry buildings (Caliò et al. 2012) has been implemented in the software 3D-Macro (2009) and validated against experimental tests by Marques and Lourenço (2014). More recently, Pantò and Rossi (2019) implemented a simplified version of the DMEM model, already proposed in Caliò and Pantò (2014), but characterised by a limited number of nonlinear links along the interfaces between elements in order to allow its implementation in the FE program OpenSees (Mazzoni et al. 2006).

In the context of simplified modelling of RC infill frames with sliding joints, Preti et al. (2019) developed an analytical formulation for calibrating the properties of an equivalent strut based on the geometrical and mechanical properties of the infill panel and of the sliding joints. This model was used by Di Trapani et al. (2020) to assess the benefits of using sliding joints in improving the seismic performance of masonry-infilled RC frames. To date, no study has investigated the use of 2D macro-models for investigating the behaviour of RC frames with sliding/flexible joints under in-plane loading.

4.2 The proposed modelling strategy

This section illustrates the modelling strategy developed for describing the hysteretic behaviour of a masonry-infilled frame with flexible/sliding joints that are horizontally placed between the infill sub-panels and vertically at the column-infill interfaces (see Figure 4.1). The same modelling strategy can also be used to describe alternative configurations (e.g., Preti and Bolis 2017) not explicitly addressed in this study.

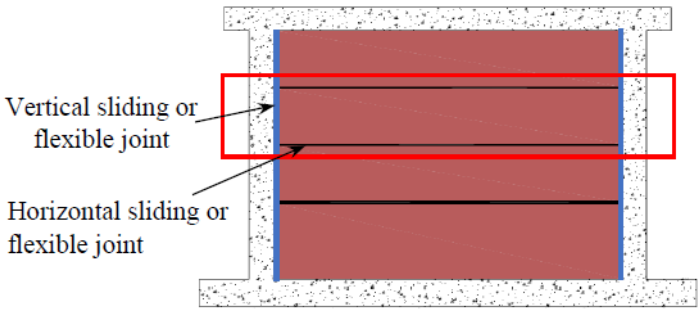

Figure 4.1. Reinforced concrete infill frame equipped with horizontal and vertical sliding/flexible joints.

The proposed modelling approach is based on the discrete macro-element method (DMEM) originally developed by Caliò and Pantò (2014), subsequently implemented in a simplified version in OpenSees by Pantò and Rossi (2019). The proposed model can be represented by an equivalent mechanical scheme consisting in an articulated quadrilateral (Figure 4.2a). Two uni-directional diagonal links and eight bi-directional perimetral links describe the shear and flexural behaviour of the represented masonry portion of masonry, respectively. The latter 2D links, also describe the normal and tangential behaviour of the infill-frame interfaces. Following the simplified formulation developed in Pantò and Rossi (2019), the two 2D links placed on each rigid edge of the panel allow the macro-element to interact with adjacent macro-elements or to frame beam/column elements. The deformability of the 2D links is concentrated in two zero-length nonlinear coupled springs connected in-series with rigid offsets (Δ_i), with i=1…4, shown in Figure 4.2a. Each link is located at one-fourth of the panel edge length (b_p or h_p) from the vertexes (V_i) ($i=1\ldots 4$), which allow for a geometrically consistent description of the interaction between infills and beam or column elements (Pantò and Rossi 2019). Each macro-element possesses eight nodes (n_i), with $i=1\ldots8$, connecting the macro-element with the adjacent macro-elements and frame elements (Figure 4.2b). Each macro-element is kinematically characterised by

twenty-eight degrees of freedom (Figure 4.2a), twenty-four of which are associated with the translations and rotations of nodes (u_i, v_i, ϕ_i) with i=1…8, and four (w_i … w_4) describing the rigid motion and shear-deformation of the panel. These dofs can be kinematically related to 17 generalised deformations: 16 deformations related to the normal (d_{n1}… d_{n8}) and tangential (d_{s1}… d_{s8}) deformations of the 2D links and the deformation of the internal diagonal link (d_d), shown in Figure 4.2b.

In the case of traditional infills, the response of the contact links along the normal direction describes the flexural response of the represented portion of the infill. The link shear response describes the sliding the infill or between the infills and the surrounding frame members. The diagonal link describes the diagonal shear failure of the infill. Being the infill built after the surrounding frame, it does not support vertical loads other than its self-weight. Therefore, it is assumed that the uniaxial response of the diagonal link depends only on the shear deformation of the articulated quadrilateral. At the same time, it is independent on the panel, vertical and horizontal, compression.

In the case of infills with sliding/flexible joints, the macro-element link properties depend on the type of discretisation adopted. For example, in Figure 4.2c the number of macro-elements is equal to the number of subpanels identified by the horizontal joints (Figure 4.1). Thus, each macro-element describes a masonry subpanel surrounded by flexible/sliding joints. The normal component of the 2D contact links describes the tensile/compressive behaviour of the masonry subpanels and of the sliding/flexible joints, working as a series mechanical system, whereas the tangential component of the 2D contact links describes the sliding of the low-friction joints or the shear displacement of the sliding/flexible joint. The diagonal link simulates the diagonal shear behaviour of the masonry subpanels, and its properties are not affected by the sliding/flexible joints. The next subsections describe the calibration of the macro-element properties for this type of discretisation. It is noteworthy that each subpanel could be discretised into more than one macro-element (Figure 4.2d). The properties of the links for the macro-elements used in Figure 4.2d can be found by combining the modelling strategy described in the following subsections with the ones already developed in Pantò and Rossi (2019) for the case of traditional masonry infills. According to the original formulation proposed by Caliò and Pantò (2014), a single macro-element could be employed for describing the entire infill-joint system. However, in presence of sliding/flexible joints, it is necessary to consider a mesh of macro-elements, consistent with the distribution of the joints, in order to describe

the interaction between adjacent horizontal subpanels and between the subpanels and the surrounding frame.

The simplified hypothesis of connecting each panel edge by two links may introduce an approximation in describing the local behaviour of the infill and its interaction with the frame members. However, as evidenced in Pantò and Rossi (2019) and confirmed by the results presented in this study, the proposed model can describe the global response of infilled frames with a reasonable level of accuracy, even employing a coarse mesh of macro-elements.

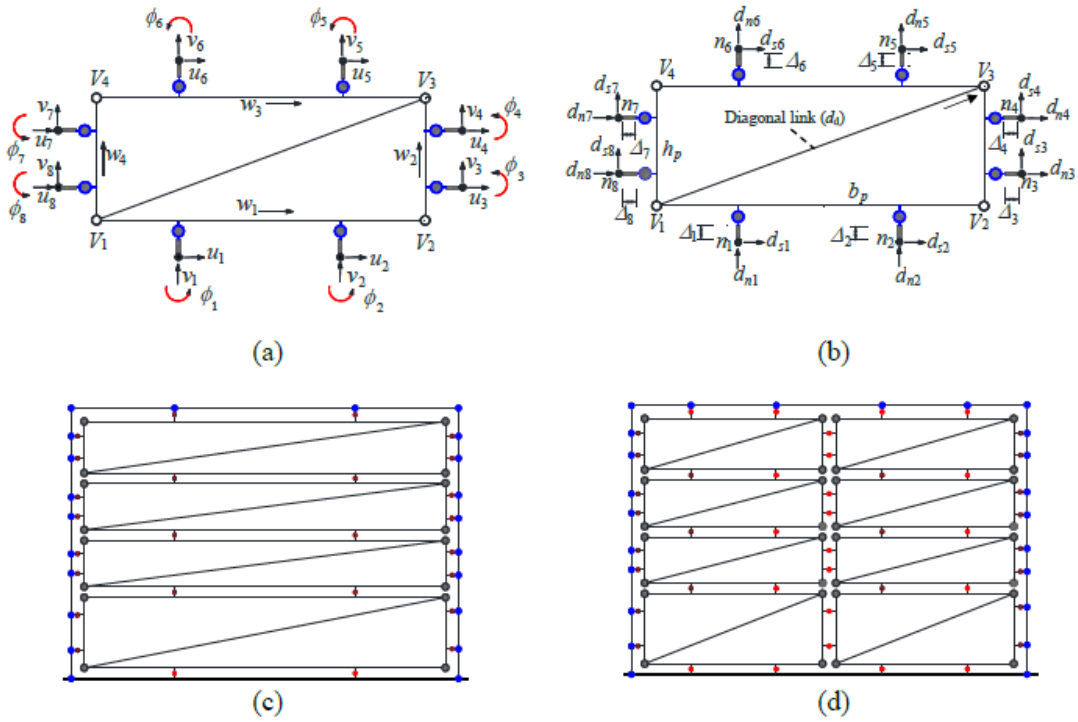

Figure 4.2. (a) Degrees of freedom of the macro-element, (b) generalised deformations, (c) discretisation of the infill with joints into minimum number of subpanels, (d) more refined discretisation.

4.2.1 The 2D Contact link

Figure 4.3a shows the equivalent mechanical scheme of the 2D nonlinear link. The relative displacements of the link along the normal and tangential direction, collected in the vector q = [d_n d_s], and the dual internal forces, collected in vector Q = [F_n F_s], are related through the expression δQ = Kδq where δ denotes the variation operator, and K denotes the tangent stiffness matrix of the link, expressed as follows:

$$\mathbf{K} = \begin{pmatrix} K_n & 0 \\ 0 & K_s \end{pmatrix} \qquad \text{Eq. 4.1}$$

where K_n and K_s are the tangent stiffnesses of the link in the normal and tangential directions, respectively.

The Concrete02 material model, implemented in OpenSees (Mazzoni et al. 2006), is used to describe the normal response of the contact link. The nonlinear elastoplastic model employed in Kent and Park (1971) is used to simulate the masonry response in compression, whereas a bi-linear constitutive law with linear strength degradation simulates the response in tension. These constitutive model's efficacy allow for cyclic stiffness degradation with the increase of the normal strain. The essential parameters to describe the normal response envelope of the 2D link Figure 4.2 (b), are: the initial elastic stiffness (K_{nm}), the maximum compressive force (F_{cm}), the maximum tensile force (F_{tm}), the ultimate displacement in compression (d_{cm}), the ultimate displacement in tension (d_{tm}) and the residual compressive strength (F_{rm}). The parameter λ represents the ratio between the unloading stiffness and the initial stiffness and controls the cyclic material behaviour

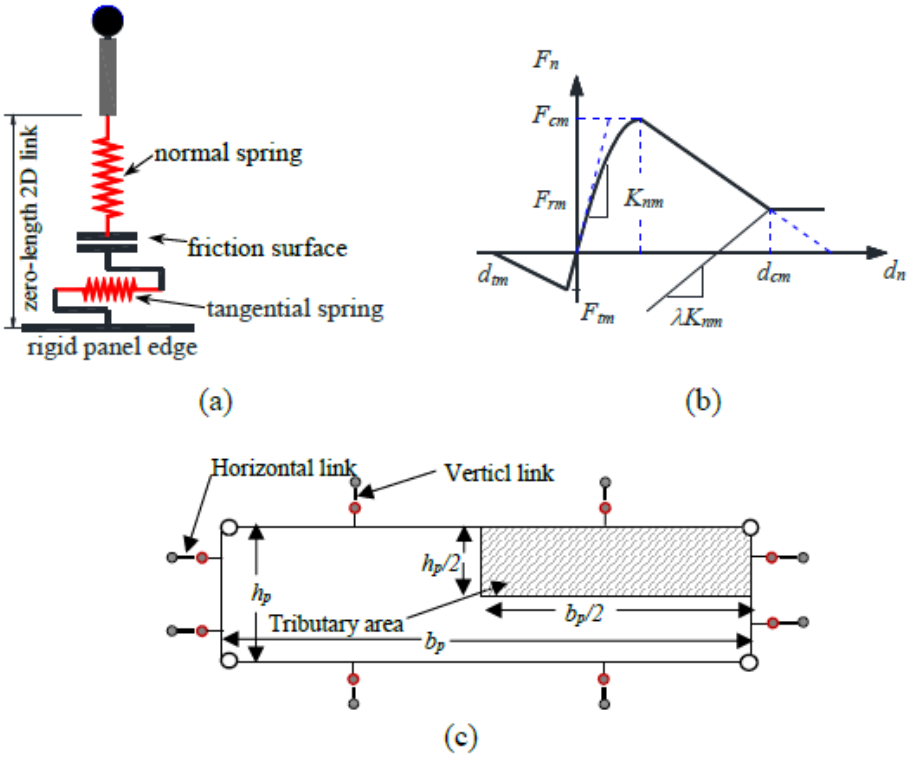

Figure 4.3. (a) Equivalent mechanical scheme of 2D contact link, (b) cyclic response in normal direction, and (c) tributary masonry area.

In general, the values of the parameters of Figure 4.3(b) depend on the geometry of the macro-element and on the mechanical properties of the masonry infill and of the flexible/sliding joints, which form a series mechanical system. The properties defining the normal behaviour of the sliding/flexible joints, assuming an elastic-perfectly plastic constitutive law, the initial normal stiffness per unit area k_{nj}, the tensile strength k_{tj}, and the compressive strength f_{cj}. The following mechanical parameters are used to characterise the constitutive behaviour of the masonry, considered as a homogenised continuous orthotropic material characterised along each direction of orthotropy by: Young modulus (E_m), compression and tensile strengths (f_{cm}, f_{tm}) and the corresponding ultimate strains in tension and compression (ε_{cu}, ε_{tu}) and a residual compressive strength f_{rm}. A tributary panel area (see Figure 4.3c) is considered for defining the contribution of the masonry subpanel. Let w_p, b_p and h_p denote respectively the thickness, width and height of the subpanel contributing to the normal link. In order to define the normal link properties (Figure 4.2b), the continuous masonry portion of the subpanel is replaced by an equivalent discrete one, whose properties are described in Table 4.1, where A_p and l_p represent respectively the cross-section area and the length of the tributary volume of the subpanel associated with the link. These are equal to respectively $w_p b_p / 2$ and $h_p / 2$ in the case of the vertical contact link of Figure 4.3(b). If flexible/sliding joints are present at the edge of the panel, then their properties must be combined with those of Table 4.1, using a series mechanical model representation.

Table 4.1. Mechanical parameters of the normal response of the equivalent spring representing the masonry panel (after Pantò and Rossi 2019).

Initial stiffness	Maximum compressive force	Maximum tensile force	Residual compressive force	Ultimate compression. displacement	Ultimate tensile displacement
$K_{nm} = \frac{E_m A_p}{l_p}$	$F_{cm} = f_{cm} A_p$	$F_{tm} = f_{tm} A_p$	$F_{rm} = f_{rm} A_p$	$d_{cm} = \varepsilon_{cu} l_p$	$d_{tm} = \varepsilon_{tu} l_p$

In the case of a macro-element representing a subpanel interacting with the frame through a horizontal or vertical sliding/flexible joint, the normal stiffness of the contact link, evaluated combining in series the stiffness representing the masonry panel (K_{nm}), and the normal stiffness of the joint (K_{nj}), is obtained as follows:

$$K_n = \frac{K_{nm} K_{nj}}{K_{nm} + K_{nj}} \qquad \text{Eq. 4.2}$$

The stiffness of the joint K_{nj} can be evaluated by multiplying the stiffness per unit area k_{nj} by the tributary area of the joint A_p.

In the case of two macro-elements representing two subpanels separated by a sliding joint, each panel link is associated to the deformability of masonry and of half joint. Eq. 4.2 becomes:

$$K_n = \frac{2K_{nm}K_{nj}}{K_{nm} + 2K_{nj}} \qquad \text{Eq. 4.3}$$

The tensile (compressive) resistance of the series system is equal to the lowest value among the tensile (compressive) resistance of the two components.

The shear response of the contact links of the macro-element is assumed to be controlled by the mechanical behaviour of the joints at the edges of the macro-element. In the case of rubber joints, the shear stiffness of the 2D link K_s coincides with that of the joint K_{sj}, which can be taken equal to the rubber stiffness assuming that the rubber compliance is much higher than that of the mortar joints (see Dhir et al. 2021). The behaviour of rubber in simple shear is very complicated, since it is rate-dependent, amplitude-dependent, and characterised by the Mullins effect (Tubaldi et al. 2017). In this study, a linearised behaviour (constant stiffness) is considered for simplicity. In the case of sliding joints, a very high value of K_{sj} can be assumed until sliding takes place. The tangent shear stiffness can be assumed to be zero during sliding.

The shear capacity of the contact links is described by an elasto-plastic model with an associated Mohr-Coulomb yield surface characterised by the following parameters: the cohesion c_j, the friction coefficient μ_j, the tributary contact area of the link A_p. For simplicity, the values of c and μ are assumed to be constant and the unloading/reloading tangential stiffness is assumed equal to the initial elastic one. It is noteworthy that also in the case of rubber joints sliding may occur following bond failure (usually at the rubber joint-mortar interface).

4.2.2 The Diagonal link

As already discussed above, it is assumed that the minimum number of macro-elements is equal to the number of subpanels identified by the horizontal joints. According to this strategy, the diagonal link represents the shear behaviour of the masonry subpanel, since the deformability of the flexible/sliding joints is described entirely by the 2D contact links along the interfaces. The uniaxial material Pinching4 which is already included in OpenSees

(Mazzoni et al. 2006) is used to simulate the axial force-displacement (F_d, d_d) response of the diagonal link shown in Figure 4.4a (Furtado et al. 2015; Mohammad et al. 2017). The constitutive law of the diagonal link is assumed not to depend on the compression forces acting on the vertical and horizontal edges of the panel. It only depends on the shear deformation of the articulated quadrilateral. This is a simplification that is not expected to lead to significant errors in the response assessment. The envelope curve describing this response is defined by eight parameters, i.e., F_{1d}, d_{1d}; F_{2d}, d_{2d}; F_{3d}, d_{3d}; F_{4d}, d_{4d}, which are indicated in Figure 4.4(b). These parameters are calibrated according to the macroscopic shear parameters of masonry, which can be identified by performing laboratory tests on masonry panels, and the panel geometry. The calibration procedure consists in imposing an equivalence between the discrete model and an equivalent continuous subpanel subjected to a pure shear stress state (Pantò and Rossi 2019). The results are summarised in Table 4.2. More specifically, the mechanical behaviour of masonry is characterised by the initial shear modulus (G_m) and the shear stress corresponding to cracking (τ_{cr}); the stress/drift at the yield (τ_y, γ_y), peak (τ_0, γ_0) and residual (τ_R, γ_r) strengths. Each strength describes a specific macroscopic level of damage. In particular, the cracking strength describes the end of the elastic response of the infill, corresponding to the activation of microcracks. In addition, the yield strength allows a better description of the change of infill shear stiffness due to the opening of macrocracks.

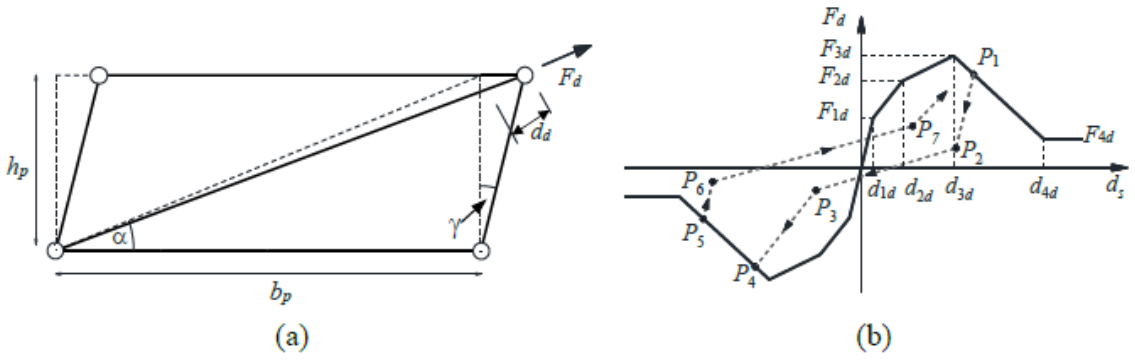

Figure 4.4. (a) Mechanical scheme and (b) cyclic response of the diagonal link.

Table 4.2. Mechanical parameters of the response envelope of the diagonal link (Pantò and Rossi 2019).

Cracking force	$F_{1d} = \frac{\tau_{cr} w_p b_p}{\cos\alpha}$	Initial stiffness	$K_{d_0} = \frac{G_m w_p b_p}{h_p \cos^2\alpha}$
Yielding force	$F_{2d} = \frac{\tau_y w_p b_p}{\cos\alpha}$	Yielding displacement	$d_{2d} = h_p \gamma_y \cos\alpha$
Peak force	$F_{3d} = \frac{\tau_0 w_p b_p}{\cos\alpha}$	Peak-force displacement	$d_{3d} = h_p \gamma_0 \cos\alpha$
Residual force	$F_{4d} = \frac{\tau_u w_p b_p}{\cos\alpha}$	Residual-force displacement	$d_{4d} = h_p \gamma_r \cos\alpha$

*α = arctan (h_p/b_p) is the angle between the diagonal and the first edge of the panel

A cyclic constitutive law with a pinching effect, already implemented in OpenSees (Mazzoni et al. 2006) and characterised by a trilinear unload-reload path (Pantò and Rossi 2019), is adopted. The model takes into account the degradation of the reloading stiffness and strength by means of two damage indexes, D_k and D_r, whose evolution is described by the following equation:

$$D_h = 1 - \alpha_h \left[E_{cum} / \left(\eta_h E_{mon} \right) \right]^{\beta_h} \leq D_{h,\lim} \; h=k,\, r \qquad \text{Eq. 4.4}$$

where the parameters α_h, β_h and η_h are constitutive parameters of the damage model, $D_{k,\,\lim}$ and $D_{r,\,\lim}$ the two limit values of damage indexes, E_{cum} the cumulative energy at the current step of the analysis, and E_{mon} is the ultimate cumulative energy corresponding to a monotonic process. The parameters of the cyclic and damage models can be adjusted to obtain the best fit to the experimental results.

4.3 Model validation

In this section, a validation study is conducted in view of the experimental tests performed by Calvi and Bolognini (2001) on a RC frame infilled with traditional hollow bricks under in-plane load (case study I). A further validation is then performed considering the numerical investigation performed with an advanced 2D modelling approach by Bolis et al. (2017) (case study II) on the same bare frame, with different infill typology and with the addition of sliding joints. Finally, the experimental tests performed within the INSYSME project (INSYSME 2016) on an RC frame with traditional masonry infills and

masonry infills with mortar-rubber joints under in-plane loading (case study III) are considered to further demonstrate the abilities of the proposed modelling approach.

4.3.1 Case Study I: Traditional Infill (after Calvi and Bolognini 2001)

The first case study consists in a masonry-infilled RC frame experimentally tested by Calvi and Bolognini (2001). Figure 4.5 provides some details of the frame and masonry infill, including the concrete member sizes, diameters of the steel rebars and masonry block dimensions. Perforated clay blocks were selected (typical of European earthquake-prone countries) and laid with holes running horizontally. The bed and head joints are 10 mm thick. Further details regarding the prototype are available in Calvi and Bolognini (2001). The experimental tests were conducted on the bare frame (BF) and the frame with traditional infills (TIF) subjected to in-plane loading. In the tests, vertical loads (400 kN) were initially applied at the top of the two columns to simulate the effect of permanent loads acting on the frame, followed by an in-plane horizontal load, monotonic or cyclic, applied at the beam's left extremity, as shown in Figure 4.5. Forced-based non-linear beam elements with two Legendre integration points are used to describe both the beams and columns, with the cross-sections discretised into fibres. The discretisation of the frame elements depends on that of the infill. In particular, since a single macro-element is used for the infill, each frame element of the RC frame is subdivided into three elements to allow the connection of the frame elements to the external nodes of the infill macro-element.

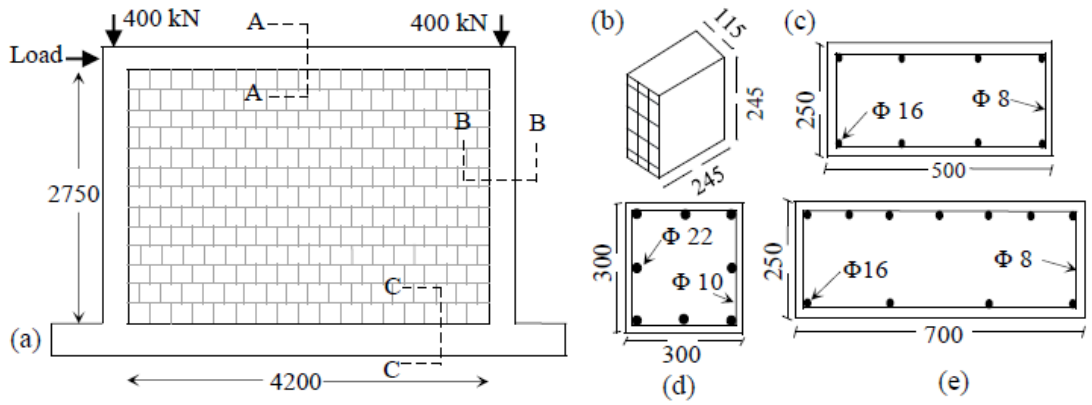

Figure 4.5. Geometric details (dimensions in mm) of (a) the tested infilled frame (b) the perforated clay block units, (c) top beam (section A-A), (d) column (section B-B), and (e) top beam (section C-C).

Table 4.3 reports the main mechanical properties of the concrete and steel reinforcement used for the RC frame members. Table 4.4 reports the parameters characterising the normal behaviour of masonry panel along the horizontal and vertical direction. Table 4.5 reports the properties of the frame-infill interfaces, namely column-masonry (CM), bottom beam-masonry (BBM), top beam-masonry (TBM), panel-panel in horizontal direction (PPH), and panel-panel in vertical direction (PPV). Table 4.6 contains the parameters that define the diagonal link envelope curve. The values of the properties displayed in Table 4.3- Table 4.6 are based on the reported material properties of concrete and steel, on the experimental tests on masonry panels carried out by Calvi and Bolognini (2001), and on the parameters adopted by Bolis et al. (2017) to simulate these tests. The values of the properties displayed in Table 4.3-Table 4.6 are based on the reported material properties of concrete and steel, on the experimental tests on masonry panels carried out by Calvi and Bolognini (2001), and on the parameters adopted by Bolis et al. (2017) to simulate these tests. G_m comes from the value of E_m assuming a poisson's ratio of 0.2 (Pantò and Rossi 2019). The values of some parameters, such as those defining the cracking and yield point, have been chosen among a range of possible values to provide the best fit to the experimental results.

Table 4.3. Mechanical properties of concrete and reinforcing steel.

Mechanical properties	Concrete	Steel reinforcement	Source
Young modulus, E [MPa]	22000	210000	(Calvi and Bolognini 2001)
Poisson ratio, v [-]	0.15	0.3	(Calvi and Bolognini 2001)
Compressive strength, f_c [MPa]	29.32 (column), 34.56 (beam)	-	(Calvi and Bolognini 2001)
Yield strength [MPa]	-	557	(Calvi and Bolognini 2001)
Tensile strength f_t [MPa]	3.9	-	(Calvi and Bolognini 2001)
Post-elastic to elastic stiffness ratio	-	0.002	(Bolis et al 2017)

Table 4.4. Mechanical parameters of the masonry for defining the contact normal links.

Direction	E_m [MPa]	f_{cm} [MPa]	f_{tm} [MPa]	f_{rm} [MPa]	ε_{cu} [-]	ε_{tu} [-]	λ
Horizontal	991	1.11	0.10	0.20	0.4	0.002	0.1
Vertical	1873	1.10	0.52	0.22	0.4	0.006	0.1

Table 4.5. Mechanical parameters of the contact links in shear describing the frame-infill interaction.

Parameter	CM	BBM	TBM	Source
k_j [N/mm^3]	150	200	100	Proposed model
c_j [MPa]	0.41	0.41	0.41	(Calvi and Bolognini 2001; Bolis et al. 2017)
μ_j [-]	0.8	1.0	0.4	(Calvi and Bolognini 2001; Bolis et al. 2017)

Table 4.6. Mechanical parameters of the masonry for defining the response envelope of the diagonal link.

G_m, Shear modulus [MPa]	τ_{cr}, Cracking stress [MPa]	τ_y, Yielding sterss [MPa]	τ_0, Peak force [MPa]	τ_r, Residual force [MPa]	γ_{cr}, diagonal shear drift [-]	γ_y, Yield shear drift [-]	γ_0, Peak shear drift t [-]	γ_r, Residual shear drift [-]
418	0.236	0.329	0.364	0.109	0.00025	0.00172	0.00343	0.01098

In Figure 4.6(a), the monotonic force-displacement response of the bare frame obtained by the proposed model (BF_MO) is compared with the experimental curve which is the is the envelope of the first cycle responses obtained by Calvi and Bolognini (2001) and the numerical response obtained by Bolis et al. (2017) using the finite-element analysis software FEAP (Taylor 2008). The load-displacement curves (experimental and numerical) are plotted for a horizontal displacement up to 110 mm, which corresponds to 4% inter-storey drift. A satisfactory agreement is observed although the initial stiffness of the system is slightly overestimated by the proposed model.

and the experimental peak load. This may be due the assumption of a rigid bond between the steel reinforcement and the concrete. Figure 4.6 (b) shows the cyclic response of the bare frame obtained using the proposed modelling approach (BF_CY) compared to the experimental response (Calvi and Bolognini 2001) and the monotonic response (BF_MO).

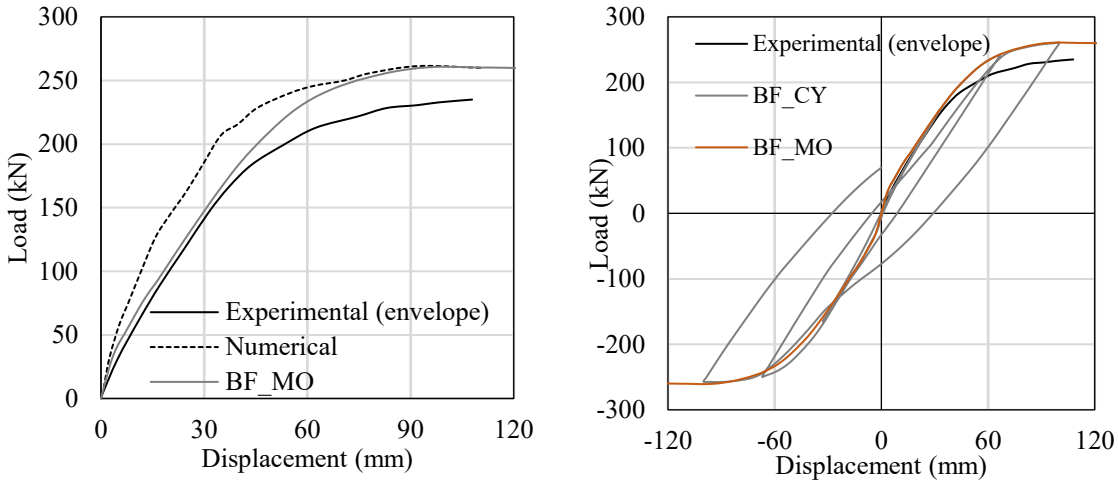

(a) (b)

Figure 4.6. Comparison between numerical and experimental load-displacement curves for bare frames against (a) monotonic and (b) cyclic loading.

Figure 4.7 (a) illustrates and compares the experimental and numerical force-displacement curves of the traditional infilled frame subjected to monotonic loading (TIF_MO). Again, the proposed model describes with good accuracy the initial as well as the post-peak behaviour of the system, up to a displacement of 25 mm. Beyond this value, both the proposed model and the model developed by Bolis et al. (2017) exhibit a hardening behaviour. This may be due to the numerical models overestimating the strength of the frame and the infills being not completely damaged at this displacement level. Figure 4.7 (b) illustrates the hysteretic response of the bare and of the infilled frame (TIF_CY). It can be observed that after a few cycles of deformation, the response of the infill frame tends to that of the bare frame due to the progressive damage accumulated in the infill. The response of the TIF_CY model is compared with that of the bare frame (BF_MO) and of the infilled frame (TIF_MO) under monotonic loading. A significant degradation of stiffness and a progressive reduction of strength is observed due to cyclic loading. This kind of behaviour strongly influences the earthquake response of infilled frame structures.

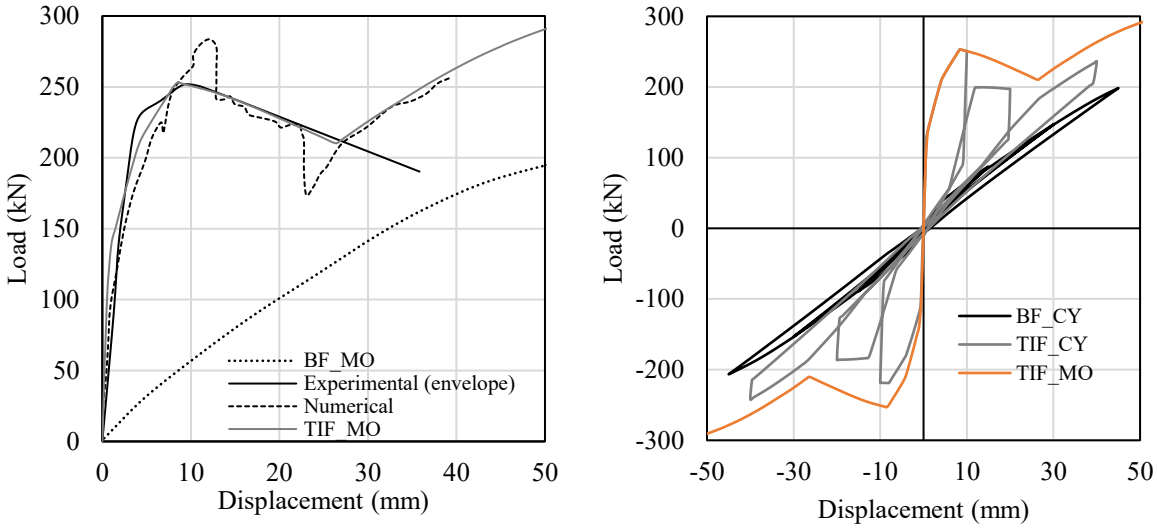

(a) (b)

Figure 4.7. Load-displacement curves of infilled frames against (a) monotonic and (b) cyclic loading.

4.3.2 Case Study II: Frame with Infill and Sliding Joints (after Bolis et al. 2017)

The capability of the proposed modelling approach to describe the behaviour of an infill with sliding joints is assessed here considering the numerical tests carried out by Bolis et al. (2017) on the RC frame of Calvi and Bolognini (2001) infilled with two different types of panels, namely a traditional one and an innovative one with sliding joints (Figure 4.8a). The infill consists of a 14-course hollow clay brick (Figure 4.8a) masonry panel arranged in a running bond pattern laid such a way that the hole axes are parallel to the vertical direction (Figure 4.8b). The bed joints and head joints are fully filled with 10 mm thick mortar. In the case of the innovative infill, the vertical and horizontal sliding joints are made using wooden boards and polyethylene sheets that reduce the friction between the boards and the masonry. The horizontal joints (Figure 4.8c) divide the infill in four subpanels. Figure 4.8 (d) illustrates the sliding vertical joints, which also present a shear key to transfer to the columns the out-of-plane forces acting on the infill.

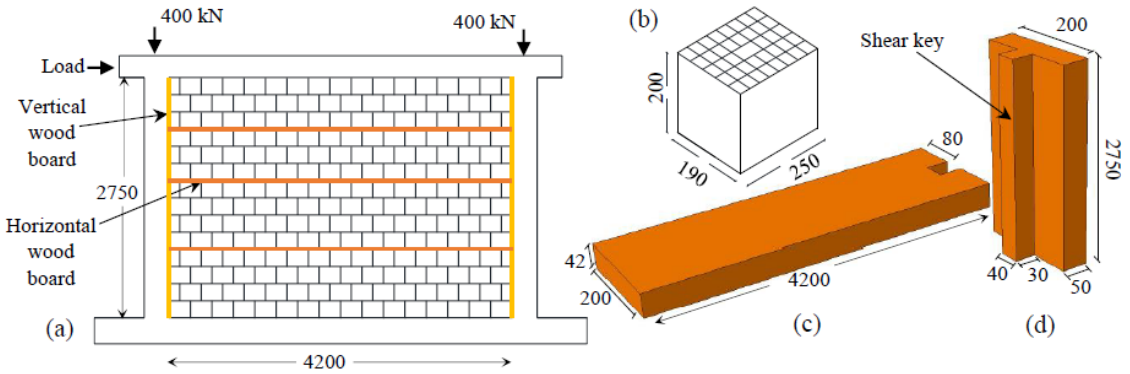

Figure 4.8. Infilled frame incorporating the proposed construction technique showing the connection details (a) Infill with sliding mechanism, (b) hollow clay brick, (c) horizontal wooden board, and (d) lateral wooden board (measures in mm).

The properties of the macro-elements, describing the infill subpanels and the joints, are calibrated using the results from the material tests presented in Bolis et al. (2015). Table 4.7-Table 4.9 show the mechanical parameters characterising the normal and shear responses of the contact links, the infill-frame interfaces and the diagonal link, for the case of traditional infill.

Table 4.7. Mechanical parameters of the masonry for defining the contact normal links.

	E_m [MPa]	f_{cm} [MPa]	f_{tm} [MPa]	f_{rm} [MPa]	ε_{cu} [-]	ε_{tu} [-]	λ
Horizontal	4408	2.70	0.52	0.54	0.4	0.0030	0.1
Vertical	16148	7.28	0.63	1.52	0.4	0.0008	0.1

Table 4.8. Mechanical parameters of the contact links in shear describing the frame-infill interaction.

Interaction Properties	CM	BBM	TBM	PPH	PPV	Source
k_j (N/mm^3)	150	200	100	200	150	Proposed model
c_j [MPa]	0.20	0.41	0.20	0.41	0.41	(Calvi and Bolognini 2001; Verlato 2017)
μ_j (-)	0.75	0.85	0.75	0.85	0.75	(Calvi and Bolognini 2001; Verlato 2017)

Table 4.9. Mechanical parameters for defining the response envelope of the diagonal link.

G_m [MPa]	τ_{cr} [MPa]	τ_y [MPa]	τ_0 [MPa]	τ_r [MPa]	γ_{cr} [-]	γ_y [-]	γ_0 [-]	γ_r [-]
2998	0.468	0.654	0.720	0.072	0.0043	0.0001	0.0021	0.0216

Figure 4.9 (a) shows the force-displacement curves for the RC frame with traditional infill under monotonic loading by Bolis et al. (2017) and according to the proposed modelling strategy (TIF). Different discretisation of the masonry panel is considered in addition to the case of a single macro-element. These include the case of a mesh of 4 macro-elements along the vertical direction (4x1 mesh) as in Figure 4.2 (c) and the case of a 4x2 mesh as in Figure 4.2 (d).

The numerical response of the bare frame obtained by Bolis et al. (2017) is also shown in the figure for comparison. The proposed models provide results that are in quite good agreement with the results obtained with the more computationally expensive model of Bolis et al (2017). Moreover, the global response of the system is not significantly affected by the infill mesh discretisation. Increasing the number of elements, the model maintains the same initial stiffness and the same strength, whereas a slightly different stiffness can be observed in the nonlinear response as well as in the residual strength. Figure 4.9 (b) shows the hysteretic response of the system with traditional infills, evaluated by imposing cyclic displacement inputs with increasing amplitude. The cyclic response of the infilled frame (TIF_CY) is compared with the cyclic response of the bare frame (BF_CY) and the monotonic capacity curve of the infilled frame (TIF_MO). A slight reduction in terms of lateral stiffness and peak load is observed due to the degradation under cyclic loading.

The normal behaviour of the sliding joints is defined by the initial normal stiffness per unit area k_{nj} = 60.7 N/mm^3, the tensile strength f_{tj} = 0 MPa, and the compressive strength f_{cj} = 6.74 MPa. The values of the mechanical parameters of the masonry subpanel defining the contact normal links properties are presented in Table 4.10. Table 4.11 report the properties of the joints defining the contact normal links and contact interfaces for the case of the modified masonry infill with the sliding joints (SJ), corresponding to model J3.LB in Bolis et al. (2017).

Figure 4.10 (a) shows the monotonic response obtained by Bolis et al. (2017) and the responses obtained with the proposed modelling approach using a 4x1, 4x2 and an 8x2 mesh for the infill (IFSJ_MO). It can be observed that the addition of the sliding joints enhances the compliance of the system compared to the frame with traditional infills, with a response that is closer to the one of the bare frames than to the infilled one. The load-displacement curves obtained by the 4x2 and 8x2 meshes are very close and result in a good agreement with the numerical results reported in Bolis et al. (2017). Some differences are observed in the non-linear response of the 4x1 model. However, the deviation in terms of the ultimate load is less than 10%. These results confirm the capability of the proposed approach of describing the global response of infilled frames equipped with sliding joints, even employing a limited number of contact links along the column or beam lengths.

Figure 4.10 (b) shows the cyclic response of the frame with infill and sliding joints (IFSJ_CY), compared to the monotonic capacity curve obtained with the 4x2 mesh (IFSJ_MO) and the cyclic response of the bare frame (BF_CY). The presence of the sliding joints strongly reduces the initial stiffness and the strength of the infilled frame. Furthermore, the system IFSJ_CY exhibits stable and good cyclic dissipative properties thanks to the frictional behaviour in correspondence of the sliding joints and this is expected to have beneficial effects for the seismic performance of the system.

Figure 4.11 illustrates the deformed shapes of the models TIF and IFSJ with different discretisation of the infill, for a displacement of 55 mm, corresponding to a 2% inter storey drift ratio. These are found to be consistent with the deformed shapes obtained by Bolis et al (2017) using a 2D modelling approach. The figures show also the contact normal links that are active in compression, thus helping to visualise the location where the infill subpanels are in contact with the frame.

It is worth noting that the joints do not completely avoid the flexural interaction between the infill and the surrounding frame. However, they provide a significant reduction of the overall stiffness and strength of the system and prevent the damage in the masonry panels, leading to a regular and dissipative cyclic response whose beneficial effects should be better investigated through experimental cyclic and dynamic analyses. Furthermore, the avoidance of the in-plane damage of the masonry panels is expected to provide a better behaviour also with respect to out-of-plane actions, which are not investigated in the present work.

Table 4.10. Mechanical parameters of the masonry for defining the contact normal links.

Direction	E_{sj} MPa]	k_{nj} [N/mm^3]	f_{cj} [MPa]	f_{tj} [MPa]	ε_{cu} [-]	ε_{tu} [-]	λ
Horizontal	3275	200	2.70	0	0.4	0.010	0.1
Vertical	2111	200	7.28	0	0.4	0.002	0.1

Table 4.11. Mechanical parameters of contact links in shear describing the frame-infill interaction.

	CM	BBM	TBM	PPH(SJ)	PPV	Source
k_j (N/mm^3)	85	100	100	36	100	Bolis et al. (2017), Proposed model
c_j [MPa]	0.020	0.4	0.2	0.020	0.4	Calvi and Bolognini 2001. Bolis et al. 2017)
μ_j (-)	0.42	0.85	0.75	0.42	0.42	Calvi and Bolognini 2001. Bolis et al. 2017)

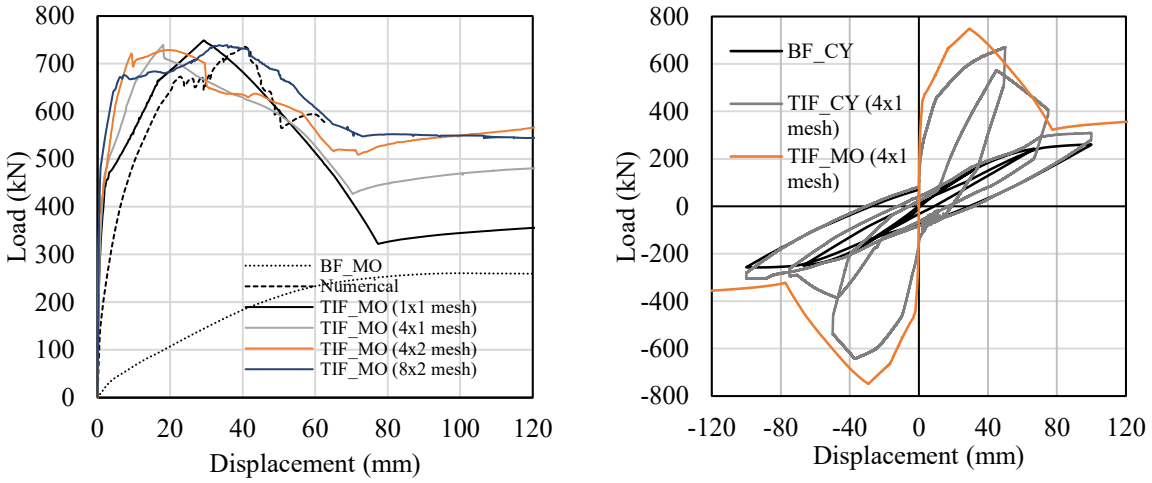

(a) (b)

Figure 4.9. Comparison of numerical responses of the RC frame with traditional infill under (a) monotonic loading and (b) cyclic loading predicted by various modelling approaches.

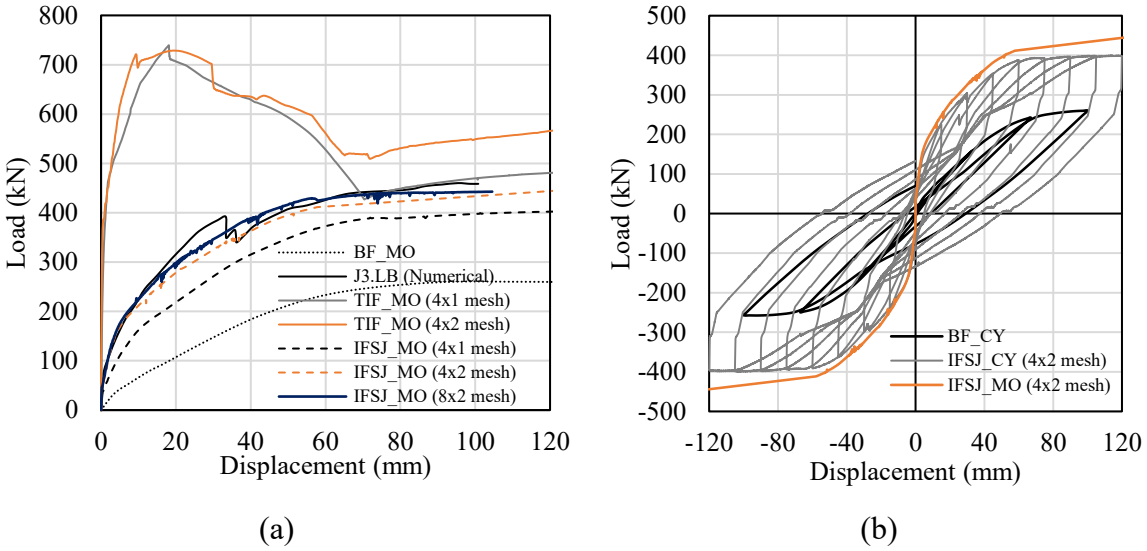

(a) (b)

Figure 4.10. Numerical response of the RC frame with masonry infill and sliding joint under (a) monotonic loading and (b) cyclic loading.

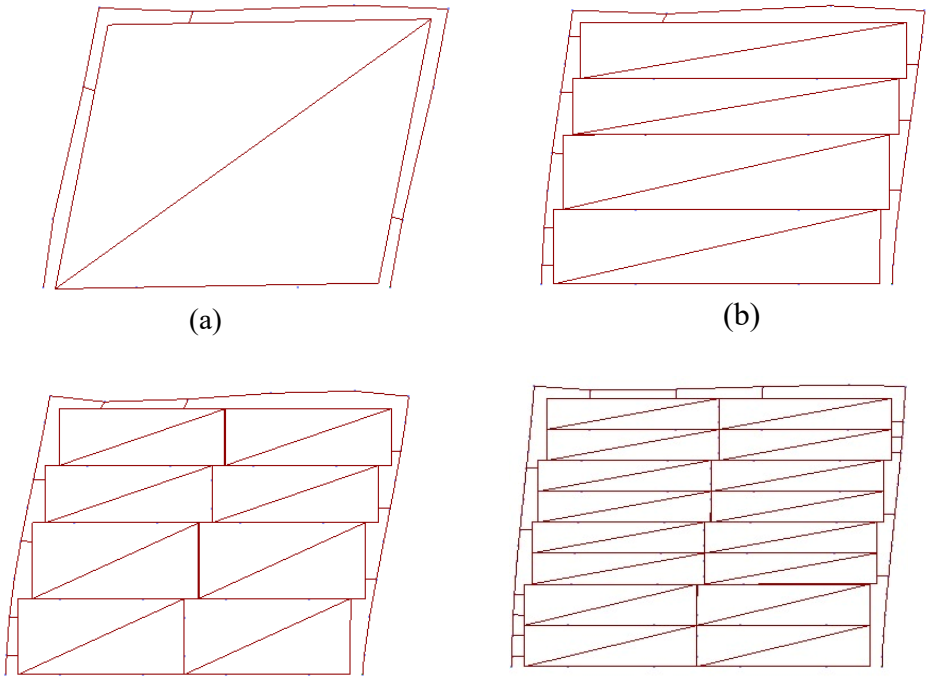

(a) (b)

(c) (d)

Figure 4.11. Deformed shapes of (a) TIF, (b) IFSJ (4 × 1 mesh), (c) IFSJ (4 × 2 mesh), (d) IFSJ (8 × 2 mesh)

In order to shed light on how the different infill typologies affect the responses of the RC frame components, the axial force, shear force and bending moment on the left (windward) and right (leeward) column is evaluated for the BF, TIF (4x1 mesh) and IFSJ models (4x1 mesh). Their diagrams are illustrated in Figure 4.12-Figure 4.14 respectively,

where (z/H) denotes the distance of the cross-section from the base of the column normalised by the column length. The reported diagrams refer to inter-storey drifts (ISD) of 0% (i.e., before application of lateral load), and 2%. The shape of the diagrams is characterised by discontinuities due to the forces transferred by the 2D contact links to the columns. It can be observed in Figure 4.12 that the axial force distribution in the two columns is almost uniform when the frame is subjected to zero or very low drift angles, as expected. At higher drift levels, the axial force distribution slightly changes showing an increased axial force (compressive) at the base of the leeward column and a decrease in the windward one, due to the transfer of tangential forces by the macro-elements and the effect of the overturning moment generated by the horizontal force eccentric with respect to the ground. At 2% drift, in the windward column, the highest values of the compressive force are observed in the BF system, and the lower in the TIF system. In the leeward column, the compressive forces are highest in the TIF system and lowest in the BF system.

Figure 4.13 shows the shear force diagrams of the columns. These diagrams are characterised by the discontinuities caused by the transmission of the normal forces in the 2D contact links. It is possible to observe that the sliding joints are effective in reducing the shear forces in the IFSJ system compared to the TIF system. However, the reduction is more significant in the leeward column than in the windward column. The distribution of the bending moments, shown in Figure 4.14, is approximately linear when only vertical loads are applied. Under a drift of 2%, the values of the maximum bending moments for the various systems are comparable, and they are generally higher for the BF model in the windward column and for the TIF model in the leeward column.

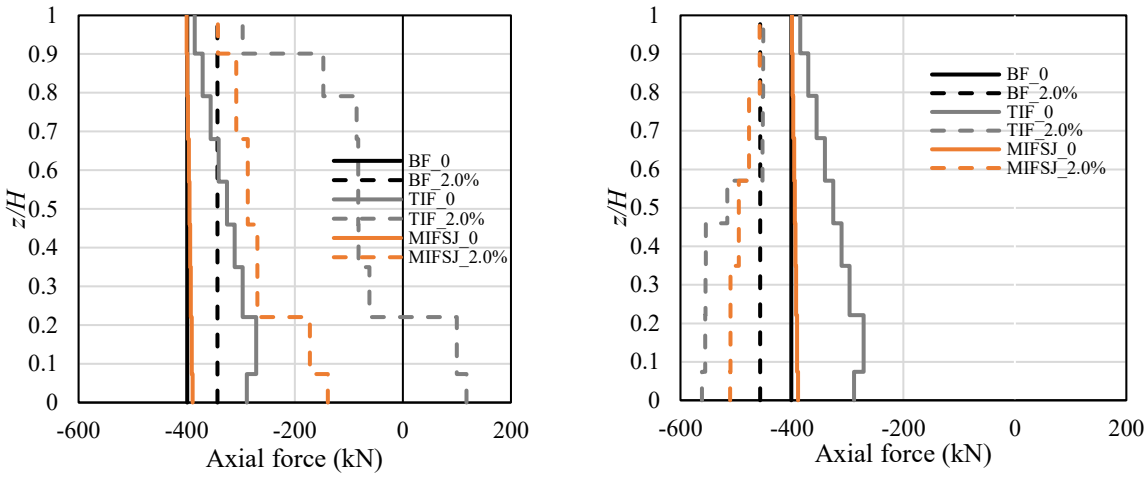

(a) (b)

Figure 4.12. Comparisons of axial forces in BF, TIF (4 × 1 mesh) and IFSJ (4 × 1 mesh) for (a) windward column (b) leeward column.

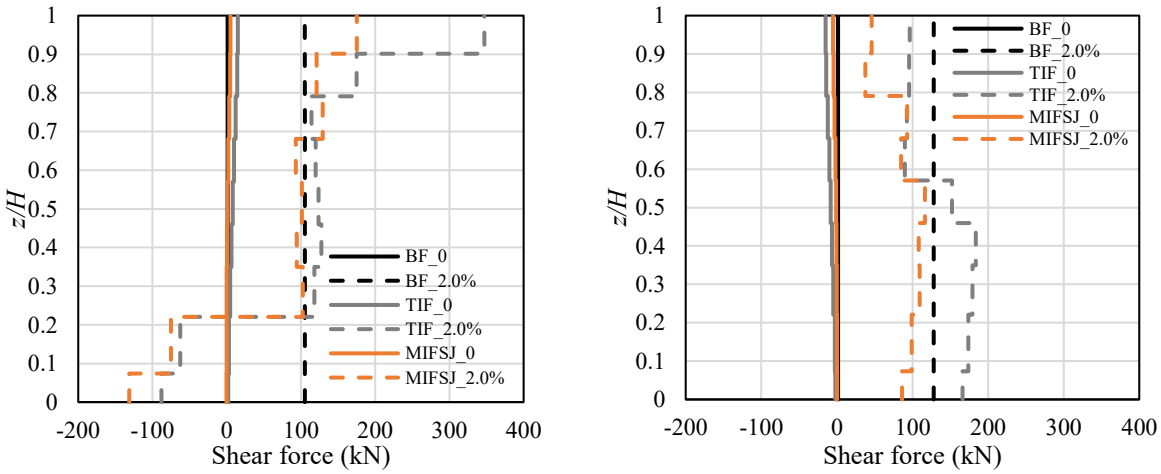

(a) (b)

Figure 4.13. Comparisons of shear forces in BF, TIF (4 × 1 mesh) and IFRJ (4 × 1 mesh) for (a) windward column (b) leeward column.

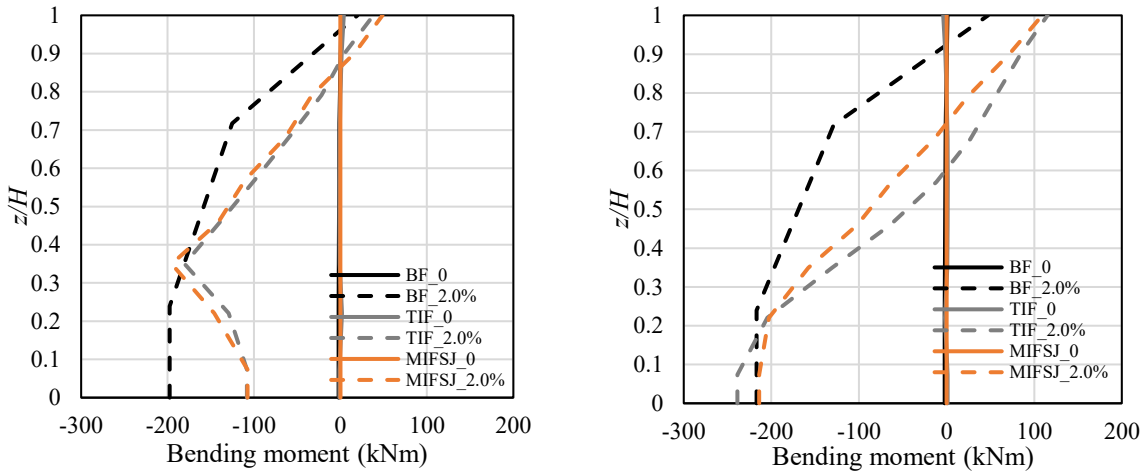

Figure 4.14. Comparisons of bending moments in BF, TIF (4 × 1 mesh) and IFSJ (4 × 1 mesh) for (a) windward column (b) leeward column.

4.3.3 Case Study III (INSYSME Project (INSYSME 2016))

The final validation study is carried out on the prototypes tested by the University of Padova within the INSYSME project (INSYSME 2016) and further described in Verlato (2017). The experimental outcomes for the bare frame, the infilled frame with mortar joints only (FC. MJ, 4th frame specimen) and the infilled frame with both mortar and specially designed rubber joints (DRES-V2) are validated against the proposed macro-modelling strategy. Hollow clay masonry blocks with a hole percentage of 50% (D-type) were used to build the infill panel. The masonry blocks were arranged in a running bond pattern and laid such a way that the hole axes are parallel to the vertical direction (Figure 4.15a). A mortar of 10mm thickness was used in the bed joints whereas there are no mortar present in the head joints and the transfer of stresses from between adjacent blocks relied on the brick inter-locking. Details of the frame cross sections, rebar diameter and detailing scheme, are given in Figure 4.15b together with the masonry block dimensions and further details are available in Verlato (2017). A constant vertical load of 200 kN was applied at the top of the column (simulating the effect of permanent load acting on the RC frame) and the experimental quasi-static tests conducted on the bare frame, the traditional infilled frame with mortar joints only and the innovative infill with both mortar and rubber joints followed by monotonically increasing in-plane horizontal load applied at the end of the beam (see Figure 4.15a.).

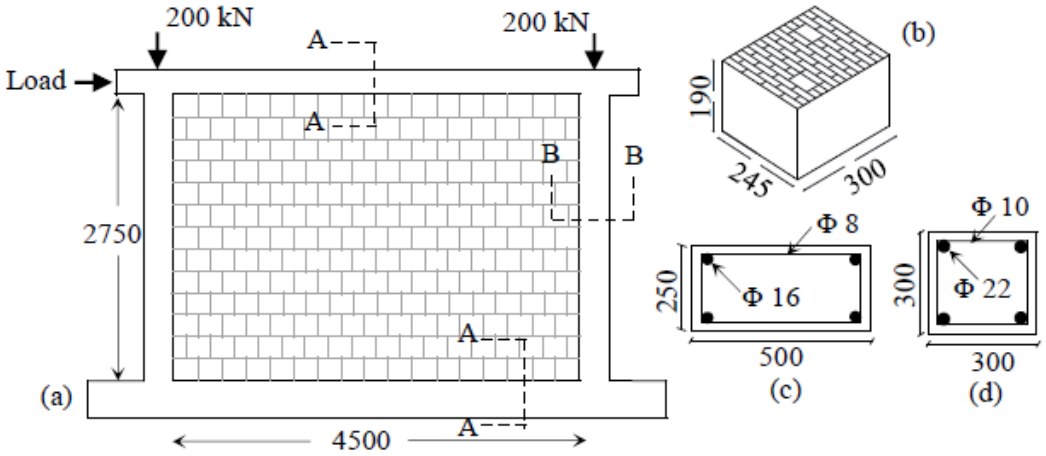

Figure 4.15. Geometric details (dimensions in mm) of (a) the tested infilled frame, (b) the perforated clay block (brick unit), (c) top and bottom beam (section A-A), (d) column (section B-B).

Table 4.12 reports the main mechanical properties of the concrete and steel reinforcement employed for the frame components. The mechanical parameters of the normal and shear responses of contact links and the response envelope of the diagonal link are presented in Table 4.13, Table 4.14 and Table 4.15 respectively. The constitutive parameters of the shear contact links, namely those describing the macroscopic sliding behaviour of masonry in the horizontal (PPH) and vertical (PPV) directions, the column-infill (CM) and beams-infill (BBM, TBM) interfaces, are assumed according to Verlato (2017) The constitutive behaviour of the contact links describing the interaction between the panel and the columns simulates the presence of mortar in the vertical joints.

Table 4.12. Mechanical properties of concrete and reinforcing steel.

Mechanical properties	Concrete	Steel reinforcement	Source
E [MPa]	22000	180000	Verlato (2017)
ν (-)	0.15	0.3	Verlato (2017)
f_c [MPa]	40	-	Verlato (2017)
Yield strength [MPa]	-	535	Verlato (2017)
f_t [MPa]	3.9	-	Verlato (2017)
Post-elastic to elastic stiffness ratio	-	0.002	Verlato (2017)

Table 4.13. Mechanical parameters of the masonry for defining the contact normal links.

Direction	E_m [MPa]	f_{cm} [MPa]	f_{tm} [MPa]	f_{rm} [MPa]	ε_{cu} [-]	ε_{tu} [-]	λ
Horizontal	1904	1.40	0.1	0.28	0.4	0.001	0.1
Vertical	6158	7.63	0.52	1.52	0.4	0.001	0.1

Table 4.14. Mechanical parameters of the contact shear links describing the masonry sliding behaviour and the frame-infill interaction.

Interaction Properties	CM	BBM	TBM	PPH	PPV	Source
k_j [N/mm^3]	100	100	100	100	100	Proposed model
c_j [MPa]	0.41	0.41	0.1	0.41	0.41	Verlato (2017)
μ_j [-]	0.8	1.13	0.4	1.13	0.8	Verlato (2017)

Table 4.15. Mechanical parameters of the response envelope of the diagonal link.

G_m [MPa]	τ_{cr} [MPa]	τ_y [MPa]	τ_0 [MPa]	τ_r [MPa]	γ_{cr} [-]	γ_y [-]	γ_0 [-]	γ_r [-]
1175	0.201	0.281	0.310	0.031	0.0040	0.0002	0.0020	0.0277

Figure 4.16 (a) compares the horizontal force-displacement response of the bare frame under monotonic loading obtained in INSYSME (2016) with the ones obtained numerically by Verlato (2017) using a 2D plane stress model and by using the proposed modelling strategy. The experimental and numerical force-displacement curves are plotted for a horizontal displacement up to 110 mm, corresponding to an inter-storey drift of 4%. The overall agreement between the numerical and experimental curves is good, although the numerical models slightly overestimate the initial stiffness of the system. Again, this may be due to the assumption of rigid bond between rebars and concrete. Figure 4.16 (b) compares the experimental and numerical curves obtained under a cyclic loading. The proposed model is characterised by a slightly larger hysteresis compared to the one observed in INSYSME (2016).

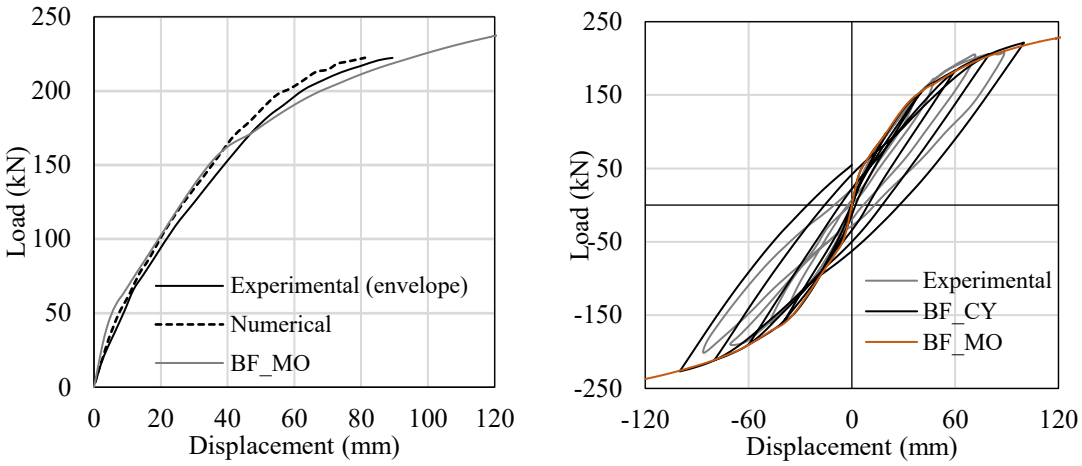

Figure 4.16. Comparison between numerical and experimental load-displacement curves of bare frame under (a) monotonic and (b) cyclic loading.

4.3.3.1 Frame with traditional infill

Figure 4.17 (a) illustrates the experimental force-displacement curve of the infilled frame under monotonic loading and compares it with the one obtained numerically (TIF_MO) considering different infill discretisation. Again, the proposed models describe with good accuracy both the initial and the post-peak behaviour of the wall. Increasing the number of macro-elements for describing the infill results in a slightly increase of stiffness and strength. A good agreement is also observed between the cyclic responses (Figure 4.17b).

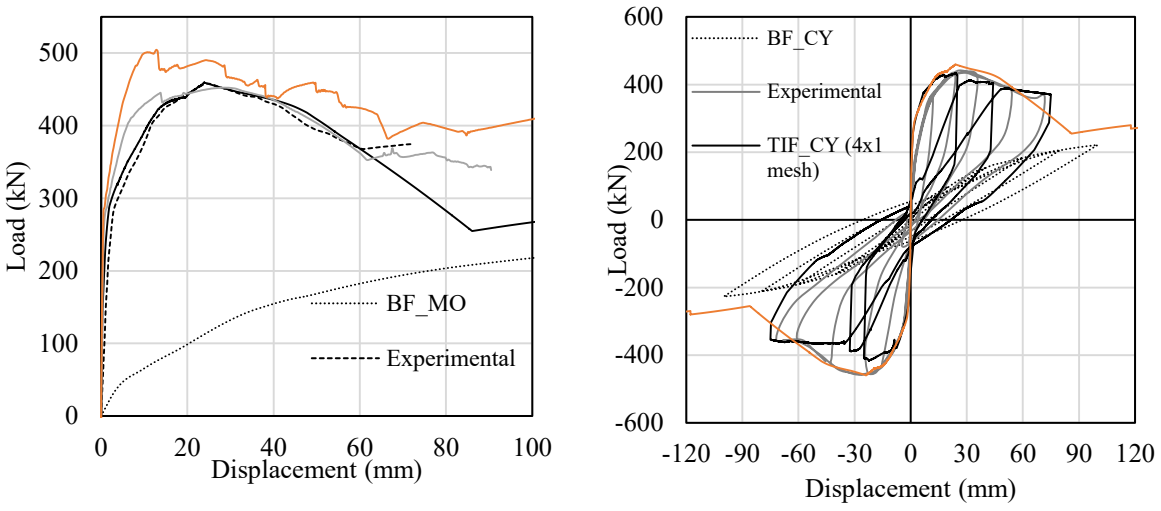

(a) (b)

Figure 4.17. Comparison between numerical responses of infilled frame with single and multi-panel approach and validation against experimental load-displacement curves for (a) monotonic and (b) cyclic loading.

4.3.3.2 Infill frames with rubber joints

Figure 4.18 (a) shows the layout of the RC frame with the infill panel and rubber joints. The rubber joints used as horizontal layers are 15mm thick and have a special shape to achieve a different stiffness in the two horizontal directions (Ahmadi et al. 2017) (Figure 4.18b) and are laid with mortar joints between them and the bricks. This rubber joint is made with natural rubber compound and possess a shear modulus of 0.5 MPa. The vertical rubber layers present between the infill and the columns are made with a different compound prepared from recycled Styrene-Butadiene Rubber and Ethylene Propylene Diene Monomer rubber anchored to a support of non-woven fabric. The normal behaviour of the horizontal rubber joints is defined by the initial normal stiffness k_{nj} = 11.73 N/mm^3, the tensile strength f_{tj} = 0 MPa, and the compressive strength f_{cj} = 1.58 MPa. The properties of the modified masonry infill and contact interfaces describing the mortar-rubber-mortar joints are presented in Table 4.16 and Table 4.17. The data reported in Table 4.12-Table 4.17 are based on the tests carried out by INSYSME (2016) and numerical models developed by Verlato (2017) to simulate these tests.

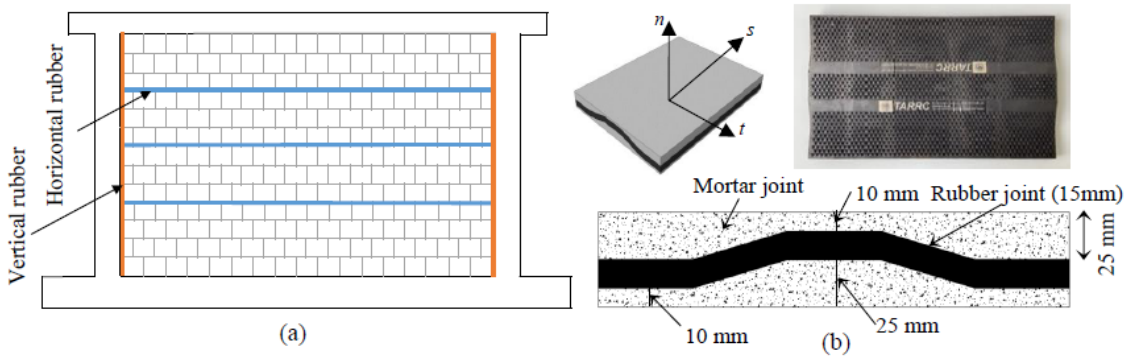

Figure 4.18. (a) Masonry infilled walls with horizontal and vertical rubber joints; (b) rubber joints developed by TARRC (Ahmadi et al. 2017).

Table 4.16. Mechanical parameters of the masonry for defining the contact normal links.

Direction	E_{rj} [MPa]	k_{nj} [N/mm^3]	f_{cj} [MPa]	f_{tj} [MPa]	ε_{cu} [-]	ε_{tu} [-]	λ
Horizontal	3275	200	1.40	0	0.4	0.001	0.1
Vertical	2111	200	1.58	0	0.4	0.001	0.1

Table 4.17. Mechanical parameters of contact links in shear for the various interfaces.

Interaction Properties	CM	BBM	TBM	PPH(RJ)	PPV	Source
k_j (N/mm^3)	1.00	100	100	11.73	100	Dhir et al. 2021
c_j [MPa]	0.001	0.4	0.1	0.05	0.3	INSYSME 2016. Verlato 2017
μ_j (-)	0.3	1.13	0.4	0.36	0.4	INSYSME 2016. Verlato 2017

Figure 4.19 (a) compares the experimental force-displacement curve with the ones obtained numerically considering two different discretisation of the infill with joints, based on a 4x1 and 4x2 mesh for the infill. The proposed models provide accurate results, with a global force-lateral displacement curve very close to the experimental one. This is despite the use of a simplified model for the shear behaviour of the mortar-rubber joints. Very good results are obtained because the proposed model is able to accurately simulate the failure of

the bond between the rubber joints and the mortar layers that was experienced in the tests for rather low drift levels, and the sliding behaviour taking place following the interface failure. Increasing the number of macro-elements results in only a slight increase of stiffness of the system. The addition of the rubber joints is found to enhance the compliance of the system, compared to the case of traditional infills (Figure 4.17a). Figure 4.19 (b) shows the cyclic response of the system according to the experiment (INSYSME 2016) and the numerical model with a 4x2 mesh for the infill. The agreement between the two is quite good. The system with rubber joints is found to be beneficial with significant energy dissipation capacity and stable loops. Figure 4.20 illustrates the deformed shape of the TIF model and two infilled frames with rubber joint (IFRJ) for different discretisation, for a 2% inter storey drift. These are found to be consistent with the experimental results obtained by Verlato (2017).

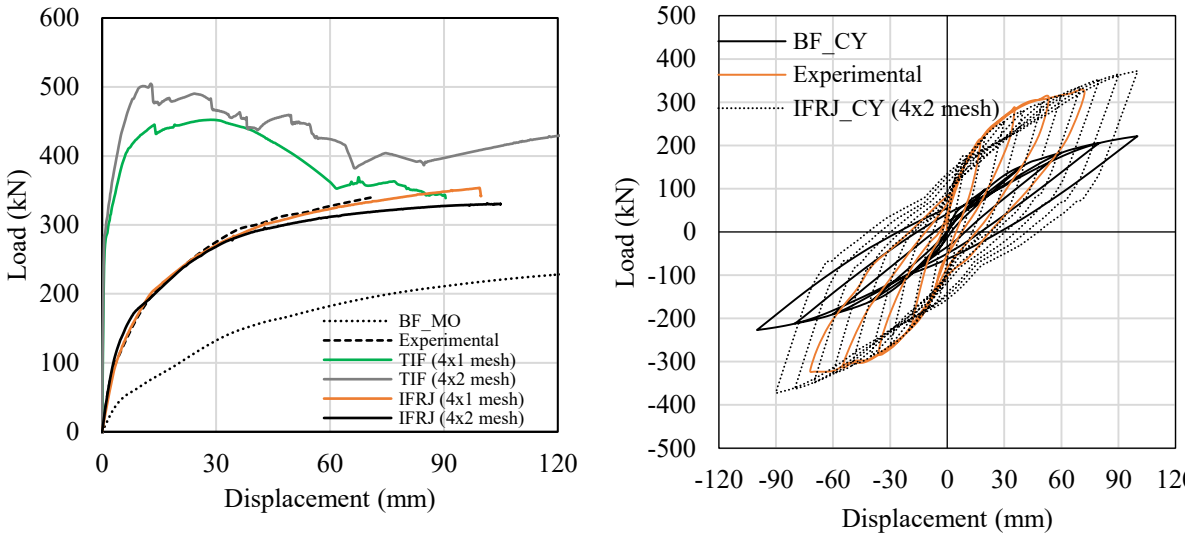

(a) (b)

Figure 4.19. Comparison between numerical responses of the bare frame, infilled frame with traditional infills and infill with innovate joints (rubber joints) for (a) monotonic and (b) cyclic loading.

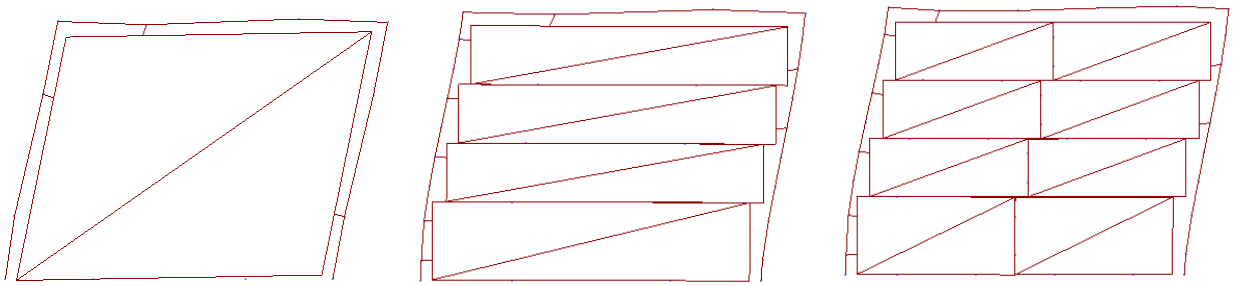

(a) (b) (c)

Figure 4.20. Deformed shapes of (a) TIF (b) IFRJ (4 × 1 mesh) (c) IFRJ (4 × 2 mesh).

The axial force, shear force and bending moment on the windward and leeward column are evaluated for the BF, TIF (4x1 mesh) and IFRJ models (4x1 mesh). Their diagrams are illustrated in Figure 4.21-Figure 4.23 respectively and they are quite similar in shape to those obtained for the model with sliding joints (Figure 4.12-Figure 4.14). Thus, similar observations hold for this case.

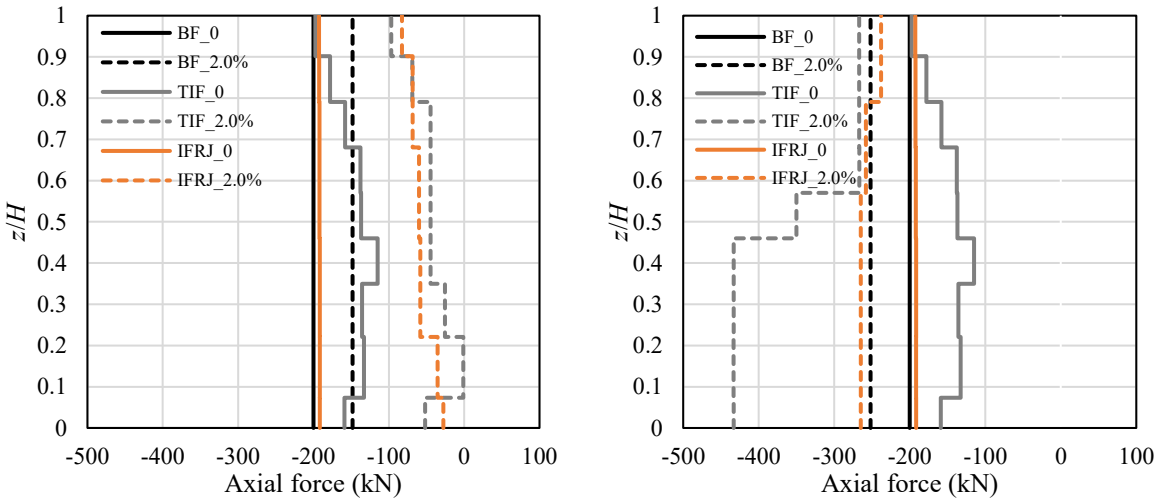

(a) (b)

Figure 4.21. Comparisons of axial forces in BF, TIF (4 × 1 mesh) and IFRJ (4 × 1 mesh) for (a) windward column (b) leeward column.

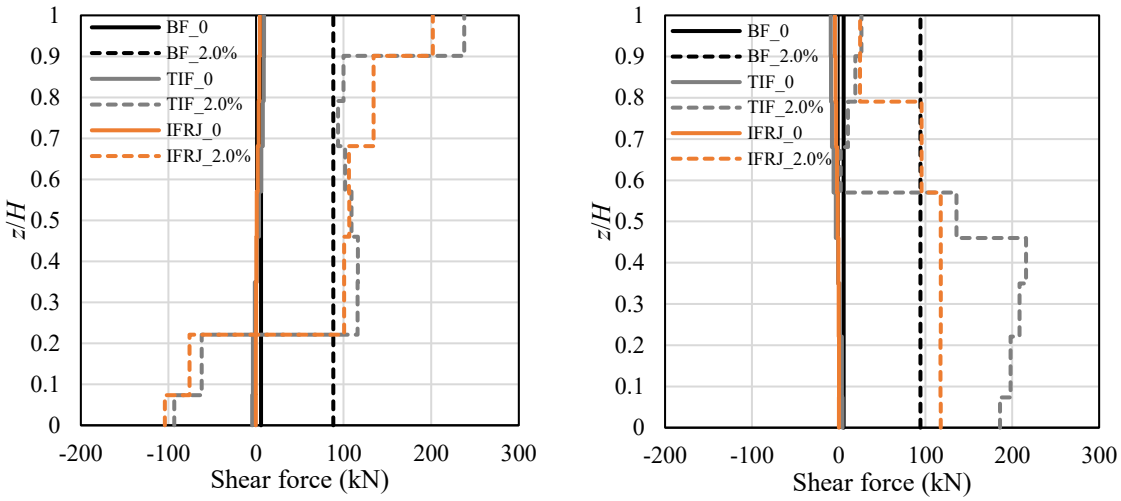

Figure 4.22. Comparisons of shear forces in BF, TIF (4 × 1 mesh) and IFRJ (4 × 1 mesh) for (a) windward column (b) leeward column.

Figure 4.22 shows the shear force diagrams of the columns. These diagrams are characterised by the discontinuities caused by the transmission of the normal forces in the 2D contact links. It is possible to observe that the rubber joints are effective in reducing the shear forces in the IFRJ system compared to the TIF system. However, the reduction is more significant in the leeward column than in the windward column. The distribution of the bending moments, shown in Figure 4.23 is approximately linear when only vertical loads are applied. Under a drift of 2%, the values of the maximum bending moments for the various systems are comparable, and they are generally higher for the BF model in the windward column and for the TIF model in the leeward column.

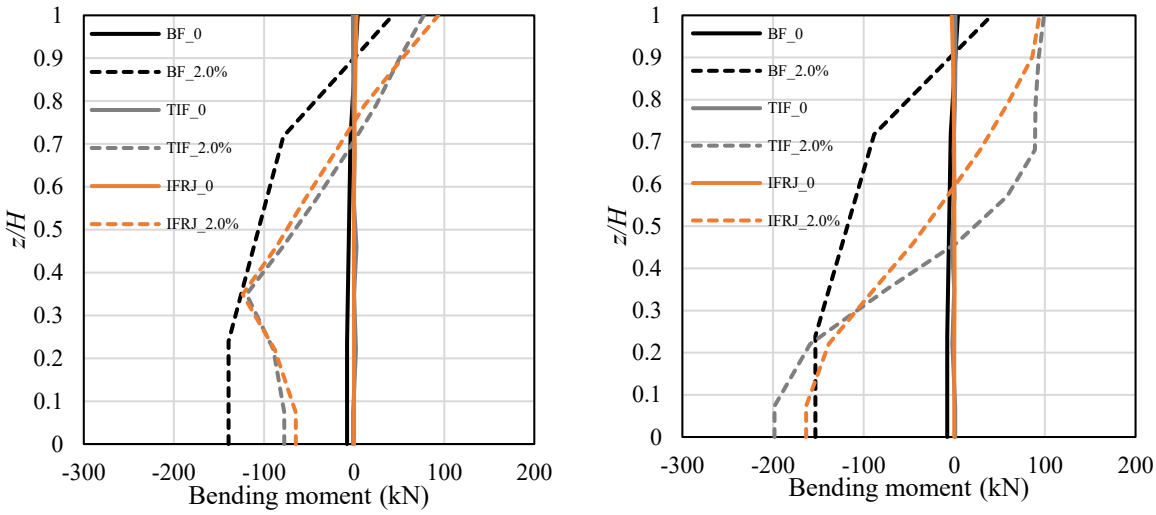

Figure 4.23. Comparisons of bending moments in BF, TIF (4 × 1 mesh) and IFRJ (4 × 1 mesh) for (a) windward column (b) leeward column.

Figure 4.24 (a, b) show and compare the diagonal spring force (F_d) vs. diagonal spring elongation (d_d) in each of the subpanel used to discretise the masonry infill in the cases of traditional infill (Figure 4.24a) and infill with rubber joint (Figure 4.24b), where SP_1 denotes the bottom subpanel and SP_4 the top. In case of TIF, all the subpanels are found to be significantly damaged, except for SP_4, whereas in the IFRJ case the diagonal spring behave linearly without any visible diagonal failure. It is also interesting to observe that SP_1 and SP_3 undergo unloading, whereas SP_2 does not unload and enters the softening regime. This corresponds to a change in the deformed shape of the frame, with horizontal deflections localised in correspondence of SP_2. Obviously, with a simpler modelling approach using an equivalent strut for representing the infills, such a behaviour would not be simulated.

Figure 4.24 (c, d) show the forces in the diagonal links vs. the top displacement of the frame. The relationship is nonlinear even in the case of linear behaviour of the diagonal links due to the nonlinear relationship between diagonal displacements of the panels and drifts. These two figures are useful to better highlight that the subpanels attain the peak load and undergo a softening behaviour in the traditional infills whereas they do not reach the peak load in the case of infills with rubber joints. Figure 4.25 compares the experimental and numerical values of the secant stiffness and of the dissipated energy. The secant stiffness is defined as the ratio between the force at the maximum displacement of each cycle and the displacement amplitude. The energy dissipated is the cumulative energy obtained by

integrating the force-displacement curve. The proposed model provides quite good estimates of the secant stiffness, which is only slightly overestimated for displacement amplitudes up to 10 mm. Moreover, the model also underestimates the dissipated energy at small displacements amplitudes and overestimates it for larger ones.

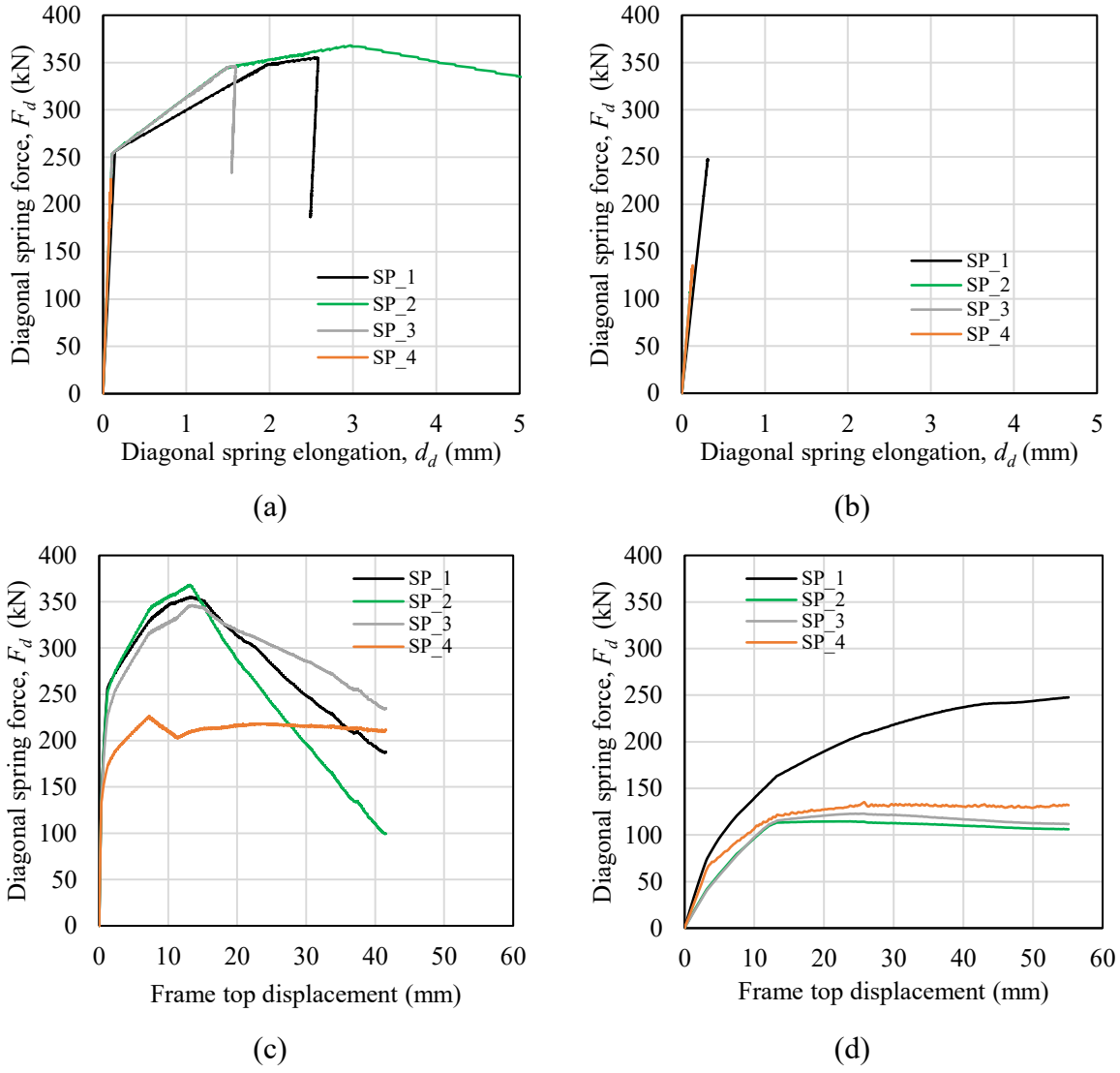

Figure 4.24. Internal force in the diagonal link against the diagonal link elongation: (a) TIF, (b) IFRJ; and against the top frame displacement: (c) TIF, (d) IFRJ.

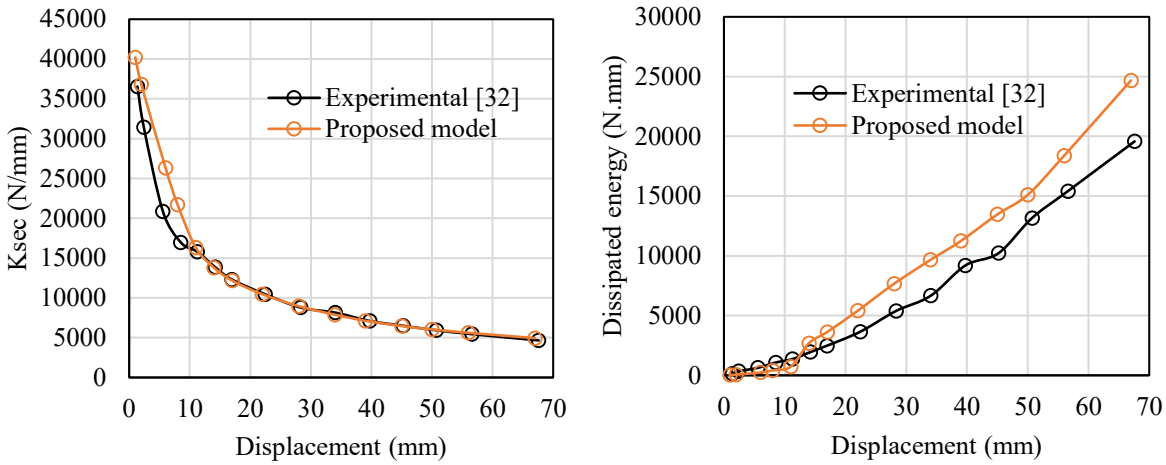

Figure 4.25. Comparison of experimental and numerical (a) secant stiffness and (b) dissipated energy.

4.4 Summary

This study has proposed an innovative and computationally efficient approach for analysing the in-plane non-linear cyclic response of RC frames with masonry infills and flexible/sliding joints. The proposed approach is based on a fiber-element based description of the frame components, and with the use of 2D discrete macro-elements, implemented in OpenSees, for describing the behaviour of the masonry subpanels and the interaction between them and with the adjacent frame components. The modelling strategy allows to evaluate the effectiveness of the sliding joints and rubber joints in minimising the negative effects of the interaction between infill and RC frame, by shedding light not only on their impact on the global force-displacement behaviour of the system, but also on the internal forces in the individual components.

The proposed modelling approach is calibrated and validated based on experimental test results and numerical results obtained by more refined FEM models available in the literature. Based on the study outcomes, the following conclusions can be made:

- the addition of the sliding/flexible joints enhances the compliance of the infilled frames, with a response that is closer to the one of the bare frames than of traditionally infilled ones. The energy dissipation capabilities are also enhanced thanks to more stable and larger hysteresis loops under cyclic loading.
- the proposed modelling strategy describes with good accuracy the initial as well as the post-peak force-displacement response of the analysed systems under horizontal loading.

- the global response of the system is not significantly affected by the infill mesh discretisation. Increasing the number of elements, the model becomes slightly stiffer and also the residual strength increases.
- for a given level of drift demand, the internal forces in the columns of the RC frame with infill and rubber joints have maximum values similar, if not inferior to those of the bare frame, with the exception of the axial and shear force in the windward column. The maximum absolute values of the internal forces in the case of infill with rubber joints are lower than the corresponding values obtained in the system with traditional infill.

In conclusion, the proposed modelling strategy can be effectively employed to investigate the optimal combination of strength, deformability and dissipation capacity of the sliding/flexible joints for enhancing the seismic performance for a wide variety of infilled frames. Further analyses will be carried out to evaluate the contribution of the sliding/flexible joints to the energy dissipation capabilities of infilled frames and to analyse the dynamic behaviour and seismic response of more complex structural systems.

5 Cyclic Shear Behavior of Masonry Triplets with Rubber Joints

5.1 Introduction

Past seismic events have revealed the significant vulnerability of masonry infilled reinforced concrete (RC) building frames and the large human and economic losses caused associated with this (Villaverde 1997; Filiatrault and Sullivan 2014; Del Vecchio et al. 2018; De Risi et al. 2019). Masonry infills are often among the most critical components of infilled RC buildings. In fact, while columns and beams are designed to be earthquake-resistant, masonry infills are often disregarded in the design stage and considered as non-structural members. Therefore, even under minor earthquakes, infills undergo severe damage, causing injury or death of occupants and hindering rescue operations.

In the recent years, a promising approach has emerged to protect infill walls from seismic damage through the use of sliding joints (Preti et al. 2012; Preti et al. 2015; Morandi et al. 2016; Thiruvengadam et al. 2018; Bolis et al. 2019; Preti et al. 2019; Di Trapani et al. 2020) and flexible/soft layers (Mojsilović et al. 2015; Vögeli et al. 2015; Calabria et al. 2016; Preti et al. 2016; Ahmadi et al. 2017; Petrović et al. 2017) for increasing the flexibility of infill panels and isolating them from the surrounding frame. These layers can be horizontal, inserted between rows of bricks or between the panel and the top beam of the frame, or vertical, placed between the infill panel and the columns (Figure 2.22a). The Tun Abdul Razak Research Centre (TARRC) has developed an innovative rubber joint (Figure 2.22b) made from a high-damping natural rubber (HDNR) compound. The joint has a non-flat profile whose shape has been defined in order to achieve different stiffness in the in-plane and out-of-plane direction and improve the out-of-plane capacity of the infills by invoking an arching mechanism (Ahmadi et al. 2017). It does not require skilled labour to be deployed and is available in two versions (DRES-V1 and DRES-V2 (Verlato 2017), which differ only for the presence of pins in the second one. These pins are introduced to enhance the bond between the rubber and the mortar and avoid sliding. In fact, even if sliding can be considered as an excellent mechanism for both reducing infill damage and

dissipating energy through friction (Morandi et al. 2016), it is not desirable since it does often result in residual displacements.

The European research project INSYSME (INSYSME 2016) has proven the effectiveness of the rubber joints during tests carried out on the seismic protection of infill walls. In particular, in-plane and out-of-plane quasi-static tests were carried out at University of Padova (Verlato 2017) on an infilled reinforced concrete frame with and without rubber joints. The tests demonstrated the "proof of concept" of the technology and showed that the introduction of the rubber joints considerably minimises the masonry infill damage and provides excellent out-of-plane performance in terms of stiffness and strength. Moreover, they showed that the rubber joints may contribute to increase the energy dissipation capabilities of the system, although this potential contribution was not investigated in depth.

Further experimental and numerical investigations are needed to fill this gap of knowledge in the dynamic behaviour of infilled frames with rubber joints. In particular, more experiments are needed to characterise the dissipation capabilities of the joints and of systems equipped with them, and the strength of the bond between the rubber joints and the mortar. Since the rubber joints introduce flexibility and dissipate the seismic energy by deforming in shear, a characterization of the cyclic shear behaviour of the HDNR compound and of the rubber-mortar joints is needed.

In order to fill this gap, an extensive experimental campaign was carried out at the University of Strathclyde. Material characterisation tests were performed to characterise the mechanical properties of bricks, mortar and HDNR. Moreover, an unconventional experimental setup was used to evaluate the cyclic shear behaviour of masonry triplets with mortar and rubber joints, rather than only the behaviour under monotonic loading as required by standards (EN 1052-3 2002). A similar test setup was recently developed and employed to characterise the shear behaviour of masonry triplets with multi-layer bed joints (Mojsilović et al. 2015; Mojsilović et al. 2019), dry stack masonry joints (Lin et al. 2017), and traditional mortar joints (Barattucci et al. 2020).

The results of the experimental investigation provide a better understanding of the mechanical properties of rubber joints. They are also useful to inform numerical studies aimed at characterising the dynamic behaviour of RC frames with masonry infill and rubber joints. On this regard, in the last decades numerous strategies have been developed for the analysis of traditional masonry infills, using macro-models (Pietruszczak and Niu 1992; El-

Dakhakhni et al. 2006; Caliò et al. 2012; Uva et al. 2012; Caliò and Pantò 2014; Pantò et al. 2017; Nicoletti et al. 2020; Ruggieri et al. 2020; Ruggieri et al. 2021), micro-models (Lourenço 1997; Mohyeddin et al. 2013; Abdulla et al. 2017), discrete-element models (Sarhosis et al. 2014), and meso-scale models (Lourenço and Rots 1997; Lourenço 1997; Dolatshahi and Aref 2011; Macorini and Izzuddin 2011, 2013, 2014; Nasiri and Liu 2017). Although some numerical studies have been carried out to evaluate the behaviour of masonry infill walls with soft or sliding joints (Preti et al. 2012; Mojsilović et al. 2015; Vögeli et al. 2015; Petrović et al. 2017; Di Trapani et al. 2020), the case of rubber joints has not been fully investigated yet. Dhir et al. (2021) has recently developed a modelling strategy in Abaqus for evaluating the in-plane quasi-static behaviour of RC frames with masonry infills and rubber joints, using a meso-scale approach. The results of the experimental campaign can be used to further expand this modelling strategy in order to investigate how the damping capabilities of the joints can effectively help reducing the seismic demand imposed on RC infilled frames. For this reason, the test results are simulated in this study by using a detailed micro-modelling strategy, with the mechanical parameters of the constituent materials of the triplets informed by material tests on mortar, brick and rubber samples. The results of the experimental and numerical investigations of this study are useful for identifying research gaps in the understanding and description of the behaviour of mortar-rubber joints. They also inform future studies on the evaluation and analysis of the seismic performance of masonry infilled frames with rubber joints, and on the evaluation of optimal mechanical and geometrical properties of the rubber joint properties.

5.2 Experimental campaign

This section describes first the characterisation tests of the materials composing the masonry triplets, namely the bricks, the mortar and the HDNR compound. In the second part of the section, the cyclic test apparatus is described, and the monotonic and cyclic shear tests on the masonry triplets with traditional mortar joints and mortar-rubber joints are presented.

5.2.1 Brick and mortar characterisation

In this study, standard fired clay bricks (Birtley old English bricks) of dimensions 215 × 102.5 × 65 mm^3 were used. Although these bricks are only one of the many types of bricks and blocks employed in masonry infill wall construction, they were chosen because they were easy to get locally, and because the main aim of the study was to investigate the behaviour of the mortar-rubber joints. Nevertheless, it must be stressed that the typology of brick and mortar is important and should be carefully considered to guarantee a good shear bond at the brick-mortar interface, allowing the deformation of the rubber device. The bricks were tested under uniaxial compressive loading (0.1 mm/min) along the horizontal and vertical directions (Figure. 5.1a, c). The Young's modulus of bricks (E_b) was calculated from its stress-strain curves assuming a linear elastic response for compressive stresses between 5% and 33% of the peak strength (see Figure. 5.1b, d). A three-point bending test was also carried out on the brick units at a rate of 0.5 mm/min to estimate the flexural strength (Figure. 5.1e) and the load displacement relation is presented in Figure. 5.1f. The test results are summarised in Table 5.1.

(a)

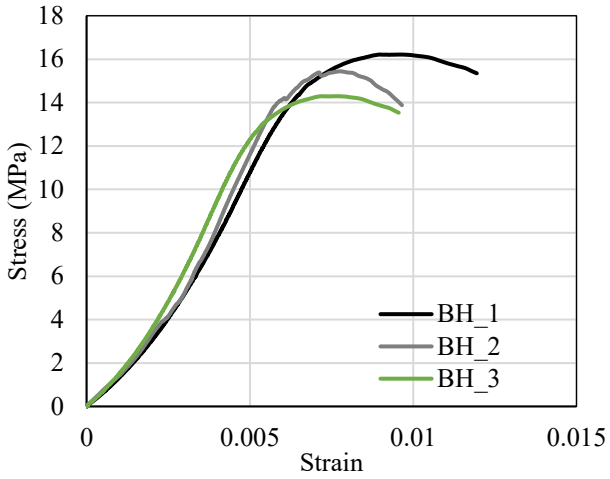

(b)

(c)

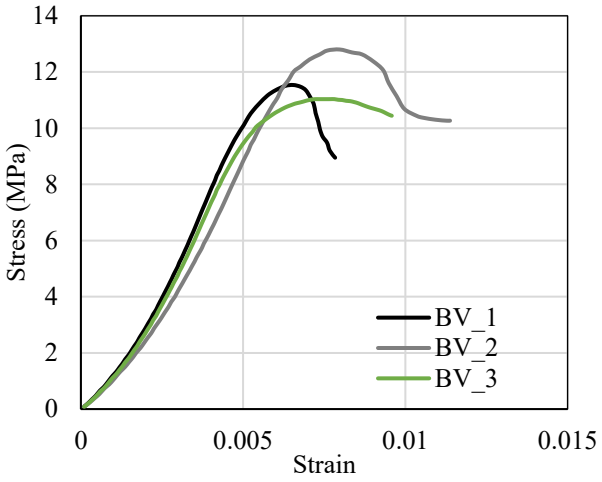

(d)

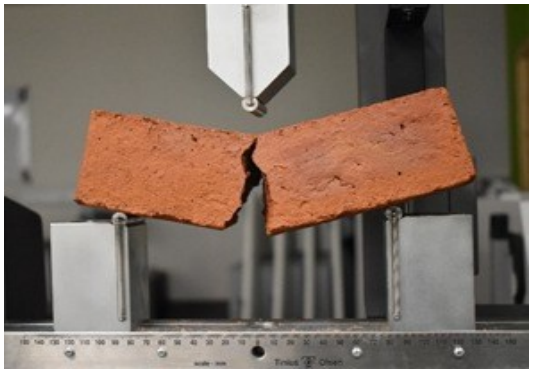

(e)

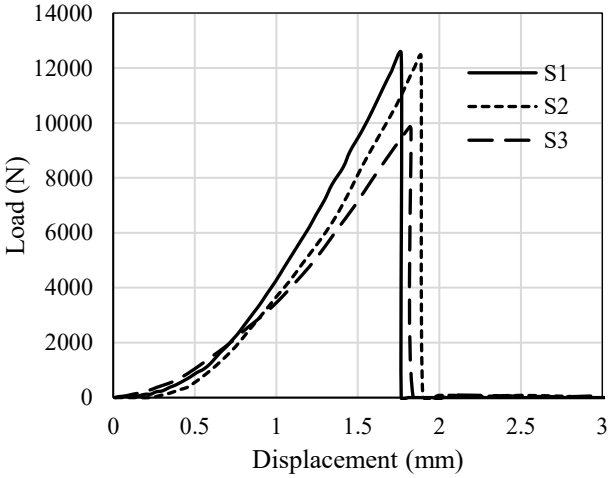

(f)

Figure. 5.1. (a, b) compressive strength test on bricks in horizontal and vertical direction, (c, d) stress-strain curves for bricks, (e) test setup for three-point bending test of brick specimens, (f) load-displacement response of brick specimens under three-point bending.

Table 5.1. Mechanical properties of clay brick specimens.

Three-point bending test				Compressive strength					
				Horizontal direction			Vertical direction		
Samples	Density (kg/m^3)	R_f [N]	f_f (MPa)	Samples	f_c (MPa)	E_b (MPa)	Samples	f_c (MPa)	E_b (MPa)
S1	1852	12523	5.61	BH_1	16.2	20125	BV_1	11.4	16882
S2	1929	12440	5.57	BH_2	15.2	19493	BV_2	12.6	17748
S3	1971	9774	4.38	BH_3	14.7	19170	BV_3	11.1	16658
Mean	1918	11579	5.19		15.37	19596		11.7	17096
(CoV)	(0.031)	(0.135)	(0.135)		(0.050)	(0.025)		(0.068)	(0.034)

General-purpose ready-mix mortar (Cement: Sand = 20-25%: 75-80%) was prepared with a water to cement ratio of 0.8:1.0 to ensure the easy workability. Flexural strength tests (Figure 5.2) and cube compressive strength tests (Figure 5.3) were conducted to characterise the mechanical properties of the mortar. Mortar specimens were left to cure at a temperature of about 25^0C for 28 days before being tested.

For the flexural strength tests of mortar, a total of 6 mortar beams of size 40 × 40 × 160 mm^3 were prepared and a three-point bending test was performed on the mortar beam specimens under a displacement rate of 0.5 mm/min (Barattucci et al. 2020). The flexural strength f_f of mortar specimens were found following EN 1015-11 (2006) as follows:

$$f_f = \frac{3}{2}\frac{R_f l}{bh^2} \tag{1}$$

where R_f is the failure load, l is the length between the two supports while testing, b and h are the width and height of the mortar specimen cross-section, respectively.

Similarly, a total of 6 mortar cubes of size 50 × 50 × 50 mm^3 were cast and subjected to compressive strength tests. The mortar cubes were tested on the 28^{th} day since casting at a constant displacement rate of 0.10 mm/min (Barattucci et al. 2020). Figure 5.4 (a, b) show the load-displacement curves obtained in the flexural and compression tests, respectively. The Young's modulus (E_m) of each mortar sample was calculated from compressive strength tests by assuming a linear elastic response for compressive stresses between 5% and 33% of the peak strength (Barattucci et al. 2020). The strain values reported in abscissa refer to the ratio between the displacement of the loading plates and the total height of the specimen. Table 5.2 summarises the values of the mortar mechanical properties from the various tests

as well as the average ones. The displacements reported are those measured by the loading machine. It is noteworthy that the compliance of the testing machine may lead to some inaccuracy in the estimate of the displacements. Local confinement effects near the loading plates may also affect the displacement estimates.

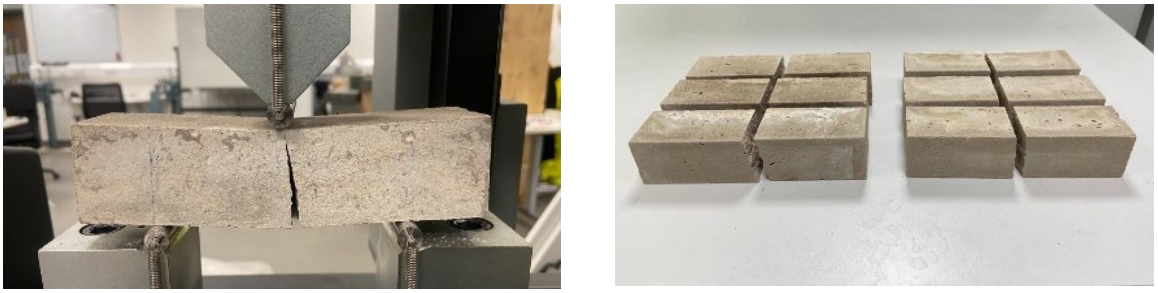

(a) (b)

Figure 5.2. (a) Three-point bending test of specimen and (b) failed mortar specimens.

(a) (b)

Figure 5.3. (a) Compressive-strength test of cubic specimen and (b) failed mortar specimen.

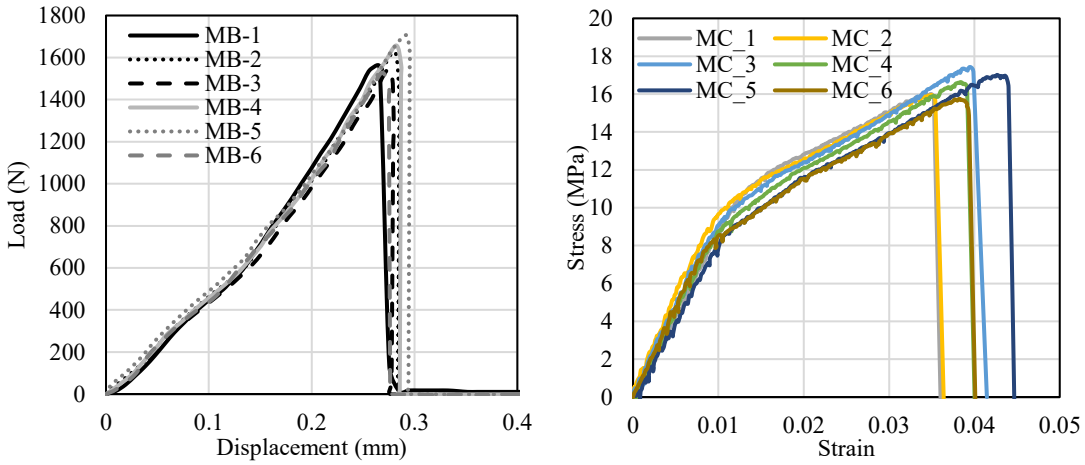

(a) (b)

Figure 5.4. (a) Three-point bending of mortar beam specimens (b) compression tests of mortar cubes.

Table 5.2. Mechanical properties of mortar specimens.

Three-point bending test				Compressive strength test		
Samples	Density (kg/m^3)	R_f [N]	f_f (MPa)	Samples	f_c (MPa)	E_m (MPa)
MB_1	2043	1556.18	3.65	MC_1	16.01	1780.87
MB_2	2094	1622.60	3.80	MC_2	15.95	1629.09
MB_3	2078	1547.13	3.63	MC_3	17.43	1875.38
MB_4	2063	1657.50	3.88	MC_4	16.64	1780.00
MB_5	2086	1706.73	4.00	MC_5	17.05	1832.10
MB_6	2070	1528.25	3.58	MC_6	15.74	1709.00
Mean (Cov)	2072 (0.009)	1603.06 (0.044)	3.76 (0.044)	Mean (Cov)	16.47 (0.041)	1767.74 (0.050)

5.2.2 Characterisation of HDNR compound

The horizontal deformable joints are the core element of the proposed system. During the experimental campaign, DRES-V2 joints (Verlato 2017) (Figure 2.22b) were used. These joints have 15 mm thickness, 300 mm width, and 500 mm length. In order to characterise the behaviour of the HDNR compound used for the joints, specimens with different dimensions were cut from the joints and tested in tension and shear.

A quasi-static tensile test, consists of a loading-unloading cycle, was performed on three rubber strips (150 mm length, 25 mm width and 15 mm thick) in a uniaxial testing machine Tinius Olsen 25ST (Tinius Olsen 2021) at a loading rate of 10 mm/min. Figure 5.5 (a) shows the schematic diagram for the test setup. Figure 5.5 (b, c) show the deformed shape of one of the three rubber specimens during and after the completion of the test. It can be seen that at the end of the test specimens was buckled, due to some viscous deformations that recovered in few minutes after the end of the tests. Figure 5.6 (a) shows the hysteretic responses of the specimens during the loading and un-loading cycle, in terms of nominal tensile stress σ and strain ε. These are defined as follows:

$$\sigma = \frac{F_t}{b_w t_w} \qquad \text{Eq. 5.1}$$

$$\varepsilon = \frac{\delta}{l_0} \qquad \text{Eq. 5.2}$$

where $b_w t_w$ denotes the nominal (i.e., initial) cross-section area of the test piece, and l_0 the initial length. F_t is the tensile force, and δ is the displacement.

The responses of the three specimens are very close to each other. Figure 5.6 (b) shows the results of the relaxation phenomenon which is linear with log of time were carried out on a specimen. These were performed by pulling the specimen at an initial rate of 10 mm/min up to 100% and 200% of its length and holding it in this position for 24 hours while measuring the change of resisting force. During the first seconds of hold time, a very rapid decrease in the stress is observed. Subsequently, the rate of decrease reduces. In the case of 100% initial amplitude, it takes about 12 hours before a constant asymptotic value can be assumed to be reached. After 12 hours, the change of stress in the subsequent 12 hours is less than 1% of the stress value at 12 hours. In the case of 200% initial amplitude, a longer relaxation time (>24h) is required to reach the asymptotic value.

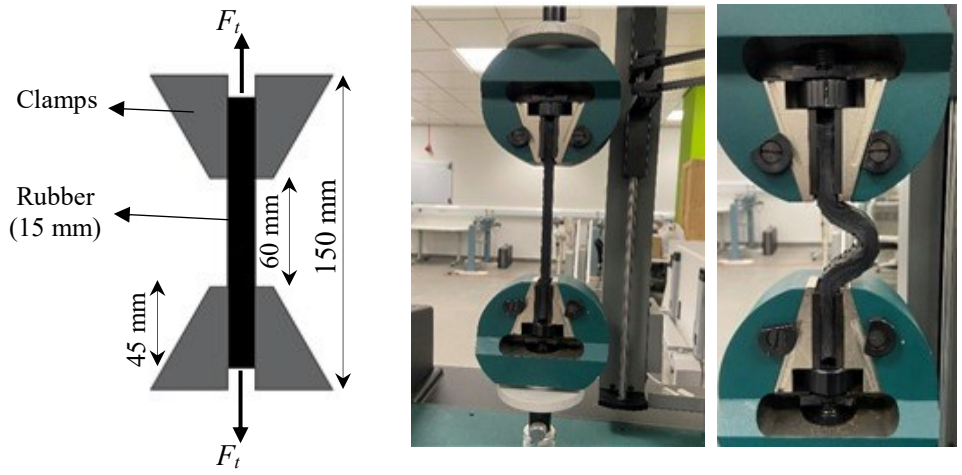

Figure 5.5. (a) Tensile test setup of rubber strip (b) deformed shape of the test piece during testing and (c) at the end of the test.

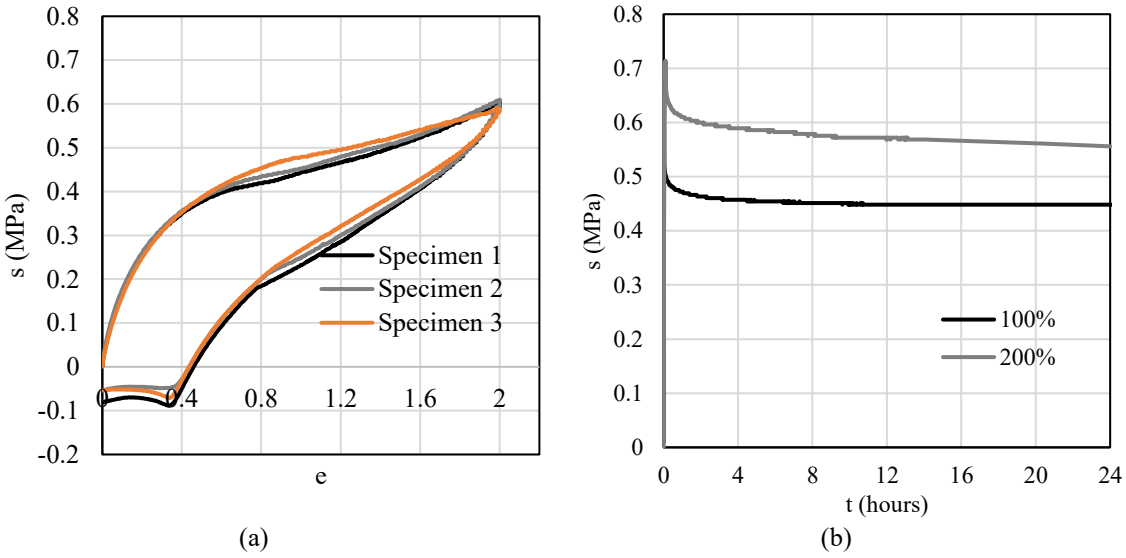

Figure 5.6. (a) Tensile stress- strain response, and (b) relaxation test of rubber specimen.

In order to study the behaviour of the rubber compound under simple shear, which is the main mode of deformation of the horizontal joints under in-plane loading of the infilled frame, multiple quadruple specimens were prepared (Figure 5.7a). Each specimen was made in our departmental laboratory by gluing four rubber pieces (60 mm × 60 mm × 15mm) to steel plates of 5 mm thick and Figure 5.7 (b) shows the testing setup of the rubber quadruplet tested at a rate of 10 mm/min. Plotted in Figure 5.8 (a, b) is the nominal shear stress-strain response of one quadruple specimen at different amplitudes of loading cycles. As there is no degradation or failure of the rubber joints expected, only five numbers of cycles were

imposed during the cyclic tests. The results obtained with the other specimens are not plotted because they are very close to each other. The nominal shear stresses and strains were obtained as follows:

$$\tau = \frac{F_s}{2A_s} \qquad \text{Eq. 5.3}$$

$$\gamma = \frac{u}{t_r} \qquad \text{Eq. 5.4}$$

where τ is the nominal shear stress, F_s= shear force, A_s= shear area of single block, γ = the nominal shear strain, u = shear displacement, t_r= thickness of block.

Relaxation tests were performed on the rubber quadruplets under shear by imposing 50%, 100%, 150% and 200% strain amplitudes. Each specimen was pulled at a rate of 10 mm/min and hold for 24 hours. The results of the tests carried out on one specimen are plotted in Figure 5.8 (c). Similar to the tensile test, after the initial seconds of hold time, a very rapid decrease in stress is observed and after 12 hours, the change of stress in the subsequent 12 hours is less than 1% of the stress value at 12 hours, corresponding to the attainment of an asymptotic value.

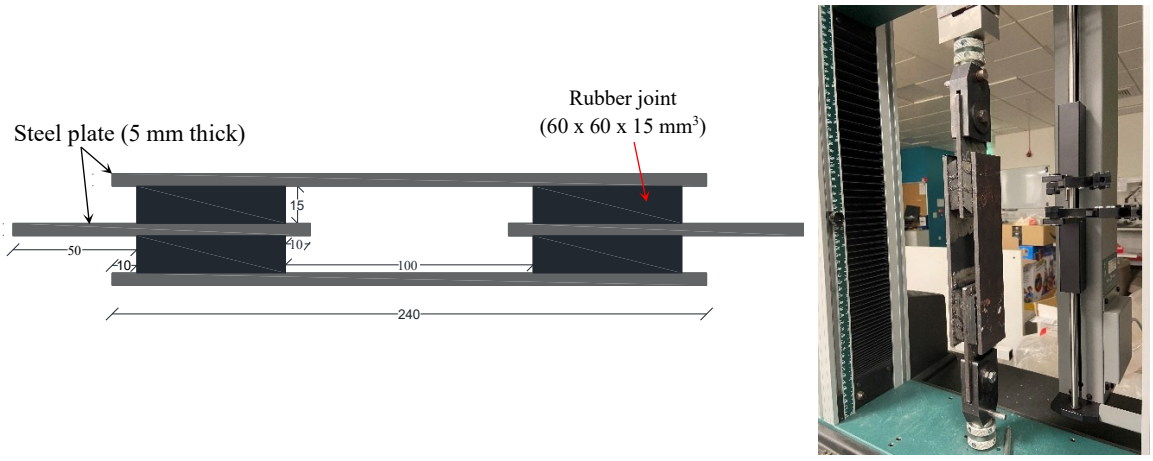

(a) (b)

Figure 5.7. (a) Quadruple test specimen (b) Test setup.

The behaviour of rubber in simple shear is very complex, since it is rate-dependent, amplitude-dependent, and characterised by the Mullins effect (Tubaldi et al. 2017). In order to further investigate the dependency of the behaviour of the rubber joint on the displacement history and rate, another test was carried out on the quadruplets by imposing a sinusoidal displacement input with frequency 0.008 Hz and amplitude 15 mm. The

corresponding hysteretic response obtained for a quadruplet is plotted in Figure 5.8 (b) and is quite similar to the one obtained with a constant-rate input of 10 mm/min. It is noteworthy that the frequency of the sinusoidal input is the same as that considered for the triplet tests presented below.

The secant shear modulus of the rubber (G_{eff}) and equivalent damping ratio (ξ_{eq}), evaluated considering the sinusoidal displacement input (γ=1), are equal to 0.25 MPa and 6% respectively. The secant shear modulus G_{eff} is obtained by dividing the values of the average shear stresses in the rubber by the values of the average shear strains corresponding to the maximum shear displacement level investigated. The equivalent damping ratio is defined as follows:

$$\zeta_{eq} = \frac{W}{4\pi G_{eff}} \qquad \text{Eq. 5.5}$$

where W denotes the energy dissipated in one cycle (i.e., the area enclosed in the hysteresis loop), $E_{el} = 1/2 G_{eff} \gamma^2$ (elastic strain energy corresponding to the maximum deformation, γ).

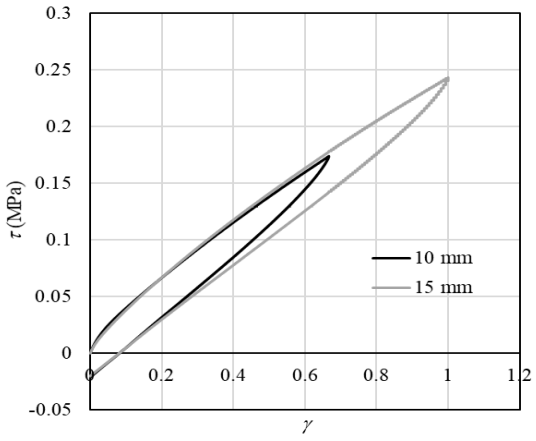

(a)

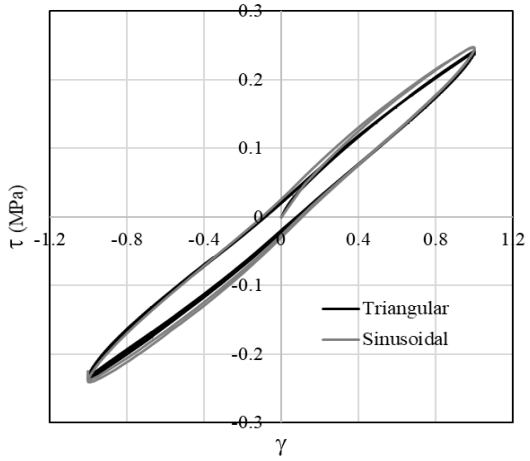

(b)

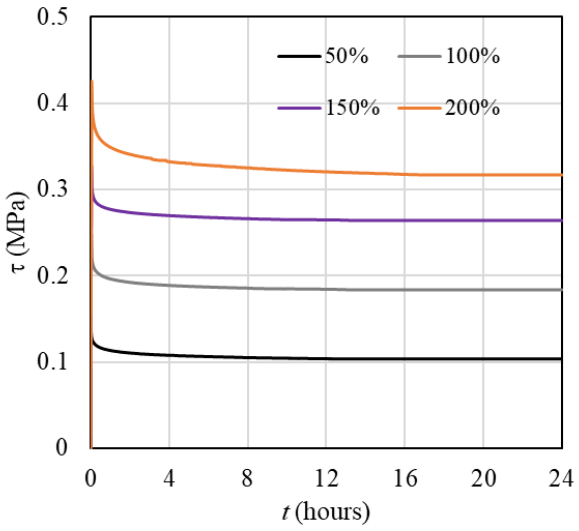

(c)

Figure 5.8. Shear stress-strain response for (a) half displacement cycle at constant rate (b) full cycle, (c) relaxation test on rubber quadruplet for different initial strain amplitudes.

5.2.3 Manufacturing of masonry triplets and test set-up

The clay brick triplets were prepared by bonding the bricks (see Figure 5.9) with the ready-mix cement mortar. 42 triplets were prepared, 12 of which with mortar joints and 30 with mortar-rubber joints. The masonry triplets with mortar joints (10 mm thick) only were casted (Figure 5.9a, c). The other triplets were prepared with mortar-rubber joints, with the rubber layers sandwiched between two layers of 10 mm thick mortar (Figure 5.9b, d). Prior to assembling the triplets, all bricks were submerged in water for a minimum time of 24 h with the aim to improve their bonding with the mortar joints. After casting of triplets, they were left in the laboratory to cure for at least 28 days at a temperature of about 25˚C.

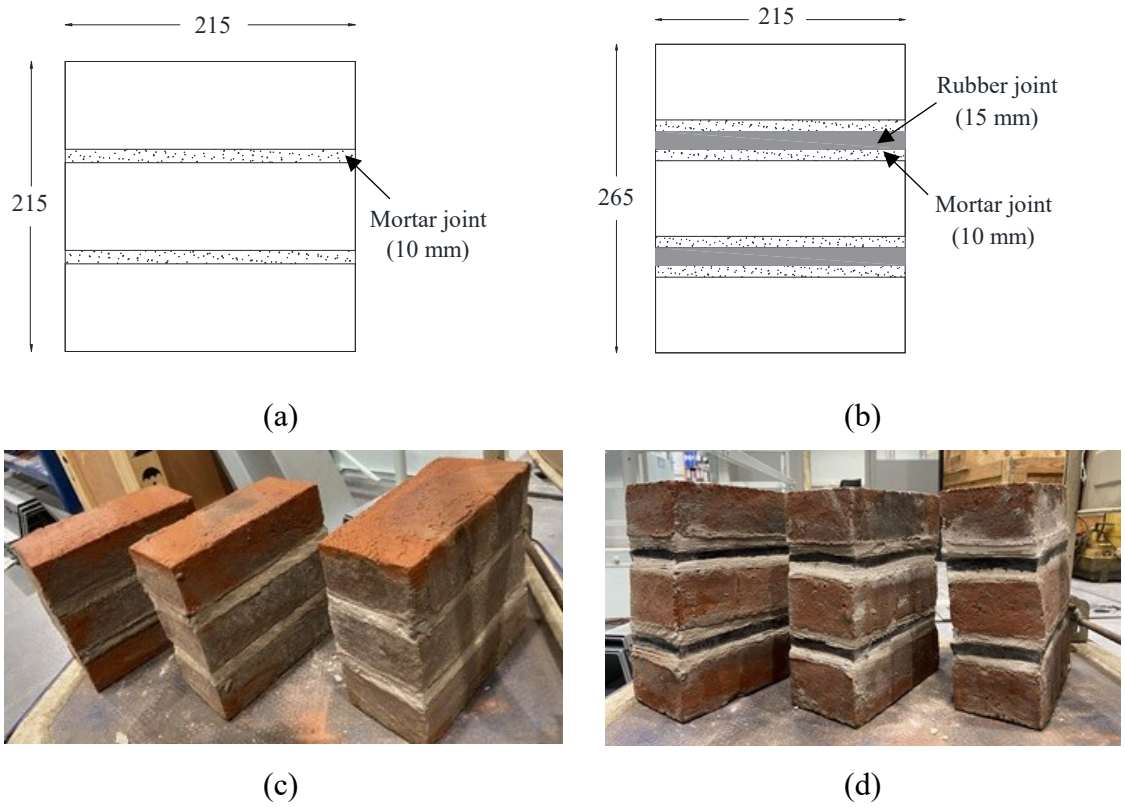

Figure 5.9. (a, b) dimensions of the triplets with mortar and mortar-rubber joints (c) triplet with mortar joint (d) triplets with mortar-rubber joints.

In order to characterise the cyclic behaviour of the triplets, the shear test set-up proposed by the European Standard (EN 1052-3 2002) was modified and expanded (Figure 5.10) in order to allow applying cyclic shear loadings. The developed apparatus is similar to the ones already employed in recent studies on the characterisation of the cyclic behaviour of masonry triplets with mortar joints (Alecci et al. 2013; Andreotti et al. 2018; Barattucci et al. 2020), dry joints (Franzoni et al. 2014; Lin et al. 2017), and multi-layer bed joints (Mojsilović et al. 2015; Mojsilović et al. 2019). Figure 5.11 describes the assembly of the testing apparatus and the various components. A hydraulic jack is used to apply the pre-compression on the triplets in the horizontal direction. The pressure is applied before the shearing displacement, and it is kept constant during the entire duration of the test. The shearing vertical displacement is applied through a computer-controlled actuator (Figure 5.10a) with a maximum load capacity of 250 kN. Both the monotonic and cyclic shearing test was performed on for three levels of pre-compressions (0.2 MPa, 0.4 MPa and 0.6 MPa).

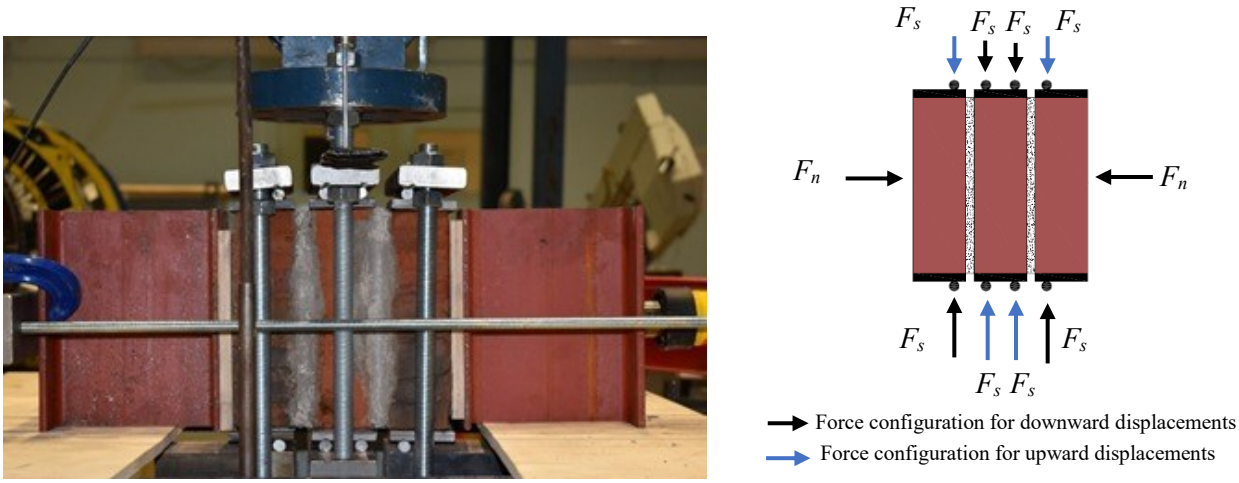

(a) (b)

Figure 5.10. (a) Shear test set-up (b) forces configuration for cyclic shear test.

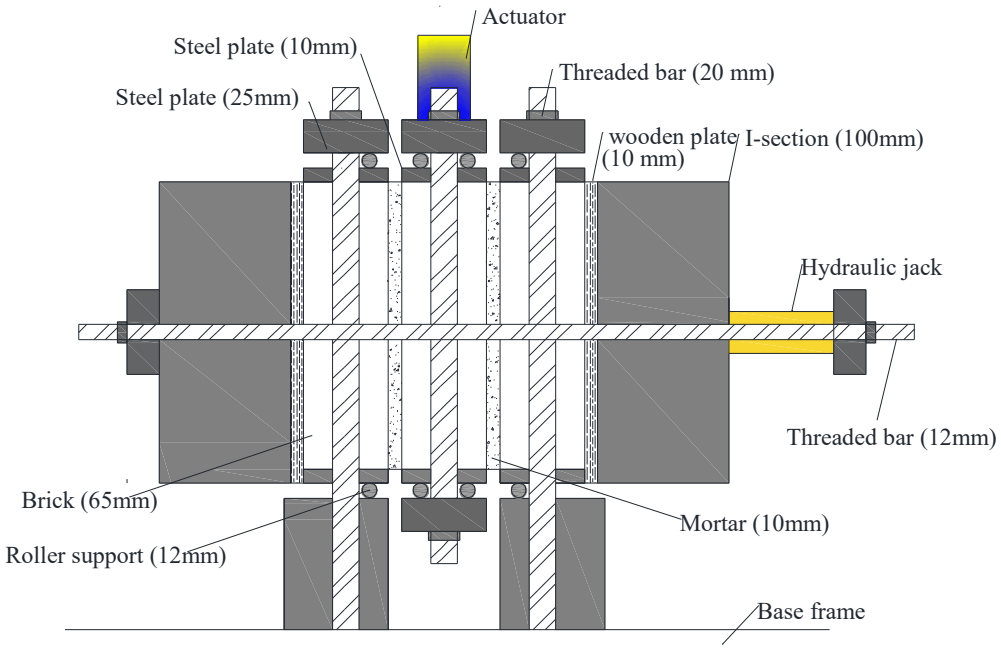

Figure 5.11. Illustration of the components of the testing equipment apparatus.

5.2.4 Monotonic and cyclic shear tests of triplets

The monotonic test was carried out by imposing a constant downward displacement rate of 1.0 mm/min on the intermediate brick through the actuator. The cyclic test was carried out by imposing downward and upward displacements over five sinusoidal cycles (frequency of 0.008 Hz). Figure 5.12 shows the load-displacement relationship of the triplets with mortar joints under monotonic (Figure 5.12a) and cyclic shear (Figure 5.12b). The monotonic tests result show that the initial stiffness of the system is not affected by the pre-

compression level, while the peak load increases for increasing pre-compression level. In the cyclic tests, lower force levels were obtained compared to the monotonic tests.

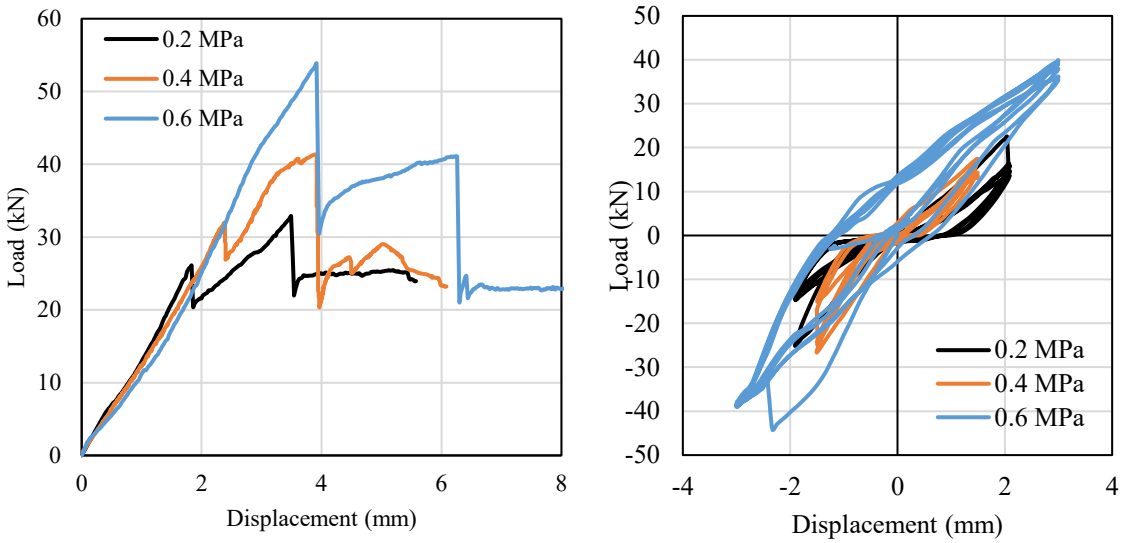

(a) (b)

Figure 5.12. (a) Monotonic (b) cyclic shear response of triplets with mortar joints.

Figure 5.13 show the failed specimens at the end of the monotonic and cyclic tests carried out at different levels of pre-compression. It can be seen from these results that the failure occurred at the mortar-brick joint interface, which was found to be weaker than the mortar layers and the bricks. The value of the cohesion and friction angle for the mortar joints (respectively 0.6 and 1.04), obtained with a mortar made with cement to sand ratio of 1:3-1:4, could be compared to those obtained by Barattucci et al. (2020) (respectively 0.932 and 1.04) with a mortar made with cement to sand ratio of 1:3.

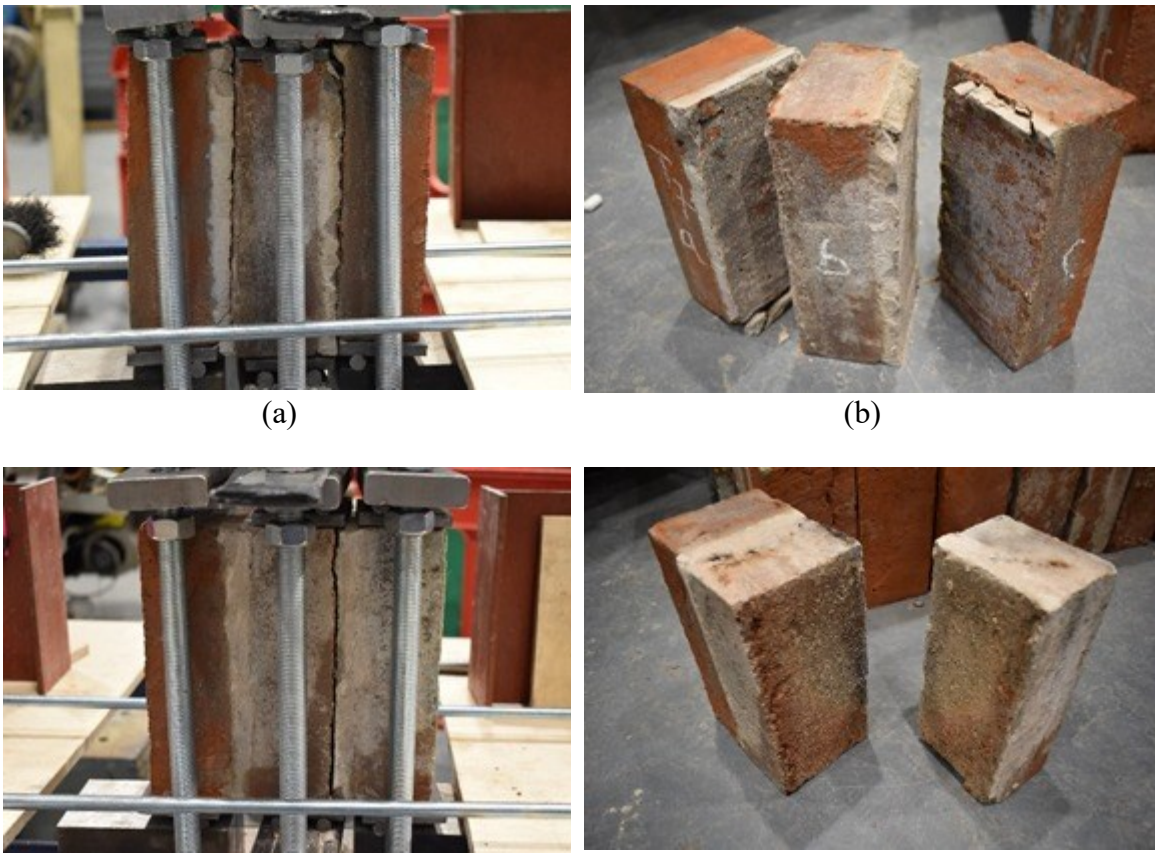

(a) (b)

(c) (d)

Figure 5.13. (a, b) Monotonic (c, d) cyclic shear test of mortar triplets with 0.6 MPa pre-compression.

The triplets with rubber-mortar joints were tested under both monotonic loading (displacement rate 1mm/min) and cyclic shear harmonic loading (frequency of 0.008 Hz). Figure 5.14 (a) shows the triplet during cyclic shear test. It can be seen that the rubber layer undergoes significant shear deformation, as expected. Figure 5.14 (b) shows the failed triplet at the end of testing. The rubber-mortar interface was found to be the weakest component in the system for all the investigated triplets. It is noteworthy that two or three tests were carried out on different triplets under the same loading condition in order to verify the repeatability of the results. Very similar responses were obtained with different specimens.

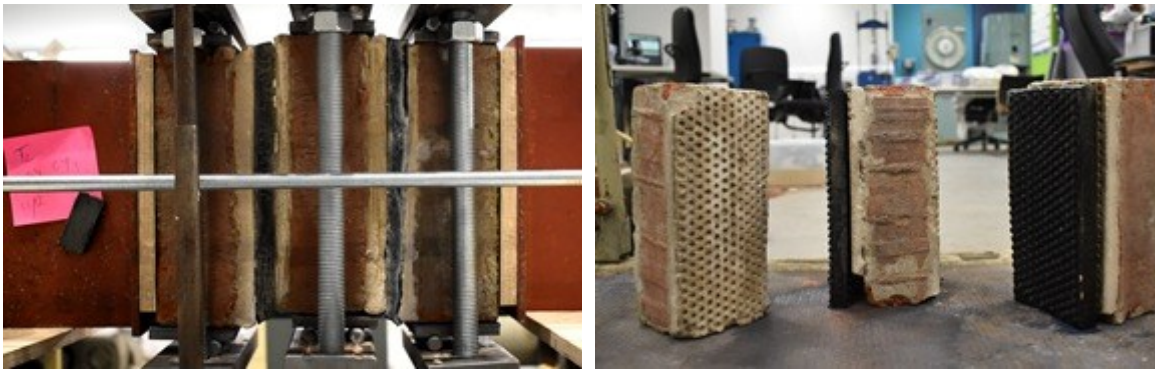

(a) (b)

Figure 5.14. (a) Cyclic shear test setup (b) failed specimens.

Figure 5.15 (a) shows the load-displacement response of the triplets with mortar-rubber joints under monotonic shear loading. Compared to the triplets with mortar joints (Figure 5.12a), the triplets with mortar-rubber joints exhibit significantly lower stiffness (about 1/10), lower peak load capacity (about 1/5), and a less brittle post-peak response. The relatively weak bond between the joints and the mortar is responsible for the lower peak strength of the system. Nevertheless, the reduction of shear stiffness due to the rubber joint compliance is an important and useful feature of the mechanical behaviour of mortar-rubber joints, since it allows to increase the flexibility of masonry infills and to reduce the interaction between the infill and the frame while reducing the forces induced by the earthquake in the system for a given seismic drift demand. Figure 5.15 (b-d) show the cyclic shear response of the triplets with mortar-rubber joints obtained for different levels of pre-compression and different maximum displacement amplitudes. For each test, the results obtained with one of the many tested specimens are reported due to space constraints and to allow the comparison between tests. It can be observed that the stiffness of the system increases slightly for increasing levels of pre-compression, whereas the dissipated energy does not change significantly. Quite surprisingly, significantly higher forces where attained in the cyclic tests without noting a complete failure of the bond compared to the monotonic tests and only in the case of low pre-compression level significant sliding at the mortar-joint interface was observed for high displacement amplitudes (i.e., 30mm). A similar observation was made by Mojsilovic et al. (2015), who observed an increased cohesion and an increase friction in cyclic tests compared to monotonic tests for mortar joints with interposed soft layers.

However, it should be noted that some sliding and energy dissipation due to friction is activated also for displacement amplitudes lower than 30mm. This explains why the

equivalent damping ratio measured with the triplet tests (discussed below, see Figure 5.16b) is higher than the one measured with the quadruplet tests (Figure 5.8b). The failure of the rubber-mortar interface for low levels of compression forces can potentially constitute a problem as it might limit the efficiency of the device and change the functioning mechanism, with the sliding at the rubber-mortar interface occurring in place of the rubber deformation. This could have consequences in terms of residual displacements at the end of the earthquake.

In order to better describe the effect of the pre-compression level and amplitude of oscillation on the hysteretic behaviour of the system, Figure 5.16 shows the variation of the secant shear modulus of the rubber (G_{eff}) and equivalent damping ratio (ξ_{eq}) for increasing average shear strains and for different pre-compression levels. G_{eff} and ξ_{eq} are slightly affected by the pre-compression level, whereas they are strongly affected by the amplitude of shear deflection. In fact, G_{eff} reduces significantly with the amplitude of shear strain, whereas ξ_{eq} increases.

Overall, the rubber-mortar joints exhibit very good dissipative properties, with high values of the equivalent damping ratio that are significantly higher than those characteristics of the rubber compound. In fact, under a shear strain amplitude of 1, ξ_{eq} =6% (measured through the quadruplet tests) whereas the rubber-mortar layer has ξ_{eq} in the range between 18% and 30%. The higher values of ξ_{eq} in the triplets can be due to the energy dissipation by friction that takes place at the interface between the mortar and the joints. This mechanism is enhanced by the presence of the pins in the rubber layers. It is noteworthy that these pins were removed before bonding the rubber to the steel plates to manufacture the quadruple test pieces. The friction between the pins and the surrounding mortar must be activated under small amplitudes, even when no significant sliding can be noticed.

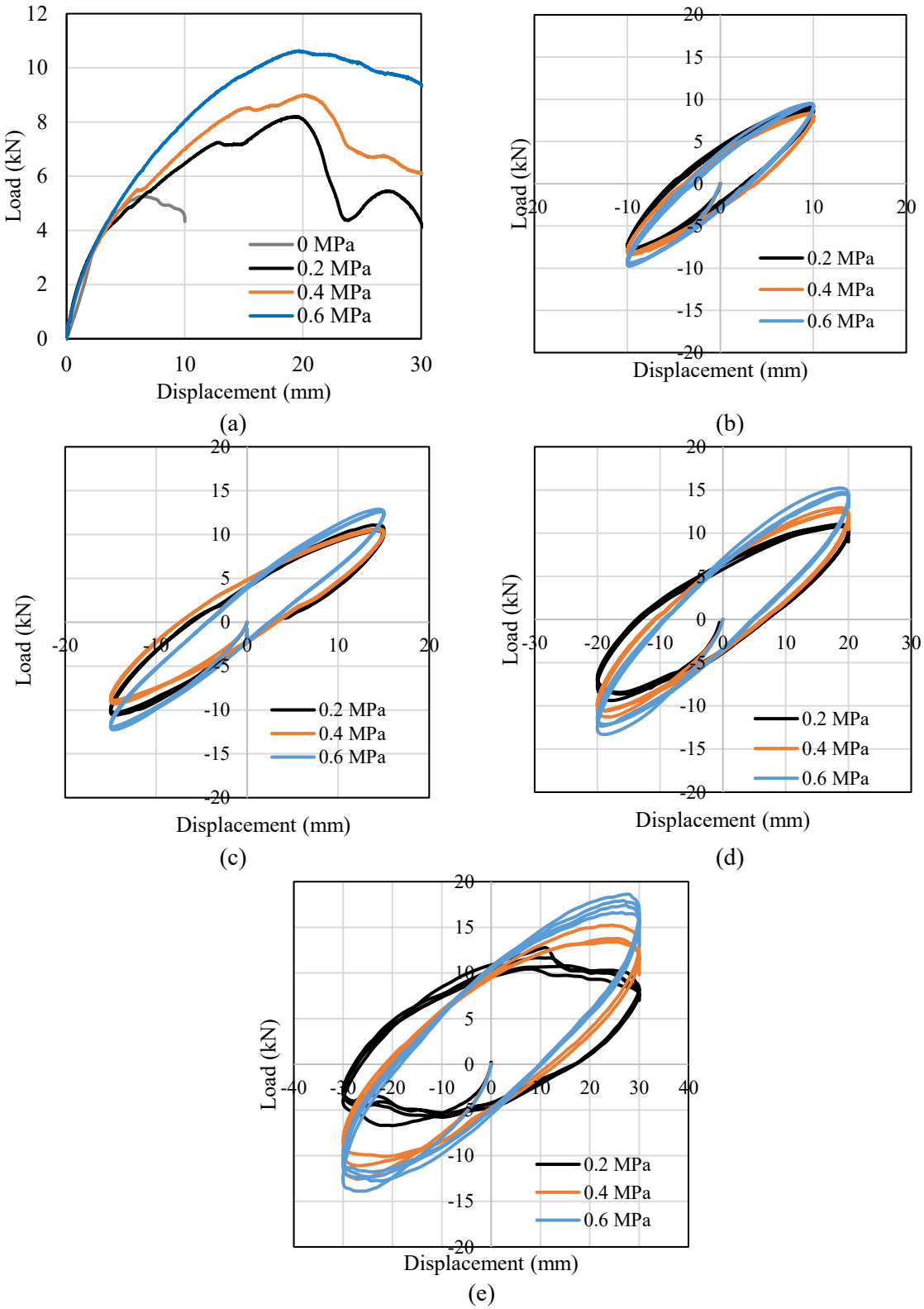

Figure 5.15. Shear response of triplets with mortar-rubber joints for various levels of pre-compressions: monotonic loading (a) and cyclic loading (b, c, d, e).

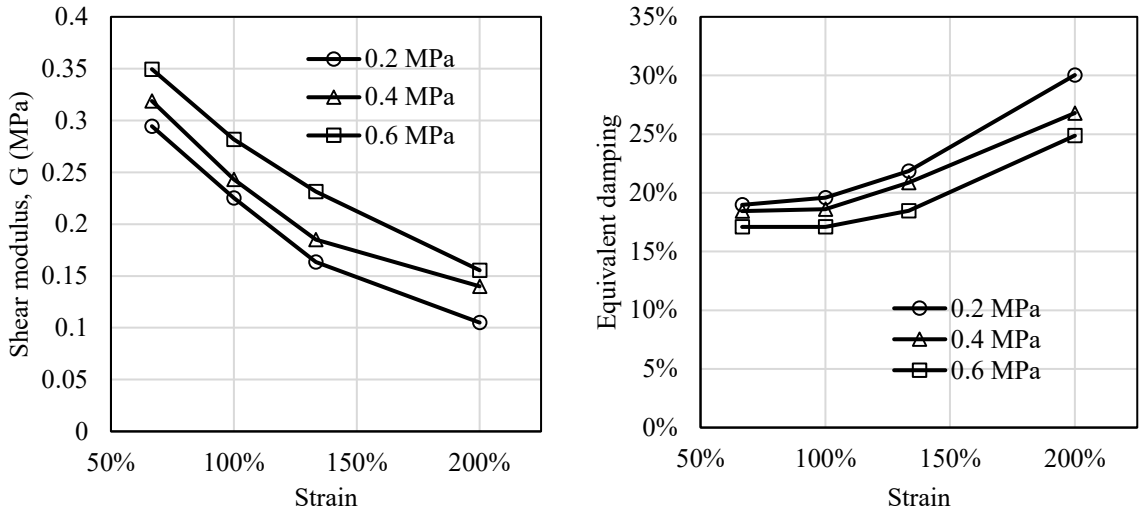

(a) (b)

Figure 5.16. Variation of the (a) secant shear modulus (b) equivalent damping with increasing shear strain at different compression levels.

Figure 5.17 shows the cyclic shear response obtained for different frequencies of oscillation. It can be seen that the stiffness of the mortar-rubber joint and the energy dissipation capacity are not significantly affected by the frequency. It is noteworthy that it was not possible to test higher frequencies, which may be more representative of those characteristics of earthquake response of RC buildings with infills (i.e., higher than 1.0 Hz).

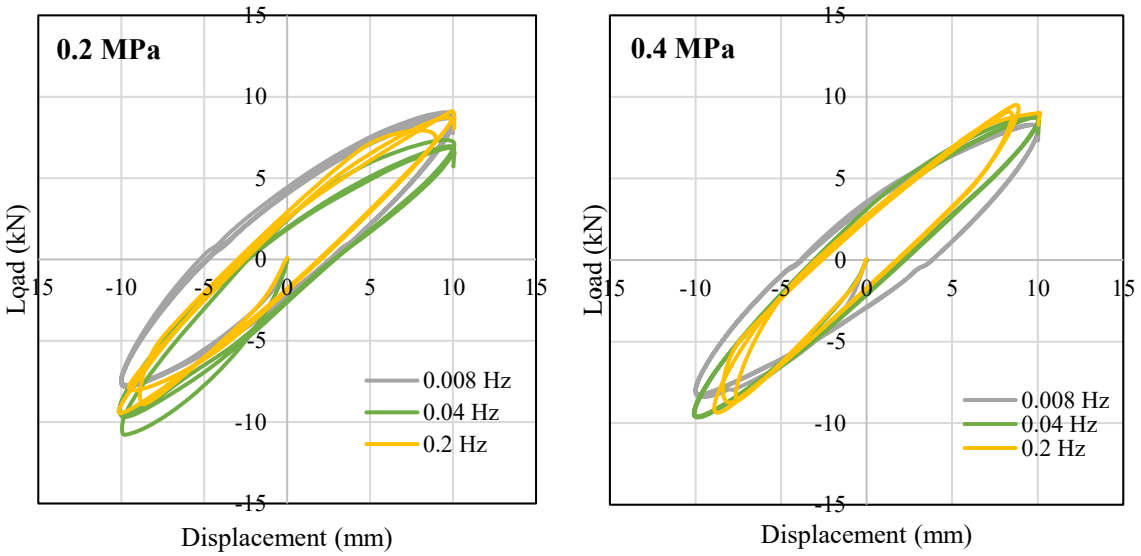

(a) (b)

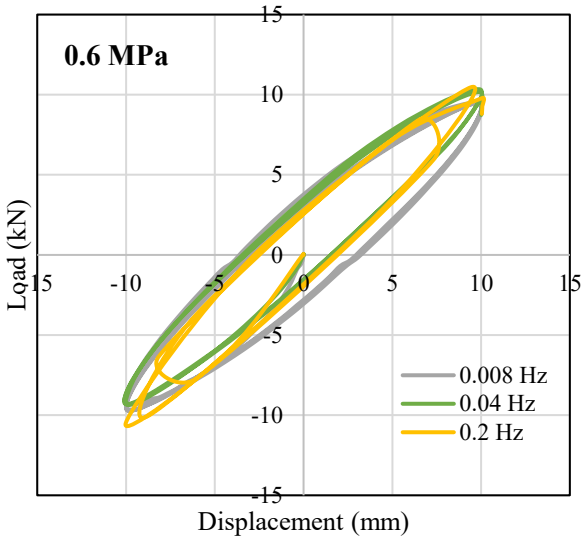

(c)

Figure 5.17. Cyclic shear response of triplets with mortar-rubber joints tested under various frequencies of oscillation for different pre-compression levels: (a) 0.2 (b) 0.4 and (c) 0.6 MPa.

Table 5.3 reports both peak loads of the masonry triplets exhibited in both the monotonic tests and the cyclic tests, for different levels of pre-compression. As already discussed, these values correspond to the rubber-mortar bond failure only in the case of monotonic loading. Figure 5.18 illustrates the relationship between the peak shear strengths, calculated as the ratio between the peak shear strength and two times the cross-sectional area of the interface, and the pre-compression stress, for the two types of triplets under monotonic loading. The

peak shear strength for the three selected levels of pre-compression can be interpolated with a straight line, representing the Mohr-Coulomb failure criterion. This is expressed as:

$$\tau = c + \sigma_p \tan(\phi) \qquad \text{Eq. 5.6}$$

where σ_p is the pre-compression, c is the cohesion, and ϕ is the friction angle. Table 5.3 shows the values of cohesion and friction angle providing the best fit of Eq. 5.6 to the experimental data. It can be seen that these values of the parameters provide a very good fit to the test results. In general, the capacity of the mortar joint is 4-5 times higher than that of the mortar-rubber joint, due to the relatively weak bond between the rubber and the mortar. The values of the cohesion and friction obtained for the mortar-rubber joints are comparable to those obtained experimentally by Verlato (2017) with triplets made with the specially shaped DRES-V2 joints of Figure 2.22b (c =0.12 MPa, $\tan(\phi)$=0.36).

Table 5.3. Peak load of masonry triplets obtained from monotonic and cyclic shear tests.

Samples	Pre-compression (MPa)	Peak stress (MPa)	
		Mortar joints	Mortar-rubber joints
1	0	-	0.12
2	0.2	0.83	0.18
3	0.4	0.94	0.21
4	0.6	1.22	0.24

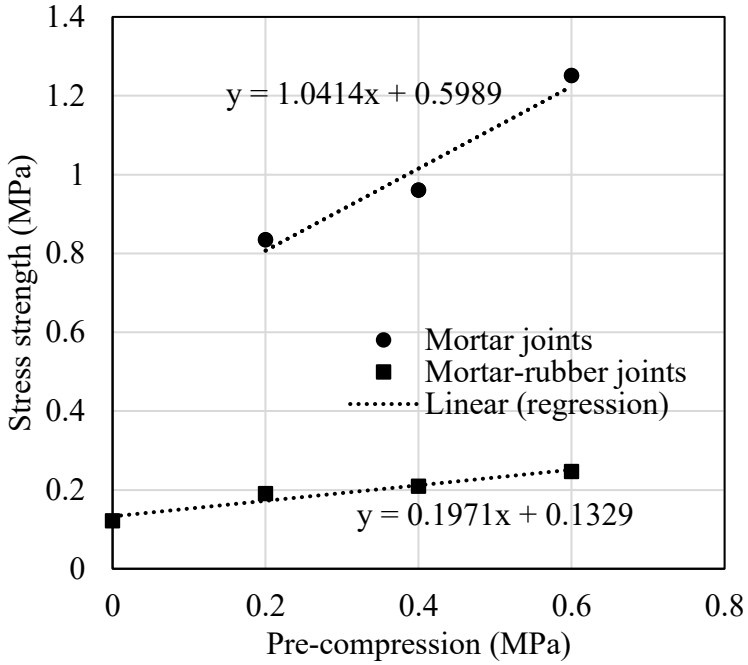

Figure 5.18. Relationship between shear strength and pre-compression stress obtained by testing the triplets with mortar and mortar-rubber joints under monotonic loading.

5.3 Simulation of experimental tests

This section illustrates the simulation of the experimental tests described in Section 2 carried out in the commercial FE software Abaqus (Dassault Systèmes 2016) using a micro-modelling approach (Rots 1997).

5.3.1 Simulation of experimental tests on triplets with mortar joints

The two components of the triplets (bricks and mortar layers) are described as a continuum and discretised using 3D 8-noded solid elements of reduced integration with hourglass control (C3D8R). The behaviour of the mortar and the brick units is described using a Concrete Damage Plasticity (CDP) model (Lee and Fenves 1998; Concrete damaged plasticity 2017). Surface-to-surface contact interfaces are used to simulate the bond between the mortar layers. The cohesive interfaces exhibit initially a linear elastic response, followed by a cracking behaviour that describes the most critical failure modes, namely, tensile cracking and shear sliding. This allows simulating the failure occurred in correspondence of the brick-mortar interfaces for the mortar triplets. The parameters of the material and interface models are based on the material characterisation tests and, on the triplet, tests discussed in the previous section. Table 5.4 and Table 5.5 illustrate the main parameters

describing the mechanical properties of the brick units, the mortar layer, and the interfaces. The last columns of Table 5.4 and Table 5.5 describe the source of the values used for the parameters of the components of the triplet models. It is noteworthy that most of these values have been taken from the characterisation tests carried out on the specimens of brick and mortar. Some parameter values (e.g., the mortar tensile test and fracture energy) have been calibrated to achieve a better fit to experimental results. Nevertheless, all the parameter values are within the ranges recommended in the literature.

Table 5.4. Mechanical properties of the triplet components (brick and mortar units).

Mechanical properties	Brick units	Mortar	Source
Young's modulus, E (MPa)	18350	1747	Material characterisation tests
Poisson's ratio, v (-)	0.16	0.15	-
Compressive strength, σ_c (MPa)	13.53	16.47	Material characterisation tests
Strain at peak compressive stress	-	0.04	-
Peak tensile strength, σ_t (MPa)	3.75	2.75	Material characterisation tests, best fit to test results
Fracture energy in tension, G_f^I (MPa·mm)	0.07	0.04	Value within the range recommended by (Lourenço 1997), best fit to test results

Table 5.5. Properties of the contact interfaces describing the brick-mortar joints.

Mortar Interaction Properties	Brick-mortar joints	Source
k_n^m per unit area (N/mm^3)	1000	Penalty parameter (Dhir et al. 2021)
k_s^m , k_t^m per unit area (N/mm^3)	500	Penalty parameter (Dhir et al. 2021)
σ_t (MPa)	0.14	Best fit to test results
Cohesion, c (MPa)	0.6	Triplet tests
Coefficient of friction, μ (-)	1.04	Triplet tests
Normal fracture energy per unit area, G_f^I (MPa·mm)	0.015	Value within the range recommended by (Lourenço 1997), best fit to test results
Shear fracture energy per unit area, G_f^{II} (MPa·mm)	0.09	Value within the range recommended by (Lourenço 1997), best fit to test results

Figure 5.19 (a) shows the model developed for the triplets with mortar joints, using a fine mesh with element size of 10mm. Figure 5.19 (b) shows the deformed shape of the model at failure and the plastic strain distribution, highlighting the high concentration of damage in correspondence of the mortar joints and at the interface.

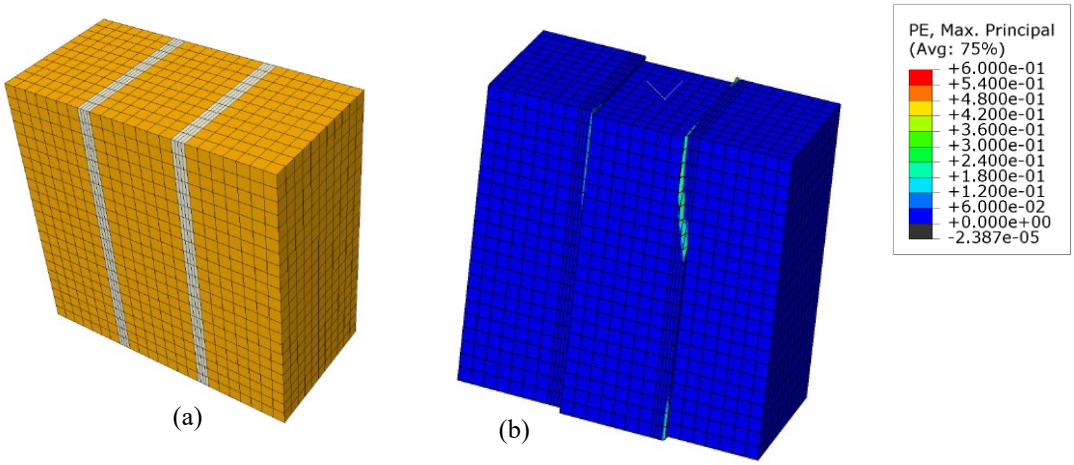

Figure 5.19. (a) FE model with refined mesh (b) plastic strain distributions for mortar triplets.

Figure 5.20 (a-d) compares the experimental and numerical responses of the masonry triplets with mortar joints under monotonic loading at different levels of pre-compression.

Two different mesh sizes were considered (with characteristic element length of 10 mm and 20 mm) without noticing significant changes in the simulated response, which is quite well described by the proposed model. In particular, the proposed model simulates with good accuracy the behaviour of the triplets up to the peak load, whereas it overestimates the post-peak stiffness of the softening branch. For the fracture energy, we assumed a value of 0.04 MPa·mm (Figure 5.20e) based on the numerical analysis carried out on the model with 0.2 MPa pre-compression considering different values in a range recommended by Lourenço (1997). Similarly, a comparison between the simulations of the triplet test obtained for five different values of the tensile resistance (with a constant fracture energy of 0.04 MPa·mm). It is noteworthy that the value of 2.75 MPa (Figure 5.20f) of the tensile resistance of the mortar was selected to obtain a better fit to the experimental results and it is less than the one obtained with the three-point bending test (i.e., 3.76 MPa).

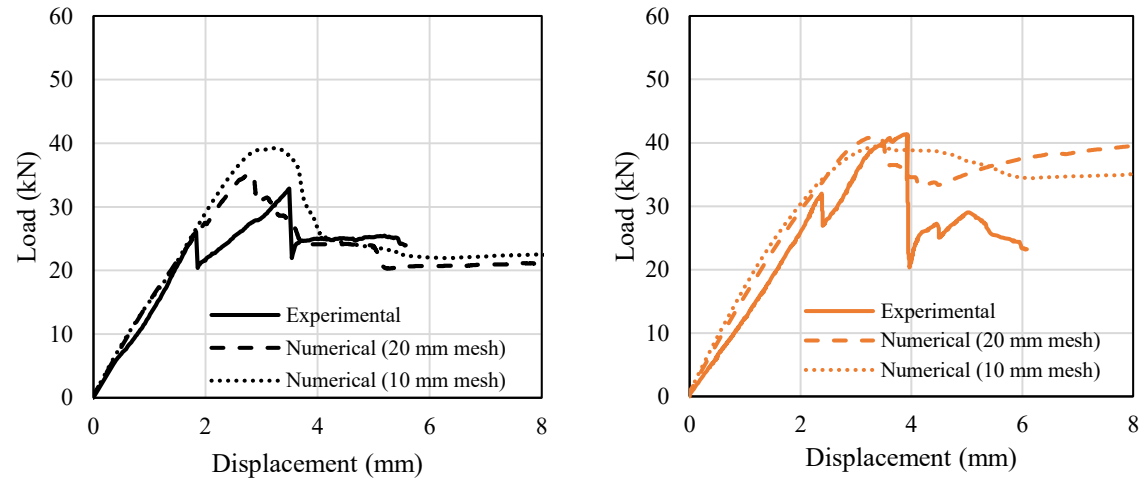

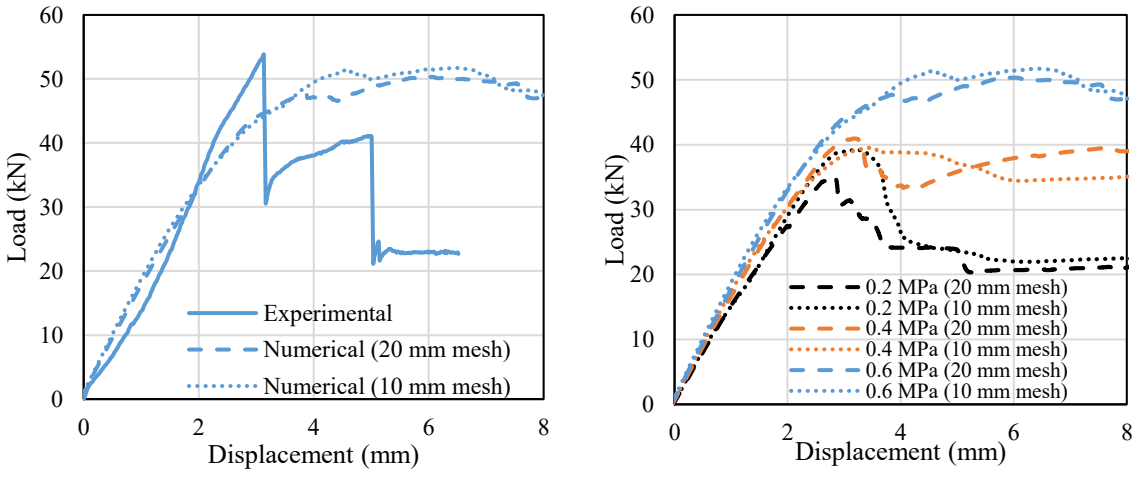

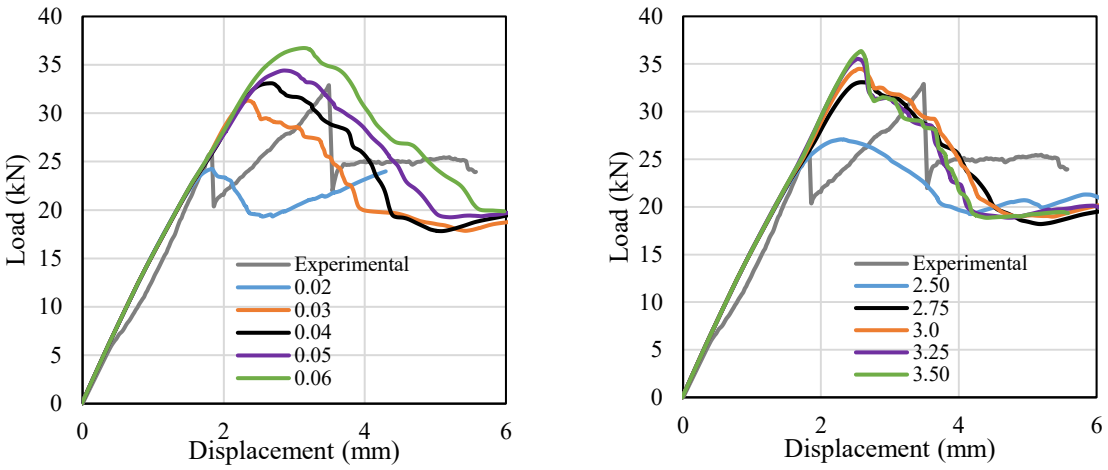

Figure 5.20. (a, b, c) Comparison of experimental and numerical response of the mortar triplets under monotonic loading at (a) 0.2 MPa (b) 0.4 MPa (c) 0.6 MPa pre-compression (d) Comparison of numerical responses only (e, f) sensitivity analysis for the selected tensile strength and fracture energy of mortar.

5.3.2 Simulation of characterization rubber material tests and cyclic tests on triplets with mortar-rubber joints

This subsection describes the simulation and results of the uniaxial and double shear tests performed on rubber test pieces and the cyclic tests performed on triplets with mortar-rubber joint. The rubber is modelled using 3D 8-noded solid elements with a first-order hybrid formulation (C3D8H) to prevent volumetric locking, which is recommended to model the almost incompressible rubber material (Dassault Systèmes 2016).

The pins in the rubber are not taken into account in the numerical model, and a tie constraint is introduced between the rubber joints and the mortar layers. The proposed model cannot describe the friction mechanism and the progressive degradation of the bond between the joints and the mortar up to failure. Thus, it is used here to simulate only the tests under small displacement amplitudes.

Following the approach developed by Bergstrom and Boyce (1998), the mechanical response of the rubber joint is described by two networks working in parallel. The first one, network A, corresponds to the time-independent behaviour of the rubber, which is described by a hyperelastic model. The other, network B, describes the non-linear rate-dependent part of the response, responsible for the hysteretic behaviour.

In particular, the Yeoh model (Yeoh 1993) is adopted for the hyperelastic component of the response, whose strain energy potential W has the following expression:

$$W = \sum_{i=1}^{3} C_{i0} \left(I_1 - 3 \right)^i \qquad \text{Eq. 5.7}$$

where I_1 is the first invariant of strain tensor and C_{i0} are material parameters.

The Bergstrom-Boyce material model (Bergström and Boyce 1998) is used to describe the rate-dependent hysteretic behaviour of the rubber. The strain-rate in network B is given by the following equation:

$$\dot{\varepsilon}_{\ldots} \quad [\ldots - 1]^c \left(\sigma_B \right)^m \qquad \text{Eq. 5.8}$$

where $\dot{\varepsilon}_{\ldots}$ is the effective creep strain rate, λ_B-1 is the nominal creep strain and σ_B is the effective stress. A, m and c are material constants. A stress scaling factor S is also required, which defines the ratio of the stress carried by network B to the stress carried by network A. The total response of the model is obtained by summing the responses of the two networks.

Table 5.6 shows the values of the parameters of the Yeoh and Bergstrom-Boyce models, which are calibrated to provide the best fit to both the shear and the relaxation tests carried out on the quadruplets and the triplet test results for maximum shear amplitudes up to 15 mm. While different sets of parameters could be found that provide a better fit to each test results than the one considered, preference has been given to a single set of values that provide a reasonable fit to all the test results. This is expected to lead to some inaccuracies, which are however unavoidable due to the complex behaviour of the rubber joint, the limitations of the models available in Abaqus for the rubber and the cohesive bond, and the simplifications introduced in the modelling strategy (e.g., the pins in the rubber are not modelled). The development of a very sophisticated model that accurately simulates the results is out of the scope of the present study.

Table 5.6 Material parameters of Yeoh model (MPa) and Bergstrom-Boyce model.

Yeoh model			Bergstrom- Boyce model			
C_{10}	C_{20}	C_{30}	S	A [$S^{-1}MPa^{-1}$]	m	c
0.112588	-0.0093778	0.000249563	1.35086	0.978683	1.48367	-0.0070551

Figure 5.21 (a-c) compare the shear tests performed on the quadruplet with the numerical results, whereas Figure 5.21 (d) compare the shear stress-strain response and the relaxation curves of the quadruplet specimen. It can be observed that the proposed model

and calibrated parameters provide a fair approximation of the complex mechanical behaviour of the rubber under different loading conditions.

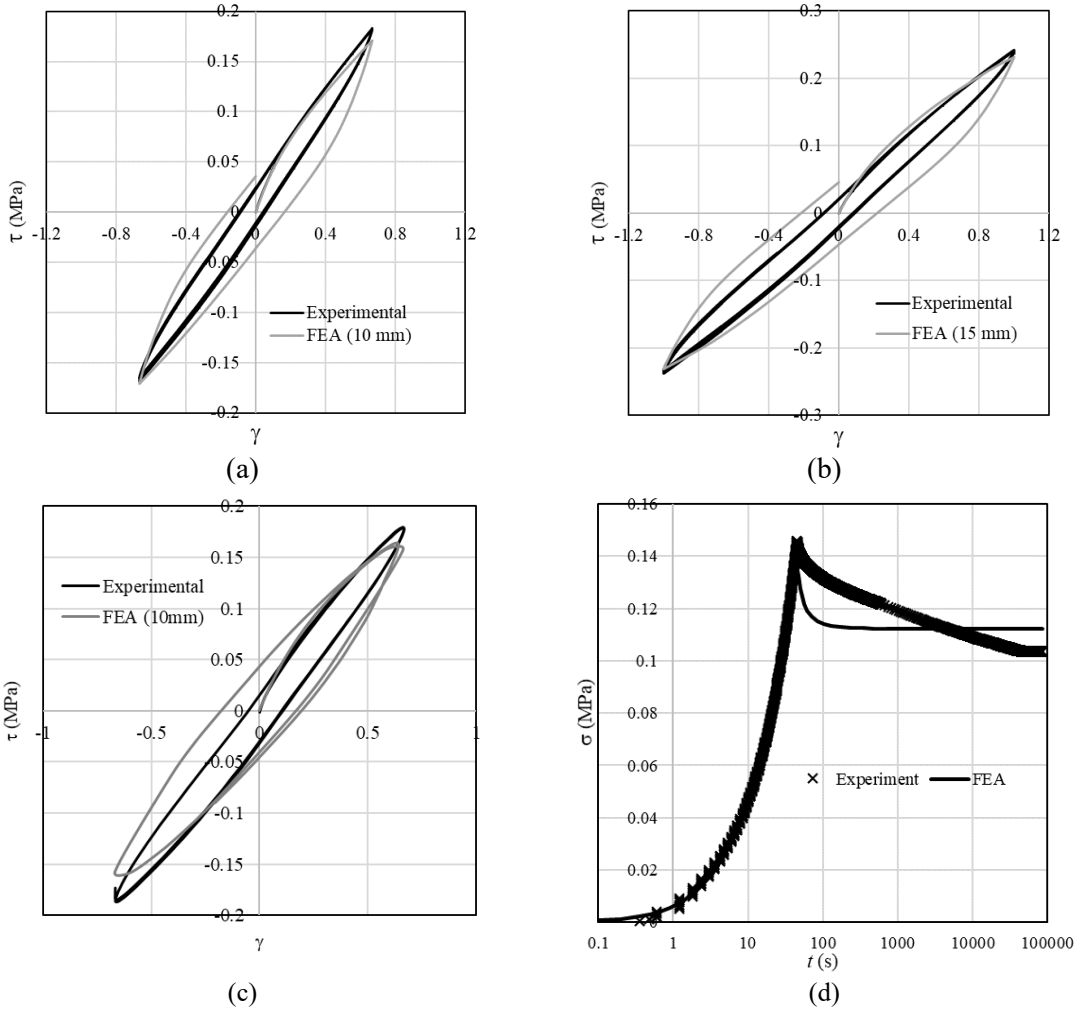

Figure 5.21. Comparison of experimental and numerical shear responses of quadruplet rubber specimen: cyclic constant rate loading with maximum amplitude of (a) γ =0.67, (b) γ =1, (c) cyclic sinusoidal input with amplitude γ =0.67, and (d) relaxation test at γ =0.5.

Regarding the triplet numerical model, tie constraints have been adopted between the brick-mortar and mortar-rubber interfaces during cyclic tests. Figure 23 (a) shows the model of the masonry triplet with rubber joints. A pressure load has been applied along the z direction to simulate the initial pre-compression levels and subsequently three cycles of sinusoidal displacement are applied along the x-direction while preventing translation along z and rotation of the external brick blocks.

Figure 23 (b) illustrates the deformed shape together with the engineering shear strain distributions of the triplet subjected to the highest pre-compression 0.6 MPa and 15 mm lateral displacement. It can be observed that the highest local shear strains are concentrated within the rubber layers. Figures 24-Figure 25 show the results of the numerical simulation of cyclic tests under 0.2, 0.4, and 0.6 MPa pre-compression and amplitudes of 10 and 15 mm respectively. A fair agreement can be observed between model predictions and experimental results.

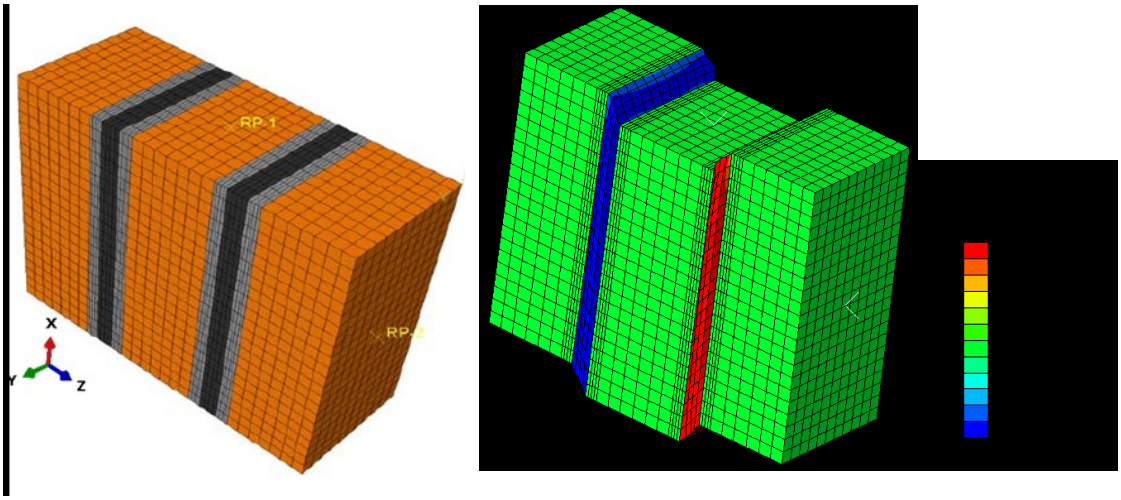

(a) (b)

Figure 5.22. (a) FE model of the masonry triplets with mortar-rubber joints, (b) nominal strain distributions for mortar-rubber triplets subjected to the maximum level of pre-compression in combination with 20 mm lateral displacement.

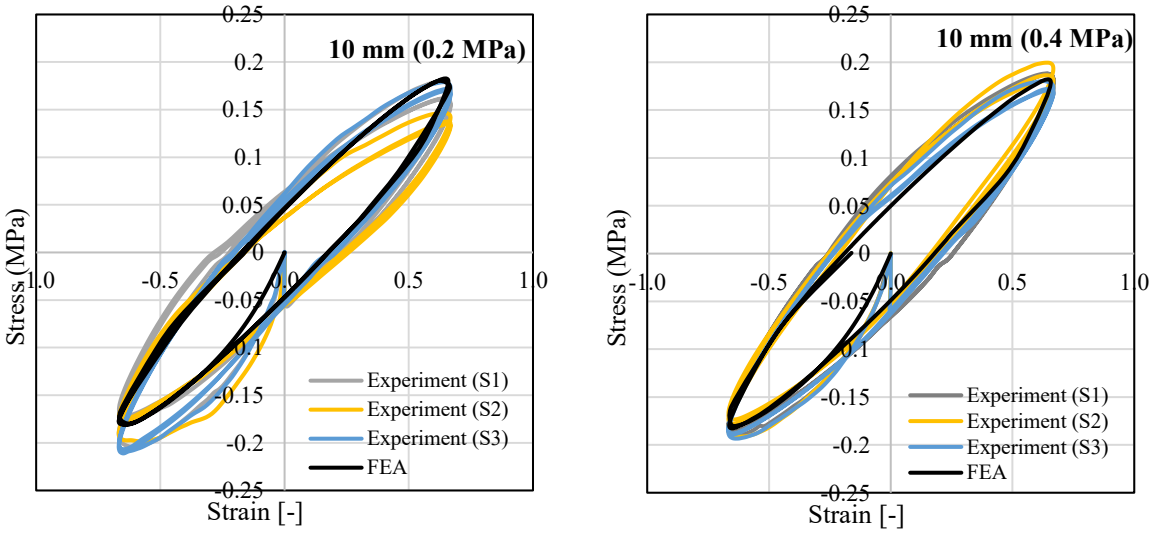

(a) (b)

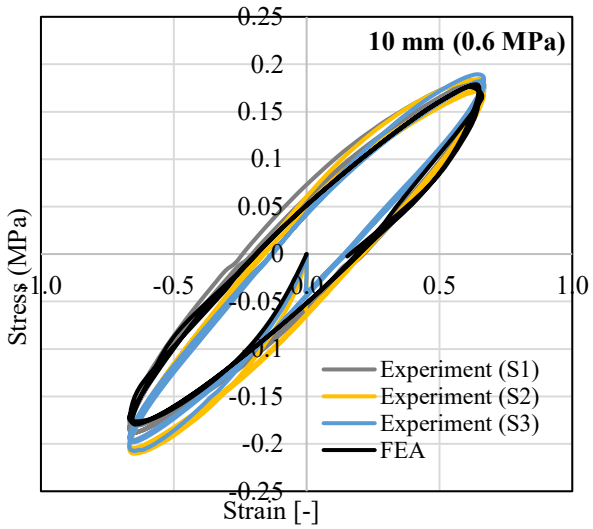

(c)

Figure 5.23. Comparison of experimental and numerical cyclic shear response of the masonry triplet at 10 mm amplitude and pre-compression (a) 0.2 MPa, (b) 0.4 MPa, and (b) 0.6 MPa.

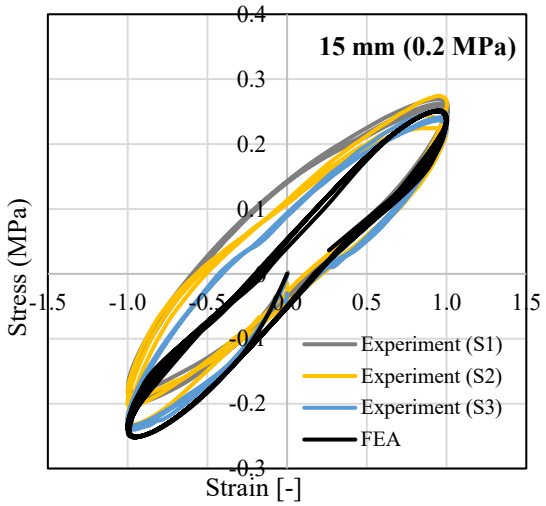

(a)

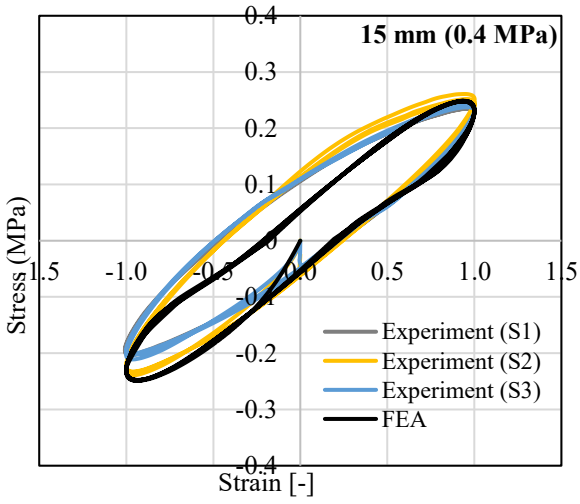

(b)

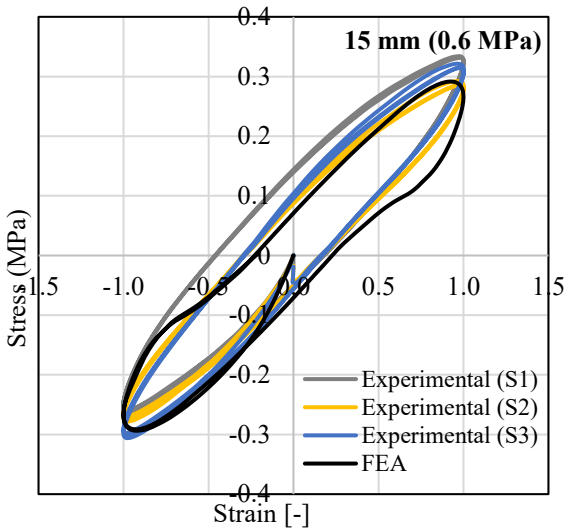

(c)

Figure 5.24. Comparison of experimental and numerical cyclic shear response of the masonry triplet at 15 mm amplitude and pre-compression (a) 0.2 MPa, (b) 0.4 MPa, and (b) 0.6 MPa.

The bond between the rubber layers and the mortar layers has been found to be the weakest component of the composite system in all the triplet tests carried out. Thus, future research efforts should be aimed to increase the bond resistance, in order to guarantee that the good energy dissipation capabilities of the rubber compounds are exploited, and avoid residual deformations associated with the bond failure. Alternatively, rubber layers with increased thickness could be employed to reduce the stresses at the rubber-bond interface.

5.4 Summary

This study has presented the outcomes of an extensive experimental and numerical campaign aimed at characterising the mechanical behaviour of mortar-rubber joints used for enhancing the performance of masonry infills in reinforced concrete frames. In the first part of the study, the experimental tests of brick, mortar and rubber are illustrated, together with cyclic shear tests of masonry triplets with mortar and mortar-rubber joints. These tests were carried out using an experimental apparatus specifically developed for the study. The numerical models used for simulating the cyclic shear tests of the masonry triplets, with the material behaviour calibrated based on the tests of brick, mortar and rubber specimens.

Based on the study results, the following conclusions can be drawn:

- The mortar-rubber joints exhibit very good dissipative properties, with an equivalent damping ratio value of the order of 20% or more which is much higher than that of the rubber compound (of the order of 6%). This is due to the frictional mechanism activated at the interface between the rubber joints and the mortar, enhanced by the presence of pins in the surface of the rubber joints.

- The measured high energy dissipation capabilities of the joints demonstrate the potential of these devices to contribute significantly to the dissipation of the seismic energy in the structures where they are inserted. This feature of the behaviour of the joints could be exploited to reduce the seismic demand in infilled reinforced concrete buildings, without requiring the use of auxiliary energy dissipation devices.

- The bond between the rubber layers and the mortar layers was found to be the weakest component of the composite system. While the failure of this bond reduces the stiffening effect of the infills and increases even further the damping capabilities of the joints due to the activation of the frictional mechanism, it may be not desirable because it may result in residual deformations and a weakening of the infill panel in the out-of-plane direction. In order to avoid bond failure, the rubber layers should be designed to undergo shear deformations below the bond capacity, for example by increasing their thickness to limit the shear deformations they would undergo.

- The bond between the rubber joints and the mortar layers exhibited higher strengths under cyclic loading compared to monotonic loading. This phenomenon, already observed in other experimental studies on similar type of joints, should be further investigated; moreover, alternative types of rubber joints, exhibiting better bond properties, should be developed and tested.

- The proposed modelling strategy provides a fair description of the behaviour of masonry triplets with mortar-rubber joints, thanks to the use of an advanced model capable to simulate the complex amplitude- and rate-dependent behaviour of the high-damping natural rubber compound. However, further investigations need to be carried out to better understand and model the complex interaction between the rubber joints and the mortar layers. Future studies should be aimed at improving the modelling of the interaction of the rubber joint and the mortar layer through the pins, and at simulating the degradation and failure of the bond between the joint and the mortar.

6 Conclusions and recommendations for future work

6.1 Conclusions

This research has presented the outcomes of an experimental and numerical study on the behaviour of masonry-infilled reinforced concrete (RC) frames with rubber joints. The seismic vulnerability of the infills commonly used in RC frames is a widely known issue, and among the various techniques proposed for enhancing their performance, the ones involving the use of sliding and rubber joints have emerged as the most promising.

The rubber joints can be introduced within the infill panels to increase their flexibility, but also at the interface between the panel and the frame, in order to reduce the contact stresses. The rubber joints are also expected to provide an additional source of energy dissipation, thanks to the use of a high-damping rubber compound, although this has not been fully investigated in past studies.

The work described in the present thesis aimed at filling some gaps in the modelling of the response of RC frames with rubber joints, particularly under in-plane loading, and in the knowledge of the mechanical behaviour of these devices.

With regards to the modelling aspects, a meso-scale approach has been developed for simulating the response of infill walls with rubber joints and their interaction with the RC frame under horizontal in-plane loads such as those induced by earthquakes. This modelling approach describes the masonry blocks with three-dimensional solid elements and uses zero-thickness interfaces to describe the mortar-rubber joints. Solid elements with embedded rebars represents the behaviour of RC frame. The proposed modelling strategy was validated against experimental tests available from the literature on RC frames with traditional infills and with infills and rubber joints, and a fair agreement was observed.

The most important results drawn from the application of the meso-scale modelling strategy to the case studies are:

- the addition of the sliding/flexible joints enhances the compliance of the infilled frames, with a response that is closer to the one of the bare frames than of traditionally infilled ones.

- In addition to the horizontal rubber joints, the use of vertical rubber joints with low stiffness further improves the performance of the infilled system by reducing the compressive stresses and the crack forming at higher displacements in the panel, as well as the plastic deformations in the frame.

This study has also proposed an innovative and computationally efficient approach for analysing the in-plane non-linear cyclic response of RC frames with masonry infills and flexible/sliding joints. The proposed approach is based on a fiber-element based description of the frame components, and on the use of 2D discrete macro-elements, for describing the behaviour of the masonry subpanels and the interaction between them and with the adjacent frame components. The modelling strategy, developed in OpenSees, allows to evaluate the effectiveness of the sliding joints and rubber joints in minimising the negative effects of the interaction between infill and RC frame, by shedding light not only on their impact on the global force-displacement behaviour of the system, but also on the internal forces in the individual components. The proposed strategy has a computational cost significantly lower than that required by the meso-scale modelling strategy, and thus it is suitable for investigating the dynamic behaviour and seismic response of large-scale frames with infills and rubber joints. Several case studies from the literature have been considered for the validation of the proposed strategy. The following conclusions were made from the proposed macro-modelling approach:

- this modelling strategy provides accurate estimates of both the initial as well as the post-peak force-displacement response of the analysed systems under horizontal loading.

- the global response of the system is not significantly affected by the infill mesh discretisation. Increasing the number of elements, the model becomes slightly stiffer and also the residual strength increases.

- for a given level of drift demand, the internal forces in the columns of the RC frame with infill and rubber joints have maximum values similar, if not inferior to those of the bare frame, with the exception of the axial and shear force in the windward column. The maximum absolute values of the internal forces in the case of infill with rubber joints are lower than the corresponding values obtained in the system with traditional infill.

With regards to the characterisation of the behaviour of the mortar-rubber joints, and particularly of the hysteretic response and capacity under cyclic loading, an extensive experimental campaign has been carried out at University of Strathclyde on individual components and on masonry triplets with both traditional and mortar-rubber joints. An unconventional test set-up has been employed to evaluate the response of the triplets under shear loading for different pre-compression levels. The study results show that the mortar-rubber joints are significantly more flexible than the traditional mortar joints, and have a very good dissipation capacity, thanks to the use of a highly dissipative rubber compound. However, in order to exploit this, particular care must be placed in the design and manufacturing stage, in order to ensure good bond properties between the rubber layers and the mortar layers, which is the weakest component of the composite system. The rubber layers should be designed to undergo shear deformations below the bond capacity. A micro-scale model has also been developed for describing the behaviour of the triplets, with the parameters of the models of the bricks, mortar and rubber calibrated based on material tests. The results of the experimental and numerical investigations of this study are useful for informing future numerical studies on the analysis of the seismic performance of masonry infilled frames with rubber joints, and on the evaluation of optimal mechanical and geometrical properties of the rubber joint properties. Based on the study results, the following conclusions can be drawn:

- The mortar-rubber joints exhibit very good dissipative properties, with an equivalent damping ratio value of the order of 20% or more which is much higher than that of the rubber compound (of the order of 6%). This is due to the frictional mechanism activated at the interface between the rubber joints and the mortar, enhanced by the presence of pins in the surface of the rubber joints.

- The bond between the rubber layers and the mortar layers was found to be the weakest component of the composite system. While the failure of this bond reduces the stiffening effect of the infills and increases even further the damping capabilities of the joints due to the activation of the frictional mechanism, it may be not desirable because it may result in residual deformations and a weakening of the infill panel in the out-of-plane direction. In order to avoid bond failure, the rubber layers should be designed to undergo shear deformations below the bond capacity, for example by increasing their thickness to limit the shear deformations they would undergo.

- The bond between the rubber joints and the mortar layers exhibited higher strengths under cyclic loading compared to monotonic loading. This phenomenon, already observed in other experimental studies on similar type of joints, should be further investigated; moreover, alternative types of rubber joints, exhibiting better bond properties, should be developed and tested.

6.2 Recommendations for future work

This thesis has confirmed the high potential of rubber joints for protecting infilled frames and enhancing the performance of RC frame structures. This opens many possibilities to expand the present research further:

- As the interaction between the in-plane and out-of-plane behaviour increases the vulnerabilities of infill systems, the meso-scale and micro-scale modelling approaches could be used to investigate the combined in-plane and out-of-plane behaviour of the infilled frame. The macro-element requires some extension in order to be able to simulate also the behaviour in the out-of-plane direction.

- The global seismic performance of a whole building with infill walls and rubber joints can be studied using the developed macro-modelling approach, whose computational efficiency and accuracy has been largely demonstrated in this study.

- Seismic fragility analyses and life-cycle cost-benefit analyses can be performed to further prove the effectiveness of rubber joints.

- Investigation of the dynamic behaviour and damping capabilities of masonry-infilled frames with rubber joints can be carried out to evaluate the effectiveness of the rubber joints in enhancing the global performance of RC infilled frames, without requiring additional sources of damping.

- Since the masonry infill construction typology, and the properties of the masonry bricks and blocks are quite diverse across the globe, the development of strategies for the optimal design of the geometrical and mechanical properties of rubber joints tailored to the specific construction technique of the infill can be an interesting work.

The present modelling strategies can be further expanded to study the development of low-cost joints made from recycled rubber (in collaboration with TARRC) and its contribution in enhancing the seismic performance of the infilled system

References

Abdulla, K.F., Cunningham, L.S. and Gillie, M., 2017. Simulating masonry wall behavior using a simplified micro-model approach. Engineering Structures, 151, pp.349-365.

Abrams, D. and Biggs, D., 2012. Hybrid masonry seismic systems. In Proceedings of the 15th International Brick and Block Masonry Conference.

Ahmadi, H., Dusi, A. and Gough, J., 2017. A rubber-based system for damage reduction in infill masonry walls. In 16th World Conf. Earthq. Eng., Santiago, Chile.

Akhoundi, F., Vasconcelos, G., Lourenço, P., Silva, L.M., Cunha, F. and Fangueiro, R., 2018. In-plane behavior of cavity masonry infills and strengthening with textile reinforced mortar. Engineering Structures, 156, pp.145-160.

Al Hanoun, M.H., Abrahamczyk, L. and Schwarz, J., 2017, January. Numerical simulation of RC frame structures with infill walls under consideration of out-of-plane behavior. In Proceedings 16th world conference on earthquake engineering (WCEE), Santiago, Chile (pp. 9-13).

Al-Chaar, G., Issa, M. and Sweeney, S., 2002. Behavior of masonry-infilled nonductile reinforced concrete frames. Journal of Structural Engineering, 128(8), pp.1055-1063.

Al-Chaar, G.K., 2002. Evaluating strength and stiffness of unreinforced masonry infill structures (No. ERDC/CERL TR 02 1). Engineer research and development center champaign il construction engineering research lab.

Alecci, V., Fagone, M., Rotunno, T. and De Stefano, M., 2013. Shear strength of brick masonry walls assembled with different types of mortar. Construction and Building Materials, 40, pp.1038-1045.

Ali, M.U., Khan, S.A., Anwar, M.Y., Aleem, A., Raza, S. and Maqbool, U., 2017. Seismic performance of deficient masonry infill reinforced-concrete structures. Proceedings of the Institution of Civil Engineers-Structures and Buildings, 170(2), pp.143-155.

Aliaari, M. and Memari, A.M., 2005. Analysis of masonry infilled steel frames with seismic isolator subframes. Engineering Structures, 27(4), pp.487-500.

Aliaari, M. and Memari, A.M., 2006. Experimental evaluation of a sacrificial system for masonry infill walls', AEI 2006: Building Integration Solutions - Proceedings of the 2006 Architectural Engineering National Conference, 2006(June), pp. 1-15.

Alwashali, H. and Maeda, M. 2013. Vulnerability assessment method of low-rise RC buildings with masonry infill walls, in 10th International Conference on Urban Earthquake Engineering. Tokyo Institute of Technology, Tokyo, Japan, pp. 1–7.

Anderson, C. 1976. Behavior of non-loadbearing block walls under wind loading.

Anderson, C., 1984. Arching action in transverse laterally loaded masonry wall panels.

Andreotti, G., Graziotti, F. and Magenes, G., 2018. Detailed micro-modelling of the direct shear tests of brick masonry specimens: the role of dilatancy. Engineering Structures, 168, pp.929-949.

Angel, R., Abrams, D.P., Shapiro, D., Uzarski, J. and Webster, M., 1994. Behavior of reinforced concrete frames with masonry infills. University of Illinois Engineering Experiment Station. College of Engineering. University of Illinois at Urbana-Champaign.

Anglada, X.R., 2014. Shear tests on masonry triplets with different soft layer membranes (Doctoral dissertation, Swiss Federal Institute of Technology, Zürich).

Anić, F., Penava, D., Abrahamczyk, L. and Sarhosis, V., 2020. A review of experimental and analytical studies on the out-of-plane behavior of masonry infilled frames. Bulletin of Earthquake Engineering, 18(5), pp.2191-2246.

Anić, F., Penava, D., Guljaš, I., Sarhosis, V. and Abrahamczyk, L., 2021. Out-of-plane cyclic response of masonry infilled RC frames: An experimental study. Engineering Structures, 238, p.112258.

Anić, F., Penava, D., Sarhosis, V. and Abrahamczyk, L., 2021. Development and Calibration of a 3D Micromodel for Evaluation of Masonry Infilled RC Frame Structural Vulnerability to Earthquakes. Geosciences, 11(11), p.468.

Anić, F., Penava, D., Sarhosis, V. and Abrahamczyk, L., 2021. Development and Calibration of a 3D Micromodel for Evaluation of Masonry Infilled RC Frame Structural Vulnerability to Earthquakes. Geosciences, 11(11), p.468.

Asteris, P.G., 2003. Lateral stiffness of brick masonry infilled plane frames. Journal of structural engineering, 129(8), pp.1071-1079.

Asteris, P.G., 2008. Finite element micro-modeling of infilled frames. Electronic journal of structural engineering, 8, pp.1-11.

Asteris, P.G., Antoniou, S.T., Sophianopoulos, D.S. and Chrysostomou, C.Z., 2011. Mathematical macro modeling of infilled frames: state of the art. Journal of Structural Engineering, 137(12), pp.1508-1517.

Asteris, P.G., Cavaleri, L., Di Trapani, F. and Tsaris, A.K., 2017. Numerical modelling of out-of-plane response of infilled frames: State of the art and future challenges for the equivalent strut macro models. Engineering Structures, 132, pp.110-122.

Asteris, P.G., Cotsovos, D.M., Chrysostomou, C.Z., Mohebkhah, A. and Al-Chaar, G.K., 2013. Mathematical micro modeling of infilled frames: state of the art. Engineering Structures, 56, pp.1905-1921.

Baker, J.W., 2007, December. Measuring bias in structural response caused by ground motion scaling. In 8th Pacific Conference on Earthquake Engineering, Singapore (Vol. 8).

Barattucci, S., Sarhosis, V., Bruno, A.W., D'Altri, A.M., de Miranda, S. and Castellazzi, G., 2020. An experimental and numerical study on masonry triplets subjected to monotonic and cyclic shear loadings. Construction and Building Materials, 254, p.119313.

Barua, H.K. and Mallick, S.K., 1977. Behavior of mortar infilled steel frames under lateral load. Building and Environment, 12(4), pp.263-272.

Basha, S.H. and Kaushik, H.B., 2016. Behavior and failure mechanisms of masonry-infilled RC frames (in low-rise buildings) subject to lateral loading. Engineering Structures, 111, pp.233-245.

Bergström, J.S. and Boyce, M., 1998. Constitutive modeling of the large strain time-dependent behavior of elastomers. Journal of the Mechanics and Physics of Solids, 46(5), pp.931-954.

Biggs, D. T. 2007. Masonry Walls and Structural Systems, in In Proceedings of the Tenth North American Masonry Conference.

Bolis, V., Migliorati, L., Stavridis, A. and Preti, M., 2015, September. In-plane behavior of innovative masonry infills based on different configurations of wooden sliding joints. In Proceedings of the 10th ERES Conference (pp. 289-301).

Bolis, V., Stavridis, A. and Preti, M., 2017. Numerical investigation of the in-plane performance of masonry-infilled RC frames with sliding subpanels. Journal of Structural Engineering, 143(2), p.04016168.

Bolis, V., Stavridis, A. and Preti, M., 2017. Numerical investigation of the in-plane performance of masonry-infilled RC frames with sliding subpanels. Journal of Structural Engineering, 143(2), p.04016168.

Bothara, J.K., Dhakal, R.P. and Mander, J.B., 2010. Seismic performance of an unreinforced masonry building: An experimental investigation. Earthquake Engineering & Structural Dynamics, 39(1), pp.45-68.

Boussabah, L. and Bruneau, M., 1992. Review of the seismic performance of unreinforced masonry walls. In Proc. of the 10th World Conf on Eq. Eng (pp. 4537-4540).

Braga, F., Manfredi, V., Masi, A., Salvatori, A. and Vona, M., 2011. Performance of non-structural elements in RC buildings during the L'Aquila, 2009 earthquake. Bulletin of Earthquake Engineering, 9(1), pp.307-324.

Brando, G., Rapone, D., Spacone, E., Barbosa, A., Olsen, M., Gillins, D., Soti, R., Varum, H., Arêde, A., Vila-Pouca, N. and Furtado, A., 2015. Reconnaissance report on the 2015 Gorkha earthquake effects in Nepal. XVI Convegno Anidis.

Breveglieri, M., Camata, G. and Spacone, E., 2018. Strengthened infilled RC frames: Continuum and macro modeling in nonlinear finite element analysis. Composites Part B: Engineering, 151, pp.78-91.

Brokken, S.T. and Bertero, V.V., 1981. Studies on effects of infills in seismic resistant R/C construction. NASA STI/Recon Technical Report N, 82, p.31576.

Bruneau, M., 1994. State-of-the-art report on seismic performance of unreinforced masonry buildings. Journal of Structural Engineering, 120(1), pp.230-251.

Cai, G. and Su, Q., 2019. Effect of infills on seismic performance of reinforced concrete frame structures—A full-scale experimental study. Journal of Earthquake Engineering, 23(9), pp.1531-1559.

Calabria, A., Guidi, G., da Porto, F. and Modena, C., 2016, November. Innovative systems for masonry infill walls based on the use of rubber joints: Finite element modelling and comparison with in-plane tests. In Brick and Block Masonry: Trends, Innovations and Challenges-Proceedings of the 16th International Brick and Block Masonry Conference, IBMAC (Vol. 2016, pp. 1155-62).

Caliò, I. and Pantò, B., 2014. A macro-element modelling approach of Infilled Frame Structures. Computers & Structures, 143, pp.91-107.

Caliò, I. and Pantò, B., 2014. A macro-element modelling approach of Infilled Frame Structures. Computers & Structures, 143, pp.91-107.

Caliò, I., Marletta, M. and Pantò, B., 2012. A new discrete element model for the evaluation of the seismic behavior of unreinforced masonry buildings. Engineering Structures, 40, pp.327-338.

Calvi, G.M. and Bolognini, D., 2001. Seismic response of reinforced concrete frames infilled with weakly reinforced masonry panels. Journal of Earthquake Engineering, 5(02), pp.153-185.

Cardone, D. and Perrone, G., 2017. Damage and loss assessment of pre-70 RC frame buildings with FEMA P-58. Journal of Earthquake Engineering, 21(1), pp.23-61.

Cavaleri, L. and Di Trapani, F., 2014. Cyclic response of masonry infilled RC frames: Experimental results and simplified modeling. Soil Dynamics and Earthquake Engineering, 65, pp.224-242.

Cavaleri, L., Di Trapani, F., Asteris, P.G. and Sarhosis, V., 2017. Influence of column shear failure on pushover-based assessment of masonry infilled reinforced concrete framed structures: A case study. Soil Dynamics and Earthquake Engineering, 100, pp.98-112.

Charleson, A. 2012. Seismic design for architects. Routledge.

Chrysostomou, C.Z., 1991. Effects of degrading infill walls on the nonlinear seismic response of two-dimensional steel frames. Cornell University.

Chrysostomou, C.Z., Gergely, P. and Abel, J.F., 2002. A six-strut model for nonlinear dynamic analysis of steel infilled frames. International Journal of Structural Stability and Dynamics, 2(03), pp.335-353.

Concrete damaged plasticity, 2017. Abaqus manual. Available at: https://abaqus-docs.mit.edu/2017/English/SIMACAEMATRefMap/simamat-c-concretedamaged.htm.

Crisafulli, F.J. and Carr, A.J., 2007. Proposed macro-model for the analysis of infilled frame structures. Bulletin of the New Zealand society for earthquake engineering, 40(2), pp.69-77.

Crisafulli, F.J., 1997. Seismic behavior of reinforced concrete structures with masonry infills, p. 404. Available at: http://hdl.handle.net/10092/1221.

Da Porto, F., Guidi, G., Dalla Benetta, M. and Verlato, N., 2013, June. Combined in-plane/out-of-plane experimental behavior of reinforced and strengthened infill masonry walls. In 12th Canadian masonry symposium (pp. 2-5).

da Porto, F., Guidi, G., Verlato, N. and Modena, C., 2015. Effectiveness of plasters and textile reinforced mortars for strengthening clay masonry infill walls subjected to combined in-plane/out-of-plane actions/Wirksamkeit von Putz und textilbewehrtem Mörtel bei der Verstärkung von Ausfachungswänden aus Ziegelmauerwerk, die kombinierter Scheiben-und Plattenbeanspruchung ausgesetzt sind. Mauerwerk, 19(5), pp.334-354.

D'Altri, A.M., de Miranda, S., Castellazzi, G. and Sarhosis, V., 2018. A 3D detailed micro-model for the in-plane and out-of-plane numerical analysis of masonry panels. Computers & Structures, 206, pp.18-30.

Dawe, J.L. and Charalambous, P.D., 1983. Finite Element Analysis for Wall-Frame Interaction. In Proceedings, Eight International Loadbearing Brickwork Symposium, British Ceramic Society, Stoke-on-Trent. UK.

Dawe, J.L. and Seah, C.K., 1989. Behavior of masonry infilled steel frames. Canadian Journal of Civil Engineering, 16(6), pp.865-876.

Dawe, JL and Seah, CK, 1989. Out-of-plane resistance of concrete masonry infilled panels. Canadian Journal of Civil Engineering, 16 (6), pp.854-864.

De Risi, M.T., Del Gaudio, C. and Verderame, G.M., 2019. Evaluation of repair costs for masonry infills in RC buildings from observed damage data: the case-study of the 2009 L'Aquila earthquake. Buildings, 9(5), p.122.

De Risi, M.T., Di Domenico, M., Ricci, P., Verderame, G.M. and Manfredi, G., 2019. Experimental investigation on the influence of the aspect ratio on the in-plane/out-of-plane interaction for masonry infills in RC frames. Engineering Structures, 189, pp.523-540.

Defining the constitutive response of cohesive elements using a traction-separation description, 2017. Abaqus manual. Available at: https://abaqus-docs.mit.edu/2017/English/SIMACAEELMRefMap/simaelm-c-cohesivebehavior.htm.

Del Vecchio, C., Di Ludovico, M., Pampanin, S. and Prota, A., 2018. Repair costs of existing RC buildings damaged by the L'Aquila earthquake and comparison with FEMA P-58 predictions. Earthquake Spectra, 34(1), pp.237-263.

Dhanasekar, M. and Page, A. W., 1986. Influence of Brick Masonry Infill Properties on the Behavior of Infilled Frames, Proceedings of the Institution of Civil Engineers (London), 81(pt 2), pp. 593–605.

Dhir, P.K., Tubaldi, E., Ahmadi, H. and Gough, J., 2021. Numerical modelling of reinforced concrete frames with masonry infills and rubber joints. Engineering Structures, 246, p.112833.

Dhir, P.K., Tubaldi, E., Panto, B. and Calio, I., 2022a. A macro-model for describing the in-plane seismic response of masonry-infilled frames with sliding/flexible joints. Earthquake Engineering & Structural Dynamics.

Dhir, P., Tubaldi, E., Orfeo, A. and Ahmadi, H., 2022b. Cyclic shear behaviour of masonry triplets with rubber joints. Construction and Building Materials.

Di Trapani, F., Bolis, V., Basone, F. and Preti, M., 2020. Seismic reliability and loss assessment of RC frame structures with traditional and innovative masonry infills. Engineering Structures, 208, p.110306.

Di Trapani, F., Macaluso, G., Cavaleri, L. and Papia, M., 2015. Masonry infills and RC frames interaction: literature overview and state of the art of macro modeling

approach. European Journal of Environmental and Civil Engineering, 19(9), pp.1059-1095.

Di Trapani, F., Shing, P.B. and Cavaleri, L., 2018. Macro element model for in-plane and out-of-plane responses of masonry infills in frame structures. Journal of Structural Engineering, 144(2), pp.04017198-04017198.

Dias, A.B., Da Porto, F., Fehling, E., Lourenço, P.B., Morandi, P., Vintzileou, E. and Yakut, A., 2014. Innovative systems for earthquake resistant masonry enclosures in RC buildings.

Dizhur, D., Ingham, J., Griffith, M., Biggs, D., Schultz, A., Modena, C., da Porto, F. and Valluzzi, M.R., 2016, November. Performance of unreinforced masonry and infilled RC buildings during the 2015 Gorkha, Nepal earthquake sequence. In Proc., 16th Int. Brick Block Masonry Conf., IBMAC (pp. 2399-2408).

Dolatshahi, K.M. and Aref, A.J., 2011. Two-dimensional computational framework of meso-scale rigid and line interface elements for masonry structures. Engineering Structures, 33(12), pp.3657-3667.

Donà, M., Tecchio, G., Domenicale, L., Saler, E., Minotto, M. and da Porto, F., 2017. Directional effects on combined in-plane and out of plane seismic behavior of masonry infills. In Proceedings of the 6th International Conference on Computational Methods in Structural Dynamics and Earthquake Engineering (COMPDYN 2015). doi (Vol. 10, No. 120117.5649, p. 18570).

DRES, 2017. Organization for Development, Renovation and Equipping of Schools of I.R. Iran (DRES). A preliminary report on school buildings performance during M7.3 Ezgeleh, Iran Earthquake of November 12, 2017.

Drougkas, A., Esposito, R., Messali, F. and Sarhosis, V., 2021. Analytical models to determine in-plane damage initiation and force capacity of masonry walls with openings. Journal of Engineering Mechanics, 147(11).

Drysdale, R.G. and Essawy, A.S., 1988. Out-of-plane bending of concrete block walls. Journal of Structural Engineering, 114(1), pp.121-133.

El-Dakhakhni, W.W., 2002. Experimental and analytical seismic evaluation of concrete masonry-infilled steel frames retrofitted using GFRP laminates. Drexel University.

El-Dakhakhni, W.W., Drysdale, R.G. and Khattab, M.M., 2006. Multilaminate macro model for concrete masonry: formulation and verification. Journal of Structural Engineering, 132(12), pp.1984-1996.

ElGawady, M., Lestuzzi, P. and Badoux, M., 2004, July. A review of conventional seismic retrofitting techniques for URM. In 13th international brick and block masonry conference (Vol. 4, No. 7).

EN 1015-11 2006. Methods of Test for Mortar for Masonry, Part 11: Determination of Flexural and Compressive Strength of Hardened Mortar, 3(1).

EN 1052-3 2002. Methods of Test for Mortar for Masonry, Part 3: Determination of initial shear strength, 3(1).

EN 1998-1 2004. Design of structures for earthquake resistance. Part 1: General rules, seismic actions and rules for buildings.

Filiatrault, A. and Sullivan, T., 2014. Performance-based seismic design of nonstructural building components: The next frontier of earthquake engineering. Earthquake Engineering and Engineering Vibration, 13(1), pp.17-46.

Filiatrault, A., Perrone, D., Merino, R.J. and Calvi, G.M., 2021. Performance-based seismic design of nonstructural building elements. Journal of Earthquake Engineering, 25(2), pp.237-269.

Fiorato, A. E., Sozen, M. A. and Gamble, W. L., 1970. An investigation of the interaction of RC frames with masonry filler walls.', (370), pp. 540.

Flanagan, R.D. and Bennett, R.M., 1999. Arching of masonry infilled frames: Comparison of analytical methods. Practice Periodical on Structural Design and Construction, 4(3), pp.105-110.

Flanagan, R.D. and Bennett, R.M., 1999. Bidirectional behavior of structural clay tile infilled frames. Journal of structural engineering, 125(3), pp.236-244.

Flanagan, R.D. and Bennett, R.M., 2001. In-plane analysis of masonry infill materials. Practice Periodical on Structural Design and Construction, 6(4), pp.176-182.

Flanagan, R.D., 1994. Behavior of structural clay tile infilled frames. The University of Tennessee.

Franzoni, E., Gentilini, C., Graziani, G. and Bandini, S., 2014. Towards the assessment of the shear behavior of masonry in on-site conditions: a study on dry and salt/water conditioned brick masonry triplets. Construction and Building Materials, 65, pp.405-416.

Fricke, K.E., Jones, W.D. and Huff, T.E., 1992, June. In situ lateral load testing of an unreinforced masonry hollow clay tile wall. In Proceedings of the Sixth Canadian Masonry Symposium, Saskatchewan, Canada (pp. 519-530).

Furtado, A., Rodrigues, H. and Arêde, A., 2014. Numerical modelling of masonry infill walls participation in the seismic behavior of RC buildings. OpenSees Days Port, pp.3-6.

Furtado, A., Rodrigues, H. and Arêde, A., 2015. Modelling of masonry infill walls participation in the seismic behavior of RC buildings using OpenSees. International Journal of Advanced Structural Engineering (IJASE), 7(2), pp.117-127.

Furtado, A., Rodrigues, H., Arêde, A. and Varum, H., 2015. Influence of the in plane and out-of-plane masonry infill walls' interaction in the structural response of RC buildings. Procedia Engineering, 114, pp.722-729.

Furtado, A., Rodrigues, H., Arêde, A. and Varum, H., 2016. Experimental evaluation of out-of-plane capacity of masonry infill walls. Engineering Structures, 111, pp.48-63.

Gent, A.N. and Lindley, P.B., 1959. The compression of bonded rubber blocks. Proceedings of the Institution of Mechanical Engineers, 173(1), pp.111-122.

Hashemi, A. and Mosalam, K.M., 2006. Shake-table experiment on reinforced concrete structure containing masonry infill wall. Earthquake engineering & structural dynamics, 35(14), pp.1827-1852.

Hendry, A.W. and Kheir, A.M.A., 1976, April. The lateral strength of certain brickwork panels. In Proceedings of the Fourth International Brick Masonry Conference (p. 4).

Hendry, A.W. and Liauw, T.C., 1994. Tests on steel frames with reinforced masonry infilling. In Proceedings of 3rd International Masonry Conference. The British Masonry Society, London (pp. 108-114).

Hendry, A.W., 1973. The lateral strength of unreinforced brickwork.

Hermanns, L., Fraile, A., Alarcón, E. and Álvarez, R., 2014. Performance of buildings with masonry infill walls during the 2011 Lorca earthquake. Bulletin of Earthquake Engineering, 12(5), pp.1977-1997.

Holmes, M., 1961. Steel frames with brickwork and concrete infilling. proceedings of the Institution of civil Engineers, 19(4), pp.473-478.

Holmes, M., 1963. Combined loading on infilled frames. Proceedings of the Institution of Civil Engineers, 25(1), pp.31-38.

Hossein, M. and Toshimi, K., 2004. Effect of infill masonry walls on the seismic response of reinforced concrete buildings subjected to the 2003 Bam earthquake strong motion: a case study of Bam telephone center.

Huang, Q., Guo, Z. and Kuang, J.S., 2016. Designing infilled reinforced concrete frames with the 'strong frame-weak infill' principle. Engineering Structures, 123, pp.341-353.

INSYSME, 2016. INnovative SYStems for earthquake resistant Masonry Enclosures in reinforced concrete buildings, FP7-SME-2013-2- GA606229GA606229. Available at: www.insysme.eu.

Jiang, H., Liu, X. and Mao, J., 2015. Full-scale experimental study on masonry infilled RC moment-resisting frames under cyclic loads. Engineering Structures, 91, pp.70-84.

Kadysiewski, S. and Mosalam, K.M., 2009. Modeling of unreinforced masonry infill walls considering in-plane and out-of-plane interaction (Vol. 70). Berkeley: Pacific Earthquake Engineering Research Center.

Kadysiewski, S. and Mosalam, K.M., 2009. Modeling of unreinforced masonry infill walls considering in-plane and out-of-plane interaction, PEER 2008/102. University of California, Berkeley, 144.

Kakaletsis, D.J. and Karayannis, C.G., 2009. Experimental Investigation of Infilled Reinforced Concrete Frames with Openings. ACI structural journal, 106(2).

Karami, K. and Ahmadi, H., 2021. Torsional control of asymmetric buildings using online 3-D damage detection and adaptive stiffness devices. Structural Control and Health Monitoring, 28(10), p.e2804.

Kariotis, J., 1995. State-of-the-Art Report on Seismic Performance of Unreinforced Masonry Buildings. Journal of Structural Engineering, 121(4), pp.789-791.

Kaushik, H.B., Rai, D.C., and Jain, S.K., 2006. Code Approaches to Seismic Design of Masonry-Infilled Reinforced Concrete Frames: A State-of-the-Art Review. Earthquake spectra, 22(4), pp.961-983.

Kent, D.C. and Park, R., 1971. Flexural members with confined concrete. Journal of the structural division, 97(7), pp.1969-1990.

Khan, M. and Raza, S., 2015. Seismic performance assessment of masonry infilled reinforced concrete (RC) frame structures. International Journal of Civil & Structural Engineering, 6(1), pp.40-57.

Korkmaz, S.Z., Kamanli, M., Korkmaz, H.H., Donduren, M.S. and Cogurcu, M.T., 2010. Experimental study on the behavior of nonductile infilled RC frames strengthened with external mesh reinforcement and plaster composite. Natural Hazards and Earth System Sciences, 10(11), pp.2305-2316.

Koutas, L., Bousias, S.N. and Triantafillou, T.C., 2014. Seismic strengthening of masonry-infilled RC frames with TRM: Experimental study. Journal of Composites for Construction, 19(2).

Koutromanos, I., Stavridis, A., Shing, P.B. and Willam, K., 2011. Numerical modeling of masonry-infilled RC frames subjected to seismic loads. Computers & Structures, 89(11-12), pp.1026-1037.

Kuang, J.S. and Wang, Z., 2014, August. Cyclic load tests of RC frame with column-isolated masonry infills. In Second European conference on earthquake engineering and seismology, Istanbul (pp. 25-29).

Kubalski, T., Butenweg, C., Marinković, M. and Klinkel, S., 2017. Investigation of the seismic behavior of infill masonry using numerical modelling approaches. In 16th World Conference on Earthquake Engineering, Santiago Chile, January (pp. 9-13).

Kubalski, T., Marinković, M. and Butenweg, C., 2016, June. Numerical investigation of masonry infilled RC frames. In 16th International Brick and Block Masonry Conference, Padova, Italy (pp. 1219-1229).

Kyriakides, M., 2011. Seismic retrofit of unreinforced masonry infills in non-ductile reinforced concrete frames using engineered cementitious composites. Stanford University.

Lawrence, S.J., 1979. Lateral loading of masonry infill panels: A literature review. Experimental Building Station, Department of Housing and Construction.

Lee, J. and Fenves, G.L., 1998. A plastic-damage concrete model for earthquake analysis of dams. Earthquake engineering & structural dynamics, 27(9), pp.937-956.

Lemos, J.V. and Sarhosis, V., 2022. Discrete Element Bonded-Block Models for Detailed Analysis of Masonry. Infrastructures, 7(3), p.31.

Lemos, J.V. and Sarhosis, V., 2022. Discrete Element Bonded-Block Models for Detailed Analysis of Masonry. Infrastructures, 7(3), p.31.

Liauw, T. and Kwan, K., 1984b. Nonlinear behavior of non-integral infilled frames', Computers and Structures, 18(3), pp. 551–560.

Liauw, T.C. and Kwan, K.H., 1983. Plastic Theory of Non-Integral Infilled Frames. Proceedings of the Institution of Civil Engineers, 75(3), pp.379-396.

Liauw, T.C. and Kwan, K.H., 1984a. New development in research of infilled frames. In Proceedings of the eighth world conference on earthquake engineering (p. 62330).

Liauw, T.C. and Kwan, K.H., 1985. Static and cyclic behaviors of multistorey infilled frames with different interface conditions. Journal of Sound and Vibration, 99(2), pp.275-283.

Liauw, T.C. and Kwan, K.H., 1985. Unified plastic analysis for infilled frames. Journal of Structural Engineering, 111(7), pp.1427-1448.

Liauw, T.C., 1972. An approximate method of analysis for infilled frames with or without opening. Building science, 7(4), pp.233-238.

Liberatore, L. and Mollaioli, F., 2015. Influence of masonry infill modelling on the seismic response of reinforced concrete frames', in 15th International Conference on Civil, Structural and Environmental Engineering Computing.

Lin, K., Liu, H., Wei, C. and Huang, Q., 2017. Effects of shear rate on cyclic behavior of dry stack masonry joint. Construction and Building Materials, 157, pp.809-817.

Longo, F., Wiebe, L., da Porto, F. and Modena, C., 2016, June. Seismic response history analysis including out-of-plane collapse of unreinforced masonry infill walls in RC frame structures. In Proceedings of the 16th International Brick and Block Masonry Conference, Padova, Italy (pp. 26-30).

Lotfi, H.R. and Shing, P.B., 1991. An appraisal of smeared crack models for masonry shear wall analysis. Computers & structures, 41(3), pp.413-425.

Lourenço, P. J. B. B., 1997. Computational strategies for masonry structures. Doctoral dissertation, Delft University of Technology, Holland.

Lourenço, P.B. and Rots, J.G., 1997. Multi-surface interface model for analysis of masonry structures. Journal of engineering mechanics, 123(7), pp.660-668.

Lourenço, P.J.B.B., 1997. An anisotropic macro-model for masonry plates and shells: Implementation and validation (pp. 34-91). Delft University of Technology, Faculty of Civil Engineering, Mechanics and Structures, Computational Mechanics.

Macorini, L. and Izzuddin, B., 2011. A non-linear interface element for 3D mesoscale analysis of brick-masonry structures. International Journal for numerical methods in Engineering, 85(12), pp.1584-1608.

Macorini, L. and Izzuddin, B.A., 2013. Nonlinear analysis of masonry structures using mesoscale partitioned modelling. Advances in engineering Software, 60, pp.58-69.

Macorini, L. and Izzuddin, B.A., 2014. Nonlinear analysis of unreinforced masonry walls under blast loading using mesoscale partitioned modeling. Journal of Structural Engineering, 140(8), p.A4014002.

Mallick, D.V. and Garg, R.P., 1971. Effect of openings on the lateral stiffness of infilled frames. Proceedings of the Institution of Civil Engineers, 49(2), pp.193-209.

Mallick, D.V. and Severn, R.T., 1967. The behavior of infilled frames under static loading. Proceedings of the Institution of Civil Engineers, 38(4), pp.639-656.

Mander, J.B. and Nair, B., 1994. Seismic resistance of brick-infilled steel frames with and without retrofit. TMS journal, pp.24-37.

Manfredi, V. and Masi, A., 2014. Combining in-plane and out-of-plane behavior of masonry infills in the seismic analysis of RC buildings. Earthquakes and Structures, 6(5), pp.515-537.

Mansouri, A., Marefat, M.S. and Khanmohammadi, M., 2014. Experimental evaluation of seismic performance of low-shear strength masonry infills with openings in reinforced concrete frames with deficient seismic details. The Structural Design of Tall and Special Buildings, 23(15), pp.1190-1210.

Marinković, M., 2018. Innovative system for seismic resistant masonry infills in reinforced concrete frame structures (PhD Thesis). University of Belgrade–Faculty of Civil Engineering.

Marques, R. and Lourenço, P.B., 2014. Unreinforced and confined masonry buildings in seismic regions: Validation of macro-element models and cost analysis. Engineering Structures, 64, pp.52-67.

Martins, A., Vasconcelos, G. and Costa, A.C., 2017. Brick masonry veneer walls: An overview. Journal of Building Engineering, 9, pp.29-41.

Mazzoni, S., McKenna, F., Scott, M.H. and Fenves, G.L., 2006. OpenSees command language manual. Pacific Earthquake Engineering Research (PEER) Center, 264(1), pp.137-158.

McDowell, E.L., McKee, K. and Sevin, E., 1956. Arching action theory of masonry walls. Journal of the Structural Division, 82(2), pp.915-1.

McDowell, E.L., McKee, K.E. and Sevin, E., 1957. Discussion of "Arching Action Theory of Masonry Walls". Journal of the Structural Division, 83(1), pp.1156-9.

McKenna, F., Scott, M.H. and Fenves, G.L., 2010. Nonlinear finite-element analysis software architecture using object composition. Journal of Computing in Civil Engineering, 24(1), pp.95-107.

Mehrabi, A.B. and Shing, P.B., 1994, February. Performance of masonry-infilled R/C frames under in-plane lateral loads: analytical modeling. In Proc., NCEER Workshop on Seismic Response of Masonry, San Francisco.

Mehrabi, A.B. and Shing, P.B., 1997. Finite element modeling of masonry-infilled RC frames. Journal of structural engineering, 123(5), pp.604-613.

Mehrabi, A.B., Benson Shing, P., Schuller, M.P. and Noland, J.L., 1996. Experimental evaluation of masonry-infilled RC frames. Journal of Structural engineering, 122(3), pp.228-237.

Milanesi, R.R., Morandi, P. and Magenes, G., 2016, November. Innovative seismic solution for clay masonry infills with sliding joints: experimental tests. In Proc., 16th International Brick and Block Masonry Conference.

Milanesi, R.R., Morandi, P. and Magenes, G., 2018. Local effects on RC frames induced by AAC masonry infills through FEM simulation of in-plane tests. Bulletin of Earthquake Engineering, 16(9), pp.4053-4080.

Milani, G. and Bertolesi, E., 2017. Quasi-analytical homogenization approach for the non-linear analysis of in-plane loaded masonry panels. Construction and Building Materials, 146, pp.723-743.

Moghaddam, H.A. and Dowling, P.J., 1987. The state of the art in infilled frames. Imperial College of Science and Technology, Civil Engineering Department.

Mohammadi, M. and Akrami, V., 2010. An engineered infilled frame: Behavior and calibration. Journal of Constructional Steel Research, 66(6), pp.842-849.

Mohammadi, M., Akrami, V. and Mohammadi-Ghazi, R., 2011. Methods to improve infilled frame ductility. Journal of Structural Engineering, 137(6), pp.646-653.

Mohyeddin, A., Goldsworthy, H.M., and Gad, E.F., 2013. FE modelling of RC frames with masonry infill panels under in-plane and out-of-plane loading. Engineering Structures, 51, pp.73-87.

Mojsilović, N., 2012. Masonry elements with damp-proof course membrane: Assessment of shear strength parameters. Construction and Building Materials, 35, pp.1002-1012.

Mojsilović, N., Petrović, M. and Anglada, X.R., 2015. Masonry elements with multi-layer bed joints: Behavior under monotonic and static-cyclic shear. Construction and Building Materials, 100, pp.149-162.

Mojsilović, N., Petrović, M. and Stojadinović, B., 2019. Multi-layer masonry bed joint subjected to shear: Analytical modelling. Construction and Building Materials, 205, pp.602-610.

Morandi, P., Hak, S. and Magenes, G., 2013. Simplified out-of-plane resistance verification for slender clay masonry infills in RC frames. Proceedings of the XV ANIDIS, L'Ingegneria Sismica in Italia, Padua, Italy, 30.

Morandi, P., Milanesi, R.R. and Magenes, G., 2016, June. Innovative seismic solution for clay masonry infills with sliding joints: principles and details. In Proceedings of 16th International Brick and Block Masonry Conference (pp. 26-30).

Moretti, M.L., Papatheocharis, T. and Perdikaris, P.C., 2014. Design of reinforced concrete infilled frames. Journal of Structural Engineering, 140(9), p.04014062.

Mosalam, K.M. and Günay, S., 2015. Progressive collapse analysis of reinforced concrete frames with unreinforced masonry infill walls considering in-plane/out-of-plane interaction. Earthquake Spectra, 31(2), pp.921-943.

Mosalam, K.M., White, R.N. and Gergely, P., 1997. Computational strategies for frames with infill walls: Discrete and smeared crack analyses and seismic fragility. In Computational strategies for frames with infill walls: Discrete and smeared crack analyses and seismic fragility (pp. 147-147).

Nasiri, E. and Liu, Y., 2017. Development of a detailed 3D FE model for analysis of the in-plane behavior of masonry infilled concrete frames. Engineering Structures, 143, pp.603-616.

Nicoletti, V., Arezzo, D., Carbonari, S. and Gara, F., 2020. Expeditious methodology for the estimation of infill masonry wall stiffness through in-situ dynamic tests. Construction and Building Materials, 262, p.120807.

Noh, N.M., Liberatore, L., Mollaioli, F. and Tesfamariam, S., 2017. Modelling of masonry infilled RC frames subjected to cyclic loads: State of the art review and modelling with OpenSees. Engineering Structures, 150, pp.599-621.

Okail, H., Abdelrahman, A., Abdelkhalik, A. and Metwaly, M., 2016. Experimental and analytical investigation of the lateral load response of confined masonry walls. HBRC journal, 12(1), pp.33-46.

Oliveira, D.V. and Lourenço, P.B., 2004. Implementation and validation of a constitutive model for the cyclic behavior of interface elements. Computers & structures, 82(17-19), pp.1451-1461.

Ozkaynak, H., Yuksel, E., Yalcin, C., Dindar, A.A. and Buyukozturk, O., 2014. Masonry infill walls in reinforced concrete frames as a source of structural damping. Earthquake engineering & structural dynamics, 43(7), pp.949-968.

Page, A.W., 1978. Finite element model for masonry. Journal of the Structural Division, 104(8), pp.1267-1285.

Pantò, B. and Rossi, P.P., 2019. A new macro model for the assessment of the seismic response of infilled RC frames. Earthquake Engineering & Structural Dynamics, 48(7), pp.792-817.

Pantò, B., Caliò, I. and Lourenço, P.B., 2017. Seismic safety evaluation of reinforced concrete masonry infilled frames using macro modelling approach. Bulletin of Earthquake Engineering, 15(9), pp.3871-3895.

Pantò, B., Caliò, I. and Lourenço, P.B., 2018. A 3D discrete macro-element for modelling the out-of-plane behavior of infilled frame structures. Engineering Structures, 175, pp.371-385.

Pantò, B., Cannizzaro, F., Caliò, I. and Lourenço, P.B., 2017. Numerical and experimental validation of a 3D macro-model for the in-plane and out-of-plane behavior of unreinforced masonry walls. International Journal of Architectural Heritage, 11(7), pp.946-964.

Panto, B., Silva, L., Vasconcelos, G. and Lourenço, P.B., 2019. Macro-modelling approach for assessment of out-of-plane behavior of brick masonry infill walls. Engineering Structures, 181, pp.529-549.

Paulay, T. and Priestley, M.N., 1992. Seismic design of reinforced concrete and masonry buildings (Vol. 768). New York: Wiley.

Pelà, L., Cervera, M. and Roca, P., 2013. An orthotropic damage model for the analysis of masonry structures. Construction and Building Materials, 41, pp.957-967.

Peng, Q., Zhou, X. and Yang, C., 2018. Influence of connection and constructional details on masonry-infilled RC frames under cyclic loading. Soil Dynamics and Earthquake Engineering, 108, pp.96-110.

Penna, A.N.D.R.E.A., Magenes, G.U.I.D.O., Calvi, G.M. and Costa, A.A., 2008, February. Seismic performance of AAC infill and bearing walls with different reinforcement solutions. In Proceedings of the 14th International Brick and Block Masonry Conference (pp. 13-20).

Petrović, M., Mojsilović, N. and Stojadinović, B., 2017. Masonry walls with a multi-layer bed joint subjected to in-plane cyclic loading: An experimental investigation. Engineering Structures, 143, pp.189-203.

Petrović, M., Stojadinović, B. and Mojsilović, N., 2017. I-Shaped unreinforced masonry wallets with a soft-layer bed joint: Behavior under static-cyclic shear. Journal of Structural Engineering, 143(11), p.04017154.

Pietruszczak, S. and Niu, X., 1992. A mathematical description of macroscopic behavior of brick masonry. International journal of solids and structures, 29(5), pp.531-546.

Polyakov, S.V., 1960. On the interaction between masonry filler walls and enclosing frame when loaded in the plane of the wall. Translations in earthquake engineering, 2(3), pp.36-42.

Pradhan, B., Sarhosis, V., Ferrotto, M.F., Penava, D. and Cavaleri, L., 2021. Prediction equations for out-of-plane capacity of unreinforced masonry infill walls based on a macro element model parametric analysis. Journal of Engineering Mechanics, 147(11).

Pradhan, B., Zizzo, M., Sarhosis, V. and Cavaleri, L., 2021, October. Out-of-plane behavior of unreinforced masonry infill walls: Review of the experimental studies and analysis of the influencing parameters. In Structures (Vol. 33, pp. 4387-4406). Elsevier.

Prawel, S.P. and Reinhorn, A.M., 1985, June. Seismic retrofit of structural masonry using a ferrocement overlay. In Proceedings of the Third North American Masonry Conference, Arlington, Texas (pp. 50-1).

Preti, M. and Bolis, V., 2017. Masonry infill construction and retrofit technique for the infill-frame interaction mitigation: Test results. Engineering Structures, 132, pp.597-608.

Preti, M. and Bolis, V., 2017. Masonry infill construction and retrofit technique for the infill-frame interaction mitigation: Test results. Engineering Structures, 132, pp.597-608.

Preti, M., Bettini, N. and Plizzari, G., 2012. Infill walls with sliding joints to limit infill-frame seismic interaction: large-scale experimental test. Journal of Earthquake Engineering, 16(1), pp.125-141.

Preti, M., Bolis, V. and Stavridis, A., 2019. Seismic infill–frame interaction of masonry walls partitioned with horizontal sliding joints: analysis and simplified modeling. Journal of Earthquake Engineering, 23(10), pp.1651-1677.

Preti, M., Migliorati, L. and Giuriani, E., 2015. Experimental testing of engineered masonry infill walls for post-earthquake structural damage control. Bulletin of Earthquake Engineering, 13(7), pp.2029-2049.

Raddington, J.R., 1984. The influence of initial gaps on infilled frame behavior. Proceedings of Institution of Civil Engineers, (Part II), pp.295-310.

Rai, D.C., Singhal, V., Raj S, B. and Sagar, S.L., 2016. Reconnaissance of the effects of the M7. 8 Gorkha (Nepal) earthquake of April 25, 2015. Geomatics, Natural Hazards and Risk, 7(1), pp.1-17.

Rasheed, M.A. and Prakash, S.S., 2018. Behavior of hybrid-synthetic fiber reinforced cellular lightweight concrete under uniaxial tension–Experimental and analytical studies. Construction and Building Materials, 162, pp.857-870.

Rodrigues, H., Varum, H. and Costa, A., 2010. Simplified macro-model for infill masonry panels. Journal of Earthquake Engineering, 14(3), pp.390-416.

Rojahn, C., Poland, C.D. and Scawthorn, C., 1988. Rapid visual screening of buildings for potential seismic hazards: A handbook (Vol. 21). Applied Technology Council.
Rots, J.G., 1991. Numerical simulation of cracking in structural masonry. Heron, 36(2), pp.49-63.

Rots, J.G., 1997. Structural masonry: an experimental/numerical basis for practical design rules. CRC Press.

Ruggieri, S., Porco, F. and Uva, G., 2020. A practical approach for estimating the floor deformability in existing RC buildings: Evaluation of the effects in the structural response and seismic fragility. Bulletin of Earthquake Engineering, 18(5), pp.2083-2113.

Ruggieri, S., Porco, F., Uva, G. and Vamvatsikos, D., 2021. Two frugal options to assess class fragility and seismic safety for low-rise reinforced concrete school buildings in Southern Italy. Bulletin of Earthquake Engineering, 19(3), pp.1415-1439.

Sachanski, S., 1960, July. Analysis of earthquake resistance of frame buildings taking into consideration the carrying capacity of the filling masonry. In Proceedings of the 2nd world conference on earthquake engineering (Vol. 138, pp. 1-15).

SAIE, 2015. SAIE. Available at: http://www.saie.bolognafiere.it/en/.

Saneinejad, A. and Hobbs, B., 1995. Inelastic design of infilled frames. Journal of Structural Engineering, 121(4).

Santos, S.P. ed., 2014. Enclosure Masonry Wall Systems Worldwide: Typical Masonry Wall Enclosures in Belgium, Brazil, China, France, Germany, Greece, India, Italy, Nordic Countries, Poland, Portugal, the Netherlands and USA. CRC Press.

Santos, S.P., 2006. Enclosure walls in the Nordic Countries. In Enclosure Masonry Wall Systems Worldwide (pp. 147-155).

Sarhosis, V., Tsavdaridis, K.D. and Giannopoulos, I., 2014. Discrete element modelling (DEM) for masonry infilled steel frames with multiple window openings subjected to lateral load variations. Open Construction and Building Technology Journal, 8, pp.93-103.

Sattar, S., 2013. Influence of masonry infill walls and other building characteristics on seismic collapse of concrete frame buildings (Doctoral dissertation, University of Colorado at Boulder).

Schmidt, T., 1989. An approach of modelling masonry infilled frames by the FE method and a modified equivalent strut method. Annual Journal on Concrete and Concrete Structures." Darmstadt, Germany: Darmstadt University.

Seah, C.K., 1998. A universal approach for the analysis and design of masonry infilled frame structures (Doctoral dissertation, PhD Thesis, Univ. of New Brunswick, Fredericton, N. B., Canada, 1998).

Sezen, H., Whittaker, A.S., Elwood, K.J. and Mosalam, K.M., 2003. Performance of reinforced concrete buildings during the August 17, 1999, Kocaeli, Turkey earthquake, and seismic design and construction practices in Turkey. Engineering Structures, 25(1), pp.103-114.

Shapiro, D.A.N.I.E.L., Uzarski, J., Webster, M.A.R.K., Angel, R.I.C.H.A.R.D. and Abrams, D.P., 1994. Estimating out-of-plane strength of cracked masonry infills. University of Illinois Engineering Experiment Station. College of Engineering. University of Illinois at Urbana-Champaign.

Sherafati, M.A. and Sohrabi, M.R., 2016. Performance of masonry walls during Kaki, Iran, earthquake of April 9, 2013. Journal of Performance of Constructed Facilities, 30(3), p.04015040.

Shing, P.B. and Mehrabi, A.B., 2002. Behavior and analysis of masonry-infilled frames. Progress in Structural Engineering and Materials, 4(3), pp.320-331.

Silva, L., Vasconcelos, G., Lourenço, P.B. and Akhoundi, F., 2016. Experimental evaluation of a constructive system for earthquake resisting masonry enclosure walls.

Silva, L.M., Vasconcelos, G. and Lourenço, P.B., 2019. Seismic performance of Portuguese masonry infill walls: From traditional systems to new solutions.

Sismica, G., 2009. 3DMacro, Computer Program for the Seismic Assessment of Masonry Buildings. Gruppo Sismica. Available at: www.grupposismica.it.

Stafford Smith, B. and Carter, C., 1969. A method of analysis for infilled frames. Proceedings of the institution of civil engineers, 44(1), pp.31-48.

Stavridis, A. and Shing, P.B., 2010. Finite-element modeling of nonlinear behavior of masonry-infilled RC frames. Journal of structural engineering, 136(3), pp.285-296.

Stavridis, A., 2009. Analytical and experimental study of seismic performance of reinforced concrete frames infilled with masonry walls. University of California, San Diego.

Stylianidis, K.C., 2012. Experimental investigation of masonry infilled R/C frames. The Open Construction & Building Technology Journal, 6(1).

Syrmakezis, C.A. and Vratsanou, V.Y., 1986, September. Influence of infill walls to RC frames response. In 8th European conference on earthquake engineering, Istanbul, Turkey (pp. 47-53).

Systèmes, D., 2016. Abaqus, RI: Dassault Systèmes. Available at: http://www.3ds.com/products-services/simulia/products/abaqus/.

Tasligedik, A.S. and Pampanin, S., 2017. Rocking cantilever clay brick infill wall panels: a novel low damage infill wall system. Journal of Earthquake Engineering, 21(7), pp.1023-1049.

Tasligedik, A.S., 2014. Damage mitigation strategies for non-structural infill walls.

Taylor, R.L., 2008. FEAP-A Finite Element Analysis Program, Theory Manual. University of California, Berkeley. http://www. ce. berkeley. edu/feap.

Tinius Olsen, 2021. Electromechanical Universal Testing Machines (ST Series). https://www.tiniusolsen.com/wp-content/uploads/2021/05/ST0000EN03-ST-Series-Tester-A4.pdf.

Tran, D. H., Behr, R. A. and Parfitt, M. K. (2014) 'Global Differences in Building Enclosures', Journal of Architectural Engineering, 20(3).

Tsantilis, A.V. and Triantafillou, T.C., 2018. Innovative seismic isolation of masonry infills using cellular materials at the interface with the surrounding RC frames. Engineering Structures, 155, pp.279-297.

Tu, Y.H., Chao, Y.F. and Chiou, T.C., 2016, November. Lateral load experiment and comparison with analytical model for in-filled masonry panels with openings in an RC

frame. In Proceedings of the 16th International Brick and Block Masonry Conference (IBMAC 2016).

Tubaldi, E., Ragni, L., Dall'Asta, A., Ahmadi, H. and Muhr, A., 2017. Stress softening behavior of HDNR bearings: modelling and influence on the seismic response of isolated structures. Earthquake Engineering & Structural Dynamics, 46(12), pp.2033-2054.

Uva, G., Raffaele, D., Porco, F. and Fiore, A., 2012. On the role of equivalent strut models in the seismic assessment of infilled RC buildings. Engineering Structures, 42, pp.83-94.

Valiasis, T.N. and Stylianidis, K.C., 1989. Masonry infilled R/C frames under horizontal loading—experimental results. European Earthquake Engineering, 3(3), pp.10-20.

Valluzzi, M.R., Da Porto, F., Garbin, E. and Panizza, M., 2014. Out-of-plane behavior of infill masonry panels strengthened with composite materials. Materials and structures, 47(12), pp.2131-2145.

Varum, H., Furtado, A., Rodrigues, H., Dias-Oliveira, J., Vila-Pouca, N. and Arêde, A., 2017. Seismic performance of the infill masonry walls and ambient vibration tests after the Ghorka 2015, Nepal earthquake. Bulletin of Earthquake Engineering, 15(3), pp.1185-1212.

Verlato, N., 2017. Development of a Clay Masonry Enclosure System with Deformable Joints: Experimental Analysis and Numerical. Doctoral dissertation, Università Degli Studi di Brescia, Italy.

Verlato, N., Guidi, G., Da Porto, F. and Modena, C., 2016, June. Innovative systems for masonry infill walls based on the use of deformable joints: combined in-plane/out-of-plane tests. In Proceedings of the 16th international brick and block masonry conference (pp. 26-30). Boca Raton, FL, USA: CRC Press.

Vicente, R., Rodrigues, H., Costa, A., Varum, H. and Mendes da Silva, J.A.R., 2010, August. Masonry enclosure walls: lessons learnt from the recent Abruzzo Earthquake. In Proc. 14th European Conference of Earthquake Engineering.

Vicente, R.S., Rodrigues, H., Varum, H., Costa, A. and Mendes da Silva, J.A.R., 2012. Performance of masonry enclosure walls: lessons learned from recent earthquakes. Earthquake engineering and engineering vibration, 11(1), pp.23-34.

Villaverde, R., 1997. Seismic design of secondary structures: state of the art. Journal of structural engineering, 123(8), pp.1011-1019.

Vintzileou, E., 2014. Typical masonry infills for buildings in Greece. In Enclosure Masonry Wall Systems Worldwide (pp. 85-99). CRC Press.

Vintzileou, E., Adami, C.E. and Palieraki, V., 2016. In-plane and out-of-plane response of a masonry infill divided into smaller wallets. Proc. of 16th IBMAC, pp.26-30.

Vögeli, C., Mojsilović, N. and Stojadinović, B., 2015. Masonry wallets with a soft layer bed joint: Behavior under static-cyclic loading. Engineering Structures, 86, pp.16-32.

Wael, W.E., Mohamed, E. and Ahmad, A., 2003. Three-strut model for concrete masonry-infilled steel frames. J. Struct. Eng, 129, pp.177-185.

Wood, R.H. and BRE, 1978. Plasticity, composite action and collapse design of unreinforced shear wall panels in frames. Proceedings of the Institution of Civil Engineers, 65(2), pp.381-411.

Xavier, F.B., Macorini, L. and Izzuddin, B.A., 2015. Robustness of multistory buildings with masonry infill. Journal of Performance of Constructed Facilities, 29(5), p.B4014004.

Yeoh, O.H., 1993. Some forms of the strain energy function for rubber. Rubber Chemistry and technology, 66(5), pp.754-771.

Yuan, F., Xiaobin, W. and Shulu, Z., 2014, July. Failure Modes of Masonry Infill Walls and Influence on RC Frame Structure Under an Earthquake. In Tenth US National Conference on Earthquake Engineering.

Yuen, T.Y., Kuang, J.S. and Ali, B.S.M., 2016. Assessing the effect of bi-directional loading on nonlinear static and dynamic behavior of masonry-infilled frames with openings. Bulletin of Earthquake Engineering, 14(6), pp.1721-1755.

Yuen, Y.P. and Kuang, J.S., 2013. Fourier-based incremental homogenization of coupled unilateral damage–plasticity model for masonry structures. International Journal of Solids and Structures, 50(20-21), pp.3361-3374.

Yuen, Y.P. and Kuang, J.S., 2014. Masonry-infilled RC frames subjected to combined in-plane and out-of-plane loading. International Journal of Structural Stability and Dynamics, 14(02), p.1350066.

Yuen, Y.P. and Kuang, J.S., 2015. Nonlinear seismic responses and lateral force transfer mechanisms of RC frames with different infill configurations. Engineering Structures, 91, pp.125-140.

Zarnic, R. and Tomazevic, M., 1988, August. An experimentally obtained method for evaluation of the behavior of masonry infilled RC frames. In Proceedings of the 9th world conference on earthquake engineering (Vol. 6, pp. 163-168).

Zhai, C., Kong, J., Wang, X. and Chen, Z., 2016. Experimental and finite element analytical investigation of seismic behavior of full-scale masonry infilled RC frames. Journal of Earthquake Engineering, 20(7), pp.1171-1198.